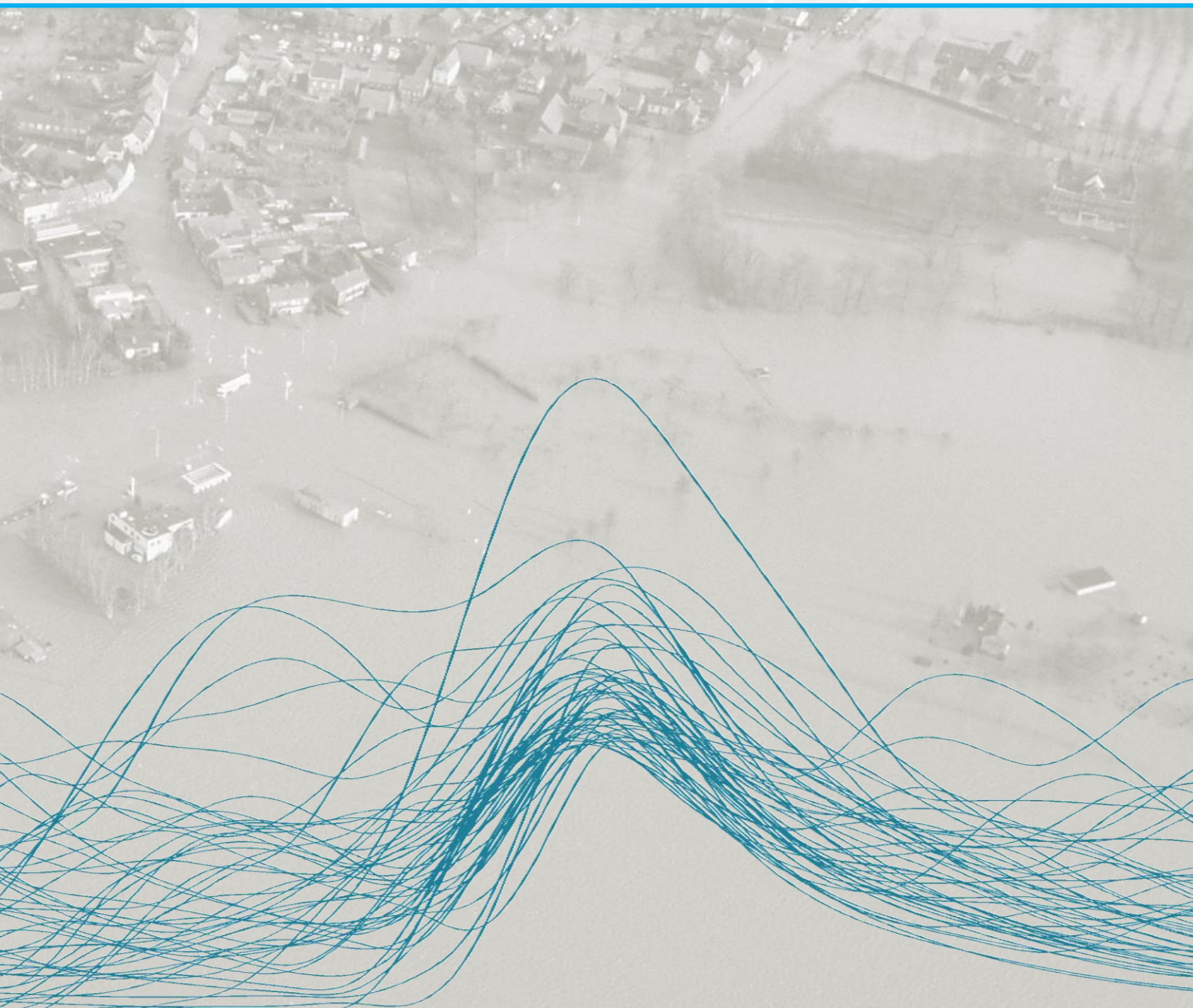


# Hydrograph shape variability on the river Meuse

Evaluation of design hydrograph methods and probabilistic methods  
to estimate design water levels on the river Meuse

**Master Thesis**

Joost Pol



Cover photo: Meuse flood of 1993. <https://beeldbank.rws.nl>, Rijkswaterstaat / Bart van Eyck

# Hydrograph shape variability on the river Meuse

Evaluation of design hydrograph methods and probabilistic methods  
to estimate design water levels on the river Meuse

## Master Thesis

### Delft University of Technology

4 November 2014

**Student:** J.C. Pol  
**E-mail:** joost.pol@gmail.com

#### Graduation committee:

prof.dr.ir. M. Kok	Delft University of Technology <i>Department of Hydraulic Engineering</i>
ir. H.J. Barneveld	HKV Consultants <i>Department Rivers and Coasts</i>
dr. O. Morales Nápoles	Delft University of Technology <i>Department of Hydraulic Engineering</i>
dr.ir. E. Mosselman	Delft University of Technology <i>Department of Hydraulic Engineering</i>
dr. R.M.J. Schielen	Ministry of Infrastructure and the Environment <i>Rijkswaterstaat WVL / Deltaprogramma Rivieren</i>

## Preface

With this Master Thesis I will finalize my Master programme in Hydraulic Engineering at Delft University of Technology. It is the result of a period of intensive work and study on the probability of floods on the river Meuse. I would like to thank all the people who have helped me to achieve the present result. First of all the graduation committee; Matthijs Kok for chairing the committee and his motivation during the process, Hermjan Barneveld for his coaching of the process and the discussions about the results, Oswaldo Morales Napoles for sharing his ideas on multivariate statistics, Erik Mosselman for his detailed comments on the reports, and Ralph Schielen for reflecting on the application in practice. I also want to thank Chris Geerse for sharing his thoughts on the probabilistic methods, and Mark Hegnauer for discussing the results with respect to GRADE. Finally I would like to thank my wife Mieke, my parents and everyone around me for their support during my study and graduation.

Delft, November 2014

Joost Pol

## Executive summary

### Introduction

Design water levels are a basic concept in flood risk management practice. These water levels with a specified return period are used for the design of dikes and other flood protection measures. Design hydrographs are used to determine these design water levels. A hydrograph is the description of the discharge of a flood wave over time. In addition to the peak discharge, the hydrograph shape affects the downstream water levels. The design water levels in their turn have considerable impact on the costs of flood protection measures. Therefore it is important that the hydrograph shape is represented correctly in the computation of the design water levels. The aim of this thesis is to investigate the influence of hydrograph shape on design water levels on the river Meuse, and to evaluate current and alternative methods to take this shape into account.

Different methods are available to determine the design water level (or the equivalent water level frequency curve) at some location along the river. The standard hydrograph method is currently used in The Netherlands to construct an average hydrograph shape based on all floods in the measured time series (100 year) at the upstream gauging station Borgharen. Recently, very long discharge time series (50,000 year) have been generated within the GRADE project, using rainfall resampling and a hydrological model of the Meuse basin. Due to its size, this GRADE discharge dataset allows to establish a reference set with hydrodynamic simulation of all floods in this dataset and evaluate the estimates of alternative methods. The evaluated methods are: the standard design hydrograph, the recently proposed vertically averaged design hydrograph and two probabilistic methods. Figure 0-3 shows the results of the methods for location Mook, 150 km downstream of Borgharen.

### Design hydrograph methods

The first step was to determine the reference set by simulation of all selected GRADE hydrographs (17,232 in total) with the 1D hydrodynamic model SOBEK. At each location along the river Meuse, a reference water level frequency curve was derived from these simulations (blue line in Figure 0-3). The second step was to investigate how the change from the measured dataset to the GRADE dataset affects the design water levels from the standard method. In Figure 0-3, this is marked by the change from \* to °.

The *standard hydrograph* method was improved by a modified selection interval. Normally, the standard hydrograph shape is the average shape of all GRADE hydrographs with a peak discharge between 1750 and 3200 m<sup>3</sup>/s, and this shape is applied to all peak discharges. Now, the selection interval was narrowed to the region around the peak discharge of interest. For example the 4400 m<sup>3</sup>/s standard hydrograph gets a shape that is the average of the GRADE hydrographs with a peak discharge between 4000 and 4600 m<sup>3</sup>/s. Simulation of these modified standard hydrographs with SOBEK results in design water levels marked by ° in Figure 0-3.

*Vertical averaging* is an alternative design hydrograph method, in which the discharge at each time step is averaged instead of the duration at each discharge level. This leads to a narrower design hydrograph (Figure 0-1). Simulation of these vertically averaged design hydrographs in SOBEK results in design water levels marked by ● in Figure 0-3 (and ● for the modified interval).

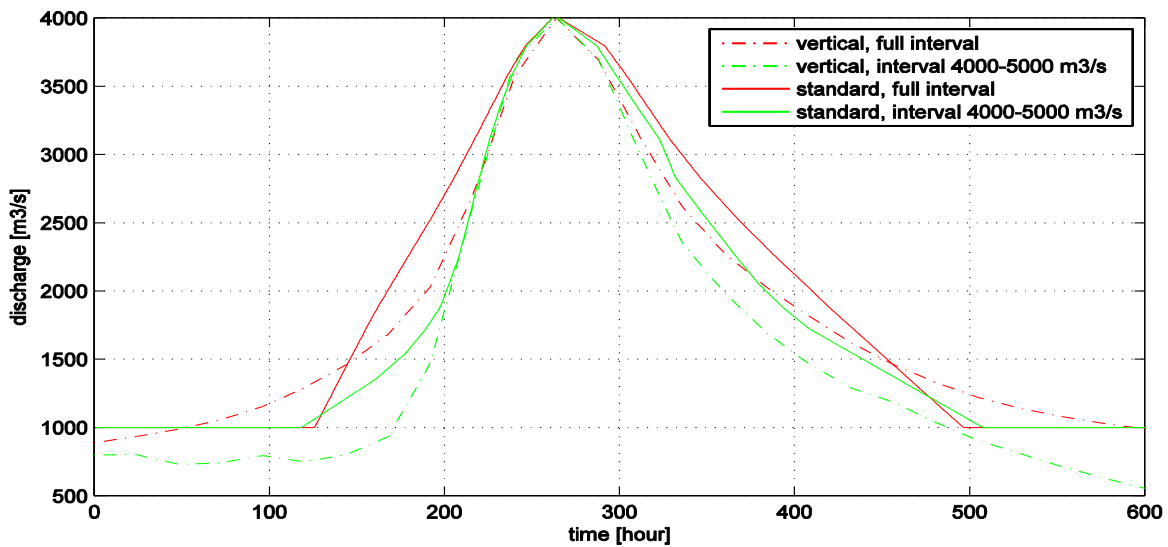


Figure 0-1 Standard and vertical design hydrographs, with full interval and modified interval

**Probabilistic methods**

The two probabilistic methods do not use design hydrographs, but combine statistics about hydrograph shapes at Borgharen with a transformation function that relates the downstream water levels to the hydrograph shape. A statistical analysis showed that in addition to the peak discharge ( $Q_p$ ), the peak curvature ( $C_2$ ) is a good predictor of downstream water levels.

The *explicit probabilistic* method derives the water level exceedance frequency for any water level by searching for the combinations of  $Q_p$  and  $C_2$  that lead to this downstream water level (red line in Figure 0-2). These combinations were found with the transformation function. The fraction of the points that is at the right side of the red line determines the exceedance probability (and so the return period) of this water level. Repeating this for a range of water levels yields the water level frequency curve (dashed line in Figure 0-3).

The *implicit probabilistic* method does not use the distributions of  $Q_p$  and  $C_2$  directly. With the transformation function, a downstream water level is estimated for each GRADE hydrograph at Borgharen (Figure 0-2 right). These estimated water levels are used to construct an estimated water level frequency curve (solid black line in Figure 0-3)

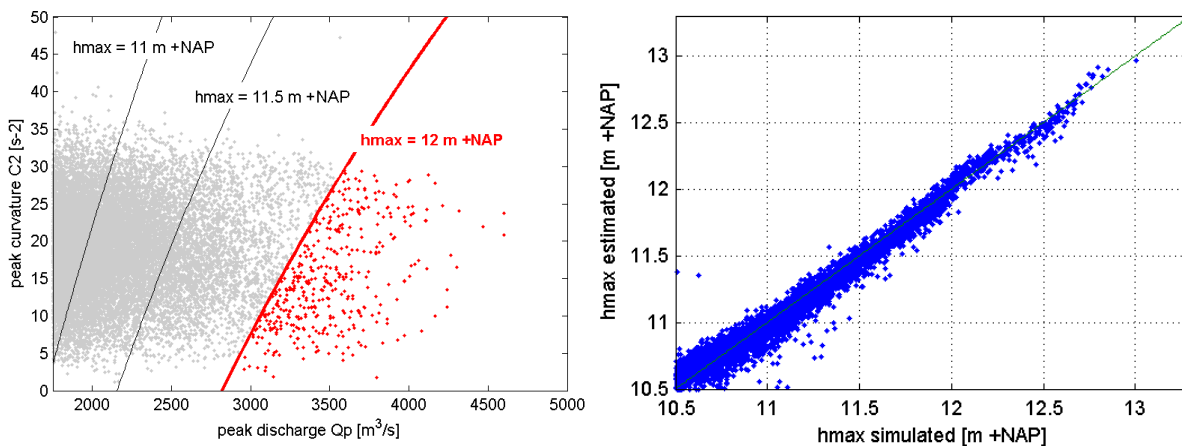


Figure 0-2 Illustration of explicit (left) and implicit (right) probabilistic methods

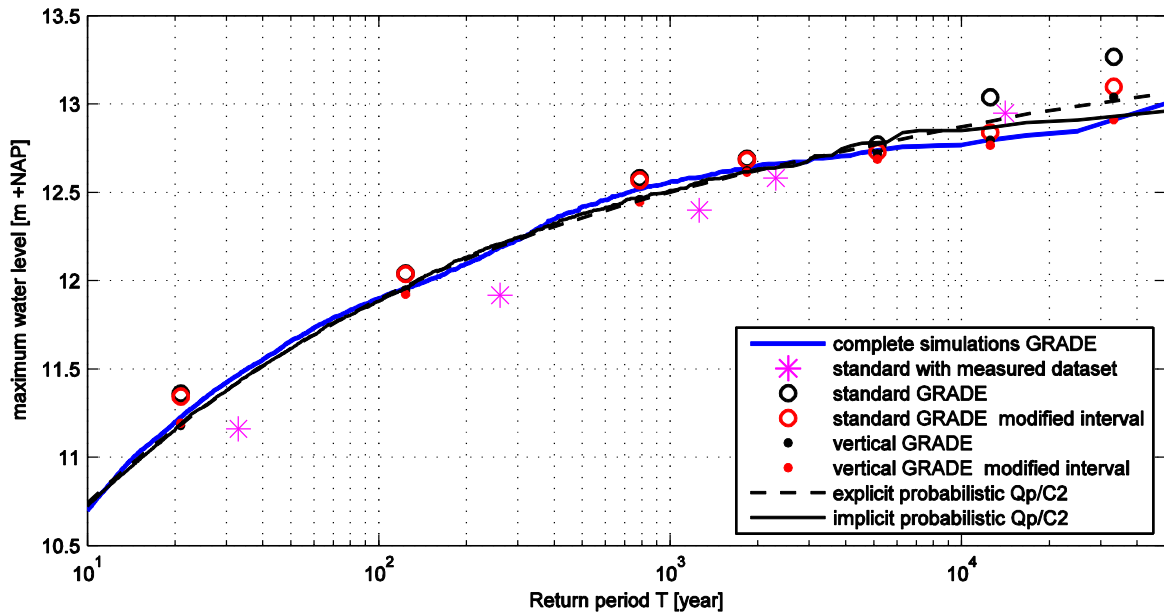


Figure 0-3 Design water levels in the different methods at Mook

### Main results

It was found that the standard hydrograph method overestimates the design water levels up to 37 cm, depending on location and return period. This was improved by a modified selection interval, but an overestimation of the design water level up to 19 cm remains. The vertically averaged hydrograph gives a more accurate estimate, with an underestimation of the design water levels up to 7 cm. The two probabilistic methods which have been applied give accurate estimates of the design water level, but do not improve the estimate of vertical averaging .

Besides the ability to estimate design water levels, the design hydrograph methods and probabilistic methods were evaluated on the ability to estimate the effect of a retention basin on the design water levels. In case of retention basin Lob van Gennep, the estimation based on the vertical hydrograph was generally closest to the reference. Besides the 1D SOBEM simulations, some extra simulations were carried out with the 2D model WAQUA to determine the transformation function for the probabilistic methods and the effect of a retention basin in WAQUA. However, these results cannot be evaluated directly because no reference set is available for WAQUA.

### Concluding remarks

The current method significantly overestimates the design water levels, meaning that more accurate methods lead to a significant reduction in the design water levels in large parts of the Meuse, which can lead to a reduction in the costs of flood protection measures. These findings suggest that the more simple design hydrograph methods (in particular vertically averaged) based on GRADE, can give an accurate estimate of the design water levels on the river Meuse, provided that the peak discharge distribution has a good fit in the extreme tail and that the selection interval is narrowed. These conditions could only be observed because GRADE was used, which implies that the use of GRADE is essential for a reliable estimation of the design water levels. The probabilistic methods are potentially valuable in case of large retention basins, but its application requires a good understanding of probabilistic concepts and the river system.

## Samenvatting

### Inleiding

Ontwerpwaterstanden zijn een belangrijk begrip in het hoogwaterbeheer. Deze waterstanden met een bepaalde herhalingstijd worden gebruikt voor het ontwerp van dijken en andere hoogwaterbeschermingsmaatregelen. Ontwerpafvoergolven worden gebruikt om deze ontwerpwaterstanden vast te stellen. Een afvoergolf of hydrograaf beschrijft het verloop van de rivierafvoer in de tijd. Naast de piekafvoer heeft ook de golfvorm een sterke invloed op de benedenstroomse waterstanden. De ontwerpwaterstanden hebben op hun beurt weer een grote impact op de kosten van hoogwaterbescherming. Daarom is het van belang dat de golfvorm op een goede manier wordt meegenomen in de bepaling van de ontwerpwaterstanden. Het doel van dit afstudeeronderzoek is om de invloed van de golfvorm op de ontwerpwaterstanden te onderzoeken, en om de nauwkeurigheid van bestaande en alternatieve methodes te evalueren.

Er zijn verschillende methoden beschikbaar om de ontwerpwaterstanden (of de equivalente waterstandsfrequentielijn) mee te bepalen. De standaardafvoergolf methode wordt momenteel in Nederland gebruikt om een gemiddelde golfvorm te bepalen, op basis van alle hoogwaters in de gemeten afvoer tijdreeks (100 jaar) bij Borgharen. Onlangs zijn in het GRADE project zeer lange afvoerreksen (50.000 jaar) gegenereerd, door gebruik te maken van resampling en een neerslag-afvoermodeel van het Maasstroomgebied. Vanwege deze grote lengte is het mogelijk om met deze dataset een referentie te bepalen die bestaat uit hydrodynamische simulatie van alle hoogwaters in de dataset, en alternatieve methodes hiermee te vergelijken. De onderzochte methodes zijn: de standaardafvoergolf, de verticaal gemiddelde afvoergolf en twee probabilistische methodes. Onderstaande paragrafen laten zien welke stappen zijn genomen. Figure 0-6 geeft de belangrijkste resultaten voor de locatie Mook, 150 km benedenstrooms van Borgharen.

### Ontwerpafvoergolven

De eerste stap bestond uit het bepalen van de referentie set door simulatie van alle hoogwaters uit GRADE (17.232) met het SOBEK model. Op basis van deze simulaties kan voor elke locatie een waterstandsfrequentielijn worden afgeleid (blauwe lijn in Figure 0-6). Verder is onderzocht welk effect het gebruik van GRADE heeft op de ontwerpwaterstanden van de standaardmethode, ten opzichte van de gemeten dataset. In Figure 0-6 is dit gemarkeerd met verschuiving van \* naar °.

De *standaardmethode* is verbeterd door een aangepast selectie interval. Normaalgesproken is de standaardgolf de gemiddelde golfvorm van alle hoogwaters met een piekafvoer tussen de 1750 en 3200 m<sup>3</sup>/s, en wordt deze vorm toegepast op alle piekafvoeren. Nu is het selectie interval versmald tot het gebied rond de gewenste piekafvoer. De golfvorm van bijvoorbeeld de 4400 m<sup>3</sup>/s standaardafvoergolf wordt bepaald uit middeling van de GRADE afvoergolven met een piekafvoer tussen de 4000 en 4600 m<sup>3</sup>/s. Simulatie van deze afvoergolven met SOBEK leidt tot de ontwerpwaterstanden gemarkeerd met ° in Figure 0-6.

*Verticaal middelen* is een alternatieve methode om een ontwerpafvoergolf te bepalen, waarbij de afvoer op ieder tijdstip wordt gemiddeld in plaats van de duur op ieder afvoerniveau. Deze methode leidt tot een smallere afvoergolf (Figure 0-4). Simulatie van deze golven in SOBEK leidt tot ontwerpwaterstanden gemarkeerd met ● in Figure 0-6 (● met aangepast selectie interval).

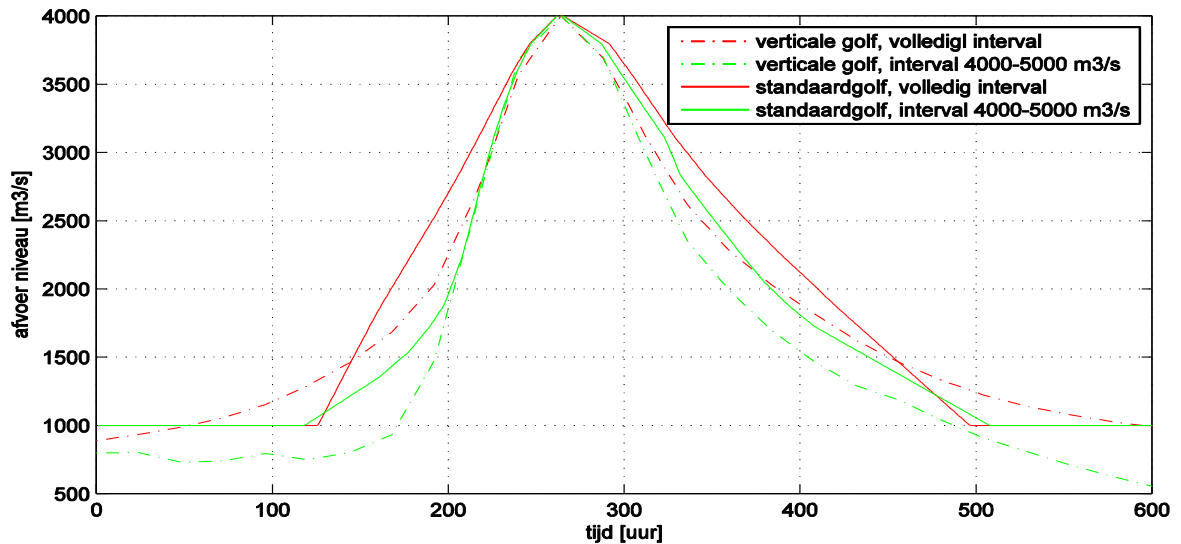


Figure 0-4 Standaard en verticaal gemiddelde ontwerpafvoergolven, incl. aangepast interval.

### Probabilistische methodes

De twee probabilistische methodes gebruiken geen ontwerpafvoergolven, maar combineren statistiek over de golfvorm bij Borgharen met een transformatiefunctie die de lokale waterstanden relateert aan de golfvorm. Een statistische analyse laat zien dat naast de piekafvoer ( $Q_p$ ), de piekkromming ( $C_2$ ) een goede voorspeller is voor de benedenstroomse waterstanden.

De *expliciete probabilistische methode* bepaalt de overschrijdingsfrequentie van een waterstand door te zoeken naar combinaties van  $Q_p$  en  $C_2$  die tot deze benedenstroomse waterstand leiden (rode lijn in Figure 0-5). Deze combinaties worden gevonden met de transformatiefunctie. Het deel van de punten dat rechts van de rode lijn ligt bepaalt de overschrijdingskans (en dus de herhalings-tijd) van deze waterstand. De frequentielijn ontstaat door deze procedure te herhalen voor een reeks waterstanden (gestreepte lijn in Figure 0-6).

De *impliciete probabilistische methode* gebruikt de kansverdelingen van  $Q_p$  en  $C_2$  niet direct. Met behulp van de transformatiefunctie wordt voor iedere GRADE afvoergolf bij Borgharen een benedenstroomse waterstand geschat (Figure 0-2 rechts). Deze geschatte waterstanden worden gebruikt om een geschatte waterstandsfrequentielijn te bepalen (zwarte lijn in Figure 0-3).

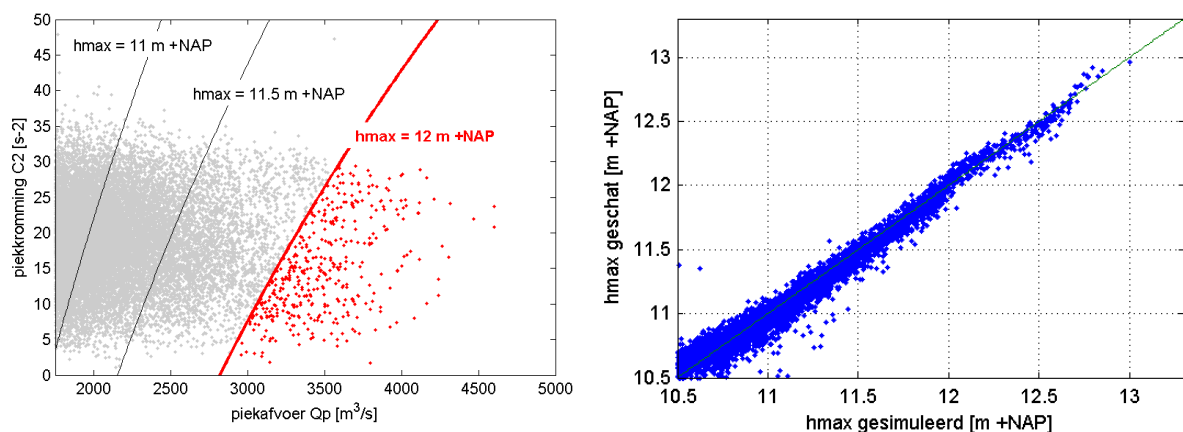


Figure 0-5 Illustratie van de expliciete (links) en impliciete (rechts) probabilistische methode

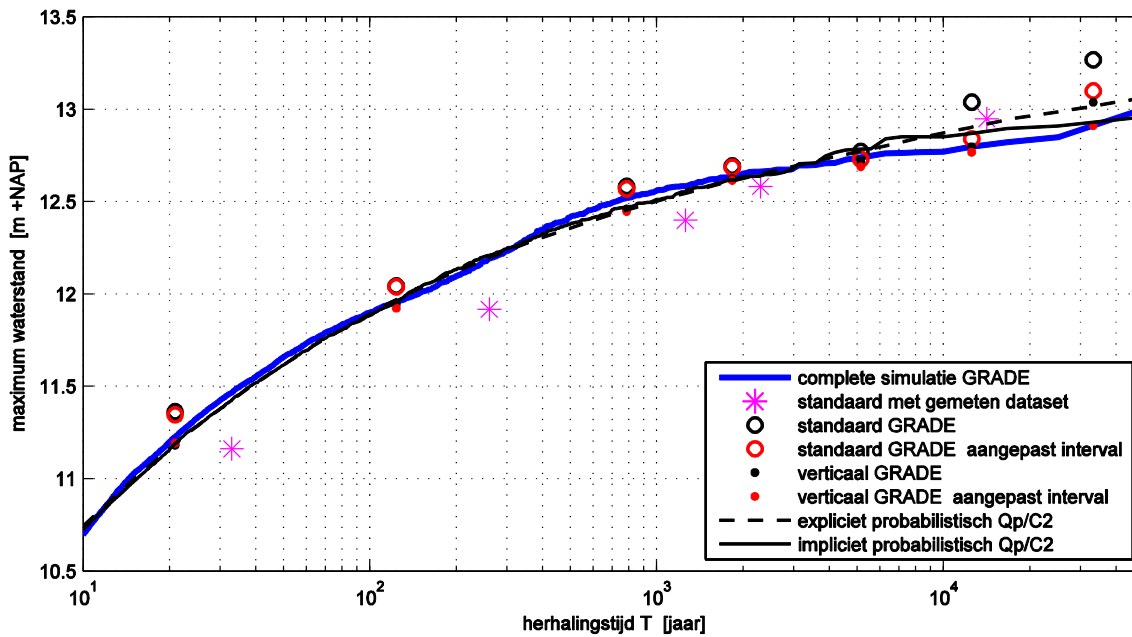


Figure 0-6 Ontwerpwaterstanden in de verschillende methodes, locatie Mook

### Belangrijkste resultaten

De standaardmethode blijkt de ontwerpwaterstanden tot 37 cm te overschatten, afhankelijk van locatie en herhalingsperiode. Dit is verbeterd door het aangepaste selectie interval, maar ook dan blijft een overschatting van 19 cm aanwezig. De verticaal gemiddelde golf geeft een nauwkeuriger schatting, en onderschatten tot 7 cm. De twee probabilistische methodes die zijn toegepast geven ook een nauwkeurige schatting, maar verbeteren de schatting van verticaal middelen niet.

Naast het vermogen om de ontwerpwaterstanden te schatten, zijn de methodes onderzocht op het vermogen om het effect van een retentiegebied op de ontwerpwaterstanden te schatten. In het geval van retentiegebied Lob van Gennep ligt de schatting van de verticaal gemiddelde golf in het algemeen het dichtst bij de referentie. Naast simulaties met SOBEK zijn er WAQUA simulaties uitgevoerd om de transformatiefunctie en het effect van retentie te bepalen. Deze resultaten kunnen echter niet direct worden geëvalueerd omdat in WAQUA geen referentie beschikbaar is.

### Conclusies

De huidige methode geeft een significante overschatting van de ontwerpwaterstanden, dus een nauwkeuriger methode leidt tot een significante verlaging van de ontwerpwaterstanden in de Maas, wat kan leiden tot een reductie in de kosten van hoogwaterbescherming. Deze resultaten suggereren dat de eenvoudigere ontwerpafvoergolf gebaseerd op GRADE (met name de verticaal gemiddelde) een goede benadering geeft van de ontwerpwaterstanden in de Maas, op voorwaarde dat de piekafvoer verdeling een goede fit in het extreme bereik heeft en dat het selectie interval voor hoge afvoeren wordt versmald. Zonder gebruik te maken van GRADE zou het belang hiervan niet zijn opgemerkt, wat impliceert dat het gebruik van GRADE essentieel is voor een betrouwbare schatting van de ontwerpwaterstanden. De probabilistische methodes zijn potentieel waardevol, met name in het geval van grote retentiegebieden, maar de toepassing ervan vraagt goede kennis van het riviersysteem en van probabilistische concepten.

# Table of Contents

Preface .....	2
Executive summary .....	3
Samenvatting .....	6
Table of Contents .....	9
List of Figures .....	13
List of Tables .....	14
List of Symbols .....	16
<b>1 Introduction .....</b>	<b>17</b>
1.1 The relevance of hydrograph shape .....	17
1.2 Problem description .....	18
1.3 Objective and research questions .....	19
1.4 Definitions of key concepts .....	20
1.5 Report structure .....	20
<b>2 The context .....</b>	<b>21</b>
2.1 The Meuse River Basin .....	21
2.1.1 Topographical overview .....	21
2.1.2 Discharge regime .....	23
2.1.3 Developments in flood protection in the Limburg Meuse .....	24
2.1.4 Strategies for the Limburg Meuse .....	25
2.2 The flood risk framework .....	25
2.2.1 The definition of flood risk .....	26
2.2.2 The failure probability of flood defences .....	27
2.2.3 The consequences of failure of a flood defence .....	29
2.2.4 Actual flood risk along the river Meuse .....	29
2.2.5 Importance of local load parameters for failure mechanisms .....	29
2.3 Current method of determining the design hydrograph .....	30
2.3.1 Design peak discharge .....	30
2.3.2 Design hydrograph shape .....	32
2.3.3 Limitations of the current method .....	33
2.3.4 Alternative methods to determine design hydrographs .....	35
2.4 The GRADE project .....	35
2.4.1 Stochastic weather generator .....	36
2.4.2 Hydrological and hydraulic modelling .....	36
2.4.3 Applicability and limitations .....	37
2.5 Peak attenuation .....	37
<b>3 Methods .....</b>	<b>38</b>
3.1 Research framework .....	38
3.2 Data .....	41
3.2.1 Measured discharge data .....	41
3.2.2 Simulated GRADE discharge data .....	41
3.3 Hydrograph selection .....	41

3.3.1	Selection for standard design hydrographs.....	42
3.3.2	Selection for vertically averaged design hydrographs.....	42
3.3.3	Modified selection for design hydrographs .....	42
3.3.4	Selection for probabilistic methods .....	43
3.4	Hydrodynamic simulations .....	43
3.4.1	Common input of SOBEK and WAQUA.....	43
3.4.2	SOBEK Meuse .....	45
3.4.3	WAQUA Meuse .....	46
3.5	Statistical analysis .....	47
3.5.1	Calculation of shape variables from selected flood wave .....	47
3.5.2	Selection of relevant hydrograph shape variables .....	49
3.5.3	Univariate distributions of shape variables.....	50
3.6	Probabilistic analysis.....	51
3.6.1	Local water level estimation based on shape variables .....	52
3.6.2	Explicit probabilistic method.....	53
3.6.3	Implicit probabilistic method .....	54
<b>4</b>	<b>Results.....</b>	<b>55</b>
4.1	Effect of using GRADE discharge data.....	55
4.2	Effects of hydrograph shape variables on local water levels .....	58
4.2.1	Correlation analysis of shape variables and water levels.....	58
4.2.2	Synthetic hydrographs: Base flow .....	61
4.3	Statistics of shape variables at Borgharen .....	62
4.3.1	Univariate probability distributions .....	62
4.3.2	Correlation structure.....	64
4.4	Design water levels based on 1D Simulations.....	64
4.4.1	Local water level distributions .....	64
4.4.2	Based on local discharge distribution and stage-discharge curve .....	65
4.4.3	Return period with plotting positions .....	66
4.4.4	Sensitivity for the number of simulations .....	67
4.4.5	Water levels based on 2D simulations .....	68
4.5	Design water levels based on design hydrograph methods .....	70
4.5.1	Standard and vertically averaged hydrographs.....	70
4.5.2	Comparison of the two design hydrograph methods with 1D simulation results.....	71
4.5.3	The impact of the selection interval.....	72
4.6	Design water levels based on a probabilistic approach .....	74
4.6.1	Transformation functions.....	74
4.6.2	Explicit probabilistic method.....	76
4.6.3	Implicit probabilistic method .....	77
4.6.4	Water level frequency curves for the probabilistic methods .....	78
4.6.5	Probabilistic methods based on WAQUA .....	78
4.7	Retention effects .....	79
4.7.1	Effect of Lob van Gennep in SOBEK.....	79
4.7.2	Effect of Lob van Gennep in WAQUA .....	82
4.7.3	Influence of shape variables on retention effect .....	83
4.7.4	Meuse system without retention basins .....	85
<b>5</b>	<b>Discussion.....</b>	<b>86</b>
5.1	Switching from measured data to GRADE data .....	86
5.2	The influence of hydrograph shape variables .....	87

---

5.3	Design hydrograph approaches .....	88
5.4	Application of probabilistic approaches.....	89
5.5	Effect of retention basins .....	90
5.6	Which method to use for the estimation of water level frequencies? .....	91
5.7	Recommendations .....	93
<b>6</b>	<b>Conclusions .....</b>	<b>94</b>
	<b>References .....</b>	<b>97</b>
	<b>Appendices.....</b>	<b>101</b>
	<b>Appendix A. Overview of programs and scripts .....</b>	<b>103</b>
	<b>Appendix B. SOBEK and WAQUA Meuse .....</b>	<b>109</b>
	<b>Appendix C. Probabilistic formulas .....</b>	<b>115</b>
	<b>Appendix D. Statistics of shape variables .....</b>	<b>119</b>
	<b>Appendix E. Results of complete simulations in SOBEK .....</b>	<b>129</b>
	<b>Appendix F. Results of design hydrograph methods .....</b>	<b>135</b>
	<b>Appendix G. Results of probabilistic methods .....</b>	<b>143</b>
	<b>Appendix H. Results of effect of retention basins.....</b>	<b>153</b>



## List of Figures

Figure 0-1 Standard and vertical design hydrographs, with full interval and modified interval .....	4
Figure 0-2 Illustration of explicit and implicit probabilistic methods.....	4
Figure 0-3 Design water levels in the different methods at Mook .....	5
Figure 0-4 Standaard en verticaal gemiddelde ontwerpafvoergolven, incl. aangepast interval.....	7
Figure 0-5 Illustratie van de expliciete en impliciete probabilistische methode.....	7
Figure 0-6 Ontwerpwaterstanden in de verschillende methodes, locatie Mook.....	8
Figure 0-1 Standard and vertical design hydrographs, with full interval and modified interval .....	4
Figure 0-2 Illustration of explicit and implicit probabilistic methods.....	4
Figure 0-3 Design water levels in the different methods at Mook .....	5
Figure 0-4 Standaard en verticaal gemiddelde ontwerpafvoergolven, incl. aangepast interval.....	7
Figure 0-5 Illustratie van de expliciete en impliciete probabilistische methode.....	7
Figure 0-6 Ontwerpwaterstanden in de verschillende methodes, locatie Mook.....	8
Figure 1-1 Hydrographs of the 1993 and 1995 floods at locations Borgharen and Lith.....	17
Figure 2-1 Topography of the Meuse River Basin .....	22
Figure 2-2 Precipitation, evaporation and discharge regime of the Meuse.....	23
Figure 2-3 Failure mechanisms of dikes.....	27
Figure 2-4 Example of fragility curves.....	28
Figure 2-5 Illustration of AM and POT methods. ....	31
Figure 2-6 Design discharge curve 2011 .....	32
Figure 2-7 Illustration of standard hydrograph method .....	33
Figure 2-8 Uncertainty in design discharge curve .....	34
Figure 2-9 Schematic representation of GRADE method.....	35
Figure 2-10 Nearest neighbour resampling .....	36
Figure 3-1 General outline of the research framework .....	38
Figure 3-2 Peak attenuation Eijsden-Borgharen as function of peak discharge Borgharen.....	44
Figure 3-3 Main output locations of hydrodynamic models .....	46
Figure 3-4 Definition of hydrograph shape variables.....	48
Figure 3-5 Pearson and Spearman correlation coefficients of non-linear relations .....	49
Figure 3-6 3D scatterplot of $h_{max}$ , $Q_p$ and $V_{1250}$ .....	50
Figure 3-7 Illustration of Kernel distribution.....	51
Figure 3-8 Illustration of the explicit probabilistic method.....	53
Figure 4-1 Standard hydrographs from GRADE and measured datasets .....	55
Figure 4-2 Water level difference between hydrographs based on GRADE and measured dataset.....	56
Figure 4-3 Peak discharge return periods, GRADE vs. measured.....	57
Figure 4-4 Water level return periods, GRADE vs Measured (T according to GPD) .....	57
Figure 4-5 Water level return periods, GRADE vs Measured (T according to Kernel).....	58
Figure 4-6 Conditional plots of $h_{max}$ versus $D_{85\%}$ , $V_{85\%}$ and $C_2$ .....	60
Figure 4-7 Synthetic hydrographs with different base flow .....	61
Figure 4-8 Downstream water levels for hydrographs with different base flow .....	61
Figure 4-9 Probability distribution fit of peak discharge $Q_p$ .....	62
Figure 4-10 Generalized Pareto and Kernel fit on logarithmic scale .....	63
Figure 4-11 Probability distribution fit of $C_2$ .....	63
Figure 4-12 scatterplot and rank scatterplot of $Q_p$ and $C_2$ .....	64
Figure 4-13 Distribution of water levels at Mook, and best parametric fit.....	65
Figure 4-14 Distribution of local peak discharge at Mook .....	65
Figure 4-15 Stage-discharge curve at Mook .....	66
Figure 4-16 Return periods of water levels at Mook .....	67
Figure 4-17 Sensitivity of water level return periods for the number of hydrographs used.....	68
Figure 4-18 Difference between WAQUA and SOBEK maximum water levels, for five locations.....	69
Figure 4-19 Differences between WAQUA and SOBEK results as function of $Q_p$ .....	69

Figure 4-20 Standard and vertically averaged hydrographs .....	70
Figure 4-21 Design water levels of the two design hydrograph methods at Mook .....	71
Figure 4-22 Standard and vertical hydrographs for different selection thresholds .....	72
Figure 4-23 Design water levels at Mook with modified selection interval .....	73
Figure 4-24 Polynomial surface fit with all 17,232 SOBEM results .....	75
Figure 4-25 Polynomial surface fit with 25 SOBEM and WAQUA results .....	75
Figure 4-26 Water level return periods at Mook in the explicit probabilistic approach .....	76
Figure 4-27 $h_{\max, \text{Mook}}$ versus $h_{\max, \text{Mook, est}}$ Borgharen and Mook .....	77
Figure 4-28 Results of the two probabilistic methods at Mook (with Kernel) .....	78
Figure 4-29 Design hydrograph- and probabilistic methods in SOBEM and WAQUA, at Mook .....	79
Figure 4-30 Effect of Lob van Gennep on $h_{\max, \text{Mook}}$ and histogram of this effect .....	80
Figure 4-31 Influence of Lob van Gennep on the hydrograph before and after .....	80
Figure 4-32 Return periods at Mook with and without retention Lob van Gennep (kernel) .....	81
Figure 4-33 Differences between WAQUA and SOBEM effects at Mook .....	82
Figure 4-34 Return periods at Mook, based on WAQUA, incl. and excl. Lob van Gennep .....	82
Figure 4-35 Relation between retention effect at Mook and shape variables .....	83
Figure 4-36 Dependence of retention effect at Mook on $C_2$ .....	84
Figure 4-37 Water level return periods based on system without any retention basins (Kernel) .....	85

## List of Tables

Table 1-1 Peak attenuation of 1993 and 1995 flood waves.....	17
Table 2-1 Importance of local load parameters for failure mechanisms. ....	29
Table 3-1 Overview of methods to determine design water levels .....	40
Table 3-2 Modified selection intervals of standard and vertically averaged hydrographs .....	42
Table 3-3 Output locations for hydrodynamic simulations.....	45
Table 3-4 Analysed hydrograph shape variables.....	47
Table 3-5 Numbers of selected hydrographs for the probabilistic approach with $C_2$ .....	52
Table 4-1 Design water levels from GRADE and measured datasets. ....	56
Table 4-2 Spearman rank correlation between local water levels and shape variables .....	58
Table 4-3 mean conditional rank correlations $\rho_{h_{\max, \text{var}}   Q_p}$ (Spearman) .....	59
Table 4-4 Peak discharge return periods at Borgharen .....	63
Table 4-5 Spearman rank correlations between $Q_p$ , $V_{1250}$ , $D_{85\%}$ and $C_2$ .....	64
Table 4-6 Results of approach with stage-discharge relationship .....	66
Table 4-7 Modified selection intervals of standard and vertically averaged hydrographs .....	73
Table 4-8 Coefficients for $h_{\max, \text{Mook}}$ as function of $Q_p$ and $C_2$ .....	75
Table 4-9 Retention effect ( $\Delta$ ) at Mook for different $Q_p$ .....	81
Table 4-10 Rank correlation coefficients between retention effect at Mook and shape variables .....	84
Table 4-11 Effect ( $\Delta$ ) of all retention basins at Mook for different $Q_p$ .....	85
Table 5-1 Comparison of the different methods for SOBEK model including retention .....	92

## List of Symbols

Symbol	Explanation	Unit
$Q$	discharge	$\text{m}^3/\text{s}$
$Q_p$	peak discharge at Borgharen	$\text{m}^3/\text{s}$
$Q_{p,x}$	peak discharge at location $x$ along the river	$\text{m}^3/\text{s}$
$Q_{p,d}$	design peak discharge at Borgharen	$\text{m}^3/\text{s}$
$Q_{\text{base}}$	base discharge at Borgharen	$\text{m}^3/\text{s}$
$V_L$	volume above level $L$	$\text{m}^3$
$D_L$	duration at level $L$	hour
$RV_L$	relative volume / shape factor above level $L$	-
$C$	peak curvature of the hydrograph	$\text{s}^{-2}$
$B_s$	storage width	$\text{m}$
$s$	bottom slope	-
$z_s$	crest level of weir	$\text{m} + \text{NAP}$
$x$	location along the river	$\text{km}$
$h$	water level	$\text{m} + \text{NAP}$
$h_{\text{max},x}$	maximum water level at location $x$ along the river	$\text{m} + \text{NAP}$
$\Delta$	retention effect	$\text{cm}$
$R$	risk of flooding	$\text{€}/\text{year}$
$K$	consequences of flooding	$\text{€}$
$P(\cdot)$	probability	-
$T$	return period	year
$\lambda$	rate of flood occurrence	$1/\text{year}$
$\rho$	plotting position	-
$\rho_{X,Y}$	correlation between variables $X$ and $Y$	-
$\rho_{X,Y Z}$	conditional correlation between $X$ and $Y$ , given $Z$	-

# 1 Introduction

## 1.1 The relevance of hydrograph shape

Design water levels are needed for the design of flood defences along the rivers in The Netherlands. These design water levels are determined by estimating the yearly probability that the design water level at that location is exceeded. Since local water levels are not only affected by the magnitude of the flood peak but also by the flood wave shape, this shape needs to be taken into account for a reliable estimate. An illustration of this influence is given by two historical flood waves (1993 and 1995) in the Meuse that have a similar magnitude but a different shape (Figure 1-1). The flood of 1993 has a larger peak discharge  $Q_p$ , but results in lower water levels  $h_{max}$  at the downstream location Grave (Table 1-1). One of the reasons for this difference is the difference in hydrograph shape.

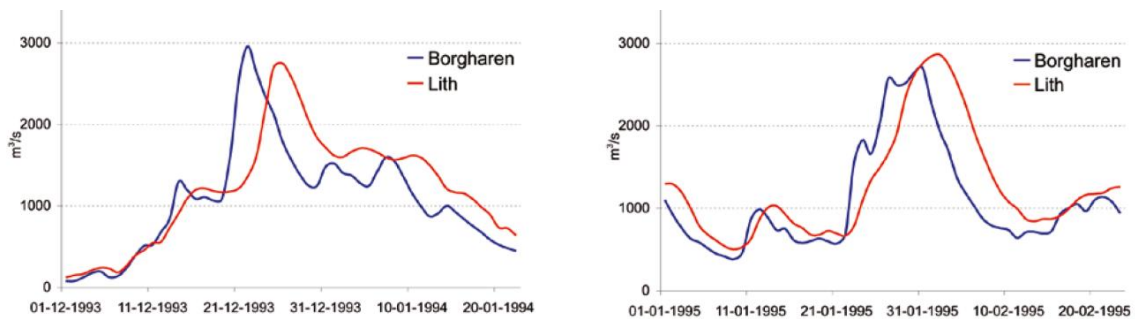


**Figure 1-1 Hydrographs of the 1993 and 1995 floods at locations Borgharen and Lith (De Wit & Buishand, 2007)**

Year	$Q_p$ Borgharen	$H_{max}$ Borgharen	$H_{max}$ Grave	Travel time
1993	2959 m <sup>3</sup> /s	+45.90 m NAP	+10.39 m NAP	81 h
1995	2702 m <sup>3</sup> /s	+45.72 m NAP	+10.58 m NAP	48 h

**Table 1-1 Peak attenuation of 1993 and 1995 flood waves (live.waterbase.nl, 24-03-2014)**

The main topic of this thesis is the manner in which these shapes are taken into account in the computation of the design water levels, and how this manner affects the design water levels. Traditionally, the design water level is determined with a hydrodynamic model simulation of one design hydrograph, which peak discharge is determined by frequency analysis and which shape is determined by averaging all flood hydrographs in the discharge record. The performance of this current method is compared to other, more advanced methods.

The effect of hydrograph shape on water levels is of great importance to the flood risk management of the Meuse river system. The current standard hydrograph method is the basis on which flood risk strategies are developed, decisions are taken and flood defences are designed. If alternative methods give a better estimation of the design water levels, this may have considerable impact on decision making. For example, a difference of 10 cm in the design water levels along the river would make a large difference in the need and costs of strengthening flood defences. Many flood risk mitigation measures, such as retention basins, are optimized for the

design hydrograph. These mitigation measures may be less effective for floods that deviate from this design hydrograph. A recent example of such measures is the strategy for the Meuse river system in the Delta programme Rivers (Berkhof, Meijer & Leushuis, 2013). An important aspect in that discussion is the safety level for the dike ring areas in Limburg, and whether they will act as retention basins during design floods, to protect downstream reaches (Meijer, 2013; ENW, 2014). In general, it is important to get a better understanding of the applicability of design hydrograph methods for the computation of design water levels. Its application to similar rivers all over the world may face the same limitations as in the case of the Meuse.

## 1.2 Problem description

The standard method to compute design water levels on the river Meuse using measured discharge series was developed for the committee Boertien (WL|Delft Hydraulics, 1993). It uses frequency analysis methods to determine a design peak discharge, and subsequently applies an averaged hydrograph shape to complete the design hydrograph (Klopstra & Vrisou van Eck, 1999). However, several researchers have pointed out that this method has fundamental limitations (Chbab, Buiteveld & Diermanse, 2006). Firstly, the derivation of the extreme design peak discharges does not directly take into account physical characteristics of the upstream or downstream river system, but it is only based on statistical extrapolation. Secondly, the historical record is short (100 years), compared to the return period of interest (1250 years and even higher). This gives considerable statistical uncertainty (Jansen, 2007). Thirdly, the assumption that the return period of a peak discharge at Borgharen equals the return period of the resulting maximum water level at any location downstream may not always be justified.

It has been suggested that the use of a rainfall simulator combined with a hydrological model (the GRADE project) can partially overcome these limitations (De Wit & Buishand, 2007). GRADE provides a very large dataset of simulated flood waves that may reduce the statistical uncertainty, takes physical characteristics into account, and allows a more extensive analysis of wave shape. This GRADE discharge dataset will be used in this thesis to compare the different methods. Some research has been carried out on differences between the GRADE discharge dataset and the measured discharge dataset (Kramer, Beckers & Weerts, 2008), also with regard to hydrograph shape (Barneveld & Van den Berg, 2010; Ogink, 2012). However, no research is known that investigates how the use of GRADE data affects the design water levels along the river Meuse, compared to the use of the 100 years of measured data.

The large GRADE dataset allows to determine the probability distributions of shape characteristics for a given peak discharge in a more accurate way than based on the measured dataset, e.g. in WL|Delft Hydraulics (1993) or Gerretsen (2009). This information on shape distributions in GRADE data is not yet included in the computation of design water levels. The (joint) effect of important hydrograph shape variables on the local water levels needs to be investigated.

Since GRADE provides much more (and more extreme) discharge data, this makes it possible to establish a reference set with hydrodynamic simulations of the complete GRADE dataset. Such a reference set based on the measured dataset is less useful because it contains too much

statistical uncertainty. In order to evaluate the accuracy of the estimation by the design hydrographs, it is needed to compare the design water levels of the standard hydrograph (Klopstra & Vrisou van Eck, 1999) and the vertically averaged hydrograph (Ogink, 2012) with the reference set.

When the influential shape variables are known, these can be taken into account in a probabilistic approach of hydrograph shape. Some research has been carried out on the probabilistic effect of flood duration, but only for measured discharge data and for a limited amount of durations (Geerse, 2013). His approach yields a design water level reduction in the order of 5-10 cm in large parts of the river Meuse. There is a need to improve this probabilistic approach and to compare the resulting design water levels to the reference set and the design hydrograph methods.

Recent studies that investigate the effect of flood risk mitigation measures use the standard hydrograph shape, or both a very wide and very narrow hydrograph to assess the sensitivity to hydrograph shape (Meijer, 2013; Van Putten & Hoefsloot, 2013). If there are differences in design water levels between the different methods, this may also affect the estimation of the effect of mitigation measures in terms of design water level reduction. A retention basin is used as an example of a mitigation measure since it is suggested that the effect of these basins is sensitive to the flood wave shape. The effect of a retention basin as estimated by the different methods needs to be compared to the effect determined by the reference set.

### 1.3 Objective and research questions

The objective of this thesis is *to investigate the influence of hydrograph shape on design water levels on the river Meuse and to compare the performance of different methods to determine these design water levels.*

The problems regarding the influence of hydrograph shape on design water levels as stated in section 1.2 were addressed by five research questions:

1. To what extent are design water levels affected by using GRADE simulated discharge data instead of measured discharge data?
2. Which hydrograph shape variables determine the downstream water levels, and how?
3. How accurate are the design water levels determined by design hydrograph methods?
4. How accurate are the design water levels determined by probabilistic methods?
5. How is the effect of a retention basin determined by hydrograph shape, and how accurately is this effect determined by the design hydrograph methods?

The following issues are beyond the scope of this thesis, though these are needed for a more complete analysis of the problem: the uncertainties in GRADE, the accuracy of the hydraulic models, a probabilistic contribution of Dutch tributaries, effects on other design conditions, effects on failure probability and risk of specific areas, and the optimization and control of retention basins.

## 1.4 Definitions of key concepts

A **flood** event is defined in the context of this thesis as the occurrence of a river discharge higher than  $1750 \text{ m}^3/\text{s}$ . A **flood wave** is the development of the discharge over time, around the moment of the flood event. A **hydrograph** is the description of the discharge of the flood wave as a function of time. So, flood wave refers to the physical event and hydrograph refers to the abstract description.

A **design hydrograph** is a hydrograph for which the peak discharge has a predefined return period or probability of exceedance, and for which the shape is determined by averaging all hydrographs in the dataset. Generally, the same hydrograph shape is applied to all peak discharges. Two averaging methods can be distinguished. The standard hydrograph is a design hydrograph that is derived according to the standard method, and is used in current practice. The vertically averaged hydrograph is a design hydrograph derived according to an alternative averaging method.

The **design water level** is the water level corresponding to a predefined return period or probability of exceedance. In the province of Limburg this return period equals 250 years, so the probability that the design water level is exceeded is  $1/250$  per year. The design water level at some location is currently found by hydrodynamic simulation using the design hydrograph.

A **probabilistic method** of hydrograph shape is a method that takes the probabilities of different hydrograph shapes into account in the estimation of the design water level.

The **effect of a retention area** is defined as the reduction in maximum water level at some location due to the functioning of the retention area. Instead of defining effects in terms of water level reduction, one could also use the flooding probability or flood risk of some area. This is particularly useful in the context of a cost-benefit analysis of the retention area.

## 1.5 Report structure

This thesis report is composed of 6 chapters. The report resumes after this introduction chapter with Chapter 2 that provides background information on topics such as the Meuse Basin and the current method to determine design water levels. Chapter 3 treats the methodology that was used, and also explains the various tools that were used in the analyses. Chapter 4 presents the results of the analyses, and Chapter 5 is a discussion of the results. Finally, in Chapter 6 conclusions are drawn with regard to the research questions. Results that are less important for the understanding of the main line, are included in one of the appendices.

## 2 The context

### 2.1 The Meuse River Basin

#### 2.1.1 Topographical overview

The river Meuse is one of the major rivers in the Netherlands, with a length of approximately 900 km and a catchment area of 33,000 km<sup>2</sup>, covering parts of France, Belgium, Luxembourg, Germany and the Netherlands (Berger, 1992; De Wit, 2008). Its origin is in Pouilly-en-Bassigny on the Plateau of Langres in France. The Meuse catchment can be divided into three major sections based on geologic characteristics (see Figure 2-1):

- the *Lotharingian Meuse* upstream of Charleville-Mézières
- the *Ardennes Meuse* between Charleville-Mézières and Liège
- the *Dutch Meuse* downstream of Liège (although not entirely in The Netherlands)

The different stretches are shown in Figure 2-1, together with a typical layout of that part of the river. The *Dutch Meuse* can be split up further into two parts: the *Limburg Meuse* between Eijsden on the Belgian-Dutch border and Cuijk close to Nijmegen, and the *Lowland Meuse* from Cuijk up to the weir at Lith where the tidal influence from the North Sea starts. In Dutch literature those stretches are often referred to as Unembanked Meuse (onbedijkte Maas) and Embanked Meuse (bedijkte Maas), but these names have become confusing since the Limburg Meuse is nowadays also partly embanked. Several smaller stretches in the Dutch part of the Meuse are: Bovenmaas (Eijsden-Borgharen), Grensmaas (Borgharen-Maaseik), Plassenmaas (Maaseik-Roermond) and Zandmaas (Roermond-Lith). This division is not universal, in other literature the stretches may be defined differently.

The main tributaries in the Netherlands are the Geul, the Roer, the Niers (in Limburg) and further downstream the Dommel and Aa. Their contribution to the discharge can be in the order of 10% (Van der Veen, 2005a), but how this contributes to the peak discharge and shape depends strongly on the timing of the peaks of tributaries and main river. An analysis of the timing of the tributaries shows that most tributaries peak on average before the Meuse, but the variation between events is large (De Wit et al., 2007).

The Ardennes Meuse (and to a lesser extent the Lotharingian Meuse) have an impermeable subsoil, causing a quick and large runoff response to rainfall. The combination of high rainfall rates, a steep and impermeable subsoil and little storage in the valleys make the Ardennes area the most important area in the generation of floods in the Meuse basin. The travel times of the flood waves upstream Borgharen are rather short; it takes approximately 20 hours from the Semois to Borgharen. From Borgharen to Lith - a comparable distance - takes approximately 50-90 hours. Large parts of the river are controlled by weirs, which influence the propagation of flood waves up to discharges of approximately 1200 m<sup>3</sup>/s (Berger, 1992).

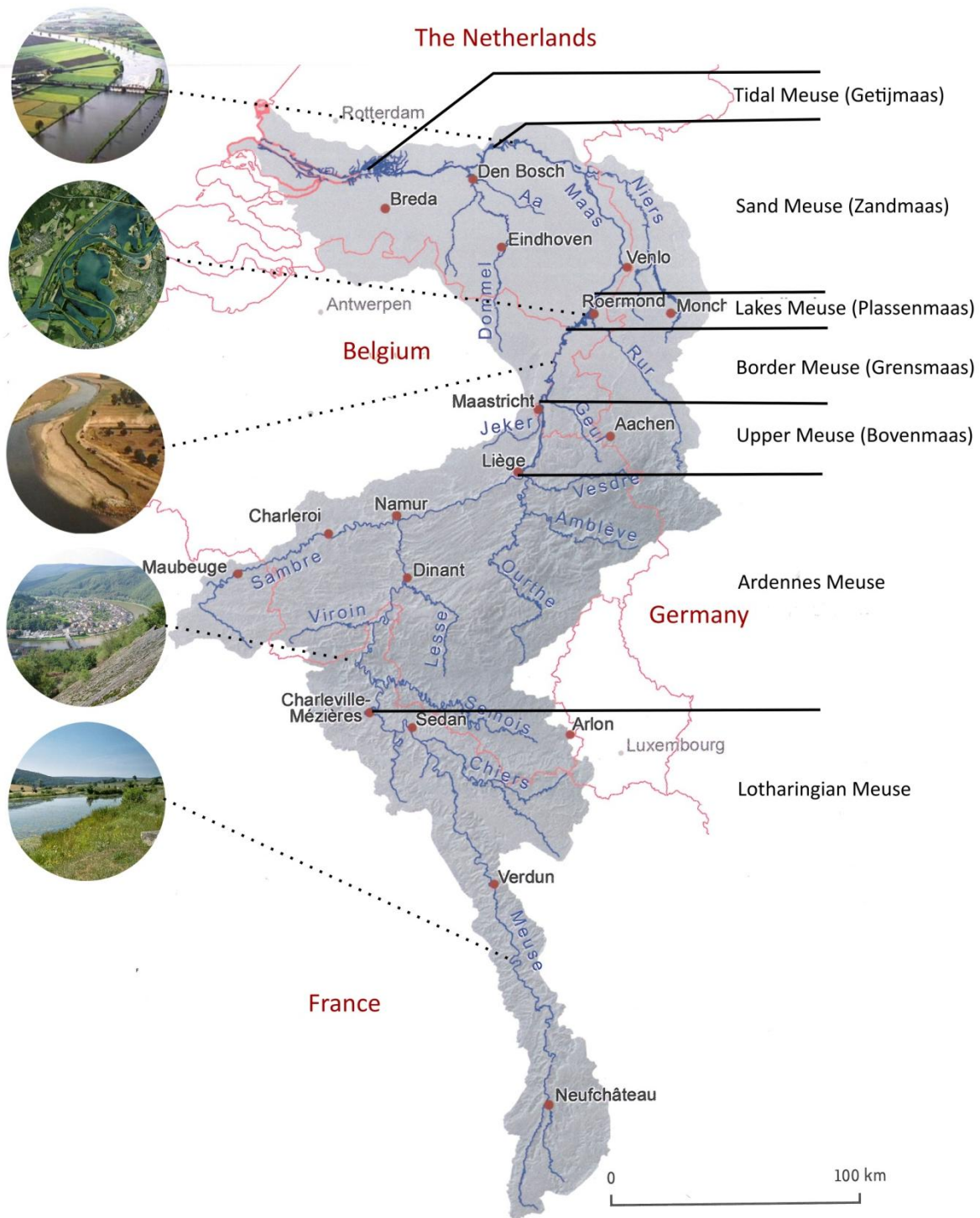


Figure 2-1 Topography of the Meuse River Basin. Map adopted from De Wit (2008)<sup>1</sup>

<sup>1</sup> Photos from Google Earth, beeldbank.rws.nl and wikipedia.com

### 2.1.2 Discharge regime

Several hydrological processes precede the moment of a flood wave entering the Dutch Meuse at Borgharen. The rainfall that leads to the extreme flood waves originates from long lasting and large-scale depressions, that are predominantly from the southwest. After precipitation falls on the earth's surface, the water finds its way via several paths. Part of the precipitation is stored on surfaces, from where it evaporates again. Another part infiltrates into the ground, where it feeds the groundwater or flows slowly underground to the river system. The remaining part will flow over or just below the surface, and quickly end up in streams. Finally, the flows of the smaller streams join to form the flood wave on the main river. This simplified picture can be refined by many detailed descriptions of processes, but for this thesis this short overview is sufficient.

The river Meuse has the character of a rain-fed river or pluvial river, what means that its discharge regime is mainly determined by rainfall. Unlike in the Rhine basin, there is little influence of ice melt during spring. Average annual precipitation amounts in the river basin vary between 750 mm in the Netherlands and 1200 mm in the higher parts of the Ardennes. On a yearly basis, approximately 60% of the precipitation evaporates and 40% discharges to the river. Precipitation over the year is relatively constant, but evaporation is much higher during summer (approx. 100 mm/month) than during winter (approx. 0 mm/month). This seasonal variation in evaporation causes the strong seasonal variation in river discharge as shown in Figure 2-2. At Borgharen, the average annual discharge is 250 m<sup>3</sup>/s, the summer discharge is on average 150 m<sup>3</sup>/s with extremes of 10 m<sup>3</sup>/s and the winter discharge is on average 500 m<sup>3</sup>/s with extremes of 3000 m<sup>3</sup>/s (De Wit et al., 2001; Tu, 2006).

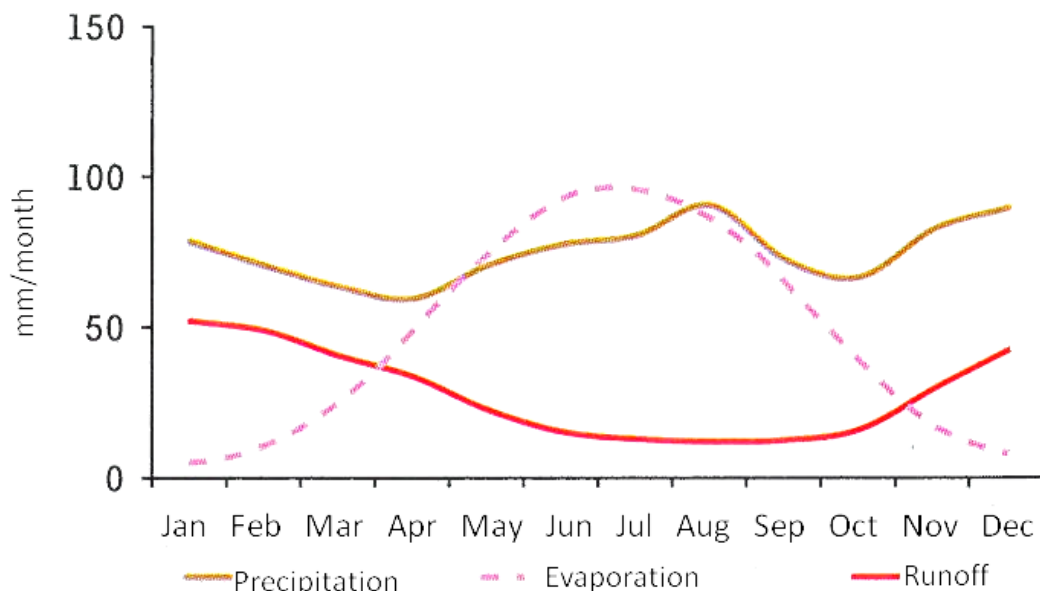


**Figure 2-2** Precipitation, evaporation and discharge regime of the Meuse (De Wit, 2008)

The Meuse peak discharge during a flood event is not simply the sum of the peak discharges of the tributaries. A flood wave is created by a complex process in which the coincidence of the tributaries is an important factor (Peeters, De Wit & Uijlenhoet, 2005; De Wit, Van der Veen & Van Hal, 2005; De Wit, 2008). Timing is important for both the peak discharge and the flood wave

shape. When the flood peaks of two tributaries coincide, the resulting flood wave will be both higher and steeper than in the case of a time lag between the two flood peaks. The complexity of the tributary inflow is one of the causes of the large variation in hydrographs shapes.

Approximately once per year, the bankfull capacity ( $Q \approx 1250 \text{ m}^3/\text{s}$ ) is exceeded. In the discharge records at Borgharen, the years 1926 ( $3175 \text{ m}^3/\text{s}$ ), 1993 ( $3039 \text{ m}^3/\text{s}$ ) and 1995 ( $2746 \text{ m}^3/\text{s}$ ) have the most extreme floods, that also led to a considerable amount of damage. Before the measurements started in 1911, extreme floods larger than  $2500 \text{ m}^3/\text{s}$  have occurred at least in the years 1571, 1643, 1740, 1850 and 1880 (Lorenz, Kwadijk & Diermanse, 2000).

### 2.1.3 Developments in flood protection in the Limburg Meuse

The property and people in the floodplains of the Limburg Meuse have been unprotected for a long time. Even after the large flood of January 1926 with a peak discharge of  $3175 \text{ m}^3/\text{s}$  at Borgharen, only minor flood protection measures were taken. The turning point in the flood protection of the Limburg Meuse is the flood of December 1993. The extreme discharge of  $3039 \text{ m}^3/\text{s}$  caused extensive flooding and considerable damage (Wind, Nierop, Blois & Kok, 1999). The Committee Boertien II (Commissie Watersnood Maas) was appointed to advise on measures to reduce flood risk. The research resulted in a proposal with different flood management strategies; both traditional dike construction, river deepening and 'room for the river' measures. Strictly speaking no choice was made for a particular strategy, but there was some preference for the option with more 'room for the river' measures (WL|Delft Hydraulics, 1994).

In January 1995 a new flood struck, this time with much larger duration than in December 1993. In response to the floods of 1995, the Delta Plan for the Major Rivers or Deltaplan Grote Rivieren (Ministerie van V&W, 1995) was written. In fact it advises to execute the proposal of Boertien II - strategy 2b - that contains widening and deepening of the river bed, and in addition the construction of low dikes (Dutch: kaden) where necessary. However, the measures had to be executed in a much shorter timeframe. The low dikes, now called DGR-kaden, had to be finished the same year, in contrary to the advice of Boertien II. Later on, it turned out that the location of the dikes was not always optimal with respect to the hydraulics (Groendijk, 2011; Van Putten & Hoefsloot, 2013). Those dikes that were built in 1995-1997 had to provide a temporary safety level of 1/50. In 2005, the Limburg part of the Meuse received a safety standard of 1/250 prescribed by law. A strict requirement at the time was that the safety measures for Limburg would not lead to negative effects downstream in Brabant and Gelderland. This requirement led to the theoretical 'floodability principle' that demands that the protected areas in Limburg act as storage areas in case of a more extreme flood than the 1/250 flood, in order to protect the downstream regions with a higher safety level.

The execution of the advised flood protection measures has led to the large project 'Maaswerken' (Maaswerken, 2002). It consists of a large set of measures including widening of the river bed, parallel flood channels, lowering of flood plains, and retention areas such as Lob van Gennep and Lateraalkanaal West. The measures in the river bed have to be completed by 2015, the reinforcement of dikes by 2020.

### 2.1.4 Strategies for the Limburg Meuse

Flood risk in the Limburg Meuse is expected to increase during this century, as a result of climate change and spatial developments. In order to cope with these future developments, a strategy for the mid-term was formulated in the project Integral Investigation of the river Meuse (Dutch: Integrale Verkenning Maas, IVM). A preferred set of measures was defined with much attention to spatial quality (Reuber, Schielen & Barneveld, 2005; Ministerie van V&W, 2006). The proposed measures are in sequence of preference:

- (1) measures in river bed (e.g. widening of main channel, creating parallel flood channels),
- (2) relocation of dikes,
- (3) retention areas and
- (4) higher dikes only if other measures are insufficient.

Retention areas in the Limburg Meuse are not seen as a robust solution. It has some practical problems coming from uncertainty in flood predictions, choices of local decision makers, and often it lacks societal and governmental support. The heightening of dikes is only a last option because it results in higher water levels downstream, and that is not in line with the European Floods Directive 2007/60/EC and the current line of thought to solve problems locally. Measures in Belgium and France were considered not very effective for The Netherlands: small scale retention far upstream has negligible effect on extreme events, and large retention basin cannot be relied on because local decision makers may choose to protect their own region.

In the framework of the Deltaprogramme Rivers, a preferred strategy (Dutch: Voorkeurstrategie, VKS) for the long term has been established (Berkhof et al., 2013). Like in IVM there is a preference for 'room for the river' measures above dike construction for the same reason as in IVM. In the VKS, the 'floodability principle' is regarded as untenable since it is not reliable, robust and explainable. The idea was smart, but in practice the system may work differently than expected. Firstly, it is difficult to avoid that the local decision makers use emergency measures to protect their area, especially in 2050 when nobody knows what the reason for this rule was. Secondly, the crest of the dikes needs to be maintained at a very precise level. Every time that the boundary conditions change slightly the dikes need to be adapted, which is very costly. Instead of raising all dikes or keeping all dikes floodable, a mixed solution is proposed: some areas will be floodable, some will get safer dikes and some dike ring areas can be optimized by relocating the dike (Deltaprogramma Rivieren, 2014). On the long term, this strategy is expected to be more flexible, manageable and robust. For all dike ring areas an optimal safety level has been established based on a cost-benefit analysis. The ENW (Expertise Network for Flood Protection) advised to leave the floodability principle, but also gave recommendations concerning amongst others the uncertainty in hydrograph shape and the use of a probabilistic approach (ENW, 2014). These recommendations are partly worked out in this thesis.

## 2.2 The flood risk framework

The Dutch have a long tradition of protecting their land and people against flooding. Before the infamous flood of 1953, design of flood defences was often based on the highest recorded water level, plus a safety margin. After 1953, the Delta Committee adopted a new safety philosophy based on economically optimal safety level. The derived optimal flooding probability was

translated into an exceedance probability of the water level, prescribed by law for all dike ring areas. This exceedance probability varies from 1/10.000 per year for the Randstad area up to 1/250 per year for the province of Limburg. The water level with this probability of exceedance is called the design water level (Dutch: maatgevend hoogwater, MHW). Those exceedance probabilities and design water levels are an important component in the design of flood defences.

After the completion of the Delta works, the developments did not stop. An important development is that the flood risk approach becomes more and more the dominant way of thinking about water safety in the Netherlands, instead of the former approach based on exceedance probabilities (TAW, 2000). The new safety standards of WTI2017 are based on flood risk, and formulated in terms of failure probabilities per dike section. This method takes into account the different failure mechanisms, the actual strength of the dike and the dependency between different dike sections. The flooding probability standard depends on the potential damage and potential fatalities in the area, and on the costs of flood protection measures.

The risk chain is a useful concept to see the relevance of this thesis for the flood risk. This risk chain consists of: hydrological load – river routing – failure of flood defences – inundation – damage. The topic of hydrograph shape variability (river routing) is rather at the beginning of a long chain of processes leading to the risk of flooding. For that reason it is useful to understand the larger frame of the flood risk approach, which will be explained in the next sections.

### 2.2.1 The definition of flood risk

Different definitions of risk are used in flood risk analysis (CUR, 1997; Merz & Thielen, 2004). A general quantifiable definition is that risk is a function of the probability and the consequences of an event. In a more specific form, this is often defined as the product of the flooding probability and the associated consequences, or the expectation of the consequences:

$$R = P \cdot K = E[K] = \int f(x) \cdot K(x) dx \quad (2.1)$$

where:

- R = risk
- P = probability
- K = consequences of flooding
- E[.] = expectation
- x = random variables that describe the flood event
- f(x) = probability density function of the random variables

A similar definition is that risk is the product of hazard (physical and statistical aspects of the flood) and vulnerability (exposure of people and assets).

What is meant exactly by flooding, probability and consequences may vary from case to case. The word 'flood' is used in different ways. In the context of flood risk, flooding can be defined as the event that leads to considerable damage due to an unmanageable amount of water. This can be the result of a dike breach, a gradual rising of the river stage in case no dikes are present, or a heavy rainstorm. The next section explains how the probability and consequences of a flood are determined in case of a dike ring system.

### 2.2.2 The failure probability of flood defences

The flooding probability of a system of flood defences, as usually is present in the Netherlands, is determined by the contribution of all (dike) sections in the system and all failure mechanisms that play a role. All contributions are combined to a flooding probability, in a way that depends on the dependence between the contributing failure probabilities.

#### Limit state functions

This section focusses on the failure probability of one such element or section. The failure probability of a section is determined by both the load on and strength of the flood defence. This is expressed in the limit state function or Z-function:

$$Z = R - S \quad (2.2)$$

Where R are the stochastic strength variables and S are the stochastic load variables. The section fails if the load becomes larger than the strength, that means it fails if  $Z < 0$ . Then the failure probability is written as  $P(Z < 0)$ . When the joint probability distribution  $f(R, S)$  of R and S is known,  $P(Z < 0)$  can be found by integration over the region where  $Z < 0$ :

$$P(Z < 0) = \int_{-\infty}^{\infty} \left( \int_{-\infty}^S f(R, S) dR dS \right) \quad (2.3)$$

This can be solved with (numerical) integration or a Monte Carlo (MC) analysis.

#### Failure mechanisms

A dike can fail due to different failure mechanisms (TAW, 1998) that have their own Z-function. The failure probability of a section is determined by the combination of the probabilities for each failure mechanism. Figure 2-3 shows several failure mechanisms for dikes. The failure mechanisms overflow (A), overtopping (B), sliding of the inner slope (C) and piping (G) are considered generally the most dominant, in the Netherlands as well as in other European countries (Vorogushyn, Merz & Apel, 2009).

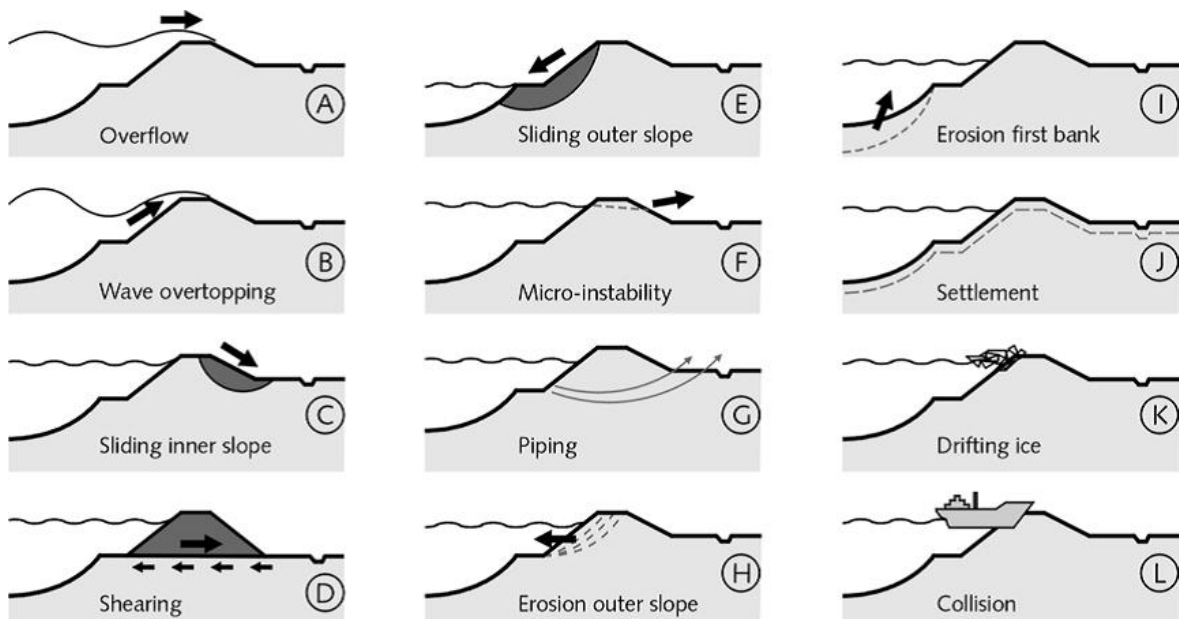


Figure 2-3 Failure mechanisms of dikes (TAW, 1998)

These three mechanisms are described briefly. More details can be found for example in VNK2 (2012). Overflow occurs when the still water level is higher than the dike crest level. Overtopping occurs when the water level is lower than the dike, but waves run over the crest. Failure due to overflow or overtopping occurs when the water erodes the inner slope and finally causes a breach. Sliding of the inner slope (called macro-instability) occurs when the soil is not in equilibrium anymore because the resistance of the soil is smaller than the weight of the soil. This is caused by infiltration of water, which both increases the weight and reduces the shear strength of the soil. Piping occurs when the water flow underneath a dike erodes the sand particles, creating a pipe. This happens when the water level difference between inner and outer side becomes too large.

The VNK2 project (VNK2, 2012) investigated the actual failure probabilities and flood risks of most dike ring areas in the Netherlands, although only a few along the Limburg Meuse. It reveals that overflow and overtopping are the dominant failure mechanisms in Limburg, but piping is dominant further downstream along the Meuse in the provinces of Gelderland and Noord-Brabant.

### Fragility curves

The failure probability depends on the load; larger loads give a higher failure probability. This behaviour is described by fragility curves (Van der Meer, Ter Horst, & Van Velzen, 2009). Fragility curves have a different characteristic shape for different failure mechanisms (Figure 2-4). Fragility curves of overflow have a strong increase around the crest level, whereas the curve of piping is smoother. This means that the failure probability due to piping is not zero during significantly lower water levels than the crest height. A first implication is that smaller flood waves, with higher probability of occurrence, may also be important for the total flooding probability. A second implication is that measures to reduce the maximum water level may be ineffective in the case that the frequency of slightly lower water levels increases as a result of the measure.

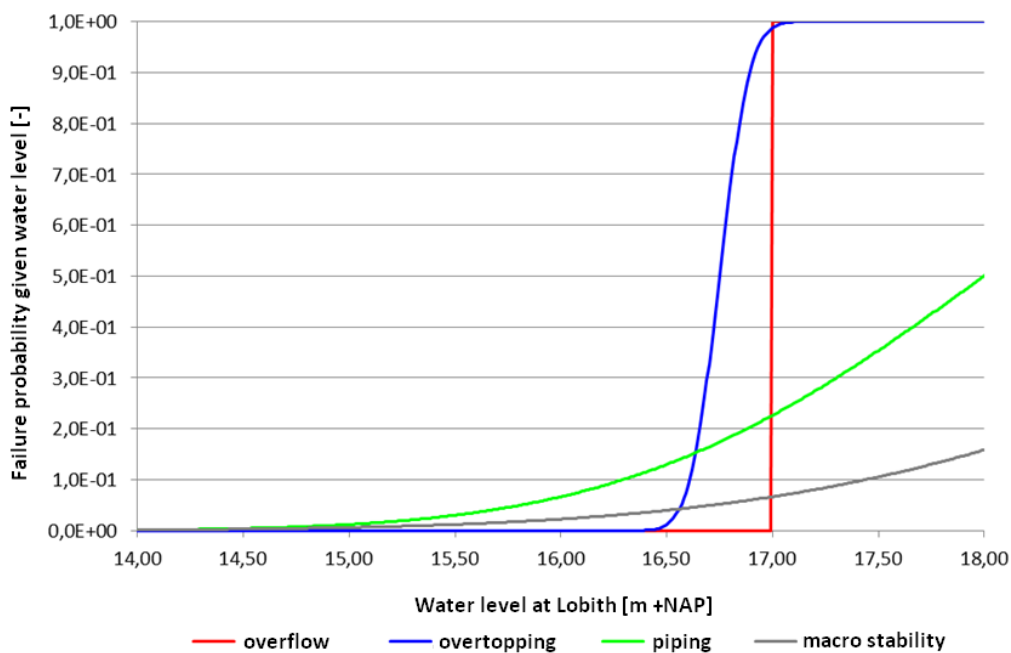


Figure 2-4 Example of fragility curves (VNK2, 2012)

### 2.2.3 The consequences of failure of a flood defence

The consequences of a flooding are usually expressed in terms of direct losses such as fatalities or economic damage. Other consequences include indirect economic damage, business disruption, social disruption and psychological damage, but these are more difficult to quantify and use in the risk analysis. The direct losses are estimated with loss (or damage) functions, that give a relation between the losses on the one hand, and characteristics of flooding and the affected area on the other hand (Jonkman et al., 2008; Apel, Merz & Thieken, 2009). Area characteristics include the surface area, land use, population of the area and evacuation fractions. Flooding characteristics are e.g. the flood extent, water depth, flow velocity, water quality and flood duration. This means that the consequences are different for different flooding scenarios with their associated probability.

### 2.2.4 Actual flood risk along the river Meuse

The VNK2 project (VNK2, 2012) attempts to compute the actual failure probabilities of flood defences and the contribution of different failure mechanisms. It reveals relatively large flooding probabilities in Limburg (1/20 to 1/35), but also further downstream along the river Meuse (1/100 to 1/550). In order to be useful for failure probability calculations, the results of the probabilistic analysis must be able to provide sufficient relevant information. Overflow and overtopping are dominant in Limburg, but piping further downstream. Since the failure probability of piping depends on the flood duration and is also significant at lower water levels, it implies that the flood duration at different water levels is an important parameter to consider. The influence of time dependence along the river Meuse is not known, but in general the duration of a flood wave is more important for short flood events. For long lasting floods, piping has completely developed and the actual duration is less important (Förster et al., 2012).

### 2.2.5 Importance of local load parameters for failure mechanisms

For different failure mechanisms, different hydrograph characteristics are relevant. Table 2-1 shows that for most failure mechanisms the shape of the local flood wave is relevant to some extent. This implies that for a good analysis of dike failure probabilities, the local joint distribution of all load variables (such as water levels and exceedance durations) must be known.

<b>Failure mechanism</b>	<b>Important hydrograph parameters for failure</b> <b>Based on Van Velzen &amp; Beyer (2007) page 42</b>
<b>Overflow</b>	maximum water level
<b>Overtopping</b>	maximum water level, waves
<b>Sliding inner slope</b>	maximum water level, duration of different water levels
<b>Shearing</b>	maximum water level
<b>Sliding outer slope</b>	height and slope of falling limb
<b>Micro-instability</b>	maximum water level, duration of different water levels
<b>Piping</b>	maximum water level, duration

**Table 2-1 Importance of local load parameters for failure mechanisms.**

## 2.3 Current method of determining the design hydrograph

Rainfall is an irregular process, and in a complex system such as the Meuse many factors influence the flood wave shapes resulting from a rainfall event. For the design of flood protection measures, it is necessary to represent the large variation in flood waves in a simplified way. A widely used method to simplify the flood wave variation is the design hydrograph. This section explains the design hydrograph method that is currently used in the Netherlands. The method can be split in two parts: (1) the peak discharge and (2) the hydrograph shape.

### 2.3.1 Design peak discharge

The current method to determine the design peak discharge is based on a frequency analysis of the discharges at Borgharen. Flood frequency analysis is widely used for the determination of design discharges. For an extensive treatment of this topic, see e.g. Hamed & Rao (2000). The basis for the application of this method to the Dutch rivers has been laid by the committees Becht and Boertien I (WL|Delft Hydraulics, 1993), and it is now incorporated in the Hydraulic Boundary Conditions (Dutch: Hydraulische Randvoorwaarden).

Starting point of determining design peak discharges is the norm frequency as prescribed by law. For the part of the Meuse in the Province of Limburg this norm frequency is 1/250 per year. For the part of the Meuse further downstream this norm frequency is 1/1250 per year.

An important assumption in the current method is that the peak discharge with a certain exceedance frequency at Borgharen leads to water levels downstream with the same exceedance frequency. This is not necessarily true because of deformation of the flood waves between Borgharen and the location of interest. This assumption has been very useful, because sufficient water level measurements at all locations along the river are unavailable and hydrodynamic computations for all historical flood events were time consuming.

#### Homogenisation

Discharge measurements at Borgharen are available since 1911. During the period of discharge measurements, several changes happened in the river system upstream of Borgharen. An important factor is the construction of large river works, which influence the water levels and discharges. Other factors include land use change, climate change and changes in measurement technique. To compensate for some of these changes, the observed discharge series is homogenised. This means that the observed discharges are modified in such a way that the homogenised discharges would occur given the observed event and the current system.

#### Frequency analysis

In order to obtain a peak discharge with a certain return period (e.g. 1250 years), the daily discharge series is transformed into two series:

- (AM) Annual Maxima
- (POT) Peaks over Threshold

Figure 2-5 illustrates the difference between the two methods. The AM series consists of the maximum peak discharge in every hydrological year. A hydrological year runs from 1 October –

31 September. In the transition period, floods are unlikely, so it is unlikely that one flood event is counted in two years. If more than one extreme flood happens in one year, only the highest flood is taken into account. The POT series consists of all peak discharges that exceed a certain threshold. A time window (e.g. 10 days) is chosen for independence between flood events. If two floods are closer than the time window, only the highest is taken into account. If the threshold is chosen in such a way that the amount of peak events equals the amount of years of data, this special case of POT is called an Annual Exceedance (AE) series. So in the AE series, the number of floods per year ( $\lambda$ ) can vary, whereas in the AM series this number is always equal to one.

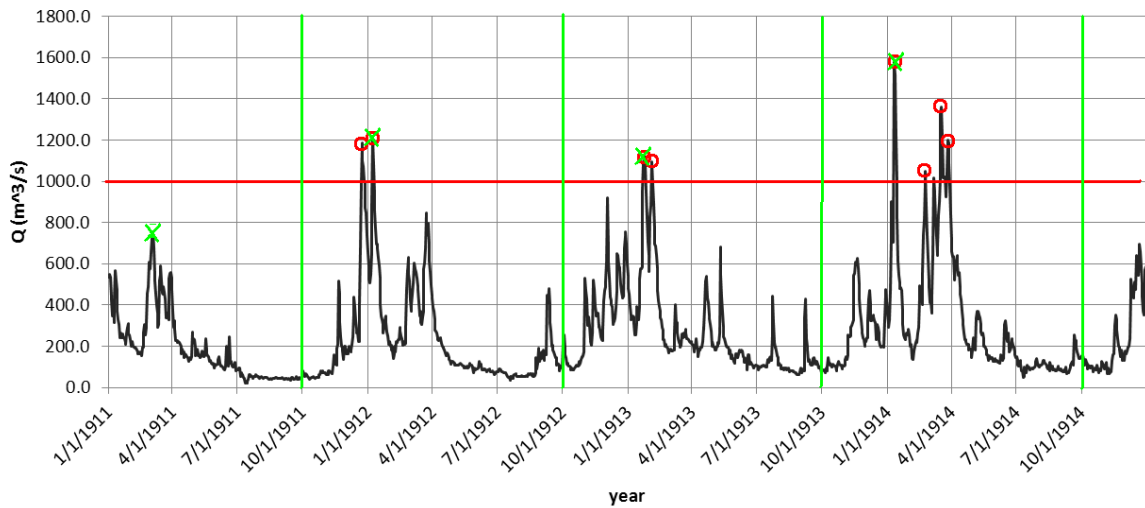


**Figure 2-5 Illustration of AM (green) and POT (red) methods.**

To determine the return period  $T$  of an event with return value  $Q_p(T)$ , all peak discharges in a series are sorted from high to low. The exceedance probability is estimated with a plotting position  $p$ , in the current methods the Weibull plotting position:

$$p = \frac{i}{N+1} \quad (2.4)$$

Then the return period is given by:

$$T = \frac{1}{p \cdot \lambda} = \frac{N+1}{i \cdot \lambda} \quad \left( \lambda = \frac{N}{t} \right) \quad (2.5)$$

Where:

- $i$  = the rank number ( $i=1$  for largest flood,  $N$  for the smallest flood)
- $N$  = the total number of peaks in the AM or POT series
- $\lambda$  = average number of floods per year
- $t$  = length of the the AM or POT series in years

The factor  $\lambda$  equals 1 in case of an AM series. The return values  $Q_p(T)$  are plotted against the corresponding return periods  $T$  (see Figure 2-6). In theory, many probability distributions are suitable to fit the plotted peak discharges. In the current method, the Lognormal, Gumbel and Pearson III distributions are used for the AM series. The exponential (for  $T > 25$  y) and Generalized Pareto (for  $T < 25$  y) distributions are used for the POT series. In order to obtain a single peak discharge value for a given return period, the applied distributions are averaged. From this average, the design discharge curve (DDC, Dutch: werklign) of the form  $Q = a \cdot \ln(T) + b$  is constructed. This DDC serves as the official relation between design peak discharge  $Q_p(T)$  and

return period  $T$ . The results are given in Figure 2-6 for the most recent DDC construction based on the period 1911-2008 (Tijssen, 2009). A threshold of  $Q_p = 1300 \text{ m}^3/\text{s}$  for the POT series has been used, and a time window of 8 days.

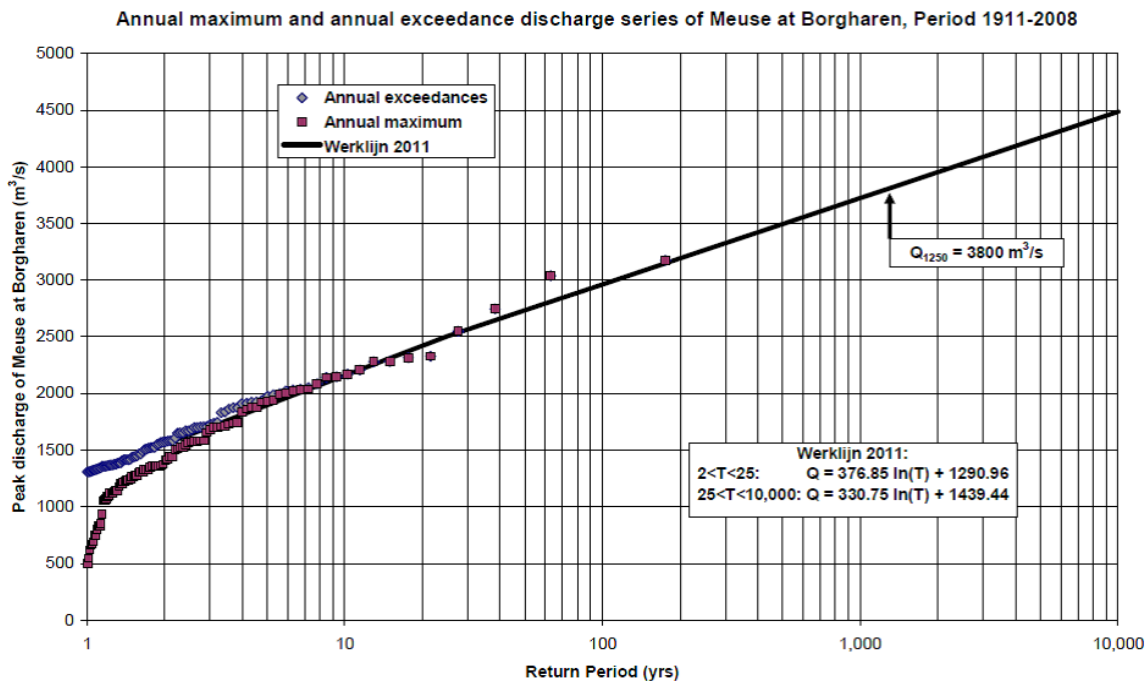


Figure 2-6 Design discharge curve 2011 (Ogink, 2012)

### 2.3.2 Design hydrograph shape

For many assessment and design problems, the wave shape is also important in addition to the peak discharge. The current method to obtain a design hydrograph shape is referred to as the scaling method (Klopstra & Vrisou van Eck, 1999). The result is a standard hydrograph shape. The method has the following steps (see Figure 2-7 for illustration):

1. For a given return period  $T$ , the design peak discharge  $Q_p(T)$  is determined according to the procedure of section 2.3.1.
2. Selection of hydrographs from the continuous discharge record; only hydrographs that have a peak discharge exceeding a threshold of  $1750 \text{ m}^3/\text{s}$  and no higher peaks in a time window of 8 days.
3. The selected hydrographs are scaled by multiplication of all discharges  $Q$  with the ratio between  $Q_p(T)/Q_p$ .
4. Double-peaked flood hydrographs are merged into hydrographs with one peak. This is done in such a way that the durations at every level are preserved.
5. At a number of discharge levels, the mean duration is determined. This is done separately for the durations of rise and fall in order to preserve the skewed character.
6. Connecting these mean durations at every level determines the design hydrograph shape.

Sometimes the 5% or 95% hydrographs are given, corresponding to the  $x\%$  percentile duration at every discharge level, based on a lognormal distribution of duration (Figure 2-7 lower).

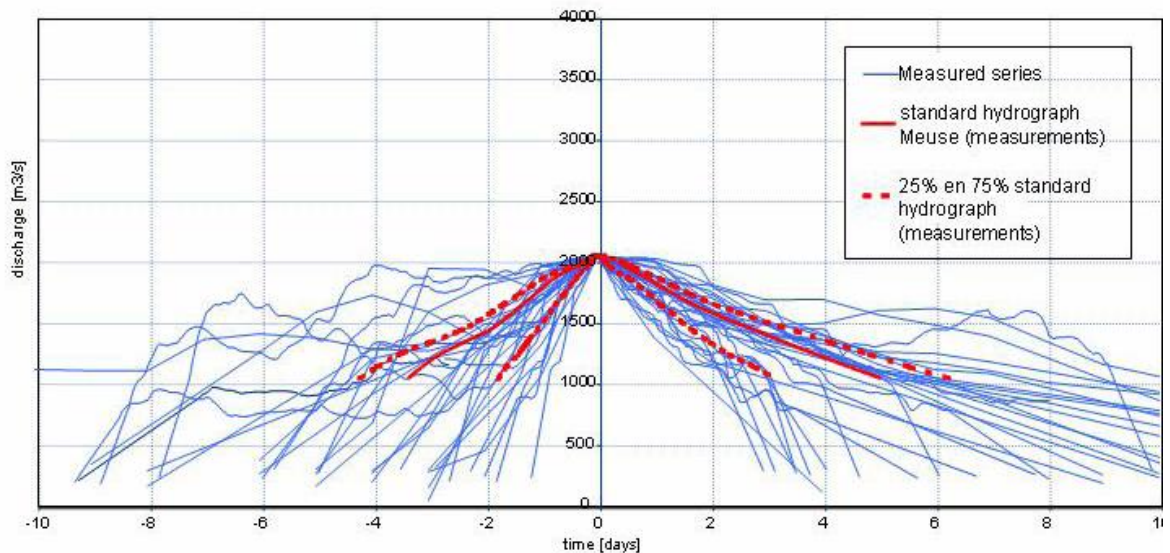
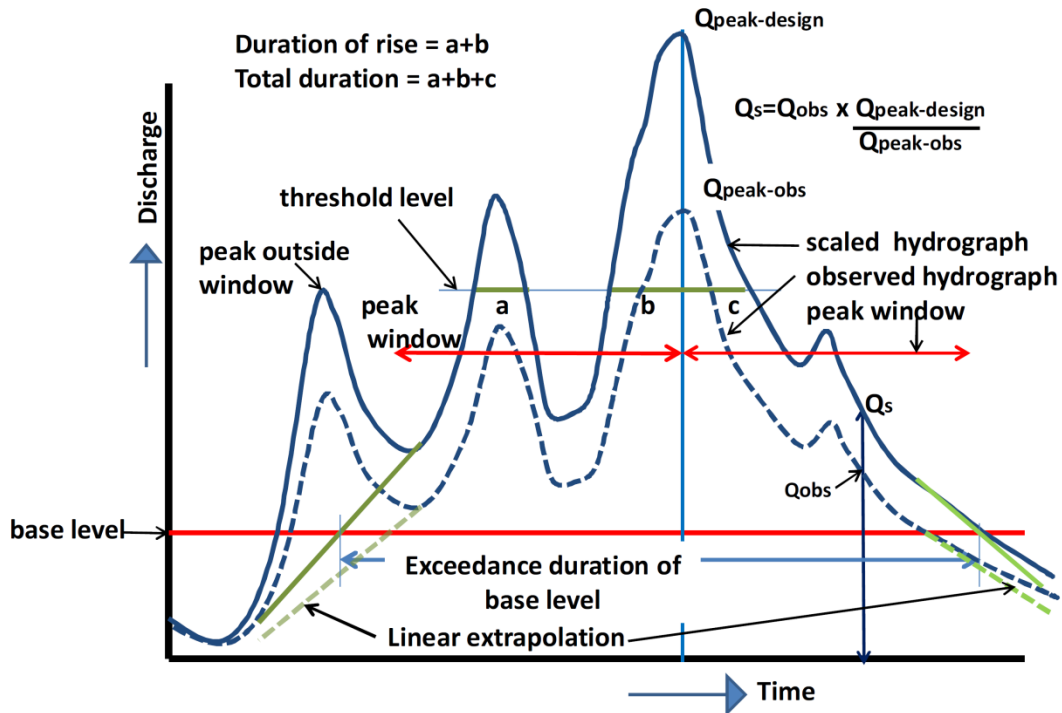


Figure 2-7 Illustration of standard hydrograph method (Ogink, 2012; Rijkswaterstaat, 2012)

### 2.3.3 Limitations of the current method

The current method that was described in sections 2.3.1 and 2.3.2 has several limitations (Klemeš, 2000; Chbab et al., 2006). The extrapolation of 100 years of data to a 1250 year return period gives a lot of statistical uncertainty (Jansen, 2007). This is partly because of the different possible probability distributions, but also because every distribution has its own confidence interval. For a return period of 1250 years this uncertainty band is approximately 1500 m<sup>3</sup>/s around the mean of  $Q_{p,d} = 3800$  m<sup>3</sup>/s (see Figure 2-8). In terms of water levels this can be estimated as 1.0 - 1.5 m, based on the local stage-discharge relationship. It is clear that this has a large impact on the dike crest height, and in that way on the costs and spatial impact of flood protection measures. The

reason for these uncertainties is that for extreme events, we are interested in the extreme tails of the distributions. But just in this part, there are few data to base the choice of distribution on.

As a result of the short record, the design peak discharge appears to be sensitive to new extreme events. The two large floods of 1993 and 1995 for example, have led to an increase of 350 m<sup>3</sup>/s in the design peak discharge compared to 1990.

Although the discharge is assumed to be homogeneous, floods can come from different meteorological causes such as snow melt, long depressions or a combination. Physical processes may be different for more extreme events, e.g. flooding of large areas. Under these heterogeneous conditions, the extrapolation can lead to deviations. The homogenisation of discharge data is difficult because of incomplete knowledge about changes in the past. In the current method homogenisation is only carried out for large river works in the main river. No corrections are carried out for changes in climate and land use.

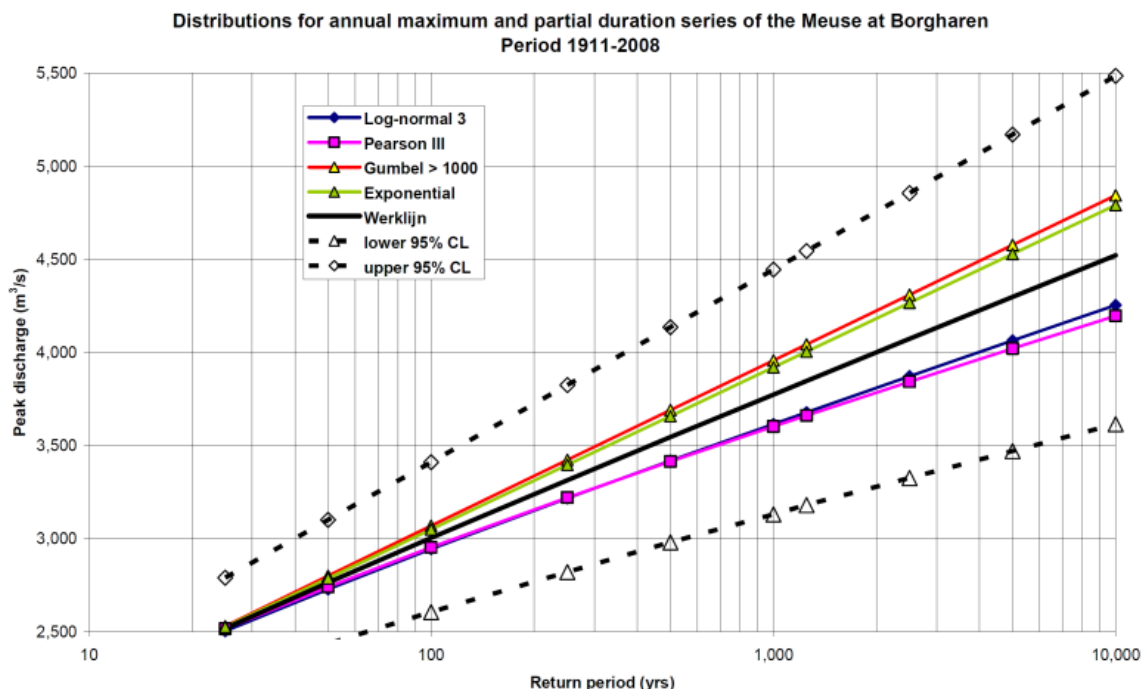


**Figure 2-8 Uncertainty in design discharge curve (Ogink, 2012)**

The method to determine the hydrograph shape has also limitations (e.g. Kramer & Schroevers, 2008; Ogink, 2012). Some have the same reason as the limitations of the design peak discharge: a small number of data, especially for the extreme events. There is an additional issue that is mainly important for the shape of the flood wave, but also for the peak discharge. In the current method it is implicitly assumed that the flood wave with a peak discharge return period of 1250 years at Borgharen leads to water levels downstream that have the same return period. But since different shapes lead to differences in peak attenuation and differences in water levels, this is not necessarily true. One could adjust the design hydrograph such that it produces the correct water levels (i.e. the assumption is valid), but it cannot be taken for granted that this will work under system adaptations too.

### 2.3.4 Alternative methods to determine design hydrographs

Beside the scaling method, there are other methods to derive the design hydrograph. The regression method (WL|Delft Hydraulics, 1993) relates duration at and volume above certain discharge levels to the peak discharge by (linear) regression. The relation between peak and volumes looks quite strong, but the one between peak and duration is much weaker. It appears that the method has the problem of a lack of data in the extreme discharges range. In that range only one or two events are available, which is definitely insufficient for regression. Also the regression for less extreme discharges may need more data to give a clear view on the relations. Apel et al. (2004) applied cluster analysis on normalized hydrographs to find a number of distinct hydrograph shapes and the corresponding probability. These hydrographs are scaled to the design discharge, and routed through a river system. Ogink (2012) and Kramer (2012) present vertical averaging (i.e. average discharge at points in time) as an alternative to the standard method which uses horizontal averaging (i.e. average duration at discharge levels).

## 2.4 The GRADE project

The limitations of the current extrapolation method as described in section 2.3.3 have led to the GRADE project (Generator of Rainfall And Discharge Extremes) by Rijkswaterstaat and KNMI. The idea of the project is to simulate long time series of rainfall and temperature by rearranging historical rainfall and temperature measurements in such a way that the statistical properties are not changed. Although the simulated *daily* events are never larger than observed events, *multiple-day* sums can be larger than ever registered as a result of the rearrangement. The simulated rainfall and temperature series are used as input for the conceptual hydrological model HBV. This model gives as output long simulated discharge time series.

GRADE contains two main elements, a stochastic weather generator and a hydrological / hydraulic model, that are explained shortly in the next sections. A more detailed description can be found in Leander et al. (2005), De Wit & Buishand (2007) and Ogink (2012). Figure 2-9 gives a schematic representation of the two elements and the input and output.

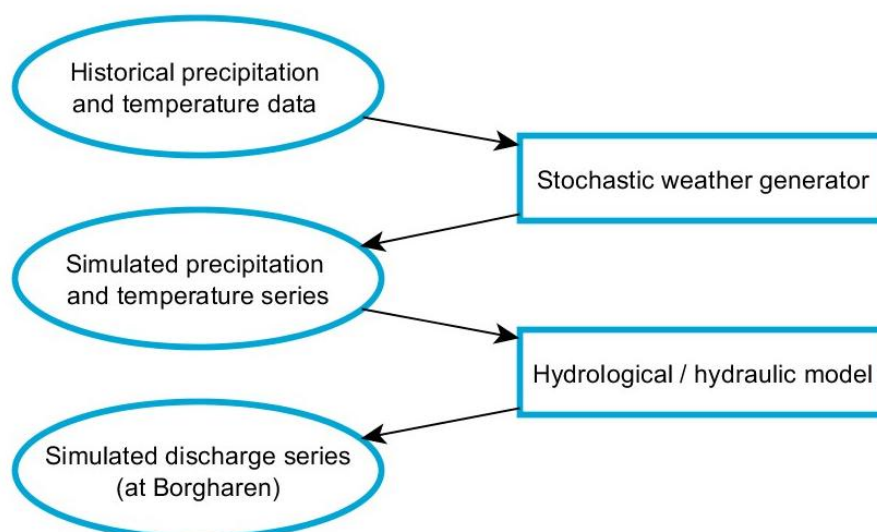


**Figure 2-9 Schematic representation of GRADE method**

The main advantages of the use of GRADE are (1) that very long series can be simulated, and (2) that meteorological and hydrological factors can be taken into account explicitly. This improves the physical basis of the determination of the design flood, and allows for varying the factors in sensitivity analyses of climate change and flood risk reduction measures in the basin.

#### 2.4.1 Stochastic weather generator

The stochastic weather generator for the Meuse basin uses rainfall and temperature measurements from several weather stations spread over the basin. These historical data are resampled using nearest-neighbour resampling. An illustration of this algorithm is given in Figure 2-10. The nearest-neighbour technique is used because it preserves the time dependent structure of the data. Starting from an observation, nearest-neighbour resampling selects an event that is very similar in terms of weather variables (blue arrow), and subsequently selects the weather variables of the day that followed historically on the randomly selected event (red arrow). This last step preserves the time dependence, while the first step makes more extreme multiple day sums possible than were in the measured record. Repeating this resampling procedure many times yields a long simulated dataset of daily rainfall and temperature.

Rainfall data from 7 stations and temperature data from 2 stations, from the period 1930-2008 (Sim30\_08), are used for the resampling procedure. The series at these stations are transformed to a finer grid of weather data for each of the 15 sub basins in the Meuse catchment.

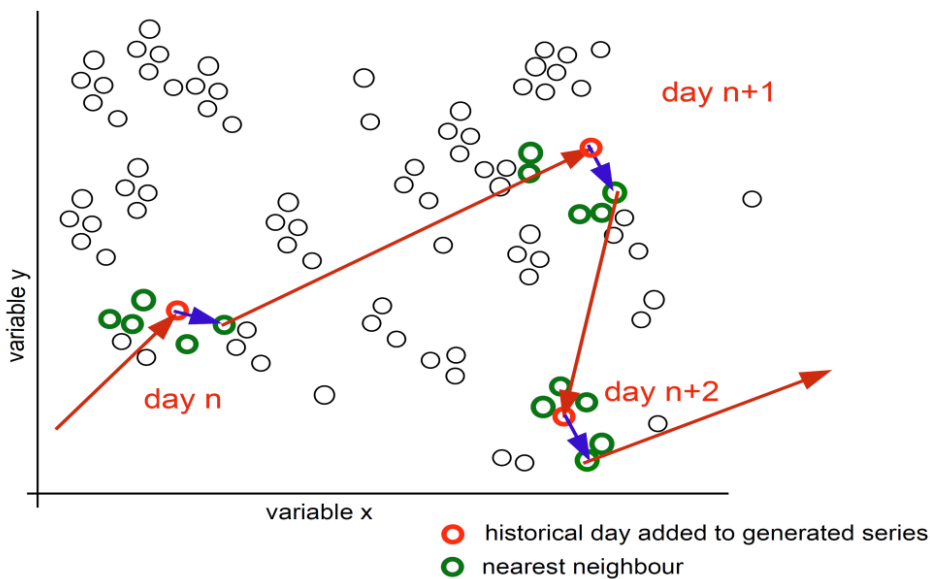


**Figure 2-10 Nearest neighbour resampling (Leander & Buishand, 2004)**

#### 2.4.2 Hydrological and hydraulic modelling

The 50,000 year weather time series per sub basin serve as input for the hydrological model. In GRADE, the conceptual model HBV is used (Lindström et al., 1997). For each sub basin it simulates the runoff for a given climate time series, taking into account processes such as interception, evaporation, snowmelt and groundwater flow. The discharge time series of each sub basin are combined and routed through the main river by a 1D SOBEM hydraulic model. The result is a discharge time series at Borgharen, in a daily time step.

### 2.4.3 Applicability and limitations

The purpose of GRADE is to reduce the uncertainties in the determination of extreme design discharges by taking the physical characteristics of the basin into account. However, GRADE also brings about new uncertainties, both in the weather generator and in the hydrological and hydraulic models (Kramer & Schroevers, 2008). Firstly, the weather data are resampled from a relatively short period. This means that daily weather characteristics reflect the weather in this period, which may be not representative. The simulated daily rainfall is never larger than measured in this period and individual extreme events (e.g. 1995) have a significant influence on the generated discharge. Secondly, the hydrological model includes uncertainties such as the model conceptualisation, parameter choices and calibration events. The HBV model is not calibrated for such extreme events as it is used for, because these events have not occurred.

Theoretically GRADE can generate very extreme discharges, but it must be kept in mind that the capacity of the Meuse at Liege is limited to approximately 4600 m<sup>3</sup>/s (Ogink & Barneveld, 2002). At this discharge level, large subsidence mining areas around Liege will flood, causing no further discharge increase. This must be taken into account in the analysis of extreme discharges. An upper limit of 4600 m<sup>3</sup>/s is used in this thesis.

## 2.5 Peak attenuation

Deformations of the flood wave can occur due to different mechanisms: wave diffusion, lateral inflow and storage in the floodplains (Woltemade & Potter, 1994). Factors in the river system geometry that contribute to the peak attenuation are: bottom slope, flow and storage width and roughness. Diffusion of the flood wave will occur, even in channels without lateral inflow and overbank storage. The peak attenuation over a part of the river can be described with the Forchheimer equation (Forchheimer, 1930):

$$\frac{dQ_{p,x}}{dx} = \frac{B_s^2 * Q_{p,x}}{2 * S * \left(\frac{dQ_{p,x}}{dy}\right)^3} * \frac{\partial^2 Q_{p,x}}{\partial t^2} \quad (2.6)$$

Where  $x$  is the distance in propagation direction [m],  $t$  is the time [s]

$Q_{p,x}$  is the peak discharge at location  $x$  [m<sup>3</sup>/s]

$B_s$  is the storage width of the river [m]

$y$  is the water depth [m]

$S$  is the bottom slope [-]

This equation shows that the peak curvature  $\frac{\partial^2 Q_{p,x}}{\partial t^2}$  is the hydrograph variable that influences the peak attenuation. The second mechanism is lateral inflow from tributaries; the magnitude and timing of this lateral inflow affects the flood wave shape. When the inflow (partly) coincides with the peak in the main river the flood wave will also become higher. The third mechanism is storage in floodplains and retention basins; when the storage is large compared to the peak volume, it can even cut off the peak (peak shaving). When the storage is relatively small, the peak attenuation is small as well. These three factors, peak curvature, coincidence of tributary flood waves and storage, contribute to the peak attenuation in a river system.

### 3 Methods

#### 3.1 Research framework

This section describes the framework that was used to answer the research questions. To recall, the research questions are:

1. To what extent are design water levels affected by using GRADE simulated discharge data instead of measured discharge data?
2. Which hydrograph shape variables determine the downstream water levels, and how?
3. How accurate are the design water levels determined by design hydrograph methods?
4. How accurate are the design water levels determined by probabilistic methods?
5. How is the effect of a retention basin determined by hydrograph shape, and how accurately is this effect determined by the design hydrograph methods?

The framework that was used to analyse the problem consists of four main tools: hydrograph selection, hydrodynamic simulations, a statistical analysis, and a probabilistic analysis (Figure 3-1). These tools are explained in detail in the sections 3.3 to 3.6. The analysis of each research questions requires different tools. Which tools were used for what question is explained in the next paragraphs.

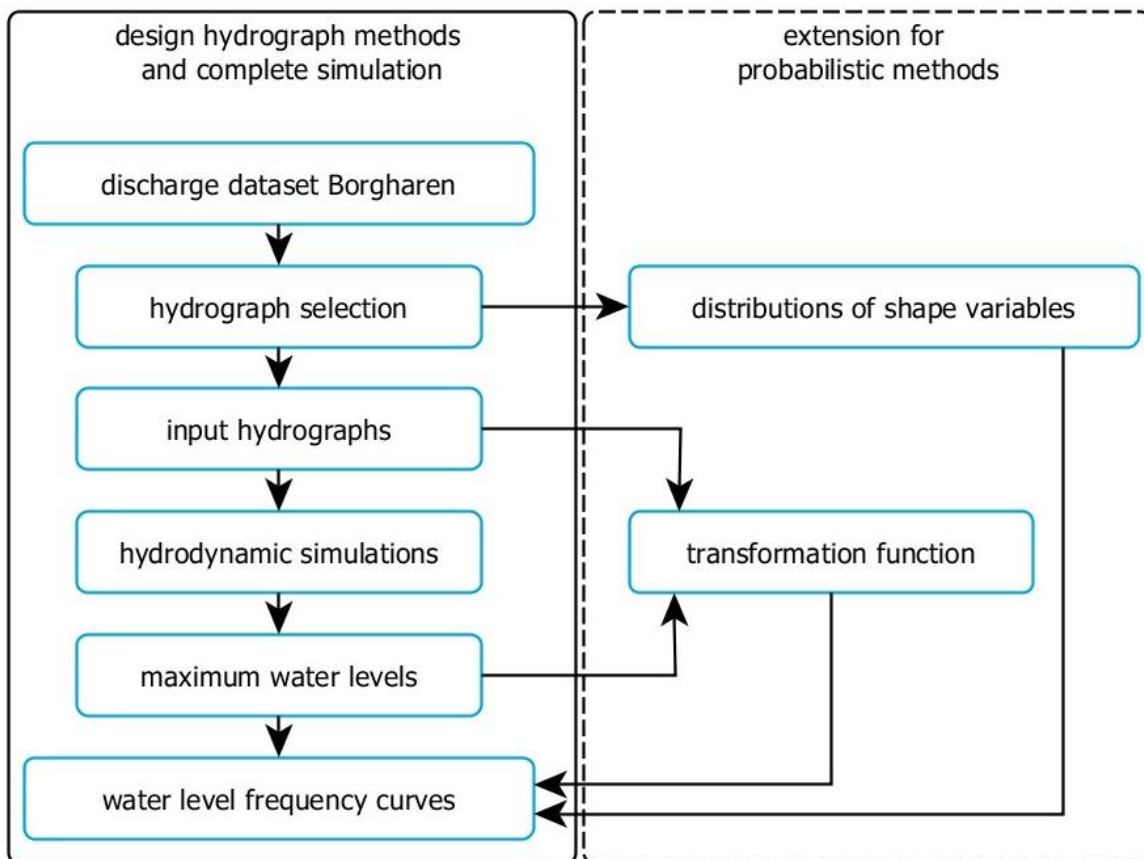
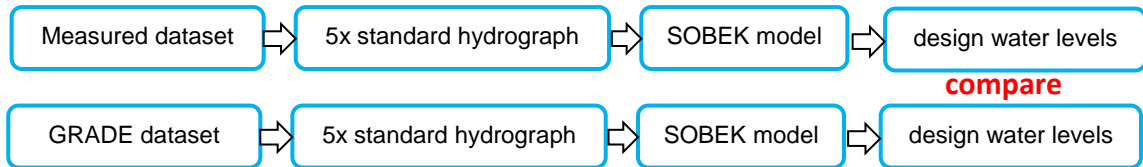


Figure 3-1 General outline of the research framework

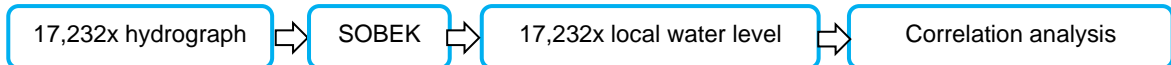
### Research question 1

To quantify the difference in design water levels between the measured and GRADE dataset, only part of the tools were used. There are two different discharge datasets (measured and GRADE) which were processed by the standard hydrograph method. Subsequently, these two hydrographs were used to simulate the downstream water levels with the 1D SOBEK Meuse model. Combining the downstream water levels with the peak discharge return period yields the design water levels of the two datasets, which were compared to each other.



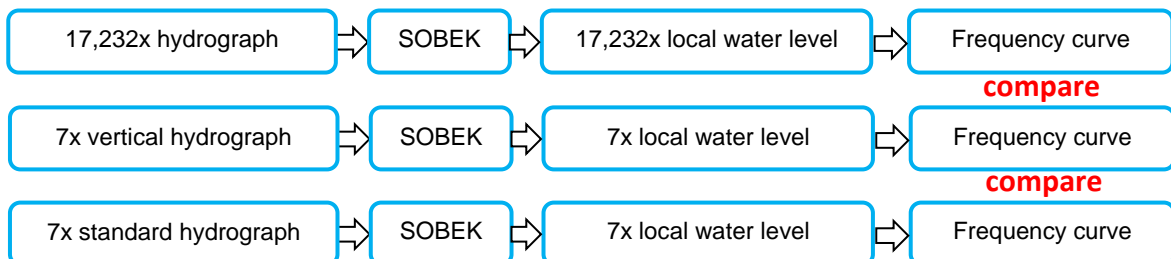
### Research question 2

To investigate the influence of hydrograph shape variables on the water levels, all hydrographs with a peak discharge larger than  $1750 \text{ m}^3/\text{s}$  were selected from the GRADE dataset (17,232 hydrographs), and the corresponding water levels simulated with SOBEK. For each hydrograph, also several shape variables like peak discharge, volume and duration were computed. A (conditional) correlation analysis between the local water levels and the hydrograph shape variables was used to show which variables have most impact on the local water levels. If strong conditional correlations are found, these shape variables can be used to predict local water levels. Transformation functions describe this relation between shape variables and local water levels, and are used in the probabilistic methods.



### Research question 3

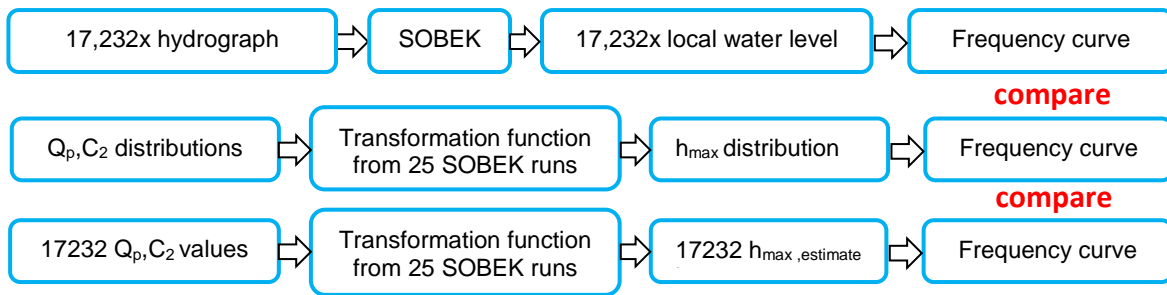
To quantify the accuracy of the design hydrograph methods, the complete simulation set of 17,232 simulations mentioned under *Research question 2* was used as reference. The standard and vertically averaged design hydrographs were derived from the GRADE dataset, and the corresponding local water levels simulated with SOBEK. The resulting design water levels were compared to the water level frequency line obtained from the reference set.



### Research question 4

To quantify the accuracy of the probabilistic methods, the complete simulation set mentioned under *Research question 2* was again used as reference. The transformation function was combined with the probability distributions (explicit method) or values (implicit method) of shape

variables at Borgharen to derive the local water level frequency line. This frequency line was compared to the one from the reference.



**Research question 5**

Next to the reference SOBEK model, an adapted SOBEK model was used in which the large retention basin Lob van Gennepe is excluded, which allows the determination of the effect of retention on the local water levels. The retention effect (= water level reduction) that is estimated with the design hydrograph methods and the probabilistic methods was compared to the effect of retention on the frequency line by simulation of the complete set (reference). To investigate the influence of shape variables on the retention effect, a similar analysis was carried out as for question 2; in this case the relation between shape variables and the retention effect is analysed.

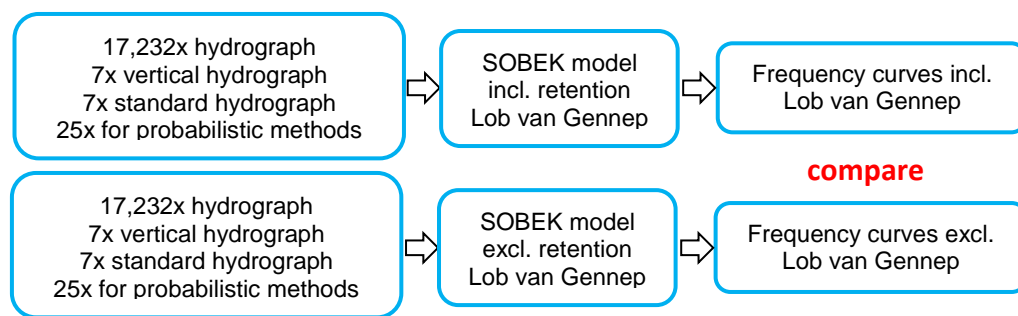


Table 3-1 gives an overview of the different methods that were used to determine design water levels or frequency curves, and shows which ones are used to answer specific research questions.

Method type	Method	Data	Hydrograph selection	Hydraulic model	Retention effect <sup>(5)</sup>
complete simulation <sup>(2)</sup>	reference	G	all hydrographs (17,232 in total)	S	yes
design hydrograph methods <sup>(3)</sup>	standard	G/M <sup>(1)</sup>	7x with standard shape	S/W	only SOBEK
	vertical	G	7x with vertically averaged shape	S/W	only SOBEK
probabilistic methods <sup>(4)</sup>	explicit	G	25x with different peak and shape	S/W	yes
	implicit	G	25x with different peak and shape	S/W	yes

G=GRADE, M=measured, S=SOBEK, W=WAQUA

<sup>(1)</sup> difference answers question 1.

<sup>(2)</sup> used to answer question 2 and reference for questions 3, 4 and 5.

<sup>(3)</sup> used to answer question 3.

<sup>(4)</sup> used to answer question 4.

<sup>(5)</sup> used to answer question 5.

**Table 3-1 Overview of methods to determine design water levels**

## 3.2 Data

The data that were used in the analyses consist mainly of discharge data at the gauging station at Borgharen, a village close to the location where the river Meuse enters The Netherlands. Two datasets were used: a measured discharge series and a discharge series that was simulated in GRADE.

### 3.2.1 Measured discharge data

Discharge measurements at Borgharen-dorp have been performed daily since 1911, and every 10 minutes since 1987. Actually, the measured water levels are transformed into a discharge series using a rating curve. More information on the measurement equipment and method that was used through the past years can be found in Jansen (2007). The measured series that was used for the construction of the standard hydrograph runs up to 31 December 2003.

### 3.2.2 Simulated GRADE discharge data

The GRADE discharge dataset is simulated with the methods described in section 2.4. The dataset used for this thesis was provided by Deltares with permission of Rijkswaterstaat. It has a 'length' of 50,000 years (previous datasets were 20,000 years) of simulated daily discharges at Borgharen. The daily discharges at Borgharen are the daily maxima of hourly discharges that are the output of the hydraulic model in GRADE. For this dataset, the HBV 50% parameter set was used for the parameters in the hydrological model (Kramer et al., 2008). This gives significantly better predictions of discharges than the original HBV parameters that were used before 2008. The GRADE instrument is still under development, so updated datasets may differ from previous ones.

## 3.3 Hydrograph selection

A basic step that is needed for all types of analyses is the selection of hydrographs from the time series of daily discharges. This selection reduces the amount of data strongly; instead of 365 data points per year, only the data that contain a flood event are kept. The rest of the data contain normal flow conditions, which are not relevant for the behaviour during extreme flood events. Different choices for hydrograph selection are possible, depending on the goal of the analysis for which they are used.

For the selection of flood events from the time series, both the AM and POT method can be used (see section 2.3.1). The AM method may lose some information when more than one extreme flood event occurs in the same hydrologic year, but the POT method has a larger risk of dependence between two successive flood events. For large datasets and large return periods, the difference between the POT and AM method is usually very small (Hamed & Rao, 2000). Since the GRADE dataset is very large (50,000 year) and the return periods of interest are usually far more than 10 years, the results will not differ significantly. For the probabilistic analysis the POT method with a threshold of  $1750 \text{ m}^3/\text{s}$  and a time window of 10 days was chosen. The value of  $1750 \text{ m}^3/\text{s}$  was chosen to avoid influence of weir operations. The time window of 10 days is more

arbitrary, but this value is used in other analyses as well and is approximately equal to the runoff time of a rainfall event. The application of these selection criteria leads to the selection of 17,232 hydrographs from the GRADE time series of 50,000 years.

### 3.3.1 Selection for standard design hydrographs

Both measured data and simulated GRADE data were transformed into a standard hydrograph (see section 2.3.2) by the wave shape generator (GVG) software. Only those hydrographs are selected that have a peak discharge between  $1750 \text{ m}^3/\text{s}$  and  $3200 \text{ m}^3/\text{s}$ , since this is the range of measured flood waves used for HR2001. Two peaks are considered two separate flood waves if the peaks are more than 10 days apart, or if the discharge drops below  $1000 \text{ m}^3/\text{s}$  between the two peaks. These selection criteria are also used in Klopstra & Vrisou van Eck (1999) and Barneveld & Van den Berg (2010).

An additional issue for the GVG is that it cannot handle a large number of data; it is limited to approximately 1800 floods. Therefore the total GRADE discharge series was cut in ten periods of 5000 years. Period 8 of the 10 gives almost the same hydrograph as the average hydrograph of the 10 periods (difference 0.01%). Therefore period 8 was considered a representative period for the 50,000 years, and thus this period was used to generate the standard hydrographs for the other peak discharges as well.

### 3.3.2 Selection for vertically averaged design hydrographs

The vertically averaged hydrograph shape was already included in the GRADE dataset, but these shapes were derived from a different selection than the standard hydrographs as stated in the paragraph above. The vertically averaged hydrograph with  $Q_p = 2600 \text{ m}^3/\text{s}$  was based on all hydrographs from the peak discharge interval  $2500 - 2750 \text{ m}^3/\text{s}$ . The hydrographs with larger peak discharges were based on all hydrographs from the peak discharge interval  $3000 - 5000 \text{ m}^3/\text{s}$ . This shape is more peaked than the one for  $Q_p = 2600 \text{ m}^3/\text{s}$ .

### 3.3.3 Modified selection for design hydrographs

A modification of the standard and vertically averaged hydrograph methods is to use only hydrographs with a similar peak discharge as the design peak discharge. This modified selection interval is used to investigate the dependence of the design hydrograph shape on the magnitude of the peak discharge. For example, to determine the design hydrograph with a peak discharge of  $4400 \text{ m}^3/\text{s}$ , only the hydrographs with a peak discharge between  $4000$  and  $4600 \text{ m}^3/\text{s}$  are used for averaging (Table 3-2). These selection intervals were set equal for both the standard and the vertically averaged hydrographs, in order to make results better comparable. This much smaller interval makes the subdivision into ten periods for use in the GVG unnecessary.

Peak discharge $Q_p$ [ $\text{m}^3/\text{s}$ ]	2600	3280	3800/4000	4200/4400/4600
Selection interval [ $\text{m}^3/\text{s}$ ]	2500-2700	3100-3500	3500-4000	4000-4600
Nr. of hydrographs [-]	1124	457	78	28

**Table 3-2 Modified selection intervals of standard and vertically averaged hydrographs**

### 3.3.4 Selection for probabilistic methods

The probabilistic methods use two different hydrograph selections. The largest selection of all 17,232 hydrographs is used to derive the probability distributions of the hydrograph shape variables. A much smaller selection of 25 hydrographs that covers the variation in hydrograph shape is used in hydrodynamic simulations to estimate the relation between hydrograph shape variables and local water levels. These 25 hydrographs are selected from the set of 17,232 hydrographs.

## 3.4 Hydrodynamic simulations

The hydrodynamic models SOBEK (1D) and WAQUA (2D) were used to simulate the flow in the river for a given input hydrograph. The following sections discuss the (common) inputs for the two hydrodynamic models.

### 3.4.1 Common input of SOBEK and WAQUA

The WAQUA and SOBEK models of the Meuse both use data from Baseline, a database that contains the river schematisation. This database includes characteristics such as surface elevation, roughness, structures, boundary conditions and initial conditions. Therefore, many model input features are the same for both model types. This section treats these common features.

The most recent Meuse schematisation that was available at the start of the research was used for this thesis (schematisation *maas-j13\_4-v3*). This schematisation was released in 2013 as result of JAMM2013 (Dutch acronym for Jaarlijkse Actualisatie Modellen Maas; Annual Update of Meuse Models). It reflects the actual river system, and does not contain planned measures such as parts of the Maaswerken project that have not been completed yet. The schematisation covers the Dutch part of the river Meuse, between Eijsden (km 2.56) and Keizersveer (km 247).

#### Lateral inflow

Discharge from Dutch tributaries, canals and outlet sluices contributes to the total flow pattern in the river. Although in reality the magnitude and timing of many lateral inflows is also an uncertain variable, deterministic relations with the discharge at Borgharen were used. The lateral discharges corresponding to each hydrograph at Borgharen were computed with a beta version of the software Hulpprogrammatuur 2.10 made available by Rijkswaterstaat. The principles of the computation of these lateral discharges can be found in Van der Veen (2005a), and are explained in short below. The discharge of the larger tributaries (Geul, Geleenbeek, Roer, Neerbeek, Niers, Dommel and Aa) is found by application of a regression function between measured discharges at Borgharen and in the tributary. The regression coefficients (see Appendix B) are based on discharges up to the year 2003. Additionally, some modifications are made for the travel times between the measuring station and the confluence with the main river. Discharges of minor tributaries are assumed to be related to a similar large tributary, proportionally by the catchment area. Some lateral discharges are limited by high water levels in the Meuse, which is taken into account.

The weakness of using these regression relations is that they assume a direct relation between tributary discharge and main river discharge. Often, the peak discharge of Dutch tributaries is caused by local rainfall, and not by the event that caused the floods in the main river (Van der Veen, 2005a). Extrapolation of regression functions also does not take into account nonlinear behaviour at high discharges, such as inundations or backwater effects. These weaknesses could be avoided when GRADE is extended to the Dutch part of the basin.

### Upstream boundary conditions

The longest record of discharge measurements is available at station Borgharen-dorp, which is 16 km downstream of the Belgian-Dutch border at Eijsden. The GRADE discharges are simulated at Borgharen as well. However, the upstream boundary of the Meuse model is located at Eijsden. To account for this difference in peak discharge and timing, Van der Veen (2005b) proposed:

$$Q_{max,Eijsden} = Q_{max,Borgharen} - \beta \quad [m^3/s] \quad (3.1)$$

$$t_{Q_{max,Eijsden}} = t_{Q_{max,Borgharen}} - \tau \quad [\text{minutes}] \quad (3.2)$$

$\beta$  depends on the peak discharges, and accounts for the combined effect of lateral discharges and flood plain storage between Eijsden and Borgharen.  $\tau$  is set to 120 or 180 minutes. Van der Veen (2005b) found a discharge-dependent value for  $\beta$  that gave reasonable results for a range of hydrographs with a standard shape (from the GVG). The term ranges from 11 m<sup>3</sup>/s for lower peak discharges to 3 m<sup>3</sup>/s for higher peak discharges.

However, these values lead to a bias in the peak discharge at Borgharen in the order of 10 - 60 m<sup>3</sup>/s when the current SOBEK Meuse model is used. This is most likely caused by a retention area in Maastricht (rkm 10) and other storage effects. Moreover,  $\tau$  and  $\beta$  were derived with standard hydrographs, whereas the peak attenuation may behave differently under other hydrograph shapes. Figure 3-2 gives the peak attenuation between Eijsden and Borgharen for 250 random GRADE hydrographs. It can be seen that there is only a weak relation between peak discharge and peak attenuation between Eijsden and Borgharen. Since this extra error was considered unacceptable for our research, it was decided to adapt the SOBEK and WAQUA models in such a way that station Borgharen serves as an upper boundary, instead of Eijsden.

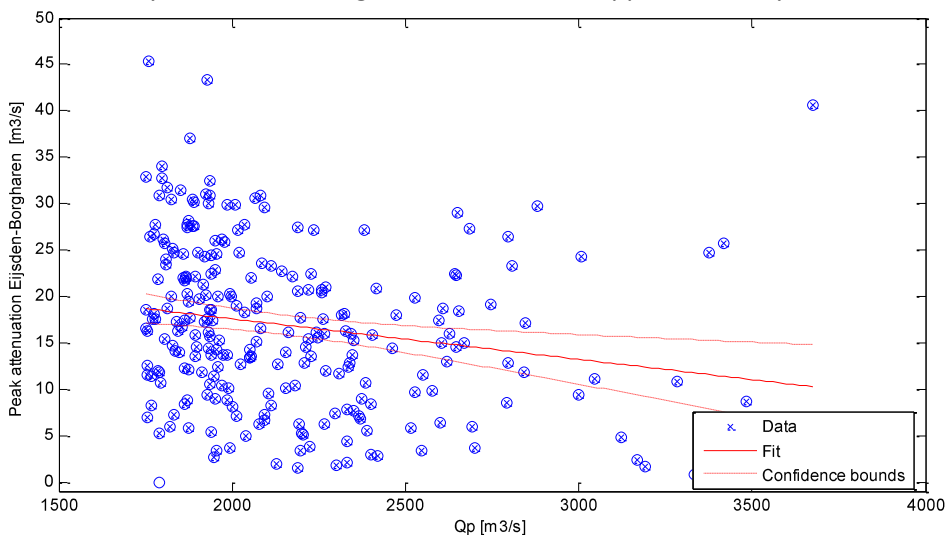


**Figure 3-2 Peak attenuation Eijsden-Borgharen as function of peak discharge Borgharen**

### 3.4.2 SOBEK Meuse

The SOBEK Meuse model is built and simulated in SOBEK-River/Estuary (RE), version 2.52.009. SOBEK is a one dimensional model; the river is schematized in stretches of approximately 500 m that have the same characteristics such as cross section or roughness. Cross sections can be composed of different parts, and roughness can be specified for each part separately. For the batch simulations a computation time step of 1 hour was used, and a simulation time of 31 days.

#### Conditions

The initial discharge at all river stretches was  $Q = 125 \text{ m}^3/\text{s}$ . In some cases, the hydrograph starts with a relatively high discharge, e.g.  $1500 \text{ m}^3/\text{s}$ . In that case, the discharge will increase quickly from 125 to e.g.  $1500 \text{ m}^3/\text{s}$  which may cause (limited) instabilities in the discharge at the first stretch of the model. For some hydrographs, this results in outliers of the maximum discharge at Borgharen.

After adaptation of the model, the upstream boundary is just upstream of Borgharen. The boundary condition at this point is simply a design hydrograph or the hydrographs from GRADE. At the downstream boundary Keizersveer a constant water level of 0 m +NAP was applied. Other boundaries (such as the locks at Nijmegen) were given a discharge of  $0 \text{ m}^3/\text{s}$ .

#### Retention in SOBEK

Retention is modelled in SOBEK as a large basin with an inflow structure and an outflow structure. The retention area Lob van Gennep has a uniform bottom depth of 12.54 m +NAP, and the area (1769 ha) is constant for all water levels. The inflow structure is a weir with a crest level at 13.75 m +NAP, a length of 1500 m and allows flow in both directions. The outflow structure is a weir with a crest level at 12.65 m +NAP and a length of 300 m, and it only allows flow back to the river. The name of the retention area is 'Otters\_ret' which refers to Ottersum, a close by village. It is located at the river reach 'zandmaas6,22650'. To get a SOBEK model without Lob van Gennep, one can simply switch it off in the user interface. In case of running SOBEK in batch (as was done in our case), one has to change the model input files. The command lines defining the retention basin can be removed, or the crest level ( $z_s$ ) of all retention areas set to 99 m +NAP.

#### Output locations

To limit the number of data and computations, the probabilistic analysis was carried out for only five locations. Therefore SOBEK output was generated only for the locations Borgharen, Maaseik, Venlo, Mook and Megen (see Table 3-3 and Figure 3-3). The full results for other locations are available for future research, but not yet transformed to readable format and not analysed.

no.	location name	river km	SOBEK location code
1	rkm 14.84	14.84	Grensms1_.00
2	Borgharen-dorp	16.00	Grensms2_.00
3	Maaseik	52.73	Grenms3a_.00
4	Venlo-Blerick	107.48	Zandmas4_.00
5	Mook	165.8	Zandmas7_.00
6	Megen	190.72	Zandmas7_24810.00

**Table 3-3 Output locations for hydrodynamic simulations**

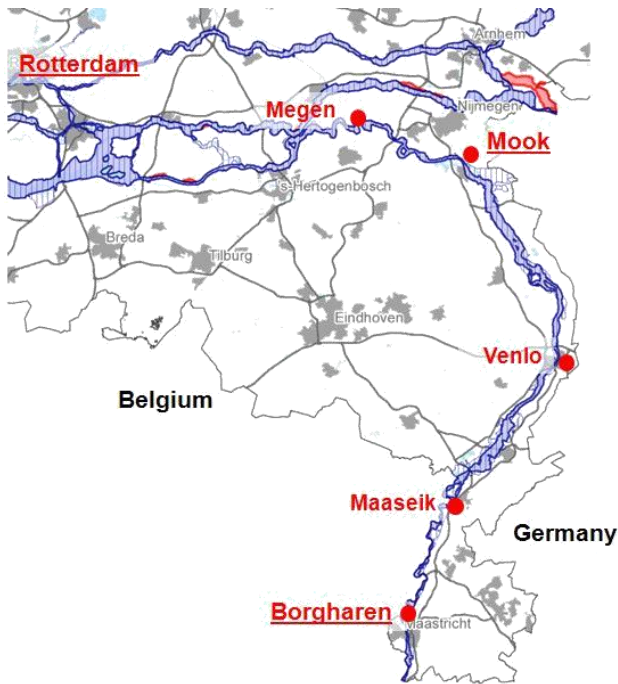


**Figure 3-3 Main output locations of hydrodynamic models**

### Batch Tool

To manage the large amount of data and simulations that is needed for the SOBEK simulations of all GRADE hydrographs, a batch tool was used. This tool automatically picks the right input files such as boundary conditions or weir height for every hydrodynamic simulation, and also writes the desired output to a predefined location. A description can be found in Appendix A.

### 3.4.3 WAQUA Meuse

The WAQUA simulations were carried out with SIMONA 2013. The 2D approach of WAQUA allows a better modelling of local effects such as the inflow to retention basins. Interaction with groundwater is not included in the model, which may have influence at locations in the southern part where large amounts of gravel are present. The spatial resolution of the WAQUA grid is generally 40 m, but in sharp river bends this can be lower than 10 m. Generally, a computation time step of 15 seconds was used.

### Conditions

The boundary conditions are similar to the ones that were used for SOBEK, except that WAQUA uses a line instead of a point as upstream boundary. After cutting off the model at the upstream side of Borgharen, the input hydrograph was imposed on this boundary (see Appendix B).

### Retention in WAQUA

Higher line elements such as dikes are represented in WAQUA with weirs with a specified crest height (per grid cell). These weirs delineate the retention area Lob van Gennepe (see Appendix B). No inflow location is defined beforehand, so inflow can occur at multiple locations depending on the water level in the river. To exclude the Lob van Gennepe from the model, all weirs that enclose the retention area were raised to 99 m +NAP.

### 3.5 Statistical analysis

From the GRADE discharge time series at Borgharen, flood waves were selected that have a peak discharge larger than 1750 m<sup>3</sup>/s and have no higher peak in a time window of 10 days to meet the condition of independence. For each selected flood wave, the shape variables peak discharge, volume, duration and peak curvature were determined.

#### 3.5.1 Calculation of shape variables from selected flood wave

From literature it is known that (relative) volume, duration and peak curvature may be influential (e.g. Gerretsen, 2009). These variables can be defined in different ways with regard to the discharge threshold level (see Table 3-4 and Figure 3-4). The duration at the 1250 m<sup>3</sup>/s level may have a different distribution than the duration at 85% of the peak discharge. Four threshold levels were chosen: 0 m<sup>3</sup>/s, 1250 m<sup>3</sup>/s (bankfull level), 50% of the peak discharge, and 85% of the peak discharge.

Variable	Definition	Unit
$Q_p$	Maximum discharge in a flood wave	m <sup>3</sup> /s
$D_{1250}$	The duration that the discharge is higher than the level $Q = 1250$ m <sup>3</sup> /s	hour
$D_{50\%}$	The duration that the discharge is higher than the level $Q = 0.5Q_p$	hour
$D_{85\%}$	The duration that the discharge is higher than the level $Q = 0.85Q_p$	hour
$V_0$	The flood volume above the level $Q = 0$ (total volume)	m <sup>3</sup>
$V_{1250}$	The flood volume above the level $Q = 1250$ m <sup>3</sup> /s	m <sup>3</sup>
$V_{50\%}$	The flood volume above the level $Q = 0.5Q_p$	m <sup>3</sup>
$V_{85\%}$	The flood volume above the level $Q = 0.85Q_p$	m <sup>3</sup>
$RV_0$	$V_0$ divided by the product of the total duration and peak discharge	-
$RV_{1250}$	$V_{1250}$ divided by the product of $D_{1250}$ and $Q_p$ relative to level $Q = 1250$ m <sup>3</sup> /s	-
$RV_{50\%}$	$V_{50\%}$ divided by the product of $D_{50\%}$ and $Q_p$ relative to level $Q = 0.5Q_p$	-
$RV_{85\%}$	$V_{85\%}$ divided by the product of $D_{85\%}$ and $Q_p$ relative to level $Q = 0.85Q_p$	-
$C_1$	Curvature around the peak discharge, between one day prior to the peak and one day after the peak, normalized with the peak discharge	s <sup>-2</sup>
$C_2$	As $C_1$ , but two days prior to the peak and two days after the peak	s <sup>-2</sup>

**Table 3-4 Analysed hydrograph shape variables**

The peak discharge of a hydrograph is by definition the maximum discharge in the hydrograph:

$$Q_p = \max(Q) \quad [\text{m}^3/\text{s}] \quad (3.3)$$

There were three events in the GRADE dataset that exceeded the maximum peak discharge of 4600 m<sup>3</sup>/s: 4605 m<sup>3</sup>/s (nr. 4731), 4622 m<sup>3</sup>/s (nr. 10100) and 4971 m<sup>3</sup>/s (nr. 6760). These hydrographs were cut off above the 4600 threshold (see section 2.4.3).

The duration at some level L is the time that the discharge is higher than that level, so secondary peaks in the time window add to the flood duration.

The flood volume above a discharge level  $L$  was calculated with the trapezium rule and an hourly time step:

$$V_L \approx \sum_{i=1}^{481} \max \left[ \frac{1}{2} (Q_{i-1} + Q_i - 2Q_L)(t_i - t_{i-1}), 0 \right] \quad [\text{m}^3] \quad (3.4)$$

The index 481 comes from 20 days \* 24 hours + 1.

The relative volume was calculated as:

$$RV_L = \frac{V_L}{D_L * (Q_p - Q_L)} \quad [-] \quad (3.5)$$

The peak curvature was approximated by the second derivative of the discharge around the peak, scaled by  $Q_p$  in the denominator:

$$C_1 = - \frac{Q_{tp-1} + Q_{tp+1} - 2 \cdot Q_p}{Q_p \cdot dt^2} \quad [\text{s}^{-2}] \quad (3.6)$$

$$C_2 = - \frac{Q_{tp-2} + Q_{tp+2} - 2 \cdot Q_p}{Q_p \cdot dt^2} \quad [\text{s}^{-2}] \quad (3.7)$$

Where:  $dt=3600$  s for  $C_1$ ,

$dt=7200$  s for  $C_2$ .

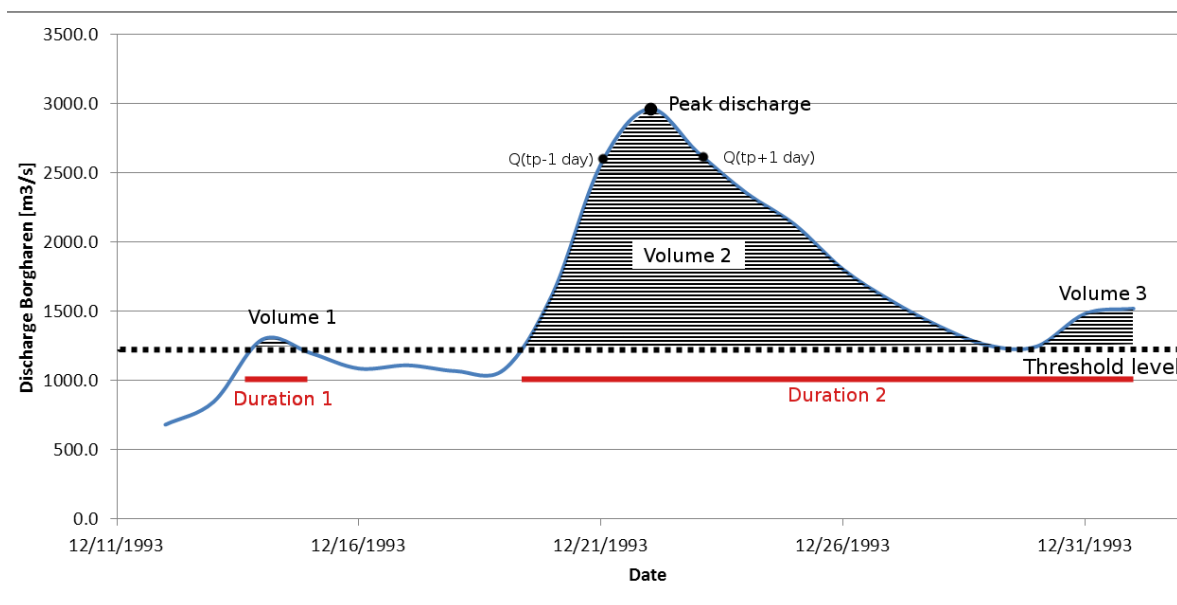


**Figure 3-4 Definition of hydrograph shape variables**

Some remarks need to be given on these variables:

- The total volume  $V_0$  strongly depends on the choice of the time interval. The arbitrariness of the choice makes this variable less useful. The same holds to a lesser extent for the other volume and duration variables in the lower discharge range.
- The level  $Q = 0.5Q_p$  is for flood waves with  $Q_p < 2500$   $\text{m}^3/\text{s}$  below the bankfull ( $1250$   $\text{m}^3/\text{s}$ ) level.  $D_{50\%}$  and  $V_{50\%}$  are therefore sometimes below bankfull and sometimes above bankfull, which may cause a different behaviour.
- The peak curvature  $C_2$  is strongly influenced in the case of a secondary peak two days before or after the peak.

### 3.5.2 Selection of relevant hydrograph shape variables

To limit the complexity of the probabilistic calculations, assumptions are to be made about which shape variables influence the design conditions most. Variables that are less influential can be left out of the analysis. The choice of variables was based on a correlation analysis and on some simulations with synthetic hydrographs.

#### Correlation analysis

Many variables such as duration, volume or peak curvature (section 3.5.1) can be quantified. The influence of these variables was analysed by a correlation analysis. A first indication of influence is given by (rank) correlation coefficients between variables  $X$  and  $Y$ , such as the ones of Pearson (Equation 3.8) or Spearman (Equation 3.9).

$$\rho_p(X,Y) = \frac{COV(X,Y)}{\sigma_X \sigma_Y} = \frac{E[XY] - E[X]E[Y]}{\sigma_X \sigma_Y} \quad (3.8)$$

$$\rho_s(X,Y) = 1 - \frac{6 \sum (x_i - y_i)^2}{n(n^2 - 1)} \quad (3.9)$$

Where  $x_i$  is the rank of  $X_i$  and  $n$  is the sample size.

The advantage of the rank correlation is that this measure is able to detect non-linear relations as well and is less sensitive to outliers. The correlation coefficients give an average correlation between two variables. To assess the correlation structure in more detail, scatterplots or rank scatterplots were used. These plots show how the correlation is distributed over the domains of the variables. For example, the behaviour in the extreme domain is often of most interest to the analysis of extreme water levels.

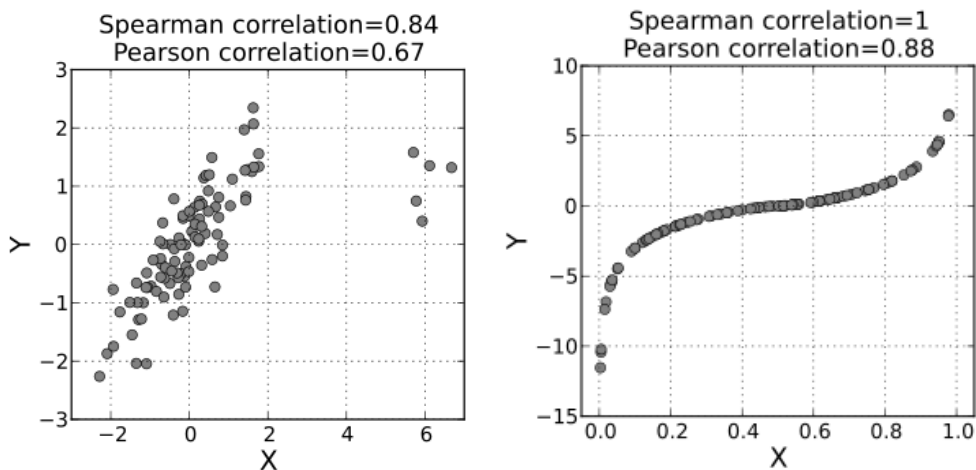
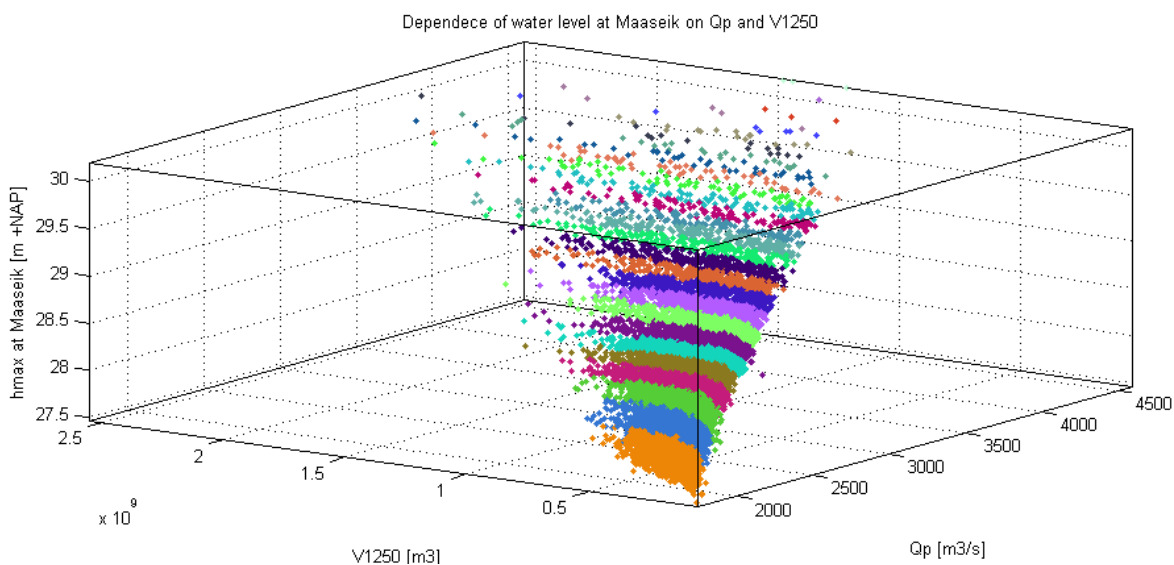


Figure 3-5 Pearson and Spearman correlation coefficients of non-linear relations

A predictor (or independent) variable that is strongly correlated to the response (or dependent) variable is considered a good predictor. However, the correlation coefficient shows only the correlation between the single predictor variable and the response variable. It does not indicate whether a second predictor variable improves the prediction in addition to another one. The amount of additional predictive value can be described with the conditional correlation coefficient  $\rho_{X,Y|Z}$ . This coefficient gives the (rank) correlation between the variables  $X$  and  $Y$ , given variable  $Z$ . In our case  $X$  equals  $h_{\max,x}$ ,  $Z$  equals the shape variable with the highest correlation  $\rho_{X,Z}$  and  $Y$  equals some other shape variable.

All data are divided into classes of  $Z$ , which are small but contain sufficient data to determine the correlation coefficient in a meaningful way. For each class, the rank correlation between  $X$  and  $Y$  is determined. In general, the conditional correlations vary over the domain of  $Z$ , and can both increase or decrease with  $Z$ . A useful statistic is the mean of the conditional correlation coefficients, averaged over  $Z$ . This mean is indicated by  $\overline{\rho_{X,Y|Z}}$ .

An illustration of the relevance of the conditional correlation is visualized in Figure 3-6. Both  $Q_p$  and  $V_{1250}$  are strongly correlated to the water level, but because of their mutual dependence  $V_{1250}$  does not give much information about  $h_{\max}$  in addition to the information from  $Q_p$ . This is indicated by the almost horizontal bands (the colours refer to different  $Q_p$  classes) in the upper peak discharge range. The conditional correlation coefficient is determined for each class (=colour) and equals approximately zero for the horizontal bands.



**Figure 3-6 3D scatterplot of  $h_{\max}$ ,  $Q_p$  and  $V_{1250}$ . Colours indicate peak discharge classes.**

### Synthetic hydrographs: base flow

There are different methods to separate the base flow in a hydrograph from the direct runoff that is directly related to a rainfall event (Gonzales et al., 2009). However, in the real Meuse hydrographs it is hard to separate base flow and rapid surface flow because flood waves are complex and composed of many contributions of tributaries. There is no clear start or end of the flood peak, which makes automated base flow separation not practical. In order to investigate the importance of a correct representation of the base flow, a number of synthetic hydrographs were constructed. The shapes of these synthetic hydrographs are based on the standard hydrograph for  $Q_p = 4000 \text{ m}^3/\text{s}$ , but have a different base flow, varying between  $125 \text{ m}^3/\text{s}$  and  $1500 \text{ m}^3/\text{s}$ .

### 3.5.3 Univariate distributions of shape variables

The hydrograph shape variables can be described by probability distribution functions. Theoretical considerations point out that the distribution type of  $Q_p$  should be a Generalized Pareto Distribution (GPD) since all Peaks Over Threshold (POT) processes lead to a GPD (Pickands, 1975).

Different parametric distributions were fitted to the realizations of each shape variable using maximum likelihood estimation of the parameters. The likelihood of a parameterset  $\theta$  given the observed variables  $x_i$  is expressed as:

$$L(\theta|x_1, \dots, x_n) = \prod_{i=1}^n f(x_i|\theta) \quad (3.10)$$

So parametersets for which the observed values are more likely, have a higher likelihood. The function type and parameterset with the maximum likelihood was chosen to model the distribution. The Matlab function *allfitdist* was used to automate this procedure.

The parametric distribution fit deviates sometimes in the tails of the distribution. For example in the case of  $Q_p$ , this leads to an overestimation of the peak discharge for a given exceedance probability. Kernel distributions are a non-parametric alternative that can also describe less smooth distributions of the data. This Kernel was applied to  $Q_p$  to eliminate the effect of the deviation from the GPD in the upper tail. A Kernel distribution is described by:

$$f(x) = \frac{1}{nh} \sum_{i=1}^n K\left(\frac{x-x_i}{h}\right) \quad (3.11)$$

where  $n$  is the sample size,  $K(\cdot)$  is the kernel smoothing function,  $h$  is the bandwidth. A Gaussian smoothing function  $K(\cdot)$  was used, so the Kernel distribution can be seen as the superposition of normal distributions at each data point (Figure 3-7, left). A larger bandwidth  $h$  produces a smoother fit, whereas a smaller bandwidth produces a more peaked fit (Figure 3-7, right). The default bandwidth was applied, which was equal to 45.

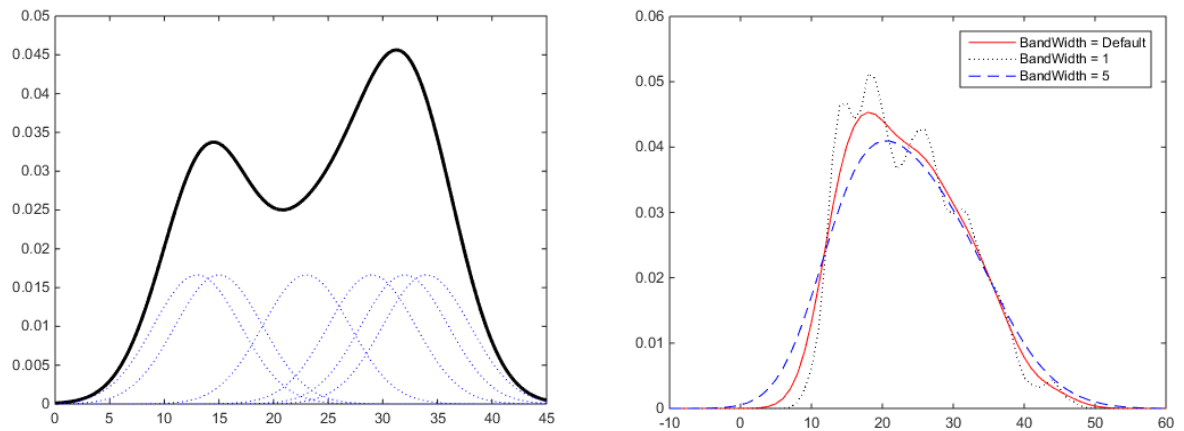


**Figure 3-7 Illustration of Kernel distribution**

### 3.6 Probabilistic analysis

The aim of the probabilistic analysis is to find the probability that a water level on a particular location at the river is exceeded per year. This exceedance probability was found by combining the statistics of GRADE hydrographs at Borgharen with hydrodynamic model results. The statistical analysis provides the (joint) probability distributions of the hydrograph shape variables (e.g.  $Q_p$ ,  $D$ ,  $V$ ,  $C$ ). The hydrodynamic calculations provide the water levels as a function of the shape variables  $h_x(Q_p, D, V, C)$ , and thus the combination of shape variables that lead to a water

level downstream. Combining the joint distribution and the transformation function gives the probability that the critical values of the shape variables (and thus the water levels) are exceeded:  $P(H > h_x)$ . The procedure to determine this probability is explained in the following sections.

### 3.6.1 Local water level estimation based on shape variables

An important aspect is the modelling of the local water levels as a function of the shape variables at Borgharen, i.e. to find a function  $h_x = f(Q, D, V, C) + \varepsilon$ . This function is called the transformation function since it transforms the hydrograph variables at Borgharen to water levels downstream. There are three different datasets on which the transformation function was based:

1. SOBEK results of the 25 selected hydrographs
2. WAQUA results of the 25 selected hydrographs
3. SOBEK results of the complete set of hydrographs

In practice, only the first two datasets are suitable for a quick analysis of the design water level since only a limited amount of hydrodynamic simulations are needed. The third dataset is used to investigate the relations in more detail and to test the suitability of simple transformation functions. The function type was limited to simple polynomials of one or two degrees. In some cases it may be useful to apply a transformation on the variables before fitting the polynomial function.

To improve the readability of these sections, it is stated in advance of the results that the variables peak discharge  $Q_p$  and the peak curvature  $C_2$  were chosen to predict the downstream water levels. The reasons for this choice are given in section 4.2.1.

#### Selection of 25 hydrographs

The 25 selected hydrographs cover five classes of  $C_2$  and five classes of  $Q_p$  (see Table 3-5) to make sure that the selection contains a varied set with different peak discharges and hydrograph shapes. The range of  $C_2$  was divided into five class intervals, with a corresponding class mean. Also, five distinct peak discharges were determined. Hydrographs which characteristics approximate the  $C_2$  class means ( $\pm 1 \text{ s}^{-2}$ ) and peak discharges ( $\pm 1 \%$ ) were selected from the complete set. If more hydrographs fulfilled the requirements, one of them was chosen randomly. These requirements were eased for the  $Q_p = 4500 \text{ m}^3/\text{s}$  class since there are only a few hydrographs in this range. As a result, those estimates will be less accurate.

C <sub>2</sub> class [s <sup>-2</sup> ] (and class mean)	Peak discharge Q <sub>p</sub> class [m <sup>3</sup> /s]				
	2500	3000	3500	4000	4500
0-12 (9.146)	nr. 12250	nr. 1251	nr. 7886	nr. 15732	nr. 15737
12-18 (15.26)	nr. 2815	nr. 8796	nr. 12399	nr. 6716	nr. 13668
18-24 (20.85)	nr. 12616	nr. 2847	nr. 576	nr. 1321	nr. 4731
24-30 (26.45)	nr. 14035	nr. 5887	nr. 9825	nr. 8442	nr. 327
30-max (32.13)	nr. 5100	nr. 9372	nr. 8508	nr. 4708	nr. 6760

Table 3-5 Numbers of selected hydrographs for the probabilistic approach with  $C_2$

### 3.6.2 Explicit probabilistic method

The explicit method uses expressions for the probability distributions of the shape variables. This analysis needs three main elements:

- The function  $h_{\max,x} = f(Q_p, C_2)$ : section 3.6.1
- The probability distribution for  $Q_p$ : section 3.5.3.
- The probability distribution for  $C_2$ : section 3.5.3

The method is an adaptation of the approach described by Geerse (2013). The differences with the approach of Geerse are that  $C_2$  is used instead of  $D_{85\%}$ , and that a polynomial is used to fit the function of  $h_{\max,x}$  instead of interpolation between the given points.

The aim is to derive an exceedance frequency for every water level at location  $x$  along the river. Figure 3-8 illustrates how this can be interpreted. To construct an exceedance frequency curve at some location, the exceedance frequency must be determined for every local water level. For any local water level of interest (e.g. 12 m +NAP at Mook) there is an equal level curve that describes the combinations of  $Q_p$  and  $C_2$  at Borgharen that lead to this water level. The equal level curves are derived from the transformation function  $h_{\max, \text{Mook}} = f(Q_p, C_2) = 12 \text{ m +NAP}$ . This function contains the results of the hydrodynamic simulations. The hydrograph shape statistics are represented by the scatterplot of the values of  $Q_p$  and  $C_2$  for each hydrograph. This scatterplot is equivalent to the joint probability density function of  $Q_p$  and  $C_2$ . The probability that the water level at Mook exceeds the level of 12 m +NAP given a flood hydrograph at Borgharen,  $P(H_{\text{Mook}} > 12 \text{ m})$ , is equal to the fraction of points that is at the right hand side of the 12 m curve (red points). These red points lead to a water level higher than 12 m +NAP. The found exceedance probability is rewritten to a return period. Repeating this computation for a range of water levels yields the water level frequency line.

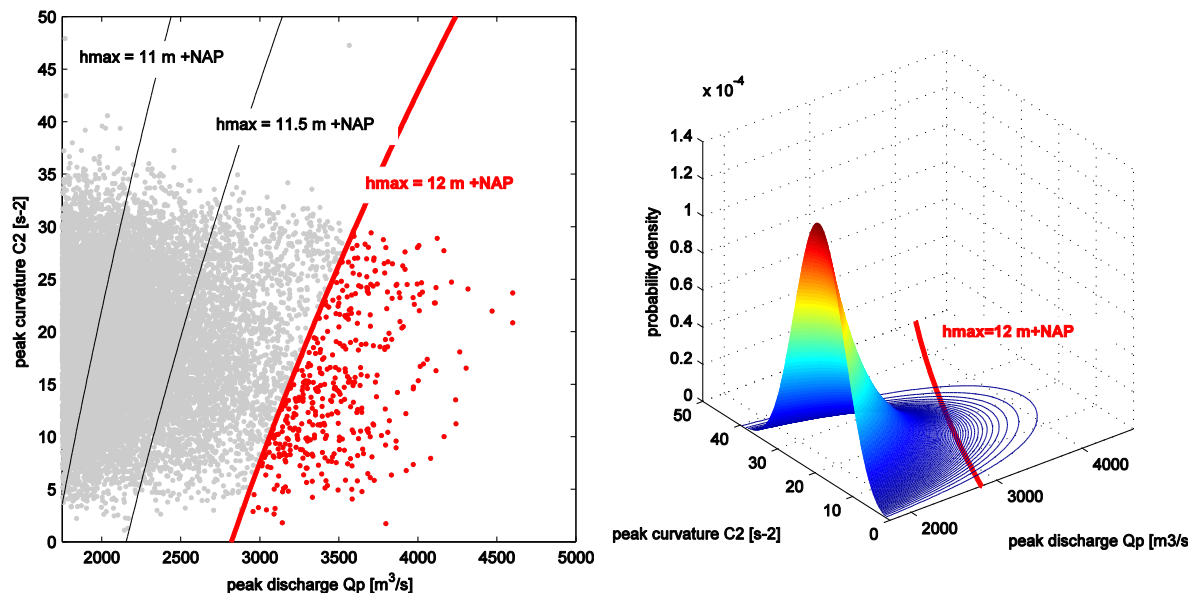


Figure 3-8 Illustration of the explicit probabilistic method

## Equations

A more formal description of the explanation given above, is given in the form of equations. First, an expression is given for the case where the probability distributions are continuous. Second, also an expression for a discrete distribution of  $C_2$  is given. To make the equations that describe the exceedance probability more compact, we define:

$$q_c = q_p(h_{max,x}, c_2), c = c_2, q = q_p, h = h_{max,x}$$

So the critical discharge  $q_c$  is the peak discharge at Borgharen that, in combination with the peak curvature  $C_2$ , leads to the local water level  $h$  at location  $x$ . This is the peak discharge on the equal level curve of  $h$  where  $C=c$ .

The probability that the water level at location  $x$  is exceeded for a hydrograph is given by the volume under the joint pdf that is at the right hand side of the equal level curve:

$$P(H > h) = \int_h^\infty f(h) dh = \int_{-\infty}^\infty \int_{q_c}^\infty f(q, c) dq dc \quad (3.12)$$

If  $Q_p$  and  $C_2$  are independent the joint pdf  $f(q, c)$  can be written as  $f(q) \cdot f(c)$ , in which case the probability of exceedance is given by:

$$P(H > h) = \int_{-\infty}^\infty f(c) \int_{q_c}^\infty f(q) dq dc \quad (3.13)$$

$P(H > h) \cdot \lambda$  is then the exceedance probability per year, where  $\lambda = \frac{17,232}{50,000} = 0.345$  is the average number of flood hydrographs in a year. The return period of the water level is the inverse of this yearly probability and is given by:

$$T(h) = \frac{1}{P(H > h) \cdot \lambda} \quad (3.14)$$

Since equation 3.13 can be written in terms of the local water level  $h$ , and a number of distribution constants, the return period  $T$  can be plotted as function of  $h$ .

In case that a discrete distribution is used for  $C_2$ , equation 3.13 is replaced by:

$$P(H > h) = \sum_c P(Q > q_c) P(C = c) \quad (3.15)$$

### 3.6.3 Implicit probabilistic method

The implicit method needs no assumptions about (parametric) probability distributions of  $C_2$  and  $Q_p$ . The transformation function  $h_{max,x} = f(Q_p, C_2)$ , which is based on a small set of hydrodynamic simulations, is used to estimate the local water level  $h_{max,x,estimate}$  of every hydrograph without using a SOBEK or WAQUA simulation. The result is a set of 17,232 estimated local water levels, which is used to construct the water level frequency line by use of plotting positions (section 2.3.1). Although this method uses no explicit distributions of the shape variables, it takes these probabilities implicitly into account by using all GRADE hydrographs. Therefore this method is also considered a probabilistic method. A disadvantage of the implicit method is that it gives no parametric function for the water level frequency line, but when GRADE is used this is no problem because of the large size of the dataset.

## 4 Results

The results are structured in sections according to the research questions: the effect of using the GRADE dataset (4.1), the influence of shape variables (4.2) and statistics of these variables (4.3), the reference set of complete simulation (4.4), the design hydrograph methods (4.5), the probabilistic methods (4.6) and the effect of retention (4.7). To keep the chapter short, sometimes only the results for location Mook are shown. Mook was chosen because at that location the effects of hydrograph shape are best visible. Results of additional locations are shown in the Appendices.

### 4.1 Effect of using GRADE discharge data

Figure 4-1 shows the standard hydrograph based on the GRADE dataset and the one based on the measured dataset, for a peak discharge of 4000 m<sup>3</sup>/s. Both shapes were determined by processing the floods with a peak discharge between 1750 and 3200 m<sup>3</sup>/s by the wave shape generator (GVG). For reference, the results from an earlier GRADE dataset (Barneveld & Van den Berg, 2010) are shown as well. Differences between the current result and the result of Barneveld and Van den Berg may be caused by differences in rainfall resampling techniques and the hydraulic routing method between the older and more recent GRADE datasets. The standard hydrographs from the GRADE dataset are wider than the ones from the measured dataset. This could be explained by the use of a daily time step in GRADE, which could be too large to capture the dynamical behaviour of the river Meuse. For the hydrograph with a peak discharge of 4000 m<sup>3</sup>/s, the duration of rise is approximately 15 hours longer and the duration of fall approximately 25 hours. The standard hydrographs for other peak discharges are given in Appendix F, and show similar results. A base flow of 1000 m<sup>3</sup>/s was applied to all standard hydrographs.

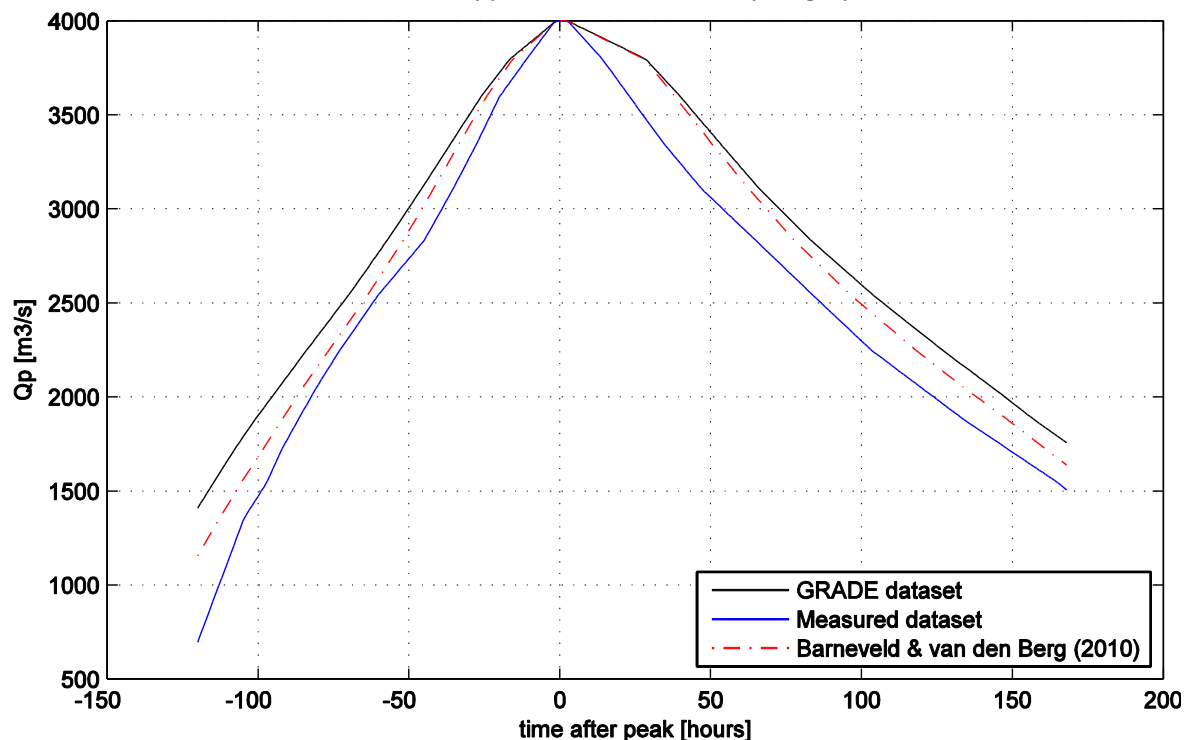


Figure 4-1 Standard hydrographs from GRADE and measured datasets

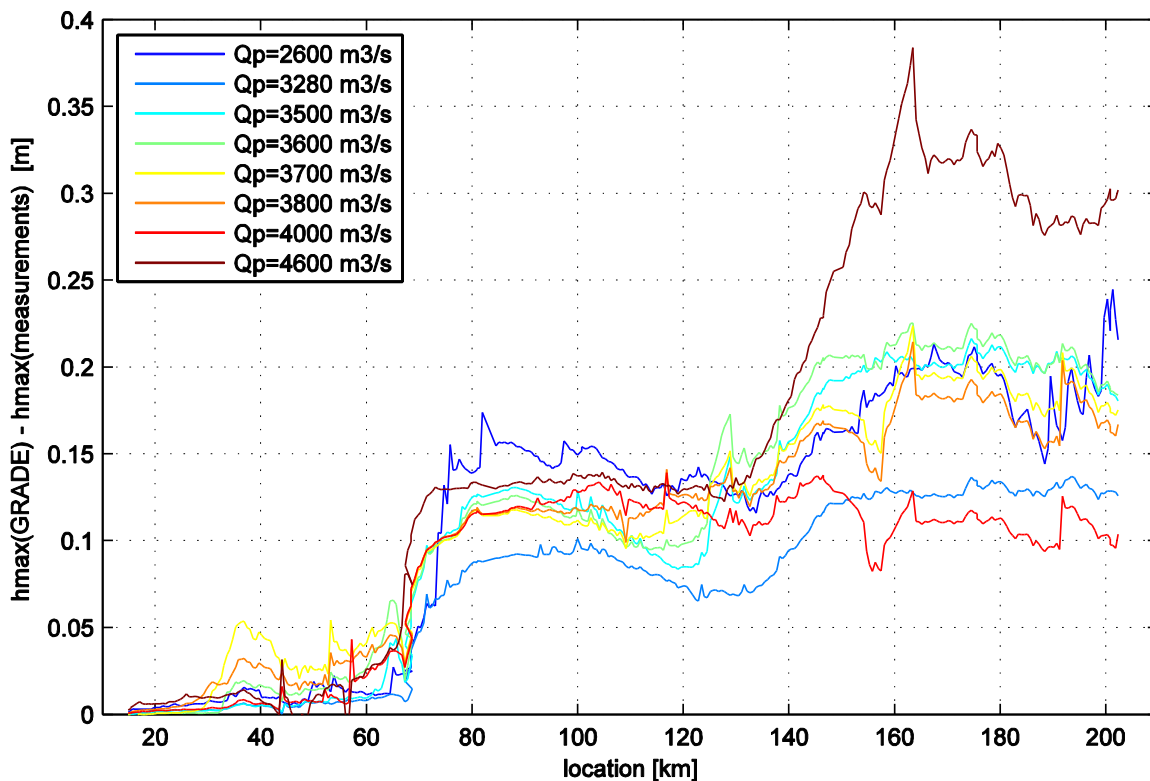


Figure 4-2 Water level difference between hydrographs based on GRADE and measured dataset

In addition to the fact that GRADE results in higher water levels for a given peak discharge, GRADE also results in higher peak discharge exceedance frequencies compared to the measured dataset (see Table 4-1 and Figure 4-3). An exception is the peak discharge of 4600 m<sup>3</sup>/s. This increase in frequency depends on the magnitude of the peak discharge and on the assumed distribution (GPD or Kernel). Results of Kramer & Schroevers (2008) are consistent with these results. Van den Boogaard et al. (2014) give an uncertainty analysis of the GRADE discharges, which shows that the 95% confidence interval at T = 250 year is 1100 m<sup>3</sup>/s and 2400 m<sup>3</sup>/s at T = 10,000 year.

Q <sub>p</sub> [m <sup>3</sup> /s]	Data	T (GRADE) <sup>2</sup>		Water level [m +NAP]				
		T (measured) <sup>3</sup>	Borgharen	Maaseik	Venlo	Mook	Megen	
2600	G	21/21	45.198	29.044	18.169	11.362	8.268	
	M	33	45.195	29.029	18.027	11.160	8.102	
3280	G	135/124	45.751	29.573	18.841	12.043	8.800	
	M	261	45.750	29.566	18.752	11.917	8.666	
3800	G	694/785	46.054	29.866	19.279	12.582	9.303	
	M	1259	46.052	29.849	19.167	12.398	9.142	
4000	G	1384/1832	46.161	29.953	19.443	12.692	9.395	
	M	2305	46.160	29.943	19.317	12.581	9.296	
4600	G	14330/33271	46.453	30.210	19.922	13.268	9.903	
	M	14144	46.448	30.196	19.789	12.948	9.616	

Table 4-1 Design water levels from GRADE and measured datasets.

<sup>2</sup> according to Generalized Pareto fit / Kernel fit. See section 4.3.1

<sup>3</sup> according to design discharge curve from Tijssen (2009)

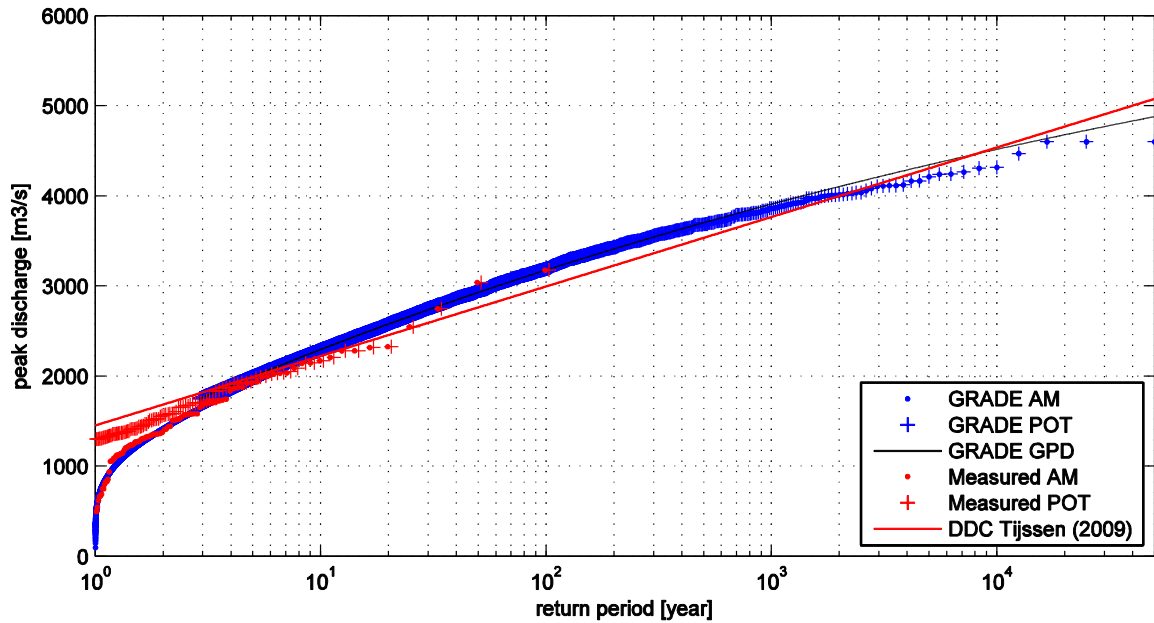


Figure 4-3 Peak discharge return periods, GRADE vs. measured

The consequence of these two effects is that if e.g. the  $T = 1250$  year design water level is to be determined, GRADE (with GPD) gives a 15 - 25 cm higher design water level at all locations. Figure 4-4 and Figure 4-5 give the relation between the maximum water level and the return period for the locations Maaseik and Mook, based on Table 4-1. The red lower line represents the measured dataset, the blue upper line the GRADE dataset, and the dashed line in the middle represents the result of wider GRADE hydrographs without considering the higher exceedance probabilities. The effect of wider hydrographs increases in downstream direction. The effect of higher exceedance probabilities decreases to zero for large return periods (with a GPD distribution), or becomes even negative (with a Kernel distribution).

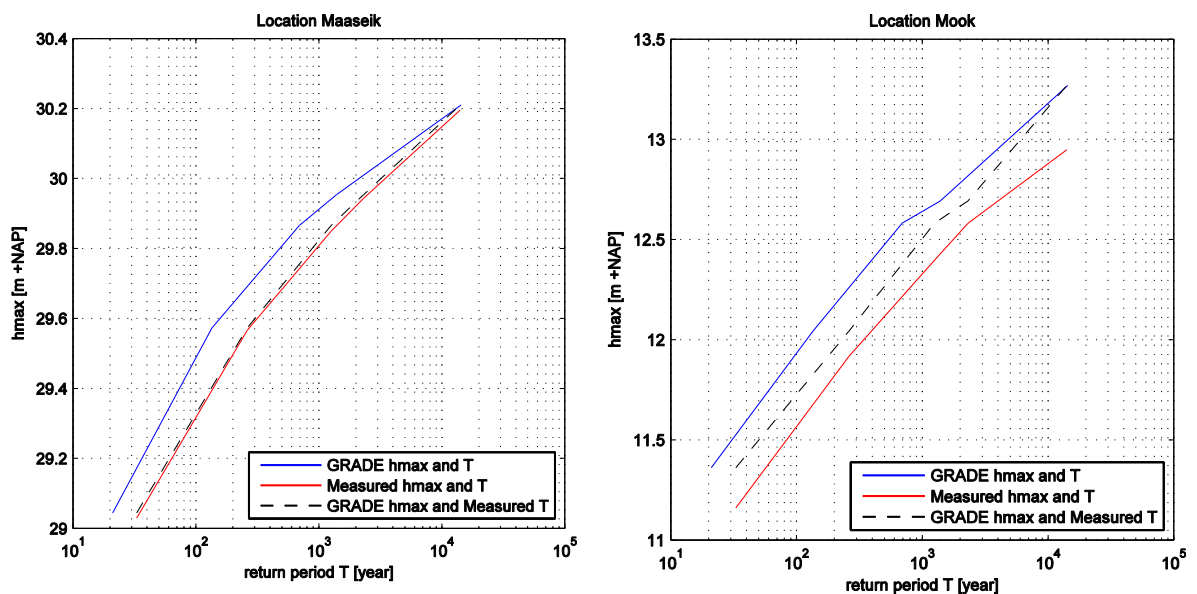


Figure 4-4 Water level return periods, GRADE vs Measured (T according to GPD)

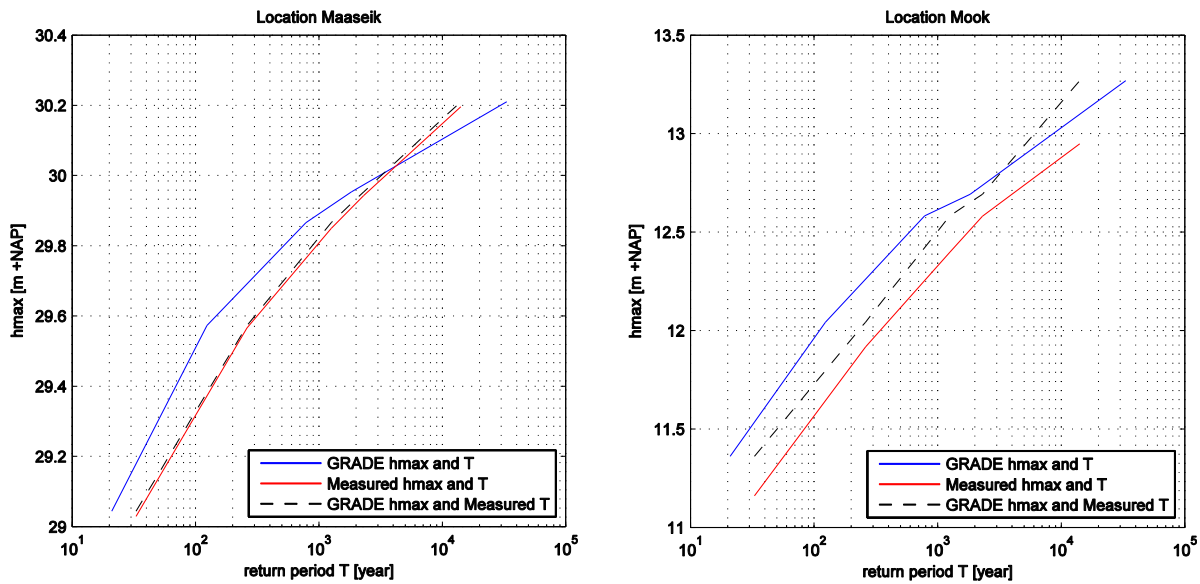


Figure 4-5 Water level return periods, GRADE vs Measured (T according to Kernel)

## 4.2 Effects of hydrograph shape variables on local water levels

### 4.2.1 Correlation analysis of shape variables and water levels

The correlation between all considered shape variables and local water levels was analysed with the Pearson, Spearman and Kendall correlation coefficients. Table 4-2 gives the Spearman rank correlations between the local water levels and shape variables.  $Q_p$  and  $V_{1250}$  show the strongest correlation with  $0.927 < \rho < 0.999$  and  $0.860 < \rho < 0.960$  respectively. The variables  $D_{1250}$ ,  $V_0$ ,  $V_{50\%}$  and  $V_{85\%}$  show moderate correlation with the water levels ( $0.355 < \rho < 0.774$ ). The other durations, relative volumes and peak curvature have the lowest correlation with the water levels ( $|\rho| < 0.339$ ). Results for Pearson and Kendall correlation coefficients show a similar pattern, but have some deviations from Spearman (see Appendix D).

Variable	$h_{\max, \text{Borgharen}}$	$h_{\max, \text{Maaseik}}$	$h_{\max, \text{Venlo}}$	$h_{\max, \text{Mook}}$	$h_{\max, \text{Megen}}$
$Q_p$	0.999	0.993	0.963	0.933	0.927
$D_{1250}$	0.520	0.562	0.644	0.695	0.704
$D_{50\%}$	-0.130	-0.085	0.009	0.072	0.084
$D_{85\%}$	-0.043	0.016	0.152	0.238	0.252
$V_0$	0.621	0.660	0.729	0.768	0.774
$V_{1250}$	0.860	0.887	0.934	0.957	0.960
$V_{50\%}$	0.355	0.405	0.512	0.580	0.593
$V_{85\%}$	0.484	0.538	0.654	0.720	0.731
$RV_0$	-0.119	-0.068	0.038	0.105	0.117
$RV_{1250}$	-0.339	-0.336	-0.310	-0.290	-0.287
$RV_{50\%}$	0.088	0.103	0.150	0.184	0.190
$RV_{85\%}$	0.057	0.007	-0.116	-0.198	-0.213
$C_1$	0.021	-0.034	-0.152	-0.216	-0.227
$C_2$	0.001	-0.061	-0.197	-0.272	-0.285

Table 4-2 Spearman rank correlation between local water levels and shape variables

Conditional correlations were used to investigate the additional predictive value of a second variable. Figure 4-6 (left) shows two/three examples of the conditional correlation structure, where each colour band represents a peak discharge class of 100 m<sup>3</sup>/s wide. The different variables show different degrees of scatter and linearity (see Appendix D for other variables). Figure 4-6 (right) shows the dependence of  $\rho_{h_{\max}, \text{var} | Q_p}$  on  $Q_p$ . The correlation of these peak variables is generally close to 1 or -1, except for the highest discharges where only a few data are available in a class. Table 4-3 shows the mean values of the conditional rank correlation coefficients, averaged over the  $Q_p$  classes of 100 m<sup>3</sup>/s wide. The conditional correlation increases in downstream direction, generally.

To identify relevant shape variables, the following procedure was used. The first variable was selected on the highest rank correlation with  $h_{\max}$  (Table 4-2). At the upstream locations this is the peak discharge  $Q_p$ . At the more downstream locations Mook and Megen,  $V_{1250}$  has a slightly higher correlation. It must be noted that  $Q_p$  and  $V_{1250}$  are also strongly correlated to each other ( $\rho_s=0.85$ ). Since the difference in  $\rho_{h_{\max}, \text{var}}$  between  $Q_p$  and  $V_{1250}$  is small and the peak discharge is widely used as most decisive variable, the peak discharge  $Q_p$  was chosen as first variable. The second variable was selected by the highest mean conditional rank correlation ( $\rho_{h_{\max}, \text{var} | Q_p}$ ). At most locations the highest values are found for  $D_{085}$ ,  $V_{085}$  and  $C_2$ ; variables that describe the shape characteristics close to the peak of the hydrograph.  $D_{085}$  and  $C_2$  have a smaller standard deviation of the conditional rank correlation than  $V_{085}$ . The relation of  $h_{\max}$  with  $C_2$  is more linear than with  $D_{085}$  and  $V_{085}$ .  $C_2$  was chosen as the second variable because this linear relation and the highest degree of independence with  $Q_p$ .

Variable	$h_{\max, \text{Maaseik}}$	$h_{\max, \text{Venlo}}$	$h_{\max, \text{Mook}}$	$h_{\max, \text{Megen}}$
$D_{1250}$	0.3597	0.5822	0.6168	0.6228
$D_{50\%}$	0.3441	0.6354	0.6724	0.6802
$D_{85\%}$	0.5155	0.8758	0.9133	0.9200
$V_0$	0.4395	0.6804	0.7119	0.7195
$V_{1250}$	0.4908	0.7998	0.8374	0.8462
$V_{50\%}$	0.4646	0.8043	0.8466	0.8549
$V_{85\%}$	0.6004	0.8821	0.8963	0.896
$RV_0$	0.4067	0.6674	0.7032	0.7112
$RV_{1250}$	0.1983	0.3775	0.3966	0.3991
$RV_{50\%}$	0.2461	0.3626	0.3778	0.3848
$RV_{85\%}$	0.2895	0.1868	0.1259	0.1108
$C_1$	-0.5889	-0.8408	-0.8448	-0.8437
$C_2$	-0.5588	-0.8993	-0.919	-0.9207

**Table 4-3 mean conditional rank correlations  $\rho_{h_{\max}, \text{var} | Q_p}$  (Spearman)**

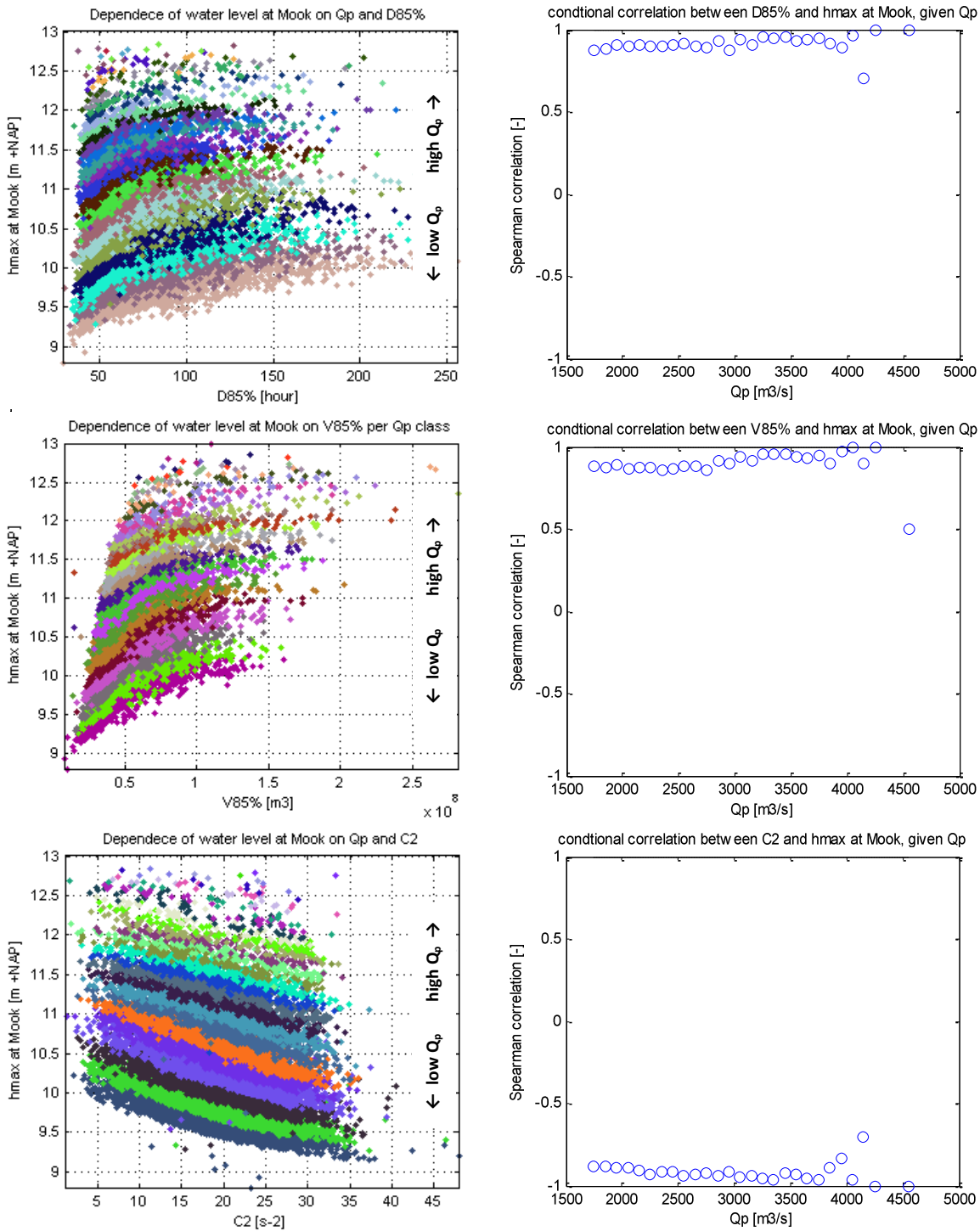


Figure 4-6 conditional plots of  $h_{max}$  versus  $D_{85\%}$ ,  $V_{85\%}$  and  $C_2$

#### 4.2.2 Synthetic hydrographs: Base flow

In order to investigate the importance of a correct representation of the base flow, a number of synthetic hydrographs were constructed (Figure 4-7). Figure 4-8 shows the effect of the different base flows on the maximum water levels. The water levels from each hydrograph are plotted relative to the water levels from the  $Q_{\text{base}} = 125 \text{ m}^3/\text{s}$  hydrograph. These results show that the magnitude of the base flow has little effect on downstream water levels, in particular if the base flow is below the bankfull discharge. In the latter case, the water level differences stay below 1 cm which is considered acceptable given the magnitude of other errors.

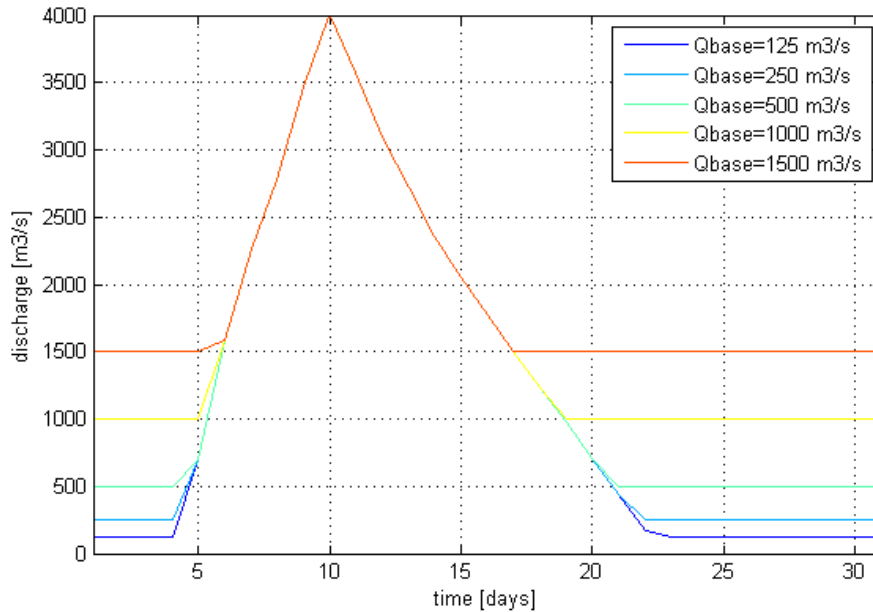


Figure 4-7 Synthetic hydrographs with different base flow

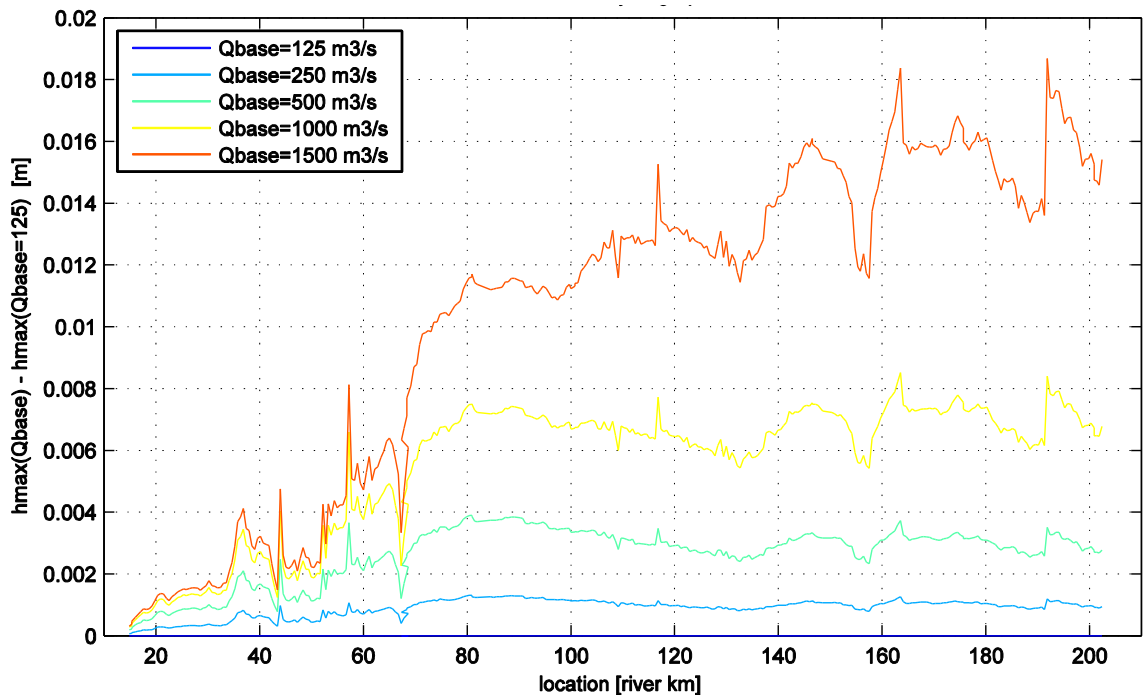


Figure 4-8 Downstream water levels for hydrographs with different base flow

### 4.3 Statistics of shape variables at Borgharen

This section describes some statistics of the input dataset, the GRADE discharge data at Borgharen. These statistics include the probability distributions of the peak discharge ( $Q_p$ ) and the peak curvature ( $C_2$ ) and their correlation. The figures of the distribution fits of  $V_{1250}$  and  $D_{85\%}$  are given in Appendix D.

#### 4.3.1 Univariate probability distributions

The distribution types and parameters were estimated with maximum likelihood estimation, as described in section 3.5.3.

##### Peak discharge $Q_p$

The Generalized Pareto distribution fits the peak discharges at Borgharen very well. This is to be expected since all POT processes converge towards the Generalized Pareto distribution. Maximum likelihood estimation shows that the best fit is obtained with shape parameter  $k = -0.080$ , scale parameter  $\sigma = 462.9$ , and location (threshold) parameter  $\theta = 1750$  (Figure 4-9). The value of  $k$  is small, so this distribution is close to exponential.

The goodness of fit of the  $Q_p$  distribution in the extreme discharge range is visualized in Figure 4-10 by plotting the return period on a logarithmic scale. For  $Q_p > 3500 \text{ m}^3/\text{s}$ , the design peak discharge is overestimated by the Generalized Pareto distribution. The alternative Kernel distribution follows the empirical points also in the extreme range.

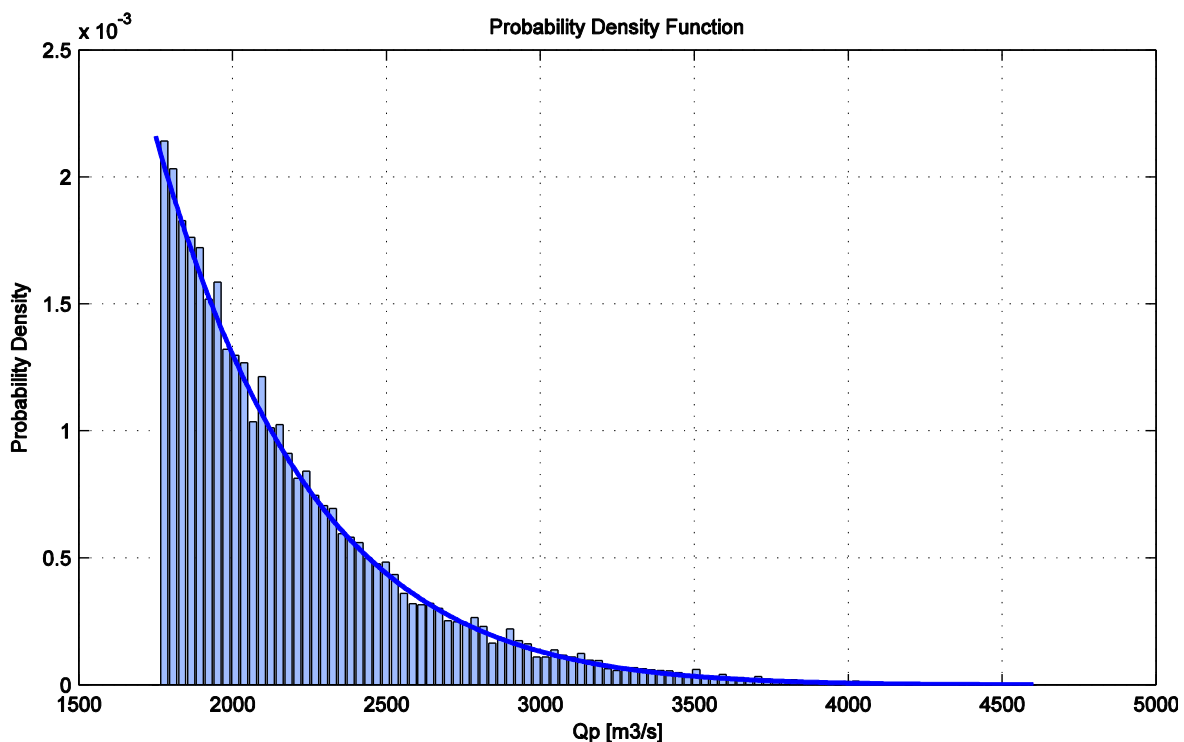
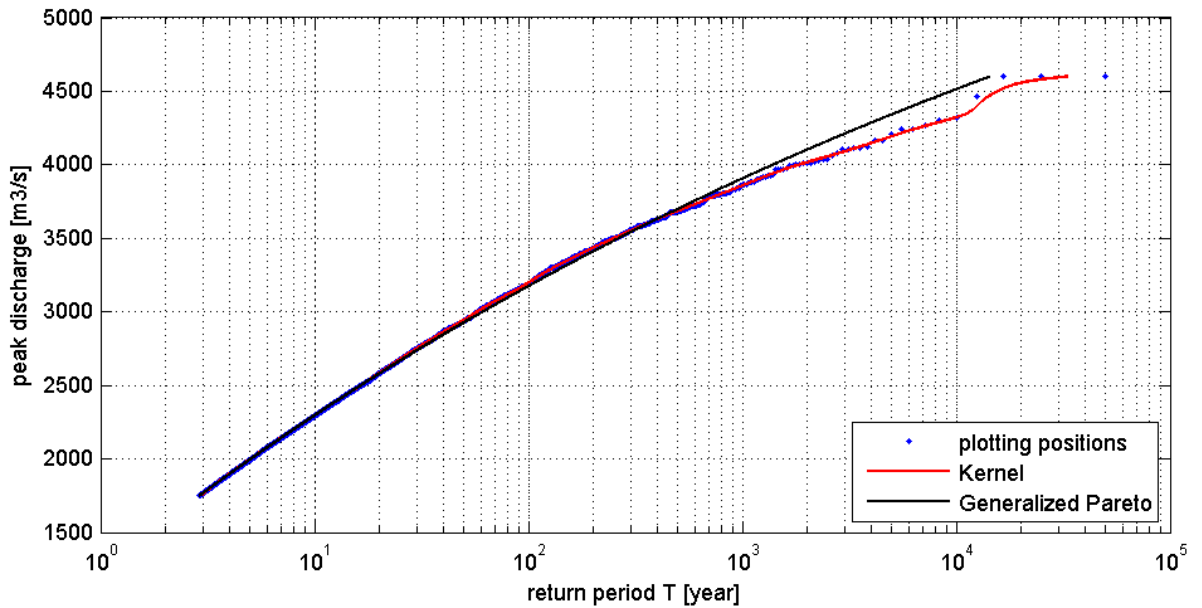


Figure 4-9 Probability distribution fit of peak discharge  $Q_p$



**Figure 4-10 Generalized Pareto and Kernel fit on logarithmic scale**

For several analyses, it is necessary to determine the exceedance probability or return period of the peak discharge. Assuming that the peak discharge at Borgharen is distributed according to the fitted Generalized Pareto or Kernel distribution, the return periods in Table 4-4 apply to the peak discharges.

$Q_p$ [m <sup>3</sup> /s]	2600	3280	3800	4000	4200	4400	4600
$T_{GPD}$ [year]	21	135	694	1384	2875	6254	14330
$T_{Kernel}$ [year]	21	124	785	1832	5129	12589	33271

**Table 4-4 Peak discharge return periods at Borgharen**

**Peak curvature  $C_2$**

The best fitting distribution type to  $C_2$  is the Weibull distribution, but it must be noted that a Normal distribution fits almost as good as Weibull. Maximum likelihood estimation shows that the best fit for  $C_2$  is obtained with scale parameter  $a = 21.055$ , and shape parameter  $b = 3.432$ .

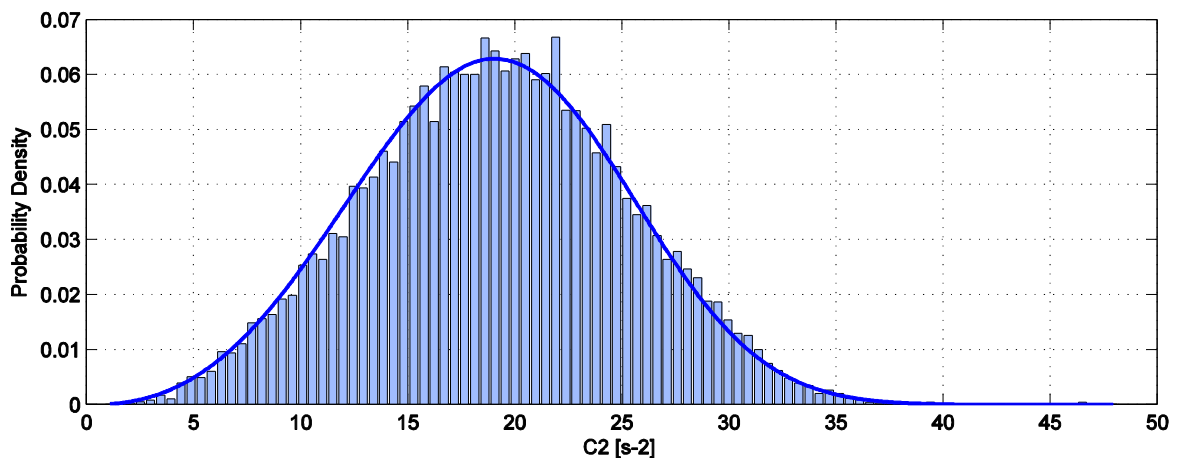


**Figure 4-11 Probability distribution fit of  $C_2$**

### 4.3.2 Correlation structure

This section shows the correlation structure between the two most important variables  $Q_p$  and  $C_2$ , both in the original space and in the ranks (Figure 4-12). Scatterplots of other variables are given in Appendix D. Table 4-5 gives the values of the Spearman rank correlation coefficient, including the ones for  $V_{1250}$  and  $D_{85\%}$ . Both the Spearman correlation coefficient (0.03) and the visual inspection of the scatterplot show that  $Q_p$  and  $C_2$  can be considered independent variables. Independence simplifies the probabilistic analysis since the joint distribution of  $Q_p$  and  $C_2$  can be determined without copulas or other multivariate dependence models.

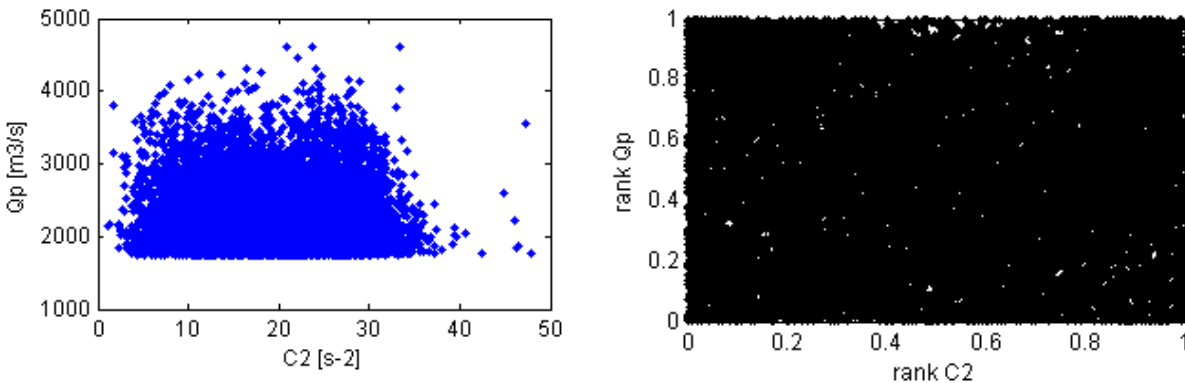


Figure 4-12 scatterplot (left) and rank scatterplot (right) of  $Q_p$  and  $C_2$

Variable	$Q_p$	$V_{1250}$	$D_{85\%}$	$C_2$
$Q_p$	1.00			
$V_{1250}$	0.85	1.00		
$D_{85\%}$	-0.07	0.39	1.00	
$C_2$	0.03	-0.36	-0.87	1.00

Table 4-5 Spearman rank correlations between  $Q_p$ ,  $V_{1250}$ ,  $D_{85\%}$  and  $C_2$

## 4.4 Design water levels based on 1D Simulations

### 4.4.1 Local water level distributions

The 1D SOBEK simulations of the complete set of 17,232 floods provide local water levels for every GRADE hydrograph. This local water level dataset can serve as reference to compare with the local water level that results from the other methods to determine the design water level. The key issue is to determine an exceedance probability for each water level. One method is to fit a parametric distribution to the local water level data. However, the distributions of the water levels at most locations downstream have a discontinuity at one or two points which is caused by a discontinuity in the stage-discharge curve. Therefore fitting a parametric distribution does not give sufficient good results (see Figure 4-13 for Mook). The distributions at other locations can be found in Appendix E. Two alternative methods that are considered in this section are:

- Parametric distribution of  $Q_{p,x}$  and a stage-discharge relationship (section 4.4.2)
- Return periods with plotting positions (section 4.4.3)

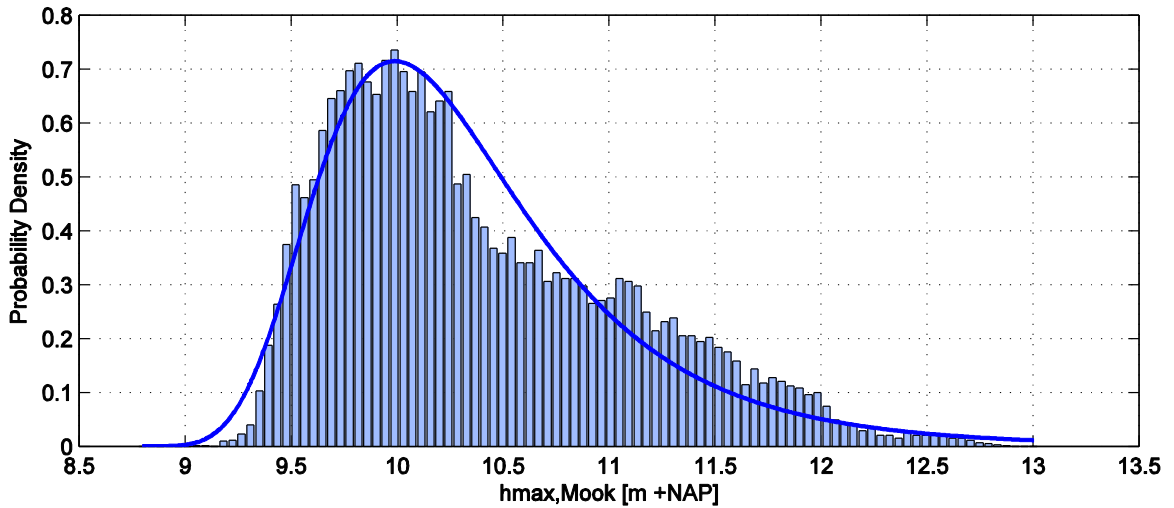


Figure 4-13 Distribution of water levels at Mook, and best parametric fit

4.4.2 Based on local discharge distribution and stage-discharge curve

The distribution of the local peak discharge shows less discontinuities than the distribution of the local water level. Therefore a parametric distribution was fitted to the local peak discharge  $Q_{p,x}$ . For a given return period  $T$ , the return value  $Q_{p,x}$  can be found with this distribution. Then the corresponding  $h_{max,x}$  can be found with the local stage-discharge relationship.

The results of this approach are given in Table 4-6 for the case of Mook. The best fit to  $Q_{p,Mook}$  was found for a GEV distribution with parameters  $k = 0.3189$ ,  $\sigma = 224.816$ ,  $\mu = 1904.73$ . It turns out that the GEV distribution gives too high values of the local peak discharge for large  $T$ , and as a consequence too high local water levels (Figure 4-14). The  $T = 500$  water level is already higher than the highest in the 50,000 year dataset. Therefore this method was considered not useful. Of course a non-parametric distribution (like Kernel) can be applied to the local discharge but that eliminates the advantages of the parametric distributions, and even the need of this approach since a Kernel could also be applied to the local water levels directly.

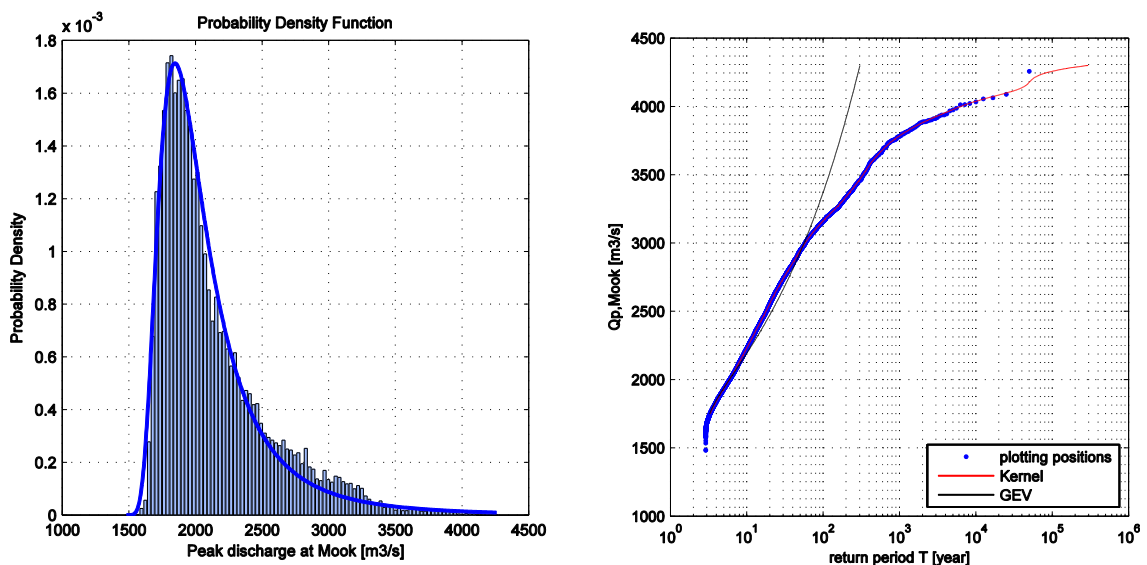


Figure 4-14 Distribution of local peak discharge at Mook

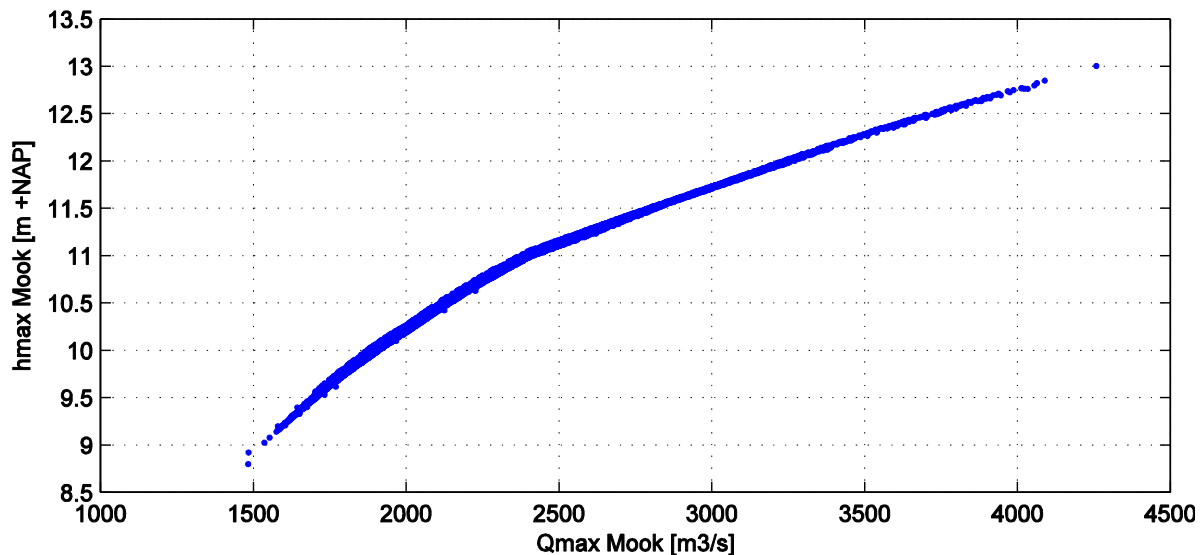


Figure 4-15 Stage-discharge curve at Mook

T (year)	$Q_{p,Mook}$ ( $m^3/s$ )	$H_{max,Mook}$ (m+NAP)	$H_{max,Mook}$ (m+NAP) with plot position
25	2574	11.3	11.33
50	2931	11.7	11.66
100	3370	12.2	11.90
250	4114	12.8	12.18
500	4838	13.5	12.42
1000	5741	14.5	12.56

Table 4-6 Results of approach with stage-discharge relationship

#### 4.4.3 Return period with plotting positions

Return period with plotting positions have the advantage that only little interpretation of the data is needed, since it does not use extrapolation or an assumed parametric distribution. The only choice is the type of plotting position. However, it is only useful when the sample is large. The result (Figure 4-16) is a relatively smooth line, which is an indication that the sample is large enough. This water level frequency curve is used as a reference for the other methods to determine the design water level.

The Weibull plotting position  $p = i / (N+1)$  was chosen in the analysis to estimate the return periods. The effect of using alternative plotting positions was assessed for:

- Hazen:  $p = (i-0.5) / N$
- Gringorten:  $p = i-0.44 / N+0.12$
- Cunnane:  $p = i-0.4 / N+0.2$

The return periods did not change significantly when other plotting positions were used. Only for the extreme range ( $T > 10,000$ ), the return periods of the alternative plotting positions were higher compared to the Weibull plotting position.

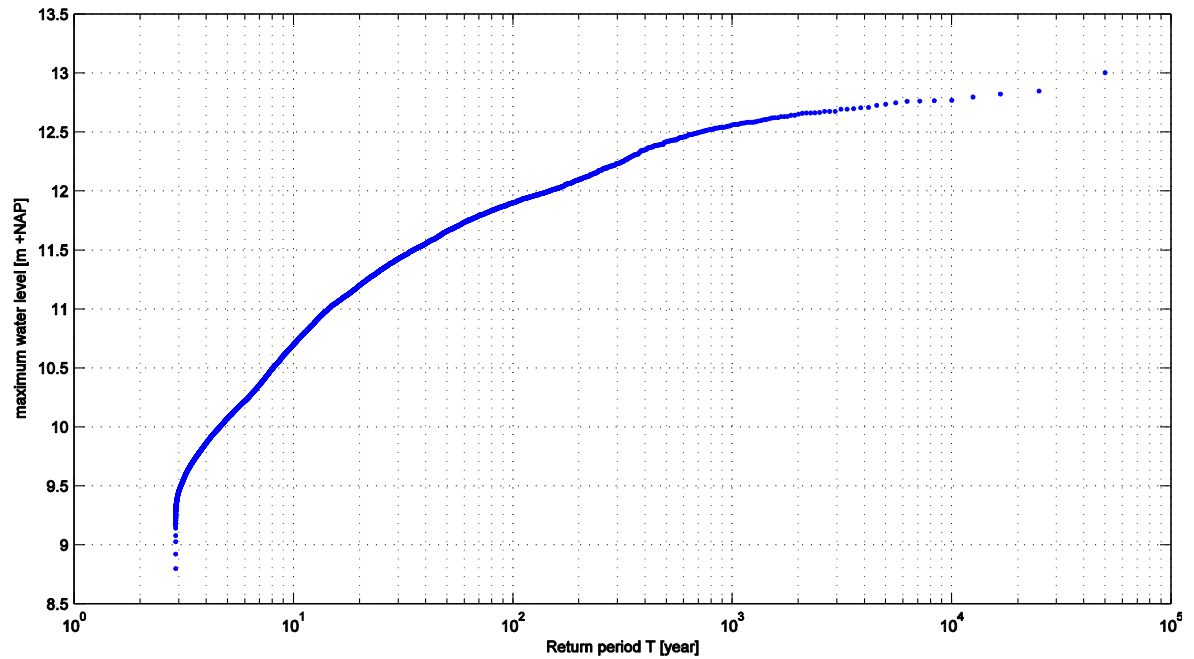


**Figure 4-16** Return periods of water levels at Mook

#### 4.4.4 Sensitivity for the number of simulations

This sensitivity analysis was carried out to show how the results of Figure 4-16 change when only a small number of hydrographs is used. From the point of computational time, it is important to know how many simulations are needed to get a reliable representation of the full set of simulations. This sensitivity analysis gives an impression of the reliability of such an approach with limited number of simulations.

$N$  random samples were drawn without replacement from the total of 17,232 simulation results. Each draw of  $N$  samples gives a line like the one in Figure 4-16. This process was repeated 100 times. The 90% confidence interval of water levels (y axis) at each return period (x axis) was then found by the 5<sup>th</sup> and 95<sup>th</sup> largest water level realisation of the 100 samples. The confidence bounds are the lines connecting the confidence intervals of all return periods.

The analysis was carried out with different values of  $N$ : 30, 100, 500, 1000, 2000, 5000, 10,000 and 17,232. Figure 4-17 shows the 90% confidence interval for these values of  $N$ . The maximum return period that can be determined with  $N$  samples is  $N / \lambda \approx 3 \cdot N$ . The confidence interval gives only information about the uncertainty due to use of smaller part of the dataset. It does not give information about model uncertainty or statistical uncertainty in the GRADE dataset. Quite a lot of simulations are needed to get a reliable estimate of the return period line. This limits the possibility to do the same analysis with a large amount of hydrographs in a 2D model. Even 100 simulations in WAQUA will cost significant computation time, and then the 90% confidence interval is still 70 cm wide for a water level of  $T = 100$  years.

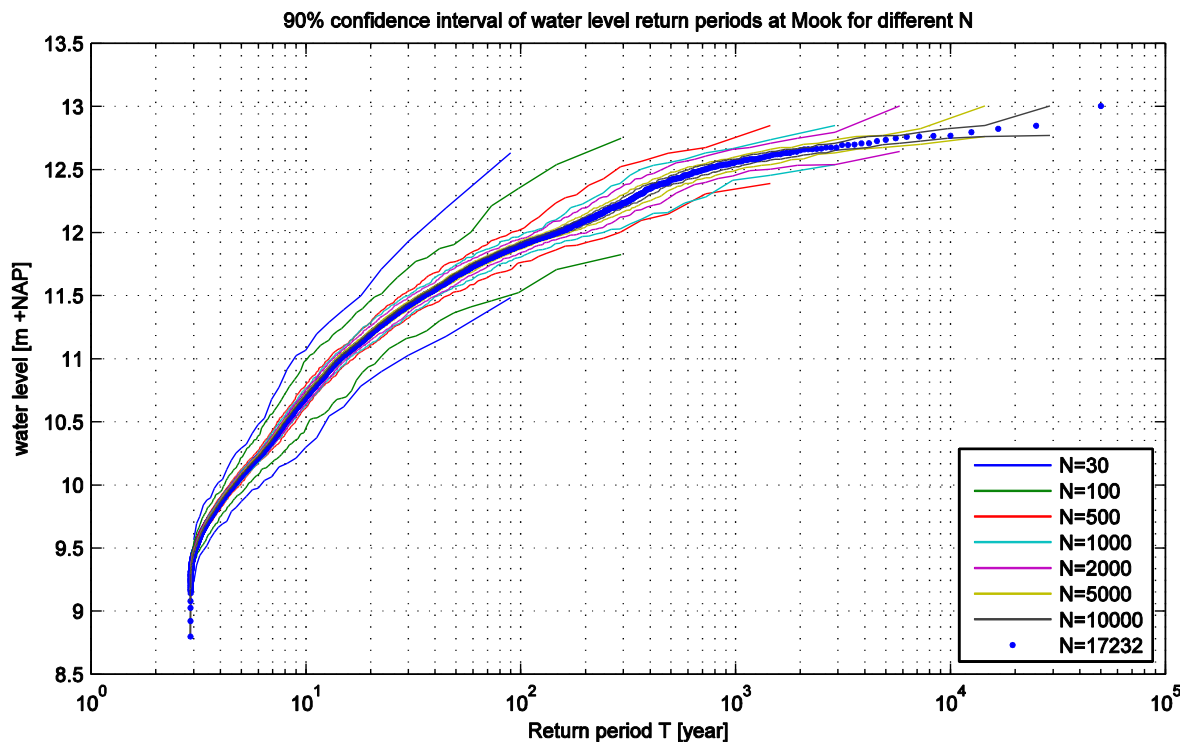


Figure 4-17 Sensitivity of water level return periods for the number of hydrographs used

#### 4.4.5 Water levels based on 2D simulations

The results of section 4.4.4 show that the method of section 4.4.3 is difficult to apply with a 2D model. If the WAQUA results have a stable deviation from the SOBEK results, one could apply this deviation as a correction factor on SOBEK results, assuming that the WAQUA results are more accurate. To assess differences between SOBEK and WAQUA results, and whether the differences are constant, a selection of 25 hydrographs was simulated in WAQUA. This particular selection covers a wide range of peak discharges, and was chosen because it was used for the analysis of section 4.6 as well.

Figure 4-18 shows that WAQUA gives 15 - 60 cm lower water levels than SOBEK at Borgharen, and that this difference decreases with higher peak discharges (Figure 4-19). At the locations Venlo, Maaseik, Mook and Megen, the difference varies between -0.1 and 0.3 m. The difference at these locations is relatively constant over the peak discharge. The spread in difference is 15 cm at Maaseik and Venlo, 35 cm at Mook and 25 cm at Megen. The results are in agreement with Table 3.17 in the report of the SOBEK model (Michels et al., 2013), in which it is stated that it is known that WAQUA gives too low water levels at Borgharen for lower floods (p. 36). The differences between SOBEK and WAQUA show a relatively large spread compared to the average difference, and in addition the difference is not in all cases constant over the peak discharge. Therefore no correction term was applied to the frequency curve based on SOBEK, but based on Figure 4-19 one could give a rough estimate of the frequency curve based on WAQUA.

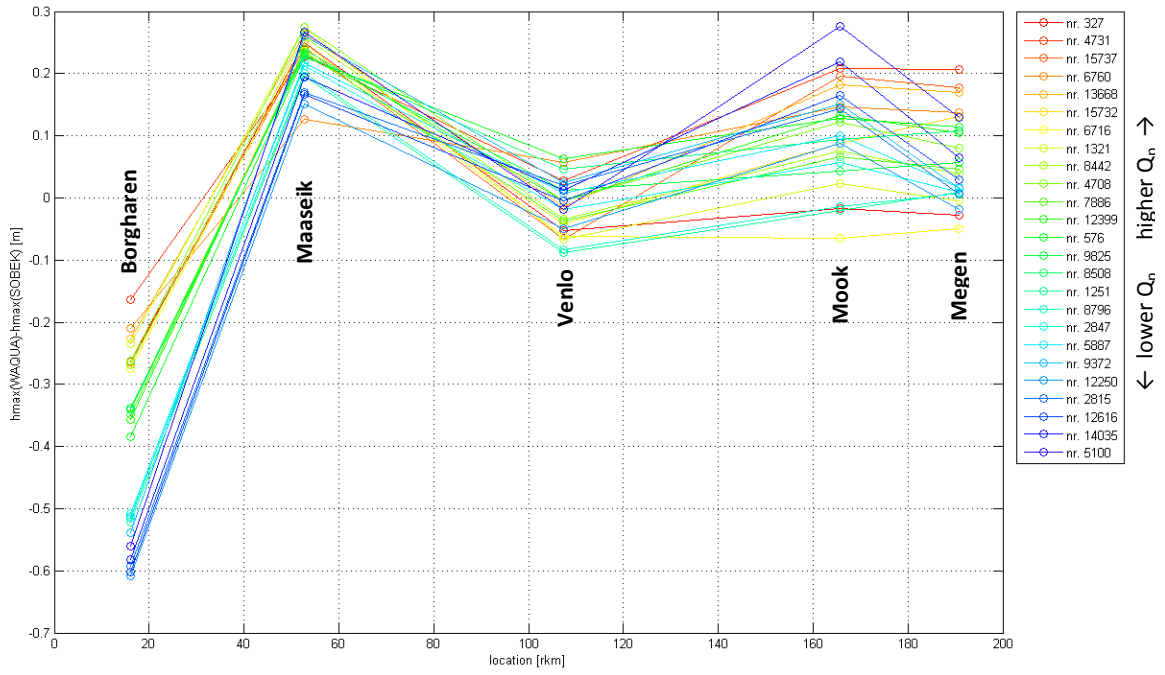


Figure 4-18 Difference between WAQUA and SOBEK maximum water levels, for five locations

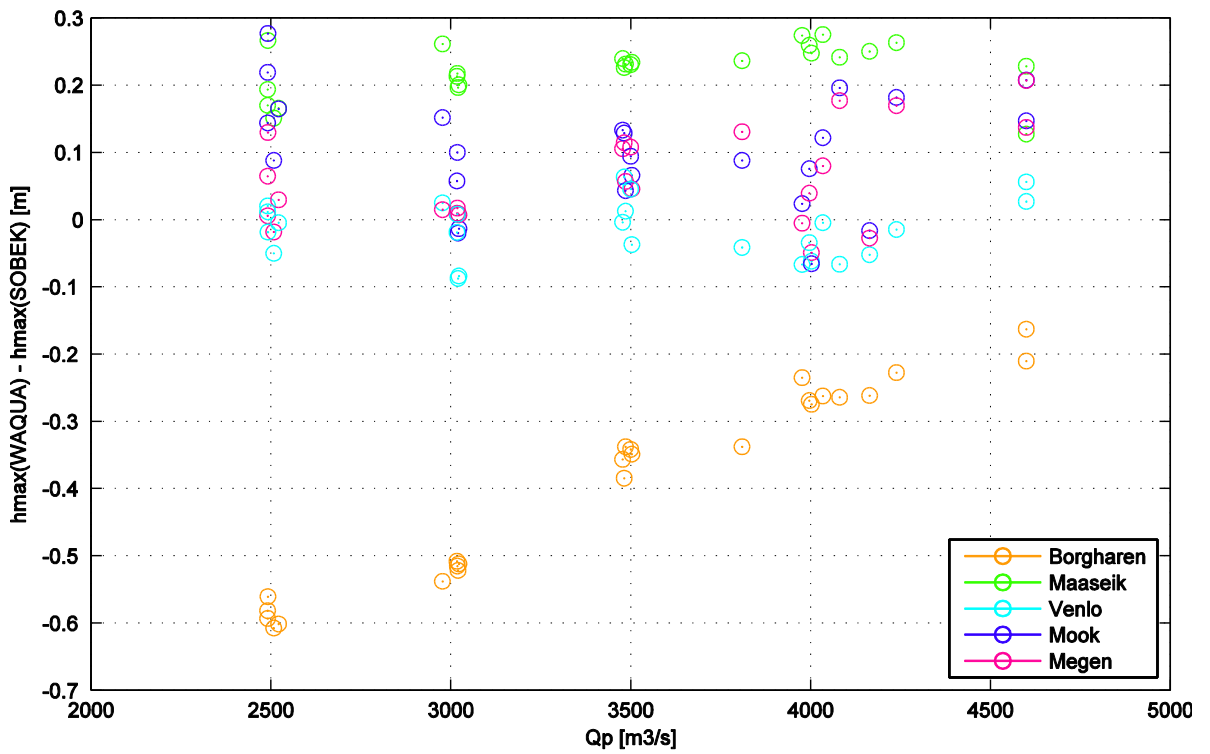


Figure 4-19 Differences between WAQUA and SOBEK results as function of Qp

## 4.5 Design water levels based on design hydrograph methods

In this section, the results of three types of design hydrograph methods are compared to the results from the complete set of simulations:

- The standard hydrograph method (see section 2.3.2)
- The vertically averaged hydrograph method (see section 2.3.4)
- The standard and vertically averaged hydrographs with a modified selection interval

Only figures of location Mook are shown in the main text. The results of other locations are given in Appendix F.

### 4.5.1 Standard and vertically averaged hydrographs

Seven standard and seven vertically averaged hydrographs were used, based on the GRADE dataset, with a peak discharge ranging from 2600 to 4600 m<sup>3</sup>/s and selection criteria according to sections 3.3.1 and 3.3.2 respectively. Figure 4-20 shows the hydrographs for a peak discharge of 4000 m<sup>3</sup>/s, which clearly shows that the standard hydrograph is wider than the vertically averaged hydrograph.

The exceedance probability or return period corresponding to each peak discharge was determined in two ways (see section 4.3.1):

- Based on the parametric Generalized Pareto Distribution
- Based on a non-parametric Kernel distribution

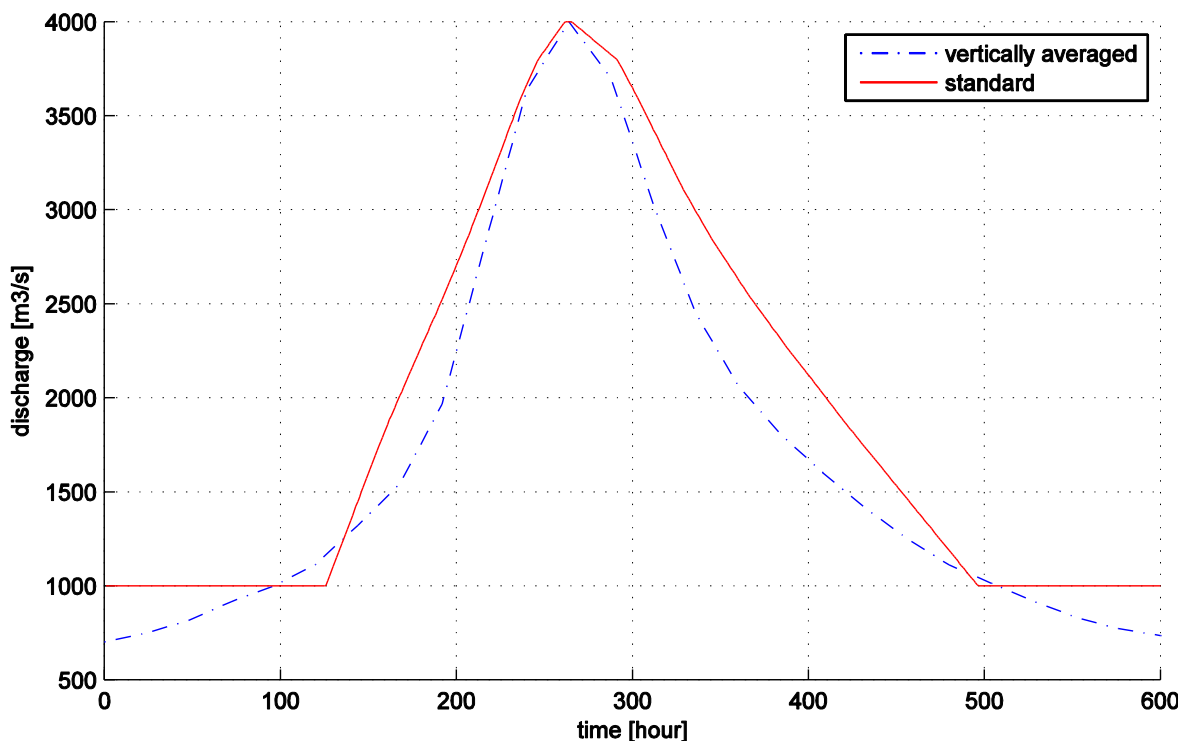


Figure 4-20 Standard and vertically averaged hydrographs

#### 4.5.2 Comparison of the two design hydrograph methods with 1D simulation results

This section shows the results of the hydrodynamic simulations of the hydrographs of Figure 4-20, and compares it to the reference (Figure 4-16). The water level return periods at Mook are shown in Figure 4-21, where the return periods are based on GPD or Kernel.

The standard hydrograph method (with Kernel) overestimates the water levels at Mook with 3 - 13 cm for return periods up to 5000 year. For the more extreme floods ( $T > 10,000$  year), the method gives a larger overestimation, up to 38 cm. The vertically averaged hydrograph method (with Kernel) underestimates the water levels at Mook with 0 - 6 cm for return periods up to 10,000 year. Only for the most extreme floods ( $T \approx 25,000$  year), the method gives an overestimation of 12 cm.

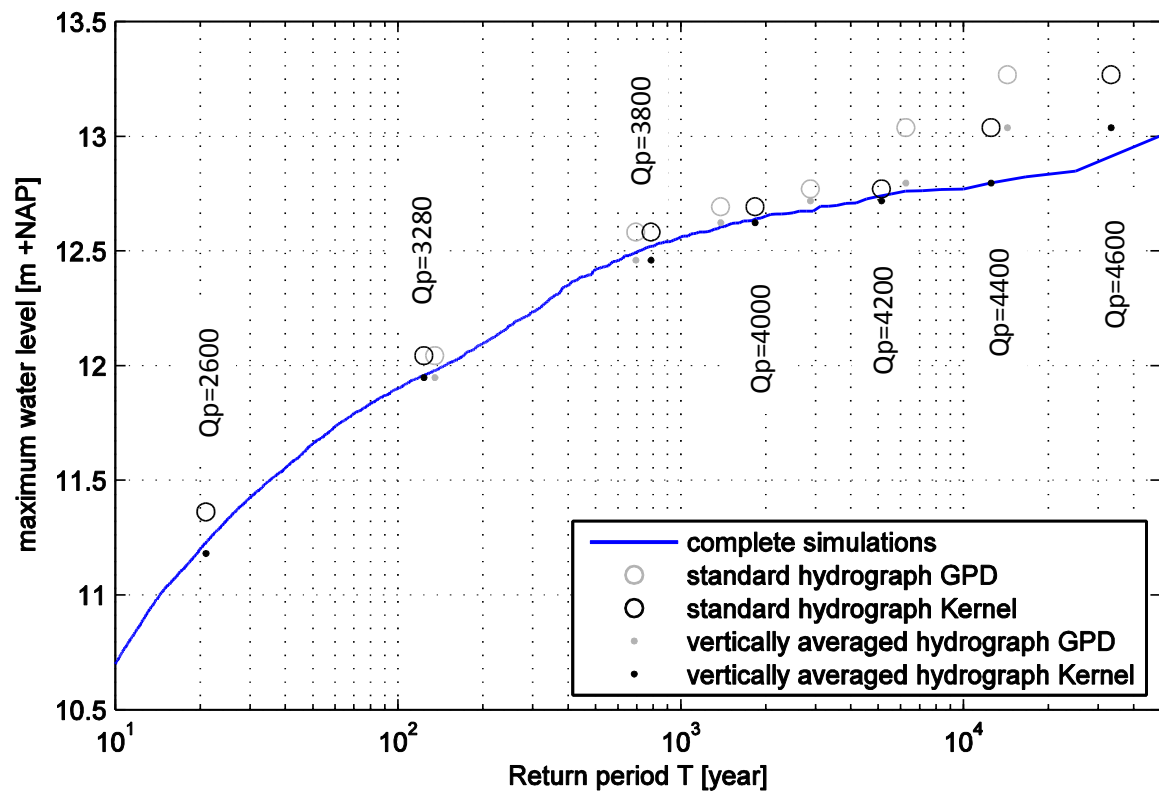


Figure 4-21 Design water levels of the two design hydrograph methods at Mook

The results at other locations are given in Appendix F. Both methods give very accurate design water levels for Borgharen and Maaseik, which is expected since at these locations the hydrograph shape is relatively unimportant compared to the peak discharge. At Venlo and further downstream, the standard method starts to overestimate the water levels. This overestimation increases strongly for large return periods at the locations Mook and Megen. For return periods between 1000 and 5000 years, the standard method seems to be a reasonable but conservative approximation.

It is observed that the influence of the hydrograph shape is not equally important at all peak discharge levels. At Venlo, the difference between standard and vertically averaged is approximately equal for all discharge levels. At Mook and Megen, the difference is larger for the

lowest peak discharges and the highest peak discharges, but for peak discharges around the  $4000 \text{ m}^3/\text{s}$  the difference is small. An explanation for this insensitivity to shape is the presence of retention basins upstream of Mook and Megen. Regardless of the peak attenuation upstream of the retention basin (which is different for the two hydrographs), these retention basins shave the peak discharge and water level to an equal level which the basin is designed for. Results of section 4.7.1 support this explanation, which show that the difference between standard and vertically averaged is constant in case of a system without retention basins.

#### 4.5.3 The impact of the selection interval

This section shows the impact of the selection threshold or interval on the difference between standard and vertically averaged hydrographs. The standard hydrograph method uses normally the floods with a peak discharge between  $1750$  and  $3200 \text{ m}^3/\text{s}$  to generate the hydrograph shape (section 3.3.1). The vertically averaged hydrograph shape is based on a different threshold:  $Q_p > 3000 \text{ m}^3/\text{s}$ . Results are better comparable if the same threshold is used.

Figure 4-22 shows standard and vertical hydrographs with  $Q_p = 4000 \text{ m}^3/\text{s}$ , but with different selection intervals. Hydrographs based on the highest selection ( $4000 - 4600 \text{ m}^3/\text{s}$ ) are more peaked than the ones based on the entire interval ( $1750 - 4600 \text{ m}^3/\text{s}$ ). This holds for both the standard and the vertical averaged hydrograph. The difference between standard and vertical in the rising limb is small for the  $4000 \text{ m}^3/\text{s}$  threshold. The solid red line in Figure 4-22 corresponds to the black line in Figure 4-1.

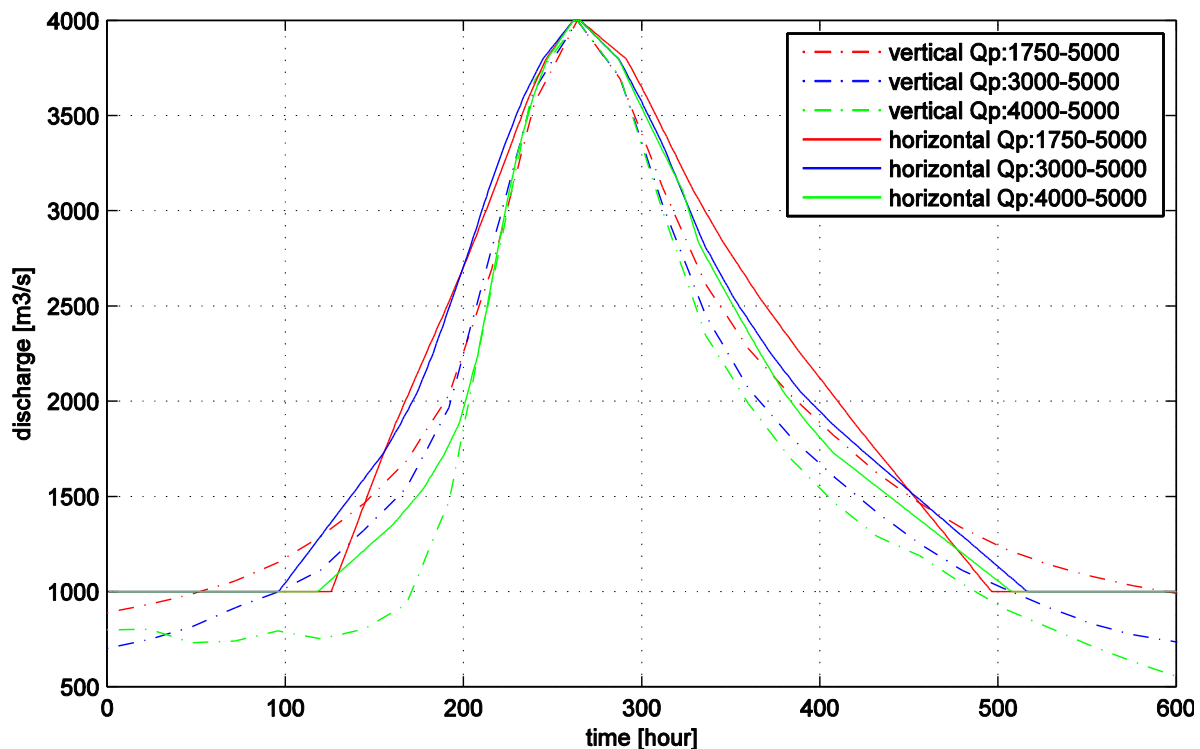


Figure 4-22 Standard and vertical hydrographs for different selection thresholds

Table 4-7 gives the modified intervals that were used for the selection of hydrographs for averaging. For the highest interval, the number of hydrographs used for averaging becomes rather small; therefore an even smaller interval for  $Q_p = 4600 \text{ m}^3/\text{s}$  does not make sense. Figure 4-23 shows the SOBEK simulation results for these modified standard and vertically averaged hydrographs at Mook. Figures of other locations and the modified hydrographs are given in Appendix F. The modified selection interval affects mainly the water levels of standard hydrographs of  $Q_p \geq 4200 \text{ m}^3/\text{s}$ . As a result, the difference between the standard and vertically averaged method becomes smaller for the extreme range.

Modification of the selection interval yields a more accurate approximation of the water level frequency curve with the standard hydrograph method. This is an important improvement to the standard method. On the other hand, results of the vertical averaging method tend to become lower than the reference by application of the modified interval.

$Q_p$ [ $\text{m}^3/\text{s}$ ]	2600	3280	3800/4000	4200/4400/4600
Selection interval	2500-2700	3100-3500	3500-4000	4000-4600
Nr. of hydrographs	1124	457	78	28

Table 4-7 Modified selection intervals of standard and vertically averaged hydrographs

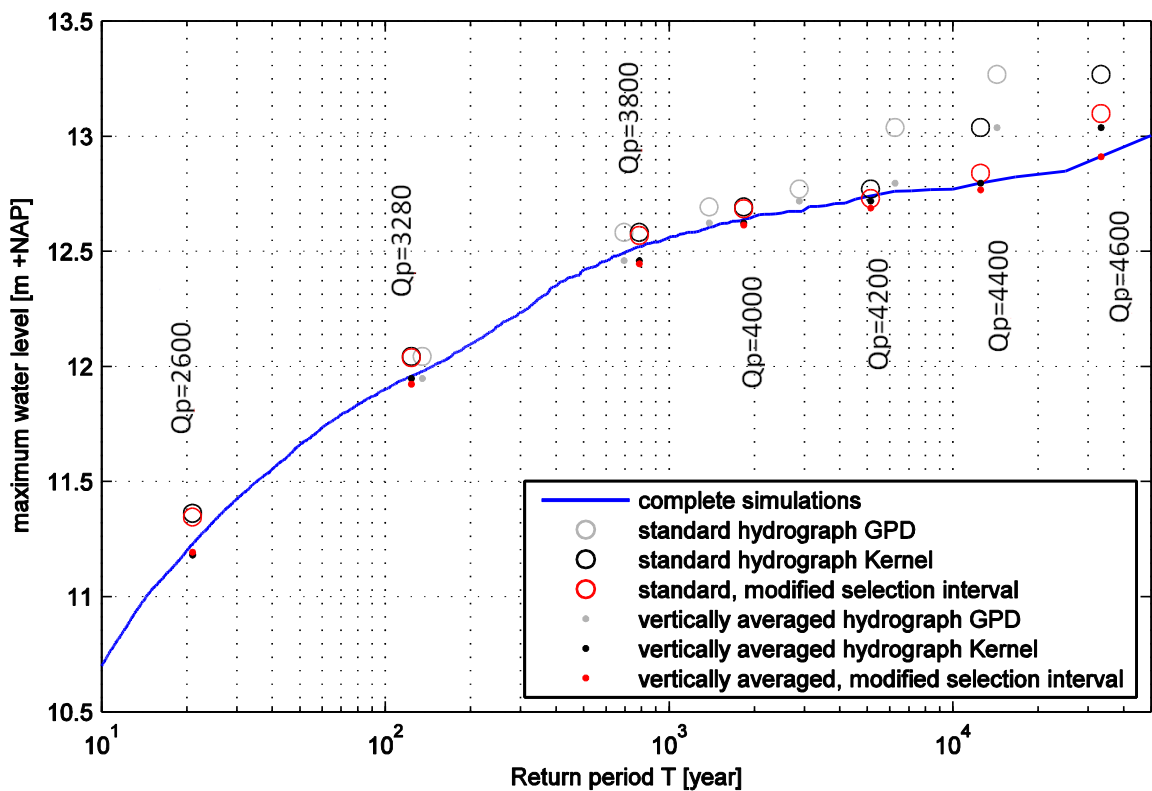


Figure 4-23 Design water levels at Mook with modified selection interval

## 4.6 Design water levels based on a probabilistic approach

The probabilistic approaches use the statistics of the shape variables in the GRADE dataset of 17,232 hydrographs, and use the results of 25 hydrodynamic simulations. Combining these two types of data yields an estimate of the water level return periods.

The variable  $C_2$  was chosen as second variable after  $Q_p$ . Firstly because the conditional correlation of  $C_2$  is very high and constant over the peak discharge (see Figure 4-6). Secondly because the relation between  $C_2$  and  $h_{\max,x}$  conditional on  $Q_p$  is approximately linear (see Figure 4-6). Thirdly because  $C_2$  and  $Q_p$  are independent (see section 4.3.2). Of course, the same analysis can be carried out for other shape variables, but then some parts of the analysis become more complex.

### 4.6.1 Transformation functions

A crucial part in the probabilistic analysis is to express the local water level ( $h_{\max,x}$ ) as function of shape variables ( $Q_p$  and  $C_2$ ). This allows to make a simple model to relate local water levels to the hydrograph shape variables that are observed (or predicted) at Borgharen. There are three different datasets on which this transformation function was based:

1. SOBEK results of the 25 selected hydrographs
2. WAQUA results of the 25 selected hydrographs
3. SOBEK results of the complete (17,232) set of hydrographs

The applied function type is a simple polynomial of one or two degrees. The relation between  $h_{\max,x}$  and  $Q_p$  is non-linear, therefore 2<sup>nd</sup> order relations and a logarithmic transformation were applied. The relation between  $h_{\max,x}$  and  $C_2$  is relatively linear, so only a 1<sup>st</sup> order relation in  $C_2$  was used, without logarithmic transformation. An overview of the applied functions for location Mook is given in Appendix G, which gives also an overview of the goodness of fits for the three different datasets, by the  $R^2$  and RMSE.

The results of the complete set give a good indication of the scatter around the transformation functions. Due to the large amount of data, this dataset can also show the goodness of fit in the extreme range. In the selection of 25 hydrographs, this is generally not seen because the function is almost perfectly fitted to the few extreme floods. Application of a 1<sup>st</sup> order relation with  $\ln(Q_p)$  leads to an overestimation of the water level for the largest peak discharges; this is improved with a 2<sup>nd</sup> order relation with  $\ln(Q_p)$ .

#### Functions of $Q_p$ and $C_2$ fitted to the three datasets

Appendix G shows that the best fit ( $R^2 = 0.984$ , RMSE = 0.087) at Mook is obtained with a function that is 2<sup>nd</sup> order in  $\ln(Q_p)$  and 1<sup>st</sup> order in  $C_2$ . This function is given by:

$$h_{\max} = p_{00} + p_{10} \cdot \ln(Q_p) + p_{01} \cdot C_2 + p_{20} \cdot \ln(Q_p)^2 + p_{11} \cdot C_2 \cdot \ln(Q_p) \quad (4.1)$$

The coefficients  $p_{00}$  to  $p_{11}$  for the three datasets are given in Table 4-8. Figure 4-24 and Figure 4-25 show the polynomial surfaces and data on which these are based.

	p00	p10	p01	p20	p11
25x SOBEK	-38.3878	9.7308	-0.2192	-0.4269	0.024
25x WAQUA	60.2372	-15.0738	-0.0017	1.1321	-0.0025
complete SOBEK	-83.984	20.7383	-0.1045	-1.0896	0.0096

Table 4-8 Coefficients for  $h_{max,Mook}$  as function of  $Q_p$  and  $C_2$

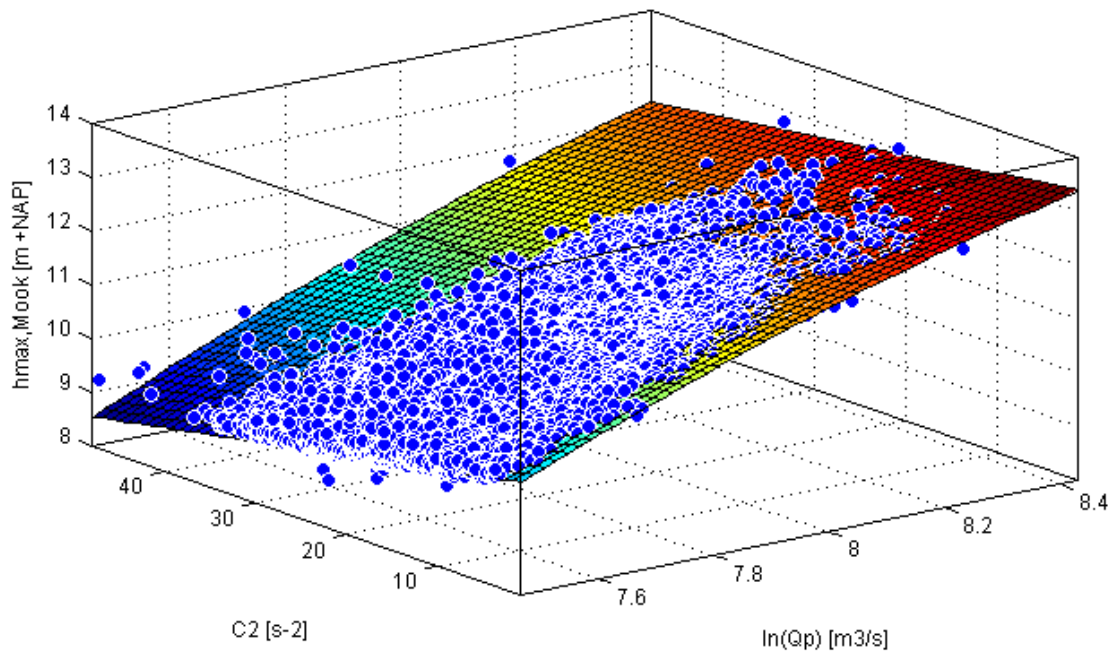


Figure 4-24 Polynomial surface fit with all 17,232 SOBEK results

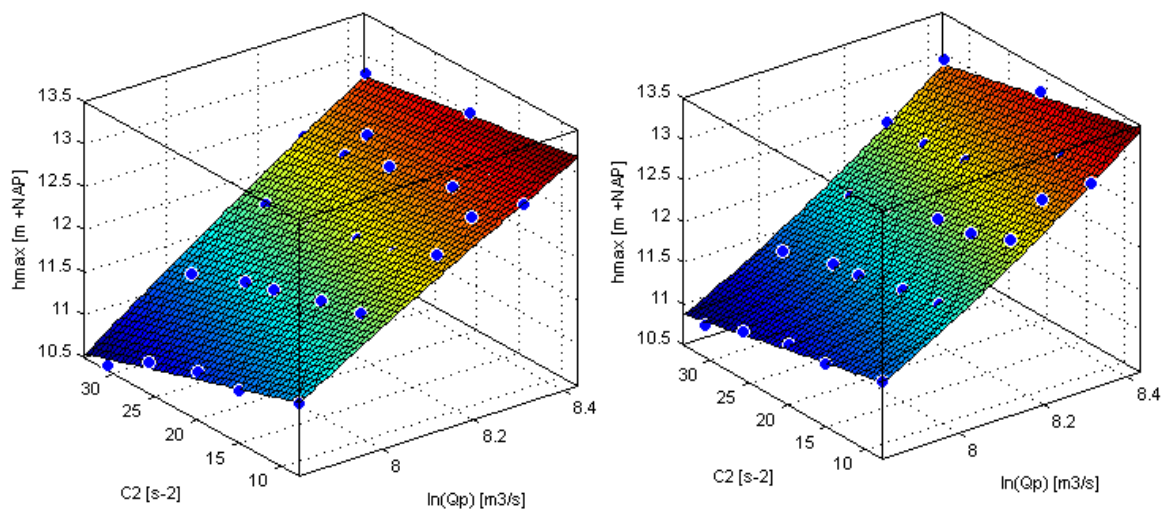


Figure 4-25 Polynomial surface fit with 25 SOBEK (left) and WAQUA (right) results

The differences between the SOBEK and WAQUA fits can be explained by the fact that WAQUA results in higher water levels at Mook, in particular for the higher and the lower range (see Figure 4-19). This turns the slightly concave SOBEK surface into a slightly convex WAQUA surface. Appendix G contains also a few figures of surface fits for the locations Venlo and Megen, and for the variables  $D_{85\%}$  and  $V_{85\%}$ . A transformation function as shown in this section, is used in the probabilistic methods of the next sections to derive the water level frequency curve, and thus the design water levels.

#### 4.6.2 Explicit probabilistic method

The explicit probabilistic approach (section 3.6.2) needs three elements:

- The function  $h_{\max,x} = f(Q_p, C_2)$ : see section 4.6.1.
- The probability distribution for  $Q_p$ : see section 4.3.1.
- The probability distribution for  $C_2$ : see section 4.3.1 and Table 3-5.

Equation 4.1 with the coefficients of the 25 SOBEK simulations is used to model the local water levels as function of  $Q_p$  and  $C_2$ . Two  $Q_p$  distributions (GPD and Kernel) and two  $C_2$  distributions (Weibull and discrete) were applied. Figure 4-26 shows the water level return periods for the different distributions. The difference between the two  $C_2$  distributions is negligible, but the Kernel distribution approaches the reference better than the GPD. With  $D_{85\%}$  as second variable comparable results were found. Appendix G (Figures G-10 and G-11) gives the water level return periods when the coefficients of the 25 SOBEK simulations and all SOBEK simulations were used ( $Q_p$  distribution: Kernel,  $C_2$  distribution: Weibull). Differences between the two are small, which gives confidence that the 25 floods are a good representation of the complete set. In section 4.6.4, the results of the explicit methods are compared to the other methods.

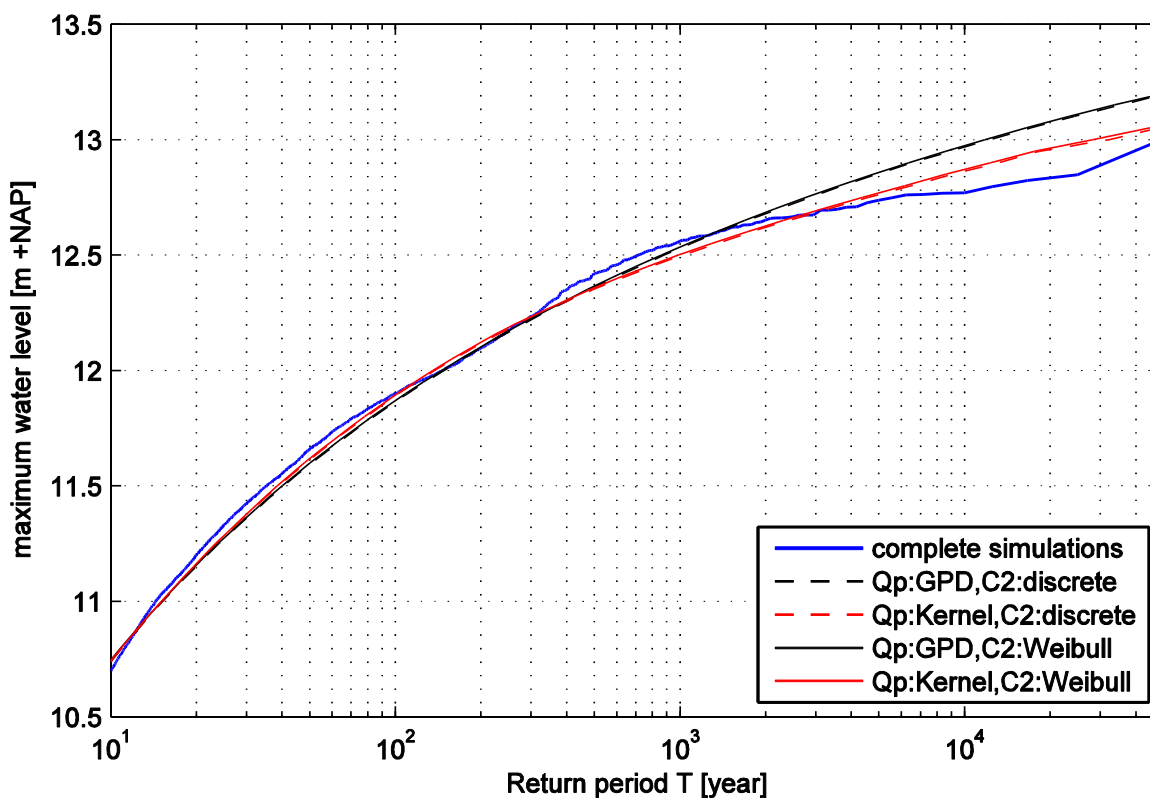


Figure 4-26 Water level return periods at Mook in the explicit probabilistic approach

### 4.6.3 Implicit probabilistic method

In this second probabilistic method, no assumptions are needed about probability distributions of  $Q_p$  and  $C_2$ . Instead, the transformation function is used to estimate the local water level  $h_{\max,x,\text{estimate}}$  of every hydrograph without using a SOBEK or WAQUA simulation. Figure 4-27 shows the error in this estimate when the transformation function is based on 25 SOBEK results. Subsequently, the  $h_{\max,x,\text{estimate}}$  was used to construct the water level frequency line (solid black line in Figure 4-28) according to the plotting position method of section 4.4.3. In section 4.6.4, the results of the implicit methods are compared to the other methods.

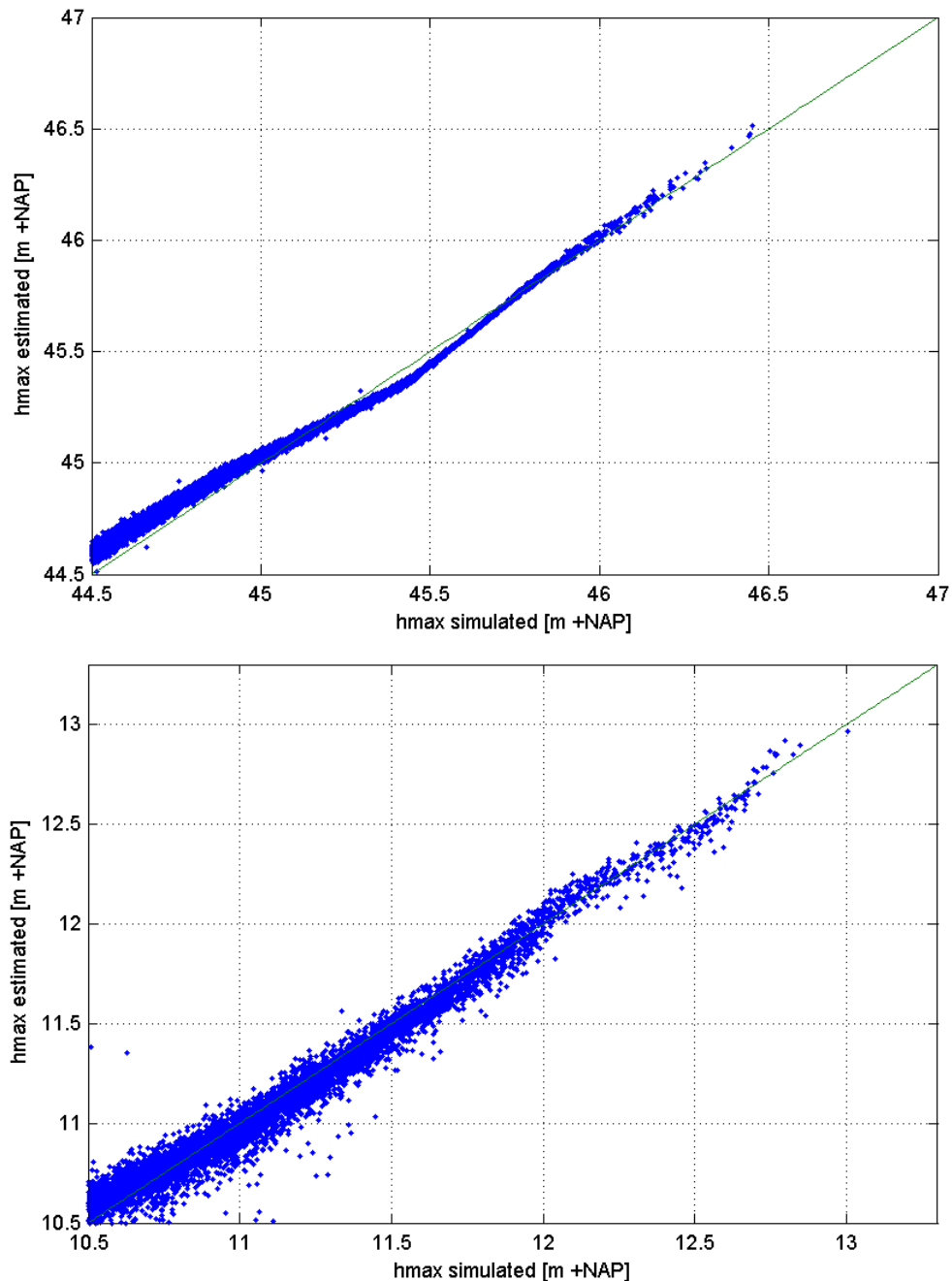


Figure 4-27  $h_{\max,\text{Mook}}$  (x axis) versus  $h_{\max,\text{Mook,est}}$  (y axis). Borgharen (upper) and Mook (lower)

#### 4.6.4 Water level frequency curves for the probabilistic methods

Figure 4-28 shows the results of the two probabilistic approaches in relation with the results of the standard and vertical hydrographs (without modified selection interval).

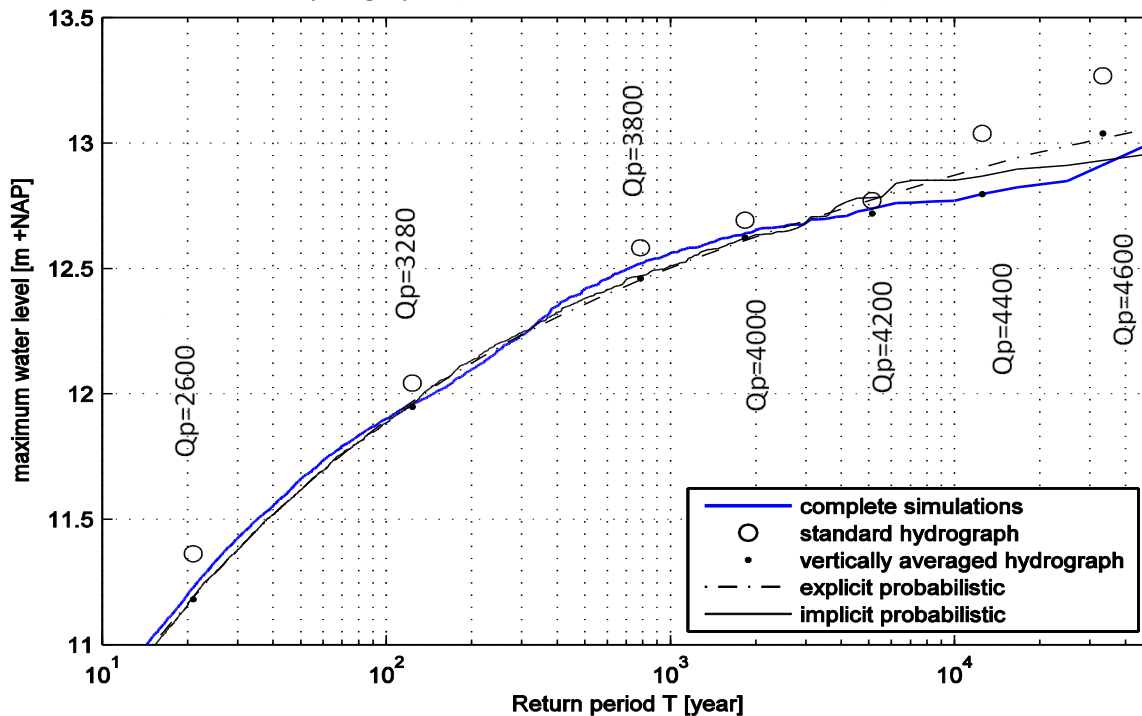


Figure 4-28 Results of the two probabilistic methods at Mook (with Kernel)

All methods show a good correspondence with the reference of the complete simulation, in particular for the most important return periods between 100 and 5000 year. The standard method shows to be an overestimation of the water level frequency. Vertically averaged hydrographs and the two probabilistic approaches give virtually the same results for return periods up to 2000 year. The overestimation of the probabilistic methods for larger return periods can be explained by the goodness of fit of the transformation function (Figure 4-27), which can be explained by inflow to large retention basins like Lob van Gennep. Improving the transformation function will yield a direct improvement of the probabilistic methods.

#### 4.6.5 Probabilistic methods based on WAQUA

Although there is no reference set with 17,232 WAQUA simulations, like for SOBEK, the results of the two probabilistic methods with the use of WAQUA are shown in Figure 4-29 for location Mook. The difference with the results of previous sections is caused by the generally higher water levels in WAQUA compared to SOBEK (see Figure 4-19). This leads to a slightly different transformation function (see Figure 4-25). However, the principle is the same and the method can be applied as well to WAQUA as to SOBEK. Since a WAQUA reference set is lacking, the accuracy of the estimate cannot be determined, and one must assume that the suitability of the method is not seriously affected by using a different hydrodynamic model.

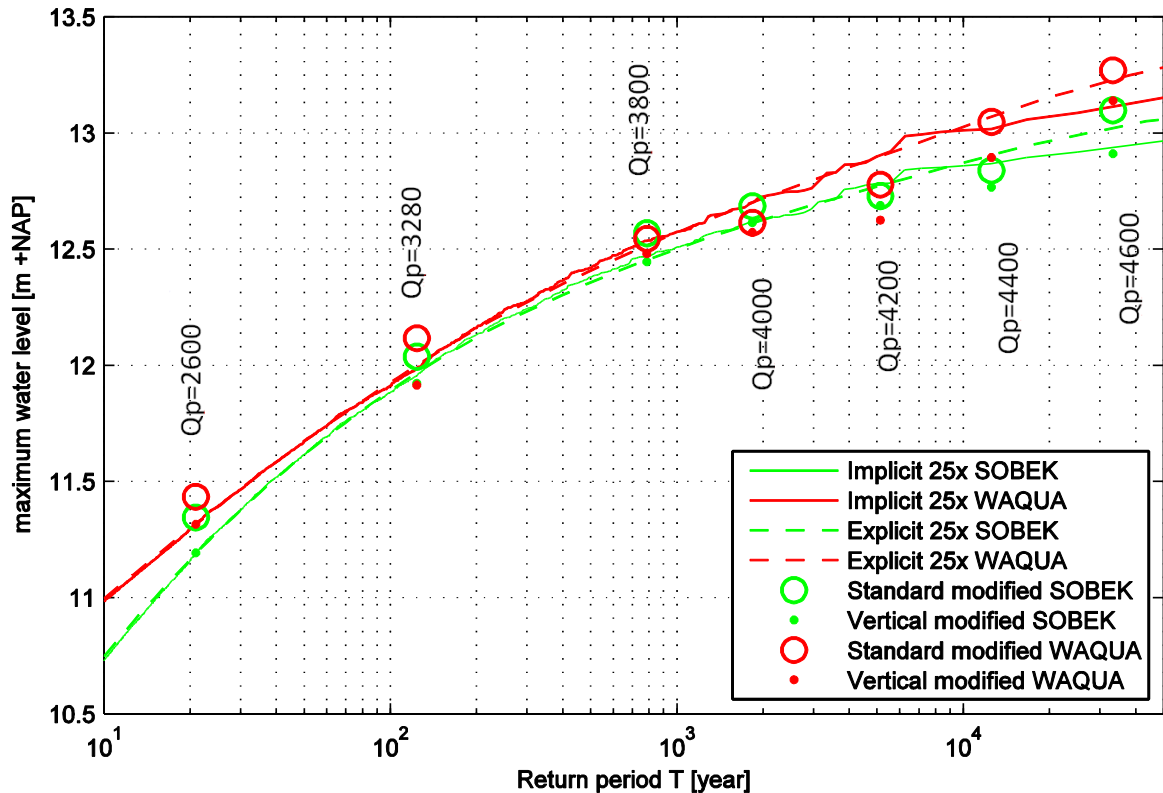


Figure 4-29 Design hydrograph- and probabilistic methods in SOBEK and WAQUA, at Mook

## 4.7 Retention effects

Previous sections show the water level frequency curves as estimated by the different methods. An additional question is how accurate the design hydrograph methods and the probabilistic methods can estimate the effect of a mitigation measure like a retention basin. Lob van Gennepe, just upstream of Mook, is taken as a case study since it is relatively large, so the effects are clearer than for small retention basins.

### 4.7.1 Effect of Lob van Gennepe in SOBEK

All 17,232 GRADE hydrographs were simulated in SOBEK, once including the Lob van Gennepe and once without the Lob van Gennepe. The effect at Mook is defined as the difference between the maximum water level at Mook with and without the Lob van Gennepe. In most cases the effect of the Lob van Gennepe is zero, since the basin will only flood during extreme floods. In approximately 40 cases, the retention basin reduces the downstream water levels, so the return period of flooding in the Lob van Gennepe is approximately 1250 years. The retention effect is 0 - 15 cm at Mook (Figure 4-30). The effect at Megen is generally 10 - 30% less than at Mook.

Figure 4-31 shows some hydrographs just before (rkm 155.3) and just after (rkm 165.8) the retention basin. A peak discharge reduction of 20 - 30 m<sup>3</sup>/s between the two points does also occur when Lob van Gennepe does not flood, and there is a time shift of a few hours. In most cases

the downstream discharge reduction is spread out over the entire period that the retention basin works (peak shaving). In some cases however, the downstream hydrographs shows a sudden increase while water is still flowing into the retention basin (e.g. hydrograph 4731). This is may be caused by a limited retention capacity due to a limited head difference over the inflow structure. More hydrographs are shown in Appendix H.

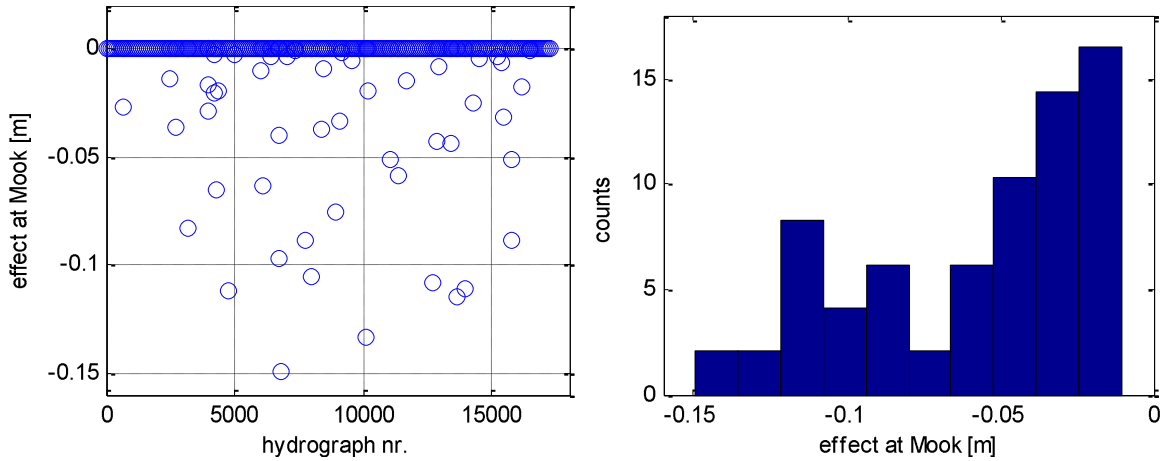


Figure 4-30 Effect of Lob van Gennepe on  $h_{max,Mook}$  (left) and histogram of this effect (right)

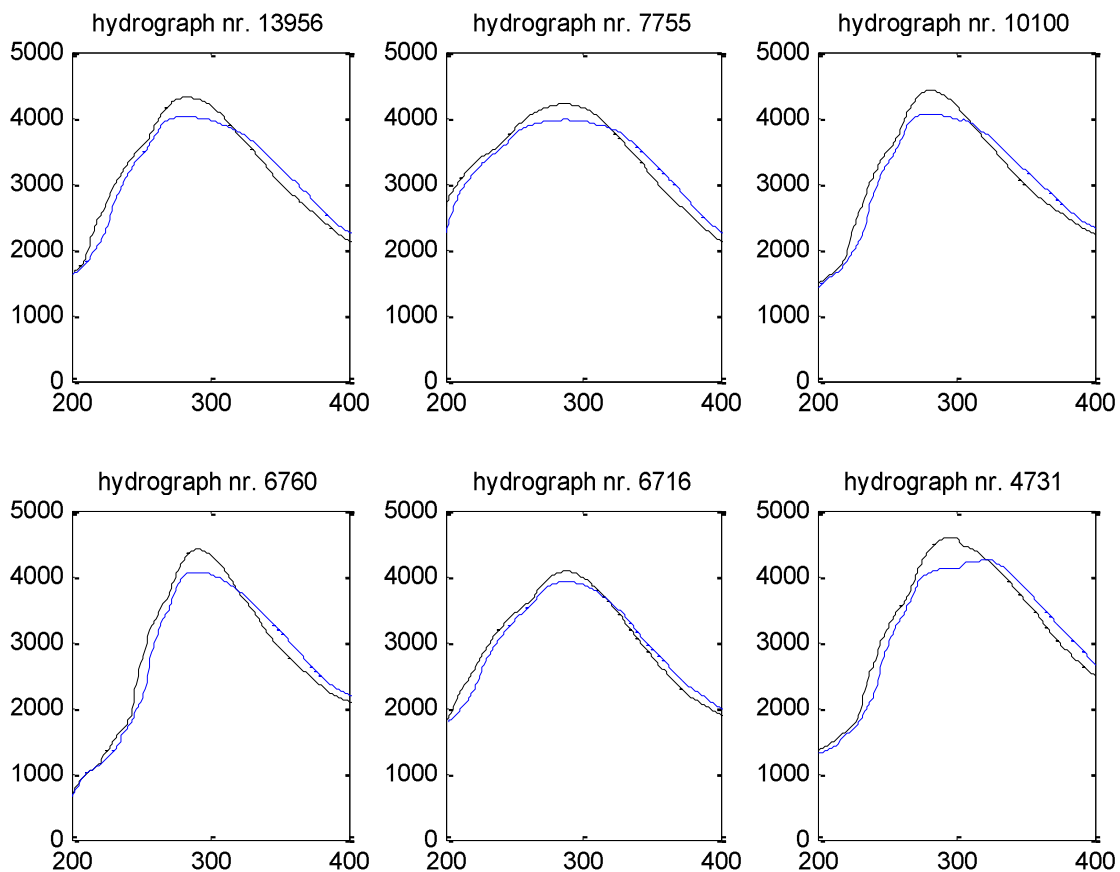


Figure 4-31 Influence of Lob van Gennepe on the hydrograph before (black) and after (blue)

Figure 4-32 shows the water level frequency curve with and without retention effect of the Lob van Genneep. It is clear that this retention area causes a drop in the extreme water levels, but at the design frequency (T = 1250 year) the effect is negligible. Reduction of the water level frequency curve starts from  $h_{max,Mook} = 12.57 \text{ m} + \text{NAP}$  which is equivalent to  $h_{max,Lob} = 13.75 \text{ m} + \text{NAP}$  which is equal to the crest height of the inlet structure. To be effective at Mook for the design frequency of 1/1250, the crest height needs to be lower.

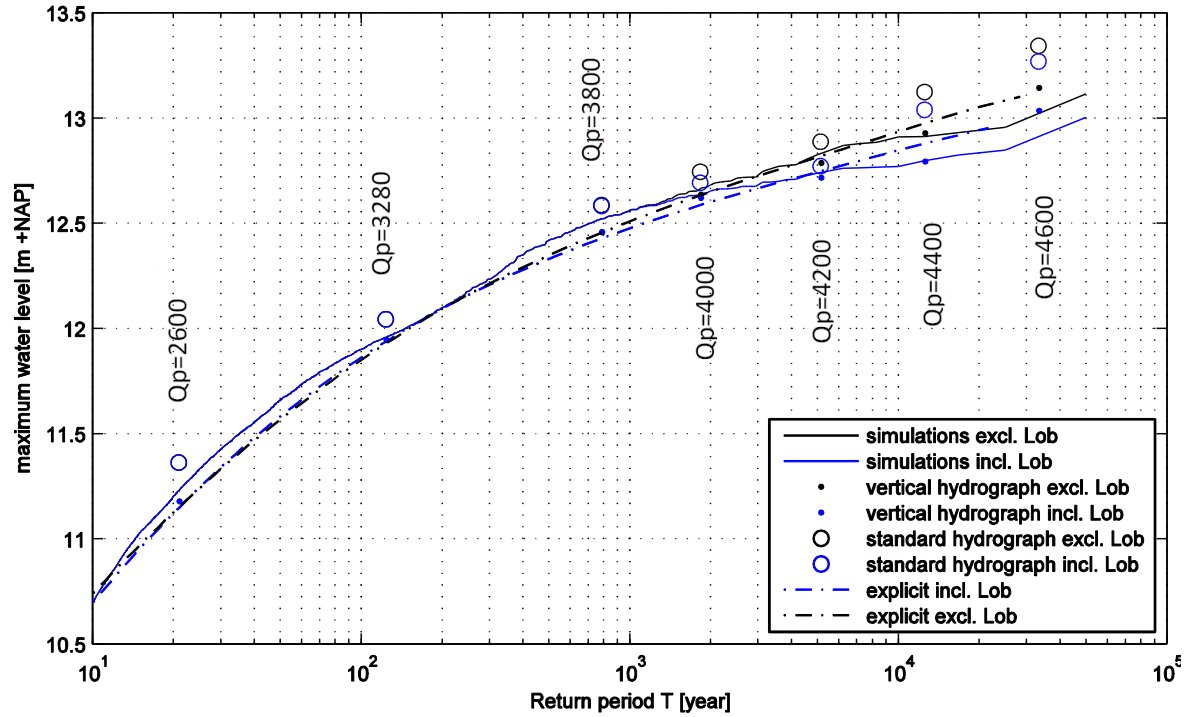


Figure 4-32 Return periods at Mook with and without retention Lob van Genneep (kernel)

T [year] ( $Q_p, \text{Kernel}$ )	21 (2600)	124 (3280)	785 (3800)	1832 (4000)	5129 (4200)	12589 (4400)	33271 (4600)
$\Delta_{\text{simulations}}$ [cm]	0	0	0	2.5	9	11	11
$\Delta_{\text{standard}}$ [cm]	0	0	0.5	5	12	9	7
$\Delta_{\text{vertical}}$ [cm]	0	0	0	1.5	7	13	11
$\Delta_{\text{explicit}}$ [cm]	0	0	3	4.5	7	10	12

Table 4-9 Retention effect ( $\Delta$ ) at Mook for different  $Q_p$

Taking  $\Delta_{\text{simulations}}$  as reference, the standard method seems to overestimate the effect for  $1000 < T < 6000$ , and seems to underestimate the effect for higher return periods. On the contrary, the vertical averaging method seems to underestimate the effect for  $1000 < T < 6000$ , and seems to overestimate the effect for higher return periods. The explicit probabilistic method overestimates for  $T < 5000$ , but is more accurate for  $T > 5000$ . It must be noted that these effects involve small differences in the order of centimetres, which makes the result sensitive to statistical uncertainty in the extreme range of the reference set.

### 4.7.2 Effect of Lob van Gennepe in WAQUA

A selection of 15 GRADE hydrographs (Table 3-5, columns  $Q_p \geq 3500$ ) was also simulated in WAQUA, once including Lob van Gennepe and once without Lob van Gennepe. Figure 4-33 shows the effect of Lob van Gennepe on the water levels at Mook, both in SOBEK and WAQUA. In a few cases, the area does not flood in SOBEK, whereas in WAQUA there is a small effect on the water levels. It is not the case that one of the two models gives systematically a larger or smaller effects.

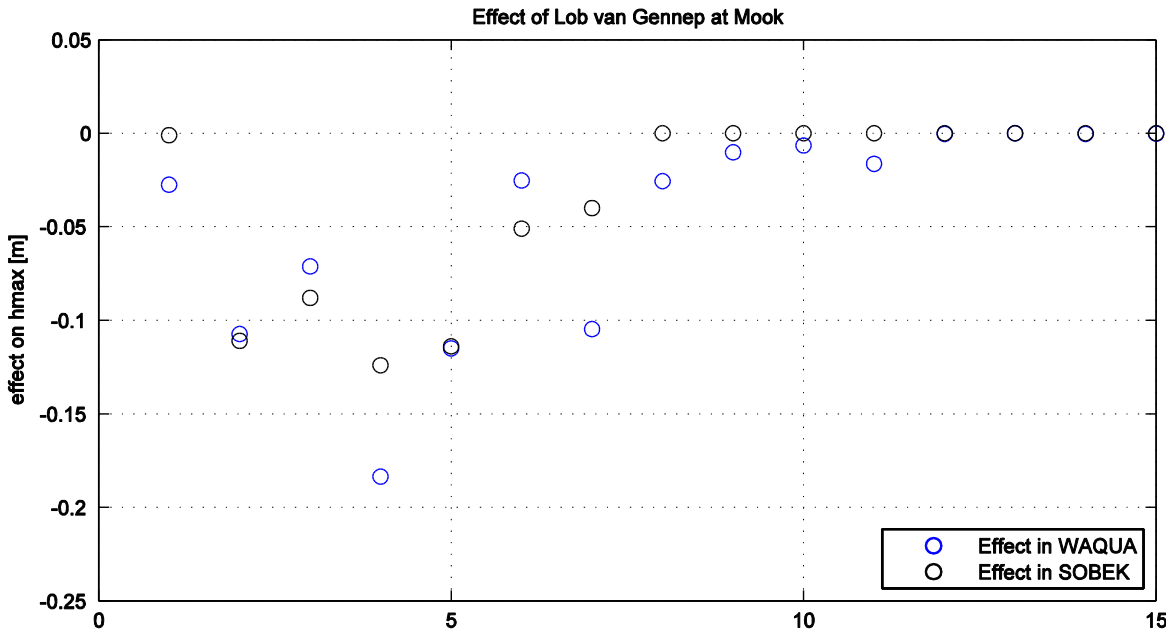


Figure 4-33 Differences between WAQUA and SOBEK effects at Mook

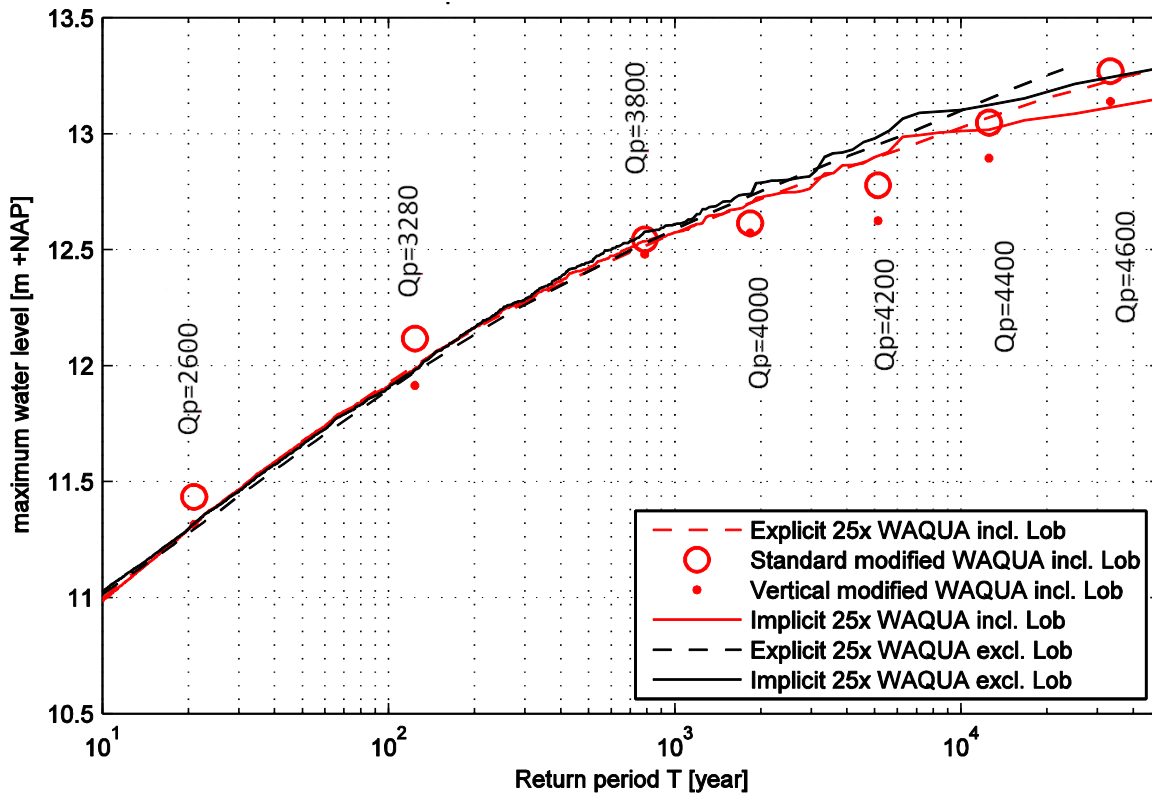


Figure 4-34 Return periods at Mook, based on WAQUA, incl. and excl. Lob van Gennepe

### 4.7.3 Influence of shape variables on retention effect

This section shows how the effect of the Lob van Gennep is influenced by the shape of the hydrograph. All results are based on SOBEK (1D) simulations. In the further analysis, only floods are taken into account that cause an effect of at least 1 cm at Mook.

A first step in the correlation analysis is the relation between the effect at Mook and the shape variables. Figure 4-35 shows the dependence on the peak discharge: a higher peak discharge above the threshold of 3800 m<sup>3</sup>/s leads generally to a larger effect. Appendix H gives these relations for other shape variables as well. Table 4-10 gives the rank correlation coefficients between all shape variables and the retention effect at Mook and Megen.

The second step in the correlation analysis is the conditional correlation. The approach with conditional correlations works less good with the retention effect since the dataset is very small. In this case, the conditional correlation depends strongly on the interval of  $Q_p$  that is chosen. E.g. in case of two points in this interval the correlation will always be 1, but with a wider interval that includes three points the correlation may suddenly be much lower. Therefore, the  $R^2$  was determined for a simple linear model that includes  $Q_p$  and one of the other shape variables (Table 4-10, right hand column). Figure 4-36 and similar figures in Appendix H give no visual reason to use a more complex than linear relation between the retention effect and the shape variables. Additionally, the use of quadratic models does not increase the  $R^2$  with more than 0.05.

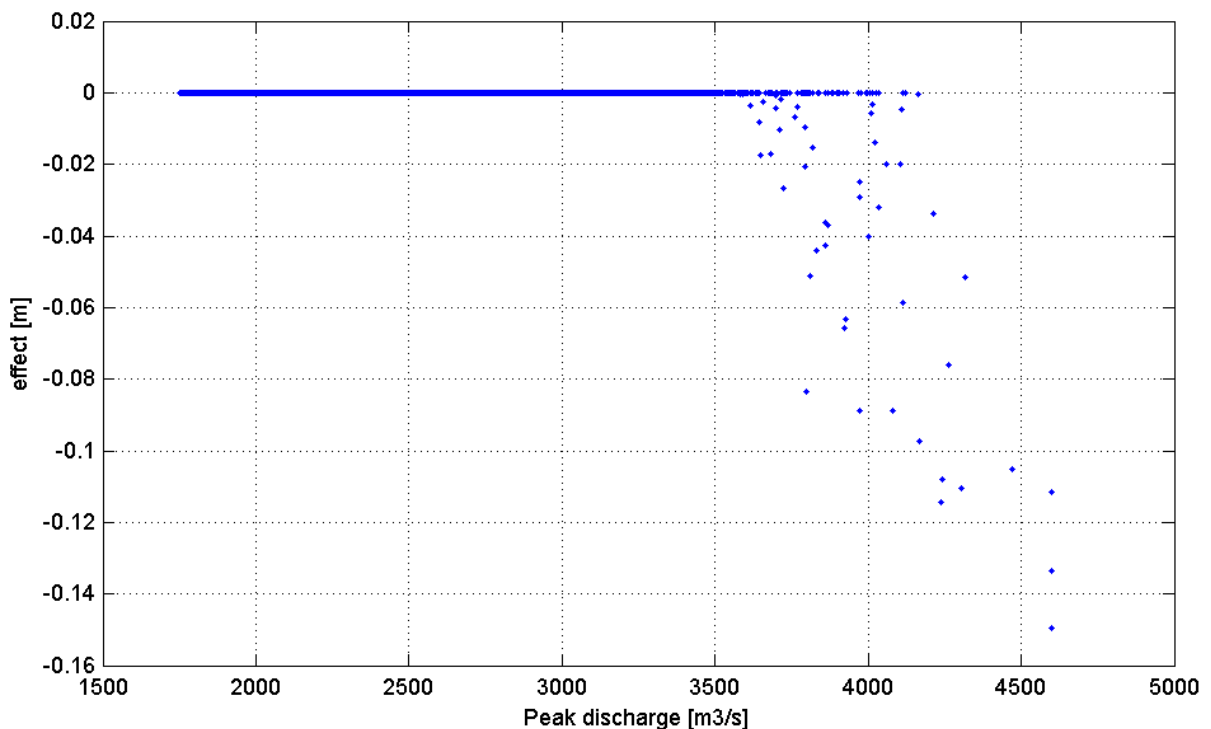
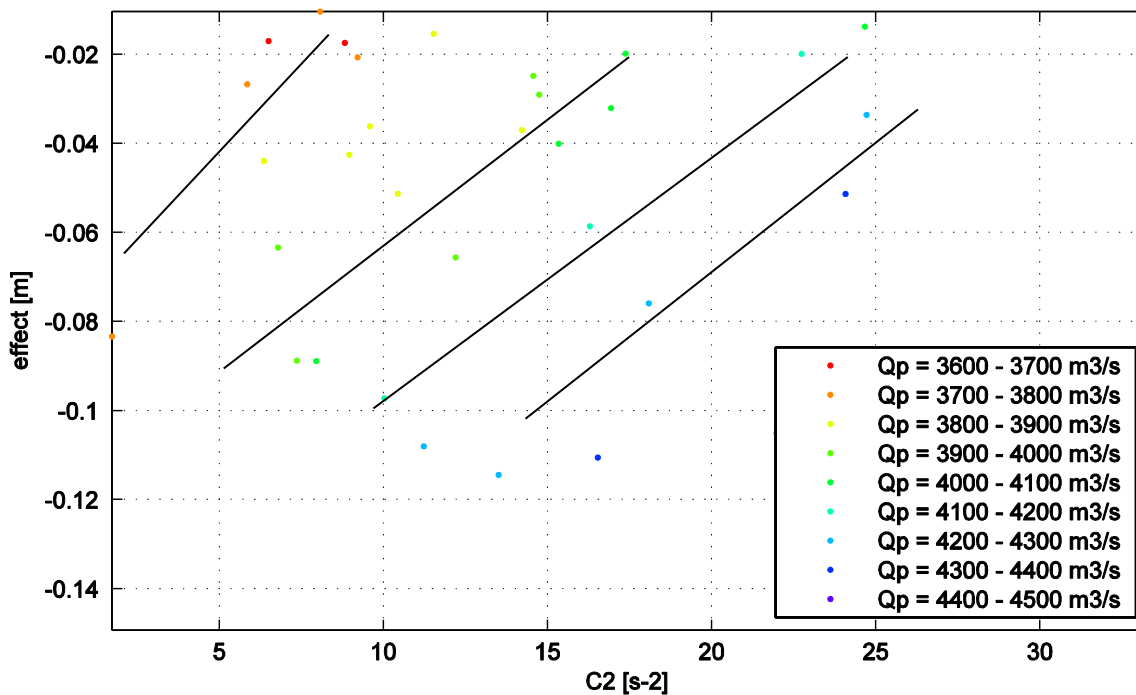


Figure 4-35 Relation between retention effect at Mook and shape variables

Shape variable	Correlation Mook (Kendall)	Correlation Megen (Kendall)	R <sup>2</sup> value (Mook)
$Q_p$	-0.689	-0.685	R <sup>2</sup> =0.580 <sup>4</sup>
$D_{1250}$	0.061	0.048	R <sup>2</sup> =0.649
$D_{50\%}$	0.220	0.209	R <sup>2</sup> =0.695
$D_{85\%}$	0.179	0.172	R <sup>2</sup> =0.773
$V_0$	-0.054	-0.067	R <sup>2</sup> =0.719
$V_{1250}$	-0.084	-0.097	R <sup>2</sup> =0.748
$V_{50\%}$	0.117	0.108	R <sup>2</sup> =0.768
$V_{85\%}$	0.060	0.051	R <sup>2</sup> =0.827
$RV_0$	0.190	0.178	R <sup>2</sup> =0.723
$RV_{1250}$	0.240	0.236	R <sup>2</sup> =0.673
$RV_{50\%}$	-0.077	-0.073	R <sup>2</sup> =0.580
$RV_{85\%}$	-0.085	-0.086	R <sup>2</sup> =0.580
$C_1$	-0.066	-0.060	R <sup>2</sup> =0.846
$C_2$	-0.174	-0.169	R <sup>2</sup> =0.858

Table 4-10 Rank correlation coefficients between retention effect at Mook and shape variables

Figure 4-36 Dependence of retention effect at Mook on  $C_2$ 

<sup>4</sup> In fact this is equal to the squared Pearson linear correlation coefficient between  $Q_p$  and  $h_{max}$  ( $\rho = -0.762$ )

#### 4.7.4 Meuse system without retention basins

In the previous sections, the effect of one retention basin (Lob van Gennepe) was shown. This section shows the cumulative effect of all retention basins that are included in the SOBEK model. Figure 4-37 shows the frequency curve for Mook. Results for other locations are given in Appendix H. The difference between standard and simulations for  $T > 10,000$  year is smaller in the model with no retention (green) than in the reference model (blue). Table 4-11 gives the retention effects  $\Delta$  as computed with the three methods.

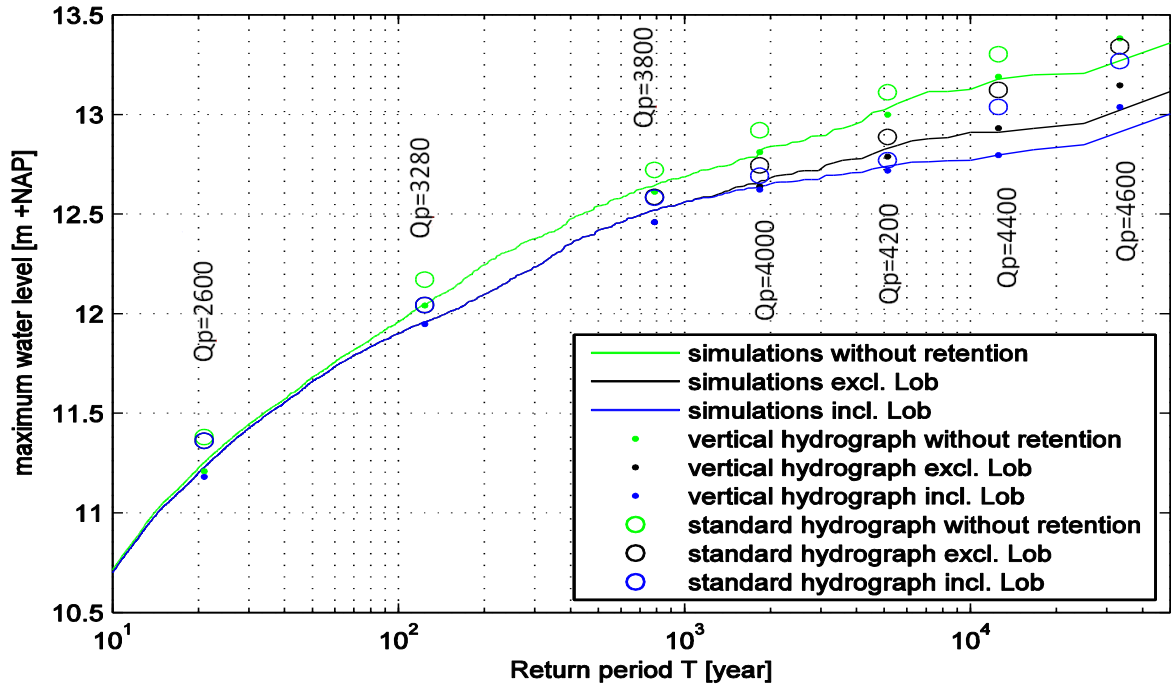


Figure 4-37 Water level return periods based on system without any retention basins (Kernel)

T [year] ( $Q_{p,Kernel}$ )	21 (2600)	124 (3280)	785 (3800)	1832 (4000)	5129 (4200)	12589 (4400)	33271 (4600)
$\Delta_{simulations}$ [cm]	2	8	12	17	29	38	35
$\Delta_{standard}$ [cm]	2	13	14	23	34	26	24
$\Delta_{vertical}$ [cm]	3	9	15	19	28	39	35

Table 4-11 Effect ( $\Delta$ ) of all retention basins at Mook for different  $Q_p$

Similar to the results for Lob van Gennepe, the standard method seems to overestimate the effect for  $T < 6000$ , and seems to underestimate the effect for higher return periods. The vertical averaging method seems to overestimate the effects as well, but estimate for  $T > 1000$  is relatively accurate compared to the estimate of the standard method. It must be noted that the probabilistic methods and design hydrographs methods with modified selection interval were not investigated for time reasons.

## 5 Discussion

The main objective of this thesis was to investigate the influence of hydrograph shape on design water levels on the river Meuse and to compare the performance of different methods to determine these design water levels. The research was guided by five research questions:

1. To what extent are design water levels affected by using GRADE simulated discharge data instead of measured discharge data?
2. Which hydrograph shape variables determine the downstream water levels, and how?
3. How accurate are the design water levels determined by design hydrograph methods?
4. How accurate are the design water levels determined by probabilistic methods?
5. How is the effect of a retention basin determined by hydrograph shape, and how accurately is this effect determined by the design hydrograph methods?

The next five sections are structured according to the five research questions. For each research question, the main findings are stated, compared to other research, interpreted and explained, and limitations, implications and recommendations are given. Subsequent sections discuss considerations about which method to use in practice, and summarize the recommendations.

### 5.1 Switching from measured data to GRADE data

The results show that using the GRADE dataset instead of the measured dataset affects the design water levels through two mechanisms; a wider standard hydrograph and generally a higher peak discharge frequency (section 4.1). The joint effect on the design water levels is 40 cm at maximum, depending on location and return period.

The present findings concerning the wider standard hydrograph (Figure 4-1) are in agreement with the results of Barneveld & Van den Berg (2010), although the presently found hydrograph is slightly wider. Differences between the present result and Barneveld & Van den Berg (2010) may be caused by differences in rainfall resampling techniques and the hydraulic routing method between the older GRADE dataset and the more recent GRADE dataset. There are at least three possible explanations for the difference in shape between the GRADE and measured datasets: (1) the calibration of the hydrological model, (2) statistical uncertainty in the hydrograph shape of the measured dataset due to the small set of 30 measured floods and (3) the use of a daily time step in GRADE which could be too large to capture the dynamical behaviour of the river Meuse. The good validation results of section 2.1.2 in Kramer & Schroevers (2008) suggest that the first explanation is not satisfactory. The second explanation can be tested by randomly drawing periods of 100 years from the GRADE set and determining the variation in the standard hydrograph shape. Concerning the third explanation, it is planned to reduce the daily time step to hourly or 6-hourly time steps in the near future. Ogink (2012) and Kramer (2012) compared the measured standard hydrograph to the GRADE vertically averaged hydrograph shape, and not to the GRADE standard hydrograph shape. Our results show the effect of using GRADE data while keeping the averaging method the same.

The peak discharge distribution of the GRADE dataset (Figure 4-3) shows higher design discharges than the design discharge curve based on the measured dataset (Tijssen, 2009), at least for return

periods between 10 and 2000 year. Depending whether a parametric Generalized Pareto or non-parametric Kernel distribution is chosen to model the GRADE peak discharge distribution, GRADE gives lower design discharges for  $T > 7000$  year or  $T > 2000$  year respectively. The found peak discharge distribution corresponds to distributions in Kramer & Schroevers (2008) and Van den Boogaard et al. (2014). Interestingly, the GRADE peak discharge frequency curve follows no straight line on a log-scale, as assumed in current practice (e.g. WL|Delft Hydraulics, 1993), but seems to flatten for large return periods. This flattening is also present in the frequency line of the simulated 10-day precipitation (Buishand & Leander, 2011), which is an indication that it is not caused by hydrological processes.

For return periods up to 2000 year, the use of GRADE leads to higher design discharges and wider hydrographs, and thus to higher design water levels along the river Meuse. For the higher return periods, it is ambiguous how the difference between measured and GRADE peak discharge distributions affects the downstream design water levels; the increase or decrease in design discharge depends on the return period, and the increase in water level for a given peak discharge depends on the location of interest.

The present results show how downstream water levels are affected by differences between measured and GRADE datasets, with respect to standard hydrograph shape and in peak discharge distribution, which was not shown before. A limitation of the present study is that the effect of using GRADE data instead of measured data was only investigated for the standard hydrograph method. Application of the vertically averaged hydrograph, standard hydrograph with a modified selection interval, or the probabilistic methods may lead to different results. The vertically averaged hydrograph was not available for the measured series, and the last two methods are hard to apply to the short measured dataset due to the lack of extreme floods. It is recommended to investigate what causes the GRADE standard hydrograph to be wider than the one from the measured dataset, e.g. by application of a hourly time step or by application of the vertically averaged hydrograph method to both the measured and the GRADE dataset. Although GRADE has its own uncertainties (e.g. Ogink, 2012; ENW, 2013; Van den Boogaard et al., 2014), it is recommended to use GRADE for the determination of the design water levels.

## 5.2 The influence of hydrograph shape variables

Hydrograph shape variables that are related to the peak of the flood hydrograph have the strongest effect on downstream water levels. Next to the most important variable peak discharge ( $Q_p$ ), good predictors are the peak duration ( $D_{85\%}$ ), peak volume ( $V_{85\%}$ ) and peak curvature ( $C_2$ ). Conditional correlation between these variables and the water levels is surprisingly strong; using a simple polynomial function and  $Q_p$  and  $C_2$  as predictors, downstream water levels can be estimated with an error (RMSE) of 4.2 - 8.7 cm. This is significantly more than the RMSE of 5.7 - 20.6 cm that follows when  $C_2$  is not used. Therefore  $Q_p$  and  $C_2$  were used as the two variables to predict downstream water levels.

The influence of duration and volume is widely recognized in literature (Gerretsen, 2009; WL|Delft Hydraulics, 1993), but the present results show that the volume and duration around the peak are better predictors for downstream water levels than the other volume and duration

variables. The present results confirm the importance of the peak curvature, as stated by e.g. Gerretsen (2009) and Woltemade & Potter (1994). An advantage of the peak curvature over the volume or duration is that it is independent from the peak discharge, and thus does not require advanced analyses including multivariate dependence (e.g. Gräler et al., 2013). Although giving good results, the choices for the duration and volume levels (at 85% of the peak discharge) and the curvature interval (2 days before and after) are arbitrary to some extent. These choices in variable definition can be optimized to achieve even stronger relations. Also base flow separation methods can be applied to achieve stronger correlations. Conditional correlation proved to be a useful statistic to identify relevant variables, but its stability depends on the size of the peak discharge class and for that reason is less useful for small datasets.

The sensitivity of the downstream water levels to differences in wave shape depends on location and on the magnitude of the peak discharge (e.g. Figure 4-2 and Figure D-3 in Appendix D). That downstream locations are more sensitive to these shape differences than upstream locations can be explained by the amount of peak attenuation, which depends both on the hydrograph shape and the river geometry (Woltemade & Potter, 1994). Peak attenuation is small in the steeper upstream reaches, and therefore the hydrograph shape is of less importance there. More downstream, the wider floodplains influence the peak attenuation to a large extent. For a given location, some peak discharges are more sensitive to hydrograph shape than other (Figure 4-2). These differences are hard to explain in general, but at Mook (km 166) for example, the insensitivity for peak discharges of 4000 m<sup>3</sup>/s can be explained by the effect of Lob van Gennep, which reduces flood waves to approximately the same level, regardless of the hydrograph shape. At other peak discharges than 4000 m<sup>3</sup>/s, the retention basin is not effective.

### 5.3 Design hydrograph approaches

Application of the standard hydrograph method (Generalized Pareto distribution, selection interval 1750-3200 m<sup>3</sup>/s) to the GRADE dataset leads to significantly higher design water levels compared to the reference set based on simulation of all GRADE flood waves, depending on location and return period.

This deviation from the reference can have two main causes: (1) the assumed Generalized Pareto distribution overestimates the peak discharges, and (2) the assumption is not valid that the peak discharge return period equals the local water level return period when the averaged hydrograph shape is used. In other words: the averaged hydrograph shape is unable to represent the peak attenuation. These two possible causes hold also for the vertically averaged hydrograph. Using a Kernel instead of a GPD minimizes the effect of the first cause. After application of the Kernel there remains an overestimation of the standard hydrograph method. The residual deviations can be explained partly by the choice of the wide selection interval for averaging. Using the modified selection interval around the peak discharge of interest for averaging, improves the results of the standard hydrograph method significantly for  $Q_p \geq 4200$  m<sup>3</sup>/s. With this improvement, the differences in design water levels between the standard and vertically averaged hydrographs become smaller, and for the most relevant return periods (250 - 10,000 year) one method is not more accurate than the other (Figure 4-23).

The overestimation of the standard hydrograph increases in downstream direction, which is expected since the influence of hydrograph shape also increases in downstream direction. An overestimation is present over the entire range of return periods, but increases strongly for return periods larger than 5000 year at Mook and Megen. Since this strong increase for large return periods is not observed for the vertically averaged hydrographs and to a lesser extent for the standard hydrograph with modified selection, it suggests that the standard hydrograph shape is not representative for the most extreme floods.

The good results of some of the design hydrograph methods support the assumption of the design hydrograph methods that the discharge return period equals the water level return period: the averaged hydrograph shapes (in particular vertically averaged and standard with modified interval) lead to approximately the same water level frequency curve as the simulation of all hydrographs. These results are based on the current Meuse system as modelled in SOBEK. It is important to note that this validation is only possible with use of GRADE data. With the measured set one cannot observe the deviation from the GPD and the different hydrograph shapes in the extreme range. The significant improvements made with these observations stress the need for a method like GRADE, providing a much larger dataset.

#### 5.4 Application of probabilistic approaches

The results of the probabilistic methods show a good agreement with the reference based on simulation of all flood waves in the GRADE dataset. The deviations of the probabilistic water level frequency line from the reference can have three causes: (1) the goodness of fit of the  $Q_p$  and  $C_2$  distributions, (2) the assumption of independence between  $C_2$  and  $Q_p$ , and (3) the goodness of fit of the transformation function (which relates local water levels to shape variables at Borgharen). The deviations are still present when the  $Q_p$  distribution was corrected with a Kernel. It is very unlikely that dependence between  $Q_p$  and  $C_2$  is the cause, given the results of the correlation analysis. The most important cause must be sought in the goodness of fit of the transformation function because this fit is the only difference between the reference and the implicit method, and the implicit method still shows the deviations.

The accuracy of the transformation function is crucial in the probabilistic approach. The simple polynomial function used in this thesis has several limitations. Due to its nature, the function cannot capture discontinuities or local effects in the relation between shape variables and water levels. One example is the discontinuity that is present in the stage-discharge curve for most locations. Another example is the effect of a retention basin that reduces the water levels only for a restricted range of discharges. Such effects are smoothed in the present approach. Alternatively, one could derive the transformation function by interpolation between the 25 simulation results, as applied in Geerse (2013), instead of fitting a parametric function. Whether this approach does capture the discontinuities depends on the number of simulations (maybe more than 25 are needed) and on the magnitude and shape of the simulated hydrographs. Further research needs to assess the suitability of these transformation functions to predict the effectiveness of measures. Although the peak curvature  $C_2$  was chosen for modelling the hydrograph shape, other variables can be used as well. The duration  $D_{85\%}$  (used in Geerse, 2013) in particular is suitable because of its independence with  $Q_p$  and its straightforward

interpretation. The choice for  $C_2$  was based largely on results at location Mook. Additionally an analysis could be valuable in which the predictor variable and transformation function are derived separately for each location. Using additional shape variables in the transformation function may increase its accuracy too.

A potential advantage of the probabilistic methods is that the hydrodynamic simulations are only used to identify the response of the river system to a flood wave, and not to deliver statistical information about the flood frequency. This allows changing of the input discharge statistics without the need to run the simulations again, which may be useful in studies on climate change for example. In the standard method, every change in discharge statistics yields a different standard hydrograph and thus requires new simulations to determine the water level frequencies. A potential disadvantage of the probabilistic methods is that when the river system changes, simulation of more hydrographs is required (25 instead of 7) to determine the response of the adapted river system.

## 5.5 Effect of retention basins

The case study of retention basin Lob van Gennep shows the accuracy of the different methods in estimating the design water level reduction by a retention basin. Estimates of the analysed methods deviate up to 4 cm from the reference set which shows an effect of up to 11 cm. Although more uncertainties generally may lead to less effective retention basins (Kok et al., 2003), it was not found that design hydrograph methods systematically overestimate the effect of the retention basin compared to the reference. Overestimation or underestimation depends on the return period, and whether standard or vertically averaged hydrographs are used. For example, the standard method seems to overestimate the effect for  $1000 < T < 6000$ , and seems to underestimate the effect for higher return periods. On the contrary, the vertical averaging method seems to underestimate the effect for  $1000 < T < 6000$ , and seems to overestimate the effect for higher return periods. The explicit probabilistic method overestimates for  $T < 5000$ , but is more accurate for  $T > 5000$ . The design hydrograph methods show a decrease in effect for the very extreme discharges and a slight flattening of the frequency curve around the inflow level of the retention basin, which is not clearly shown in the probabilistic methods.

The reason that the probabilistic approaches have difficulty to capture the shape of the reference frequency curve is most probably that the method uses only five discharge levels to determine the transformation function. As a result, the behaviour between those discharge levels is not captured well, especially when a retention basin becomes active in between. Local discontinuities in the frequency curve that occur around the point where the retention basin starts to flood, are then smoothed. As mentioned in the previous section, this could be improved by interpolation, but then still a denser grid of simulation results is needed. Therefore, one should be careful when applying the probabilistic methods to assess the effects of local measures or in a system with discontinuities in the relation between local water levels and shape variables. One should make sure that sufficient and representative floods are selected for hydrodynamic simulation. Effects of retention on the frequency curve are shown in the probabilistic methods, but are more smooth than what follows from complete simulation.

The analysis of the influence of the shape variables on the retention effect is limited by the small amount of hydrographs that actually flood the retention basin (approximately 40). Despite the dataset size, a pattern can be distinguished in the conditional correlation plots, indicating that the peak curvature is also a suitable predictor for the retention effect. More peaked hydrographs have a smaller effect than wide hydrographs with the same peak discharge. This can be explained by the peak attenuation upstream; peaked floods attenuate more, and so lead to lower water levels at the location of the retention basin and lead to less inflow of the retention basin. Additional research could investigate the influence of the local hydrograph shape on the effect of the retention basin.

The discussion above is mainly based on the results from the SOBEK model, since this is the only model for which the reference is available. But WAQUA results reveal some other issues. The design hydrograph methods show a rather horizontal part in the frequency curve that includes Lob van Gennep, which is even stronger in WAQUA (Figure 4-34) than in SOBEK (Figure 4-32). From the SOBEK reference we know that this flattening around the Lob van Gennep inflow threshold is less sharp than suggested by the design hydrograph methods. If this is also the case in WAQUA, the retention effect may be overestimated more by the design hydrograph methods than in SOBEK. Therefore additional research is needed which method is more accurate in predicting the effect of retention in WAQUA. It could be valuable to run a few thousands of WAQUA simulations including and excluding a retention basins, which would enable validations like this thesis research for the WAQUA Meuse model.

## 5.6 Which method to use for the estimation of water level frequencies?

Sections 4.4 up to 4.7 show how the estimated water level frequencies from the different methods relate to the reference and to each other. This section gives an evaluation of the different methods, and puts the results into perspective. An important question is which (dis)advantages the different estimation methods could have for water management practice in The Netherlands. Important considerations include the accuracy of the design water level estimate, the simplicity of the analysis, and the number of hydrodynamic simulations required.

The most simple indication that can be given of the accuracy of the method is the average RMSE. For a more complete picture of the accuracy of the different methods, the reader is referred to Figure 4-23, Figure 4-28 and similar figures for the other locations. Table 5-1 (second column) shows that vertical averaging reduces the RMSE with 50% compared to the standard hydrograph (current practice), without making the analysis more complex or increasing the number of simulations. The standard method can be considered a more conservative choice. Again a reduction of the RMSE with more than 50% can be reached by using vertical averaging with a modified selection interval. This requires the derivation of a design hydrograph shape per peak discharge class, but once these shapes are available, the method involves no more effort than without the modified selection. So a significant improvement of the current practice can be achieved by adopting the vertical averaging method with modified selection intervals.

The probabilistic methods are generally more demanding, in complexity of the analysis or in simulation time. Complete simulation (reference) is the most accurate method, but requires many

simulations when applied to GRADE, and is virtually impossible to use in WAQUA because of computational time. Only when 1D simulations like SOBEK would be acceptable, this approach could be a good choice. The explicit and implicit methods require only a limited number of simulations and hence are also feasible in WAQUA. An advantage of the explicit method is that it is also applicable to short time series (e.g. measured discharge series), as long as the probability distribution show a good fit. Therefore it can also be applied without GRADE, in any river system where upstream discharge time series are available. Additionally, this method yields an expression for the water level frequency curve, providing information for dike safety assessments that take other failure mechanisms into account. Although the implicit method gives no expression for the frequency curve, it has the advantage that it is a more simple method than the explicit method, especially in case of dependent hydrograph shape variables (dependency does not matter). The explicit method becomes more complex in case of dependency, since a multivariate distribution of different distribution types is needed. Both the explicit and implicit methods are very suitable to study the effects of climate change, since hydrodynamic simulation results are not coupled to flood statistics at Borgharen. The accuracy of the explicit and implicit methods depends strongly on the accuracy of the transformation function, and the currently used polynomial function requires that the relation between shape and water levels is relatively smooth. When this is not the case, small adaptations are needed for good results.

Method	Accuracy RMSE [cm] <sup>(1)</sup>	Simplicity analysis <sup>(2)</sup>	Hydrodynamic simulations	WAQUA feasible?
Complete simulation (section 4.4.3)	-	2	17,232 <sup>(3)</sup>	no
Standard hydrograph (section 4.5.2)	15.2	1	7 <sup>(3)</sup>	yes
Vertical hydrograph (section 4.5.2)	7.5	1	7 <sup>(3)</sup>	yes
Standard, modified interval (section 4.5.3)	6.5	2	7 <sup>(3)</sup>	yes
Vertical, modified interval (section 4.5.3)	3.1	2	7 <sup>(3)</sup>	yes
Explicit probabilistic (section 4.6.4)	4.2	4	25 <sup>(4)</sup>	yes
Implicit probabilistic (section 4.6.4)	3.5	3	25 <sup>(4)</sup>	yes

<sup>(1)</sup> Mean error w.r.t. reference, averaged over return period and over locations

<sup>(2)</sup> 1=most simple, 4=most complex

<sup>(3)</sup> Approximately, per river system and per discharge dataset

<sup>(4)</sup> Approximately, per river system and independent of discharge dataset

**Table 5-1 Comparison of the different methods for SOBEK model including retention**

A summary of the considerations mentioned above is given in Table 5-1. Due to the limited scope of this research, the decision for a method should not be made only based on the present results. Firstly, all results of this research are based on the GRADE dataset, which is still under development. Secondly, the reference set was only simulated with the 1D model SOBEK, so only an indirect evaluation of WAQUA results is possible. Furthermore, the present study considers only the effect on water levels, not on other design variables, dike failure probabilities and flood risk. Especially the impact on flood risk is much more relevant to investigate than the impact on design water levels only. Finally, the conclusions were based on the case of the river Meuse. In other river systems, the evaluation of the different methods may lead to different results. Before a trade-off can be made between methods, it is needed to apply the present evaluation to other rivers like the Rhine and particularly to look at more factors than design water levels only.

## 5.7 Recommendations

This research gives rise to several recommendations for current practice with regard to the determination of the design water level:

- Use the GRADE results to determine design water levels.
- Do not use the standard hydrograph shape anymore to determine design water levels.
- Apply complete simulation of all GRADE hydrographs when 1D modelling is sufficient.
- Apply the vertical averaging method (with modified selection interval) when 2D or 3D modelling is required, or for quick analyses.
- Apply the probabilistic method parallel to the vertical averaging method.

Additional research on several related topics is recommended:

- A better representation of Dutch tributary hydrographs, by extending the hydrological models of GRADE to the Dutch part of the Meuse basin. When GRADE is extended to the Dutch part of the basin, it is important that water level and discharge series are available at more than a few locations along the river.
- Explain and validate the wider standard hydrograph from GRADE and the more peaked hydrograph shape in the extreme range.
- Investigate the influence of secondary peaks on the design hydrograph shape and on the design water levels (especially in case of large retention basins). Evaluate the way in which these peaks are treated in the averaging procedure.
- Improve the transformation functions in the probabilistic methods, e.g. by interpolation, including other shape variables, or determining the function type per location. Provide clear guidelines on how to determine and use the transformation function in a wide range of situations, in particular how to select flood events that are used to find the transformation function.
- Establish a reference set by simulation of a large number of flood events in WAQUA, and use this reference set to evaluate the effect of large retention basins as predicted with both the design hydrograph methods and probabilistic methods.
- Apply a similar approach as the present study to evaluate the accuracy of design hydrograph estimates of other design variables and of failure probabilities along the river Meuse and along other rivers (Rhine). Focus on the vertical averaging method (with modified selection interval) as this is the most promising design hydrograph method.

## 6 Conclusions

The purpose of this thesis was to investigate the influence of the hydrograph shape on the design water levels on the river Meuse, and to compare the performance of different methods to determine these design water levels. Based on the results in Chapter 4, we draw the following conclusions, which are structured according to the five research questions.

### The use of GRADE data instead of measured data:

- The use of the GRADE dataset leads to wider standard hydrographs compared to the standard hydrographs based on the measured dataset (Figure 4-1). Consequently, higher water levels for a given peak discharge are found (Figure 4-2).
- For a wide range of return periods, the GRADE peak discharge distribution leads to higher peak discharges than the currently used design discharge curve (Figure 4-3).
- These two effects together generally lead to higher design water levels.

### The influence of hydrograph shape variables

- In addition to the peak discharge  $Q_p$ , the hydrograph shape variables peak duration  $D_{85\%}$ , peak volume  $V_{85\%}$ , and peak curvature  $C_2$  have the strongest influence on the local water levels (Table 4-3). Both the peak duration and peak curvature can be considered independent of the peak discharge (Figure 4-12).
- Using a simple polynomial function of  $Q_p$  and  $C_2$ , one can estimate the downstream water levels with an error (RMSE) of 8.7 cm at maximum.

### Design hydrograph approaches

- The standard hydrograph method with GRADE data overestimates the design water levels up to 37 cm, depending on location and return period, compared to the reference set with simulation of all GRADE hydrographs (e.g. Figure 4-21). An overestimation is present over the entire range of return periods, but increases strongly for return periods larger than 5000 year at locations downstream of Venlo.
- When the selection interval of GRADE hydrographs that are used for generating the standard hydrograph is modified to the region around the design discharge, this increased overestimation is reduced strongly to 19 cm (e.g. Figure 4-23). The modification of the selection interval has limited effect for return periods smaller than 5000 year.
- The results of the vertically averaged hydrograph – with both the full selection interval and the modified interval – show an underestimation of the design water levels up to 7 cm, depending on location and return period (e.g. Figure 4-23).
- Vertical averaging is more accurate on average, whereas the standard hydrograph with modified selection interval is a more conservative choice.

### Probabilistic approaches

- The explicit probabilistic method, with peak discharge and the peak curvature as variables and a Kernel peak discharge distribution, shows an underestimation of the design water levels up to 9 cm and an overestimation of up to 14 cm, depending on location and return period (e.g. Figure 4-28).

- The implicit probabilistic method, with peak discharge and the peak curvature as variables, shows an underestimation of the design water levels up to 7 cm and an overestimation of up to 9 cm, depending on location and return period (e.g. Figure 4-28).

#### **The effect of retention basins**

- Retention effects of Lob van Genneep are overestimated with the standard hydrograph method for peak discharges between 4000 m<sup>3</sup>/s and 4200 m<sup>3</sup>/s, but underestimated for peak discharges between 4200 m<sup>3</sup>/s and 4600 m<sup>3</sup>/s. The vertically averaged hydrograph estimates the retention effects more accurately than the standard hydrograph. This holds for both the effect of one basin (Lob van Genneep) and the effect of multiple retention basins (Figure 4-37). The probabilistic approaches yield also good estimates of the retention effect, but it is essential that the hydrographs used for simulation have the correct characteristics to show the behaviour of the retention basin.

These findings suggest that the more simple design hydrograph methods (in particular vertically averaged) based on GRADE, can give an accurate estimate of the design water levels on the river Meuse, provided that (1) the peak discharge distribution has a good fit in the extreme tail and (2) the selection interval is modified to the interval around the peak discharge. These conditions imply that the use of GRADE is essential for a reliable estimation of the design water levels. The vertically averaged hydrograph gives design water levels closer to the reference than the standard hydrograph, but the standard hydrograph can be considered a more conservative approach. The present results do not prove that a probabilistic approach leads to a more accurate estimate of the design water level than the design hydrograph approaches, at least in this particular case with the SOBEM Meuse model. However, the probabilistic method does have potential, which needs to be developed further.



## References

- Apel, H., Merz, B., & Thielen, A. (2009). Influence of dike breaches on flood frequency estimation. *Computers & Geosciences*, 35(5), 907-923.
- Apel, H., Thielen, A. H., Merz, B., & Blöschl, G. (2004). Flood risk assessment and associated uncertainty. *Natural Hazards and Earth System Science*, 4(2), 295-308.
- Barneveld, H. J., & Van den Berg, T. (2010). *Effect herijking HBV op de golfvorm van de Maas te Borgharen*. Lelystad: HKV Lijn in Water.
- Berger, H. E. J. (1992). *Flow forecasting for the river Meuse* (Ph.D. Thesis). Delft: Delft University of Technology.
- Berkhof, A., Meijer, D., & Leushuis, H. (2013). *Deltaprogramma Rivieren: Voorkeurstategie Maasvallei. Onderzoeksrapportage fase 2 Regioproces*. Provincie Limburg.
- Van den Boogaard, H. F. P., Hegnauer, M., & Beersma, J. J. (2014). *GRADE Uncertainty Analysis*. Delft: Deltares.
- Buishand, T. A., & Leander, R. (2011). *Rainfall generator for the Meuse basin. Extension of the base period with the years 1999-2008*. De Bilt: KNMI.
- Chbab, E. H., Buiteveld, H., & Diermanse, F. (2006). Estimating exceedance frequencies of extreme river discharges using statistical methods and physically based approach. *Österreichische Wasser-und Abfallwirtschaft*, 58(3-4), 35-43.
- CUR. (1997). *CUR-publication 190. Probability in Civil Engineering. Part 1: The theory of probabilistic design*. Gouda: Stichting CUR.
- Deltaprogramma Rivieren. (2014). *Systeemwerking en bescherming langs de Maas - Onderzoek naar een robuust hoogwaterveiligheidssysteem*.
- ENW. (2013). *Advies over status en kwaliteit GRADE*, Document ENW-13-09.
- ENW. (2014). *Advies veiligheidssysteem Maas*, Document ENW-14-07.
- Forchheimer, P. H. (1930). *Hydraulik (3 Auflage)*. Leipzig, Berlin.
- Förster, U., van den Ham, G., Calle, E., & Kruse, G. (2012). *Onderzoeksrapport Zandmeevoerende Wellen*. Deltares & RWS Waterdienst.
- Geerse, C. P. M. (2013). *Belastingmodellen WT12017, Gevoeligheidsanalyses en adviezen voor eventuele aanpassingen aan Hydra-Ring*. Lelystad: HKV Lijn in Water.
- Gerretsen, J. H. (2009). *Flood level prediction for regulated rain-fed rivers* (Ph.D. Thesis). Enschede: University of Twente.
- Gonzales, A. L., Nonner, J., Heijkers, J., & Uhlenbrook, S. (2009). Comparison of different base flow separation methods in a lowland catchment. *Hydrology and Earth System Sciences*, 13(11), 2055-2068.
- Gräler, B., van den Berg, M. J., Vandenberghe, S., Petroselli, A., Grimaldi, S., Baets, B. D., & Verhoest, N. E. C. (2013). Multivariate return periods in hydrology: a critical and practical review focusing on synthetic design hydrograph estimation. *Hydrology and Earth System Sciences*, 17(4), 1281-1296.
- Groendijk, L. (2011). *Limburgse primaire waterkeringen* (MSc. Thesis). Delft University of Technology.
- Hamed, K., & Rao, A. (2000). *Flood frequency analysis*. Boca Raton: CRC press.
- Jansen, P. C. (2007). *Beoordeling van de kwaliteit van hoogwaterparameters berekend voor de Nederlandse Maas* (MSc.Thesis). University of Twente.

- Jonkman, S. N., Bočkarjova, M., Kok, M., & Bernardini, P. (2008). Integrated hydrodynamic and economic modelling of flood damage in the Netherlands. *Ecological Economics*, 66(1), 77–90. doi: 10.1016/j.ecolecon.2007.12.022
- Kok, M., Stijnen, J. W., & Silva, W. (2003). Uncertainty analysis of river flood management in the Netherlands. In *Proceedings of ESREL 2003 (European Safety and Reliability Conference 2003), 15–18 June 2003, Maastricht, The Netherlands*.
- Klemeš, V. (2000). Tall tales about tails of hydrological distributions. I. *Journal of Hydrologic Engineering*, 5(3), 227–231.
- Klopstra, D., & Vrisou van Eck, N. (1999). *Methodiek voor vaststelling van de vorm van de maatgevende afvoergolf van de Maas bij Borgharen*. Lelystad: HKV Lijn in Water.
- Kramer, N. (2012). *GRADE 2012. Procedure to derive design hydrograph. Draft*. Delft: Deltares.
- Kramer, N., Beckers, J., & Weerts, A. (2008). *Generator of Rainfall and Discharge Extremes (GRADE), part D&E*. Delft: Deltares.
- Kramer, N., & Schroevers, R. (2008). *Generator of Rainfall and Discharge Extremes (GRADE), part F*. Delft: Deltares.
- Leander, R., Buishand, T. A., Aalders, P., & De Wit, M. J. M. (2005). Estimation of extreme floods of the river Meuse using a stochastic weather generator and a rainfall–runoff model/Estimation des crues extrêmes de la Meuse à l'aide d'un générateur stochastique de variables météorologiques et d'un modèle pluie–débit. *Hydrological Sciences Journal*, 50(6), 1089–1103.
- Leander, R., & Buishand, T. A. (2004). *Rainfall generator for the Meuse Basin: Development of a multi-site extension for the entire drainage area*. De Bilt: KNMI.
- Lindström, G., Johansson, B., Persson, M., Gardelin, M., & Bergström, S. (1997). Development and test of the distributed HBV-96 hydrological model. *Journal of hydrology*, 201(1), 272–288.
- Lorenz, N. N., Kwadijk, J. C. J., & Diermanse, F. L. M. (2000). *Bepaling van de maatgevende afvoer bij Borgharen. Representativiteit meetreeks, verdelingsfuncties en statistische extrapolatie*. Delft: WL|Delft Hydraulics.
- Maaswerken. (2002). *Tracebesluit Zandmaas/Maasroute*.
- Meijer, D. G. (2013). *Analyse overstroombaarheid Limburgse waterkeringen + addendum*. RiQuest & Acima
- Merz, B., & Thielen, A. (2004). Flood risk analysis: Concepts and challenges. *Österreichische Wasser-und Abfallwirtschaft*, 56(3-4), 27–34.
- Michels, C., Agtersloot, R., van der Veen, R., & van der Veen, S. (2013). *Actueel SOBEK-model FEWS 2013. JAMM 2013*. Arnhem: Rura-Arnhem, AHA & Acima.
- Ministerie van V&W. (1995). *Deltaplan Grote Rivieren. Basisrapport*.
- Ministerie van V&W. (2006). *Integrale Verkenning Maas, advies, hoofd rapport en achtergrond documenten (cd-rom)*. Den Haag: Rijkswaterstaat
- Ogink, H. J. M. (2012). *Design discharge and design hydrograph computation for Meuse and Rhine rivers. Comparison of computational methods*.
- Ogink, H. J. M., & Barneveld, H. J. (2002). *Quick scan maximale wateraanvoer Maas*. Delft: WL|Delft Hydraulics.
- Pickands, J. (1975). Statistical Inference Using Extreme Order Statistics. *The Annals of Statistics*, 3(1), 119–131.
- Peeters, H. A., De Wit, M. J. M., & Uijlenhoet, R. (2005). Floods in the Meuse basin: contribution of tributaries. *Proceedings of NCR-days 2004 (pp. 50-52)*.

- Putten, D. R. van, & Hoefsloot, F. V. J. (2013). *Hydraulische analyse dijkringen Maas*. Bunnik: CSO Adviesbureau.
- Reuber, J., Schielen, R., & Barneveld, H. (2005). Preparing a river for the future-The river Meuse in the year 2050. *Proceedings of the 3rd International Symposium on Flood Defence*. (pp. 25-27)
- Rijkswaterstaat. (2012). *GRADE, beoordeling / advies ENW rivieren. Presentation at 20 september 2012*.
- TAW. (1998). *Fundamentals on Water Defences*. Delft: Technische Adviescommissie voor de Waterkeringen.
- TAW. (2000). *Van Overschrijdingskans naar Overstromingskans. Hoofdrapport*. Delft: Technische Adviescommissie voor de Waterkeringen.
- Tijssen, A. (2009). *Herberekening werklijn Maas in het kader van WTI2011*. Delft: Deltares.
- Tu, M. (2006). *Assessment of the effects of climate variability and land use changes on the hydrology of the Meuse River Basin* (Ph.D. Thesis). Vrije Universiteit Amsterdam and UNESCO-IHE Institute for Water Education.
- Meer, J. van der, Ter Horst, W., & Van Velzen, E. (2009). Calculation of fragility curves for flood defence assets. *Flood Risk Management: Research and Practice*, 567-573.
- Veen, R. van der (2005a). *Laterale toestroming Maas en Rijn onder maatgevende omstandigheden*. Arnhem: Rijkswaterstaat - RIZA.
- Veen, R. van der (2005b). *Vertaalslag Borgharen-Eijsden voor WAQUA*. Arnhem: Rijkswaterstaat - RIZA.
- Velzen, E. H. van, & Beyer, D. (2007). *Technisch Rapport Ontwerpbelastingen voor het Rivierengebied*. Den Haag: Ministerie van V&W and ENW.
- VNK2. (2012). *Flood Risk in The Netherlands. VNK2: the method in brief*. VNK2 project office.
- Vorogushyn, S., Merz, B., & Apel, H. (2009). Development of dike fragility curves for piping and micro-instability breach mechanisms. *Natural Hazards & Earth System Sciences*, 9(4).
- Wind, H. G., Nierop, T. M., De Blois, C. J., & De Kok, J. L. (1999). Analysis of flood damages from the 1993 and 1995 Meuse floods. *Water Resources Research*, 35(11), 3459-3465.
- Wit, M. J. M. de (2008). *Van regen tot Maas*. Diemen: Veen magazines.
- Wit, M. J. M. de, & Buishand, T. A. (2007). *Generator of Rainfall And Discharge Extremes (GRADE) for the Rhine and Meuse basins*. Lelystad: Rijkswaterstaat and KNMI
- Wit, M. J. M. de, Peeters, H. A., Gastaud, P. H., Dewil, P., Maeghe, K., & Baumgart, J. (2007). Floods in the Meuse basin: event descriptions and an international view on ongoing measures. *International Journal of River Basin Management*, 5(4), 279-292.
- Wit, M. J. M. de, Van der Veen, R., & Van Hal, L. (2005). Het samenvallen van hoogwatergolven op de Maas en zijrivieren. *Stromingen*, 11(4), 33-41.
- Wit, M. J. M. de, Warmerdam, P. M. M., Torfs, P. J. J. F., Uijlenhoet, R., Roulin, E., Cheymol, A., Van Deursen, W. P. A., Van Walsum, P. E. V., Ververs, M., Kwadijk, J. C. J., Buiteveld, H. (2001). *Effect of climate change on the hydrology of the river Meuse*. Wageningen: Wageningen University.
- WL|Delft Hydraulics. (1993). *Toetsing uitgangspunten rivierdijkversterkingen. Aanvullend rapport 1: Maatgevende Afvoer Maas*.
- WL|Delft Hydraulics. (1994). *Onderzoek Watersnood Maas, Hoofdrapport*.
- Woltemade, C. J., & Potter, K. W. (1994). A watershed modeling analysis of fluvial geomorphologic influences on flood peak attenuation. *Water Resources Research*, 30(6), 1933-1942.



# Appendices



## **Appendix A. Overview of programs and scripts**

## Scheme for hydrodynamic SOBEEK simulations

This section gives an overview of the programs and Matlab scripts used for the simulation of the (complete series of) GRADE hydrographs.

	Input	Tool	Output
1	GRADE full series 50000\store_sobek_50000.hdf5	grade_to_hulpprogrammatuur.m	run_maas.bat Borghare.dat som(i).inp
2	run_maas.bat Borghare.dat som(i).inp maas_sobek_ini.csv	Hulpprogrammatuur 2.10 (run_maas.bat)	q_Borgharen.som(i) q_lateraal.som(i)
3	defcnd2_constants.txt defcnd3_constants.txt q_Borgharen.som(i) q_lateraal.som(i)	hulpprog_to_sobek_defcnd.m	defcnd_var(i).2 defcnd_var(i).3
4	parsen.inv	make_parsen.m	parsen.NZK
5	Sobek Meuse model files defcnd_var(i).2 defcnd_var(i).3 hisvs_input_flowhis.txt hisvs_input_minmax.txt parsen.NZK	Maasbatch (SOBEKbatch.bat)	hisvs_output_flowhis.txt hisvs_output_minmax.txt hisvs_output_flowhis.his hisvs_output_minmax.his
6	hisvs_output_flowhis.txt hisvs_output_minmax.txt	check_sobek_runs.m	
7	hisvs_output_flowhis.txt hisvs_output_minmax.txt	read_sobek_output.m	sobekout.mat hmax.mat qmax.mat
8	wavestruct.mat wavetable.mat	shapevariables.m	wavestruct.mat wavetable.mat

**Table A-1 Scheme for hydrodynamic batch simulations**

### Hulpprogrammatuur 2.10

The program Hulpprogrammatuur 2.10 determines the lateral discharges for a given flood wave at Borgharen. The file Borghare.dat contains the discharge time series at Borgharen. The file som999.inp contains instructions for Hulpprogrammatuur 2.10: regression functions, event name, output directory, begin/end date, and some optional specifications. The file *maas\_sobek\_ini.csv* gives the relations between main and tributary hydrographs. These files are generated by the Matlab code *grade\_to\_hulpprogrammatuur.m*, based on the GRADE discharge series .

Executing the file *run\_maas.bat* runs Hulpprogrammatuur 2.10 for all simulations.

Output files of Hulpprogrammatuur 2.10 are *q\_lateraal.som999* and *q\_Borgharen.som999* which contain the discharge time series used for further processing.

## Maasbatch

### Folder 'Invoer'

Contains the defcnd\_var999.2 and defcnd\_var999.3 files (boundary conditions of Borgharen and tributaries respectively) for each simulation. Contains the hisvs\_input.txt files with instructions for hisvs.exe (see below).

### Folder 'Model'

Contains the definition files of the SOBEK Meuse model.

### Folder 'Programmas'

Contains three executables:

- parsen.exe combines all definition files before SOBEK simulation starts
- sobeksim.exe is the main computational core of SOBEK
- hisvs.exe writes the needed SOBEK results to a readable text file

### Folder 'Uitvoer'

Contains a folder Som999 for every simulation. The folders contain a file *parsen.NZK* that lists which model files should be used by parsen.exe. After the simulation it will also contain files with the results of the SOBEK simulation. SOBEKbatch.bat is executed to run the SOBEK simulations. The file *opdrachtloop.txt* was used to run SOBEKbatch.bat automatically for every simulation on the computation cluster of HKV.

### Folder 'Werk'

For every simulation, this temporary directory is created and deleted after simulation is finished.

## Matlab codes

### *grade\_to\_hulpprogrammatuur.m*

This Matlab code reads the daily discharge series from the GRADE HDF5 database, selects flood waves, and write each flood wave in a format that is readable for Hulpprogrammatuur2.10. Choices for hydrograph selection:  $Q_{\text{threshold}}=1750 \text{ m}^3/\text{s}$ .  $Z_{\text{pot}}=10$  days. Interpolate daily discharge values linearly to hourly discharge values. Dates of all hydrographs are set to start from 2000/01/01;00:00:00

### *hulpprog\_to\_sobek\_defcnd.m*

This Matlab code transforms the output files of Hulpprogrammatuur2.10 to boundary condition files (defcnd.2 and defcnd.3) in the correct input format for SobekRE.

### *make\_parsen.m*

This Matlab code changes the file *parsen.inv* to *parsen.NZK*, changing the lines that specify the locations of the boundary condition input files defcnd.2 and defcnd.3.

### *check\_sobek\_runs.m*

This Matlab code checks whether for each simulation a flowhis and minmax file are present.

### *read\_sobek\_output.m*

This Matlab code reads the hisvs\_output.txt files and writes all results to a Matlab structure called sobekout.mat and the matrices hmax.mat and qmax.mat that contain the maximum water levels

and discharges at the five locations. These matrices and structure are used for the statistical and probabilistic analyses.

#### *shapevariables.m*

This Matlab code derives the hydrograph shape variables and adds these variables to wavestruct.mat and wavetable.mat.

## **Statistical and probabilistic analyses**

### **Matlab codes**

#### *analyse\_sobek\_output.m*

This Matlab code is used for many different analyses on the SOBEK results of the complete simulations. The main inputs for these analyses are wavetable.mat containing the hydrographs and the shape variables, and hmax.mat containing the local maximum water levels. The analyses include:

- Plotting water level frequency curve of complete simulation and design hydrograph methods.
- Sensitivity analysis on the number of simulations used for this frequency curve.
- Retention
- Fitting distributions to water levels, discharges and shape variables
- Plotting local stage-discharge curves
- (Rank) scatterplots between water levels and shape variables
- (Rank) correlations between water levels and shape variables
- Plotting equal water level curves

#### *analyse\_sobek\_retention.m*

This Matlab code is used for a number of analyses on the effect of retention, both of retention basin Lob van Gennep and all retention basins. The main inputs for these analyses are wavetable.mat containing the hydrographs and the shape variables, and hmax.mat, hmax\_nLob.mat and hmax\_noret.mat containing the local maximum water levels in case of reference, no Lob van Gennep and no retention.

#### *probabilistic\_C2.m*

This Matlab code carries out the probabilistic analysis. A choice must be made for the type of method (implicit or explicit), the simulation set used for fitting the transformation function (25x SOBEK, 25x WAQUA or 17232x SOBEK), method to construct the transformation function (polynomial fit or linear interpolation), and the distribution used for  $Q_p$  (GPD or Kernel). It uses wavetable.mat and hmax.mat, and hmax\_waqua\_sobek.mat which contains the water levels of the 25 selected SOBEK and WAQUA simulations. The code returns the water level frequency curves for the different probabilistic methods and datasets.

```

% Matlab code probabilistic_C2.m
%=====
clear;close all;clc;addpath 'Data';
load('wavetable.mat');
Qp = wavetable(:,2);
C2 = wavetable(:,30);
hmaxstore = 'D:\Users\Data_Thesis\Matlab\Data\after_sobek\hmax.mat';
load(hmaxstore);

%=====
% Give the choices for the analysis
%=====
loc = 5; %6 locations [Boundary Borgharen Maaseik Venlo Mook Megen]
% fitting source data: 1 = 25x SOBEK, 2 = 25x WAQUA, 3 = all SOBEK
fitsource=1;
% probabilistic method: 1 = Qpfit,C2 classes, 2 = Qpfit,C2fit, 3 = implicit
probmeth=2;
% distribution fit to Qp: 1 = GPD, 2 = Kernel
probdist=2;
% fitting method: 1 = poly21 fit, 2 = interpolation
fitmethod=1;

%=====
% Fitting the transformation function to the simulation set
%=====
nrs = [327 4731 15737 6760 13668 15732 6716 1321 8442 4708 7886 12399 576
9825 8508 1251 8796 2847 5887 9372 12250 2815 12616 14035 5100]'; % see
thesis report
load('hmax_waqua_sobek_25x')
for i=1:length(nrs)
hloc_waq(i,1) = hmax_waqua_sobek(3+loc,4*i-2);
hloc_sob(i,1) = hmax_waqua_sobek(3+loc,4*i);
end
if fitsource==1
Y = hmax(nrs,loc);
var1 = log(Qp(nrs));
var2 = C2(nrs);
elseif fitsource==2
Y = hloc_waq;
var1 = log(Qp(nrs));
var2 = C2(nrs);
else %fitsource==3
Y = hmax(:,loc);
var1 = log(Qp);
var2 = C2;
end
[surfacefit gof] = fit([var1 var2],Y,'poly21');
formula = formula(surfacefit)
coeffs = coeffvalues(surfacefit)
Rsquare = gof.rsquare
RMSE = gof.rmse
p00=coeffs(1);
p10=coeffs(2);
p01=coeffs(3);
p20=coeffs(4);
p11=coeffs(5);

```

```

%=====
% Probabilistic computation
%=====
lambda = 17232/50000; plotpos = [1:17232]/(17232+1); % Weibull
plotposition
if probmethod==2 % Qpfit,C2fit
    pd_C2 = fitdist(C2,'Weibull');
    if probdist==1 %GPD
        pd_Qp = fitdist(Qp,'GeneralizedPareto','theta',1750);
    else % Kernel
        pd_Qp = fitdist(Qp,'Kernel');
    end
    % integration of fitted distributions over area where h is exceeded
    c2start=min(var2);c2end=max(var2);c2step=1;
c2range=c2start:c2step:c2end;
hstart=min(Y); hend=max(Y); hstep = 0.05; hrange=hstart:hstep:hend;
Pexceed_h(1:length(hrange),1:4)=-999;
for h=1:length(hrange)
    Pexceed_h(h,1) = hrange(h); % h
    Pexceed_h(h,2) = 0; % P(H>h) in a hydrograph
    for c2 = 1:length(c2range)
        if fitmethod==1 % in case of poly21 fit on ln(Qp) and C2:
            qx(h,c2) = exp(-0.5*((p11*c2range(c2)-sqrt((c2range(c2)^2)*
            (p11^2)-4*c2range(c2)*p01*p20+2*c2range(c2)*p10*p11+
            4*hrange(h)*p20-4*p00*p20+p10^2)+p10)/p20));
        elseif fitmethod==2 % in case of linear interpolation
            F = scatteredInterpolant(Y,var2,var1,'linear','linear');
            qx(h,c2) = exp(F(hrange(h),c2range(c2)));
        end
        Pexceed_qx(h,c2) = cdf(pd_Qp,qx(h,c2),'upper');
        Pin_c2 = cdf(pd_C2,c2range(c2)-0.5*c2step,'upper')-
            cdf(pd_C2,c2range(c2)+0.5*c2step,'upper');
        % P(Hmax>h) in a hydrograph:
        Pexceed_h(h,2) = Pexceed_h(h,2) + Pin_c2*Pexceed_qx(h,c2);
    end
    Pexceed_h(h,3) = Pexceed_h(h,2)*lambda; % P(Hmax>h) per year
    Pexceed_h(h,4) = 1./(Pexceed_h(h,3)); % return period [year]
end
else % implicit
    if fitmethod==1 % polynomial fit

h_estimate(:,loc)=p00+p10*log(Qp)+p01*C2+p20*log(Qp).^2+p11.*log(Qp).*C2;
        elseif fitmethod==2 % linear interpolation
            F = scatteredInterpolant(var1,var2,Y,'linear','linear');
            h_estimate(:,loc) = (F(log(Qp),C2));
        end
end
end

%=====
% Figure of results, including all simulations
%=====
figure
semilogx(1./(lambda.*plotpos),flipud(sort(hmax(:,loc))),'b');
hold on ; grid on ; xlim([10 50000])
if probmethod==1
elseif probmethod==2
plot(Pexceed_h(:,4),hrange,'r-')
elseif probmethod==3
semilogx(1./(lambda.*plotpos),flipud(sort(h_estimate(:,loc))),'k');
end
xlabel('Return period T [year]'); ylabel('maximum water level [m +NAP]');

```

## **Appendix B. SOBEK and WAQUA Meuse**

## Lateral discharges

Table B-1 gives the coefficients that were used to derive the lateral discharges of the larger tributaries from the hydrograph at Borgharen.

- $\Delta t_p$  is a coefficient for the difference in timing of the flood peak
- $\alpha$  is a coefficient for multiplication of the discharge
- $\beta$  is a coefficient for translation of the discharge
- $\gamma$  is a coefficient for the scaling of the durations ( $\gamma=0.5$  gives half the duration)
- $Q_{min}$  is the minimum discharge
- $Q_{max}$  is the maximum discharge

	$\Delta t_p$ (hour)	$\alpha$ (-)	$\beta$ (m <sup>3</sup> /s)	$\gamma$ (-)	$Q_{min}$ (m <sup>3</sup> /s)	$\tau$ (hour)	Translation to mouth
<b>Geul</b>	-13	0.0130	0.0	0.129	9.18	0.86	No
<b>Geleenbeek</b>	-19	0.0124	-4.2	0.256	5.57	9.46	No
<b>Roer</b>	-9	0.0466	0.0	0.904	57.86	26	dt=20-10 h dQ=10 m <sup>3</sup> /s
<b>Neerbeek</b>	-24	0.0062	0.0	0.326	5.44	32	No
<b>Niers</b>	11	0.0120 0.0087	0.0 6.02	1.046	16.98	55	dt=3h
<b>Aa</b>	-24	0.0266	0.0	0.564	26.67	80	Use SOBEK
<b>Dommel</b>	0	0.0330	0.0	0.605	39.82	80	Use SOBEK

**Table B-1 Main tributary discharges at measuring station (Van der Veen, 2005a)**

Main tributary	Minor tributaries	SOBEK lateral	Factor to main lateral
<b>Geul</b>	Jeker + smaller		0.67 if $Q < 1500$ , 0.51 if $Q > 2500$ , linear in between
<b>Geleenbeek</b>	Vlootbeek		0.31
<b>Neerbeek</b>	Minor Neerbeek	Zandmas5	0.76
	Belgian streams	Grenmas4	1.01 if $Q < 1500$ , 0.50 if $Q > 2500$ , linear in between
	Uffeltse beek Thornerbeek	Grenmas6	0.41
	Peel	Grenmas6	1.31
<b>Niers</b>	Gemaal Bloemers)	Zandmas9	0.09
	Gemaal Quarles v. Ufford	Getymas1	0.09
	Hertogswetering	Getymas2	0.21
	gemalen afgedamde Maas	Andelms2	0.08
<b>Dommel&amp;Aa</b>	Dieze & Drongelens kanaal		1
Julianakanaal depends on Q Borgharen: 16 for $Q < 1275$ , 5 for $Q > 1900$ , and linear in between			
Zuid-Willemsvaart depends on Q Borgharen: 15 for $Q < 1275$ , 8 for $Q > 1900$ , and linear in between			

**Table B-2 Minor tributary discharges (Van der Veen, 2005a)**

## SOBEK Meuse Model

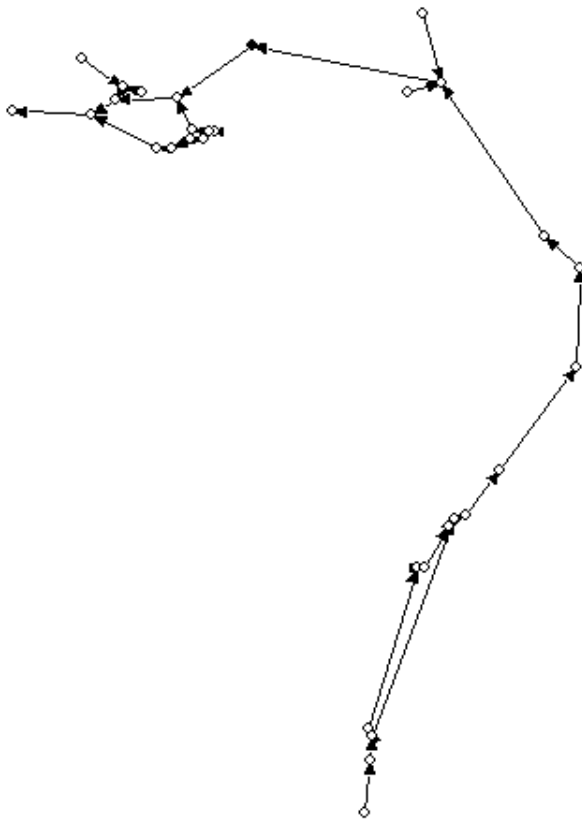


Figure B-1 Overview of SOBEK Meuse model

Retention areas in the SOBEK model j13\_4-v3

Name	Area (m <sup>2</sup> )	Type	Bottom height (m +NAP)
LKW2	2316068	2-zijdig	18.39
DGR_Blitterswijck	11672848	2-zijdig	14.95
DGR_Bergen	962209	2-zijdig	13.28
VL_Thorn	3752698	1-zijdig	22.72
<b>DGR_Ottersum</b>	<b>17688667</b>	<b>1-zijdig</b>	<b>12.54</b>
DGR_Maastricht_Oost	3529070	1-zijdig	48.22
DGR_Borgharen	548159	1-zijdig	44.69
DGR_Itteren	621054	1-zijdig	43.25
DGR_Aan_de_Maas	1059613	1-zijdig	41.27
DGR_Meers_Maasband	1968108	1-zijdig	36.43
Negenoord	991820	1-zijdig	28.63
LKW1	2943964	1-zijdig	19.48
DGR_Middelaar	6577161	1-zijdig	10.71

Table B-3 Retention basins in the SOBEK Meuse model

## Numerical parameters

Parameter	Value	Parameter	Value
g [m/s <sup>2</sup> ]	9.81	Max. nr. of Iterations	100
Theta [-]	0.55	If no Convergence on Non-linearity	Continue
Psi [-]	0.5	Max. nr. of Iter.s Nodal Adm. Matrix	50
Density of Fresh Water [kg/m <sup>3</sup> ]	1000	Stop Criterion Nodal Adm. Matrix	1e-007
Pseudo Courant number	10	Stop Criterion Variation in Water Level [m]	0.001
Under Relaxation	1	Stop Criterion Variation in Discharge [m <sup>3</sup> /s]	0.005
Under Relax. Structures	0.35	Relative Stop Criterion Discharge [-]	1.3e-005
Extra Resist. in General Structures	4	Increment for Num. Diff. in Structures	1e-007
Calculation	Unsteady	Transition height for summerdikes [m]	0.75

Ok Cancel

Figure B-2 Numerical parameters SOBEK

## WAQUA Meuse model

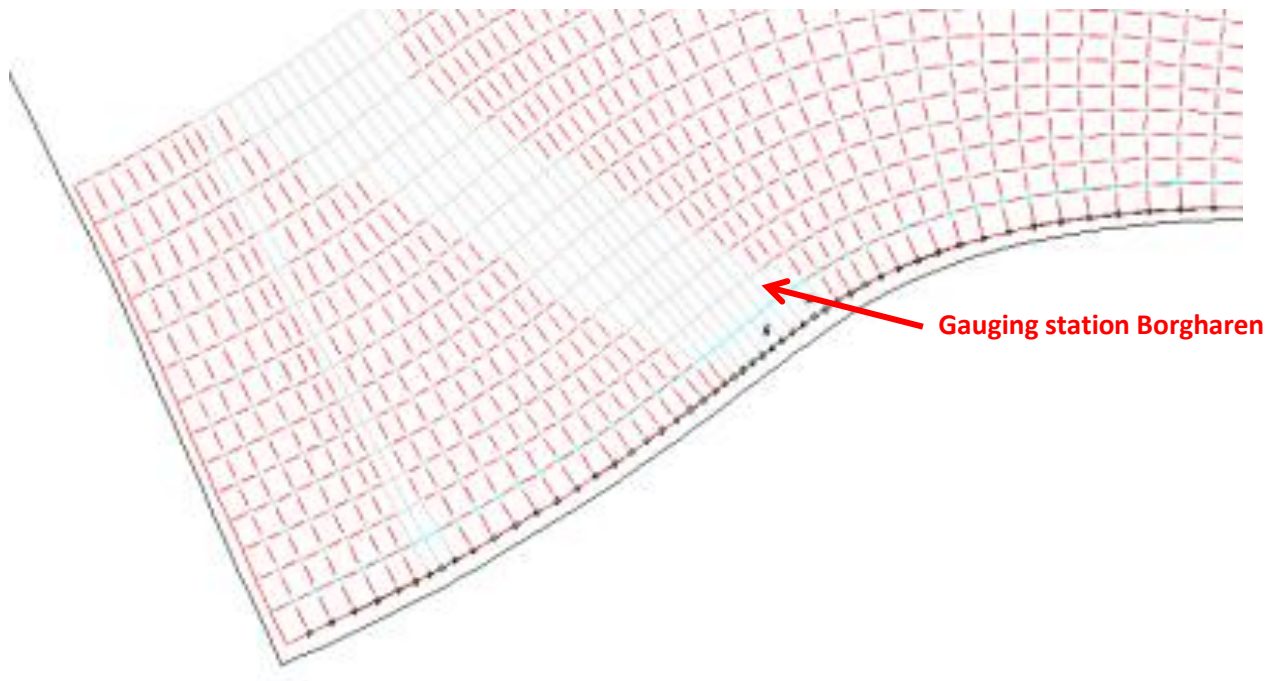
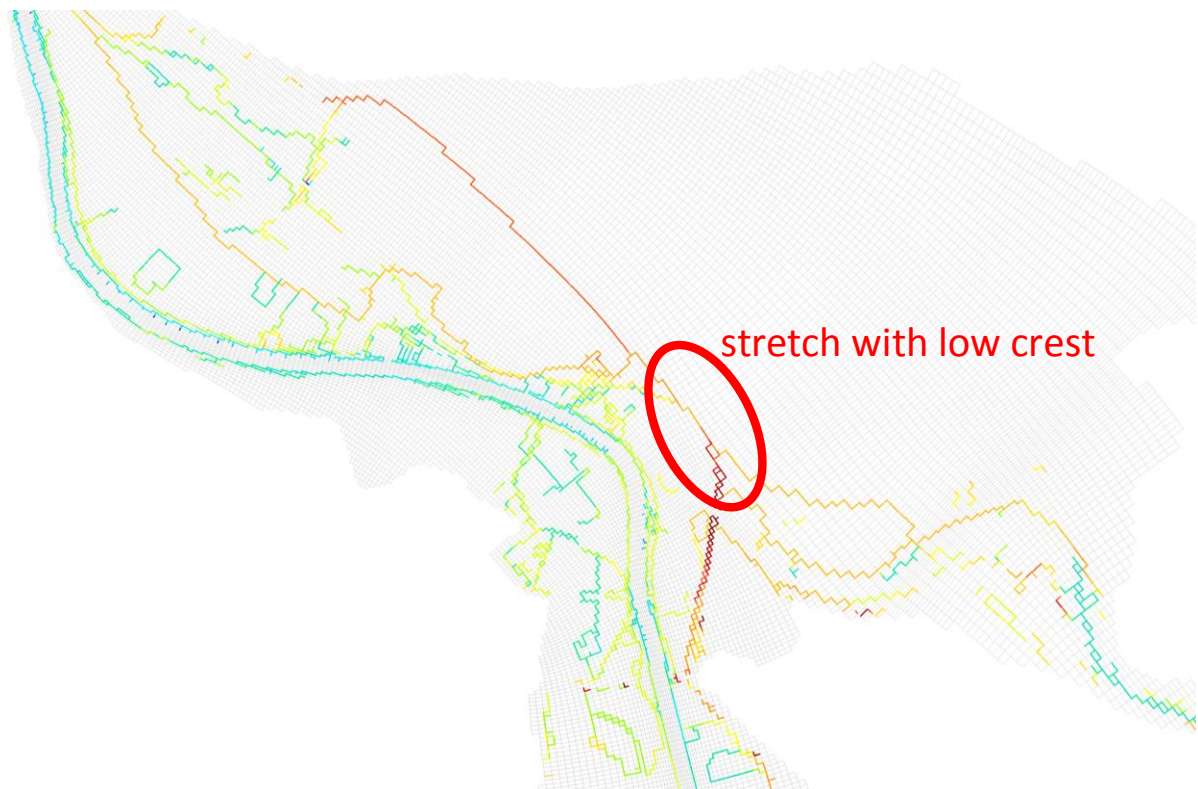


Figure B-3 Upstream boundary after cutting off





## Appendix C. Probabilistic formulas

## Univariate probability distributions

### Generalized Extreme Value distribution (GEV):

$$F(x) = \exp\left(-\left(1 + k \frac{x-\mu}{\sigma}\right)^{-\frac{1}{k}}\right) \quad k \neq 0 \quad (\text{C.1})$$

$$F(x) = \exp\left(-\exp\left(-\frac{x-\mu}{\sigma}\right)\right) \quad k = 0 \quad (\text{C.2})$$

$$f(x) = \frac{1}{\sigma} \exp\left(-\left(1 + k \frac{x-\mu}{\sigma}\right)^{-\frac{1}{k}}\right) \left(1 + k \frac{x-\mu}{\sigma}\right)^{-1-\frac{1}{k}} \quad k \neq 0 \quad (\text{C.3})$$

$$f(x) = \frac{1}{\sigma} \exp\left(-\left(\frac{x-\mu}{\sigma}\right) - \exp\left(-\left(\frac{x-\mu}{\sigma}\right)\right)\right) \quad k = 0 \quad (\text{C.4})$$

$k$  = shape,  $\sigma$  = scale,  $\mu$  = location

If  $k = 0$  this is a Gumbel distribution

If  $k < 0$  this is a Weibull distribution

If  $k > 0$  this is a Frechet distribution

### Negative Weibull distribution:

$$F(x) = 1 - \exp\left(-\left(\frac{x}{a}\right)^b\right) \quad (\text{C.5})$$

$$f(x) = \frac{b}{a} \left(\frac{x}{a}\right)^{b-1} \exp\left(-\left(\frac{x}{a}\right)^b\right) \quad (\text{C.6})$$

$a$  = scale,  $b$  = shape

### Generalized Pareto Distribution (GPD):

$$F(x) = 1 - \left(1 + k \frac{x-\theta}{\sigma}\right)^{-\frac{1}{k}} \quad (\text{C.7})$$

$$f(x) = \frac{1}{\sigma} \left(1 + k \frac{x-\theta}{\sigma}\right)^{-\frac{1}{k}-1} \quad (\text{C.8})$$

$k$  = shape,  $\sigma$  = scale,  $\theta$  = threshold

If  $k = 0$  and  $\theta = 0$ , this is equivalent to exponential

If  $k > 0$  and  $\theta = \sigma/k$ , this is equivalent to Pareto

## Correlation coefficients

Pearson

$$\rho_{X,Y} = \frac{COV(X,Y)}{\sigma_X \sigma_Y} = \frac{E[XY] - E[X]E[Y]}{\sigma_X \sigma_Y} \quad (C.9)$$

Spearman

$$\rho_{X,Y} = 1 - \frac{6 \sum (x_i - y_i)^2}{n(n^2 - 1)} \quad (C.10)$$

Where  $x_i$  is the rank of  $X_i$  and  $n$  is the sample size

## Return period and return value

The return period  $T$  is given by:

$$T = \frac{1}{(1-F(x))\lambda} \quad (C.11)$$

where  $\lambda$  is the rate of peak occurrence [1/year].  $\lambda$  equals 1 for AM series.

The return value of the Generalized Pareto Distribution for return period  $T$  is given by:

$$x_T = \begin{cases} \theta + \frac{\sigma}{k} ((\lambda T)^k - 1) & k \neq 0 \\ \theta + \sigma \ln(\lambda T) & k = 0 \end{cases} \quad (C.12)$$

The return value of the Generalized Extreme Value distribution for return period  $T$  is given by:

$$x_T = \begin{cases} \mu + \frac{\sigma}{k} \left(1 - \left(-\log\left(1 - \frac{1}{T}\right)\right)^{-k}\right) & k \neq 0 \\ \mu - \sigma \log\left(-\log\left(1 - \frac{1}{T}\right)\right) & k = 0 \end{cases} \quad (C.13)$$



## **Appendix D. Statistics of shape variables**

## Correlation coefficients

	$h_{\max, \text{Borgharen}}$	$h_{\max, \text{Maaseik}}$	$h_{\max, \text{Venlo}}$	$h_{\max, \text{Mook}}$	$h_{\max, \text{Megen}}$
$Q_p$	0.976	0.968	0.960	0.942	0.936
$D_{1250}$	0.520	0.553	0.621	0.660	0.669
$D_{50\%}$	-0.145	-0.103	-0.018	0.030	0.043
$D_{85\%}$	-0.022	0.025	0.142	0.209	0.225
$V_0$	0.688	0.715	0.779	0.805	0.810
$V_{1250}$	0.832	0.842	0.887	0.904	0.905
$V_{50\%}$	0.393	0.431	0.526	0.578	0.590
$V_{85\%}$	0.463	0.497	0.595	0.644	0.655
$RV_0$	-0.132	-0.084	0.016	0.070	0.085
$RV_{1250}$	-0.322	-0.317	-0.282	-0.256	-0.252
$RV_{50\%}$	0.098	0.112	0.162	0.192	0.199
$RV_{85\%}$	0.067	0.026	-0.074	-0.136	-0.151
$C_1$	0.001	-0.049	-0.161	-0.208	-0.219
$C_2$	-0.003	-0.060	-0.190	-0.252	-0.267

**Table D-1 Pearson correlation between local water levels and shape variables**

	$Q_p$	$D_{1250}$	$D_{50\%}$	$D_{85\%}$	$V_0$	$V_{1250}$	$V_{50\%}$
$Q_p$	1.000						
$D_{1250}$	0.506	1.000					
$D_{50\%}$	-0.144	0.675	1.000				
$D_{85\%}$	-0.066	0.606	0.644	1.000			
$V_0$	0.608	0.914	0.587	0.498	1.000		
$V_{1250}$	0.850	0.849	0.268	0.395	0.866	1.000	
$V_{50\%}$	0.338	0.947	0.766	0.778	0.871	0.755	1.000
$V_{85\%}$	0.463	0.803	0.443	0.807	0.770	0.815	0.857
$RV_0$	-0.135	0.666	0.920	0.711	0.651	0.291	0.766
$RV_{1250}$	-0.345	-0.481	-0.335	0.213	-0.449	-0.329	-0.292
$RV_{50\%}$	0.080	0.068	-0.298	0.401	-0.026	0.220	0.151
$RV_{85\%}$	0.075	-0.640	-0.695	-0.913	-0.515	-0.379	-0.785
$C_1$	0.050	-0.407	-0.440	-0.778	-0.353	-0.278	-0.551
$C_2$	0.027	-0.542	-0.584	-0.867	-0.482	-0.362	-0.690

**Table D-2 Spearman rank correlation between local water levels and shape variables (part 1)**

	$V_{85\%}$	$RV_0$	$RV_{1250}$	$RV_{50\%}$	$RV_{85\%}$	$C_1$	$C_2$
$V_{85\%}$	1.000						
$RV_0$	0.511	1.000					
$RV_{1250}$	0.013	-0.225	1.000				
$RV_{50\%}$	0.426	-0.137	0.579	1.000			
$RV_{85\%}$	-0.694	-0.743	-0.039	-0.290	1.000		
$C_1$	-0.633	-0.503	-0.226	-0.311	0.678	1.000	
$C_2$	-0.714	-0.654	-0.143	-0.276	0.801	0.901	1.000

**Table D-3 Spearman rank correlation between local water levels and shape variables (part 2)**

## Conditional plots of shape variables at Mook

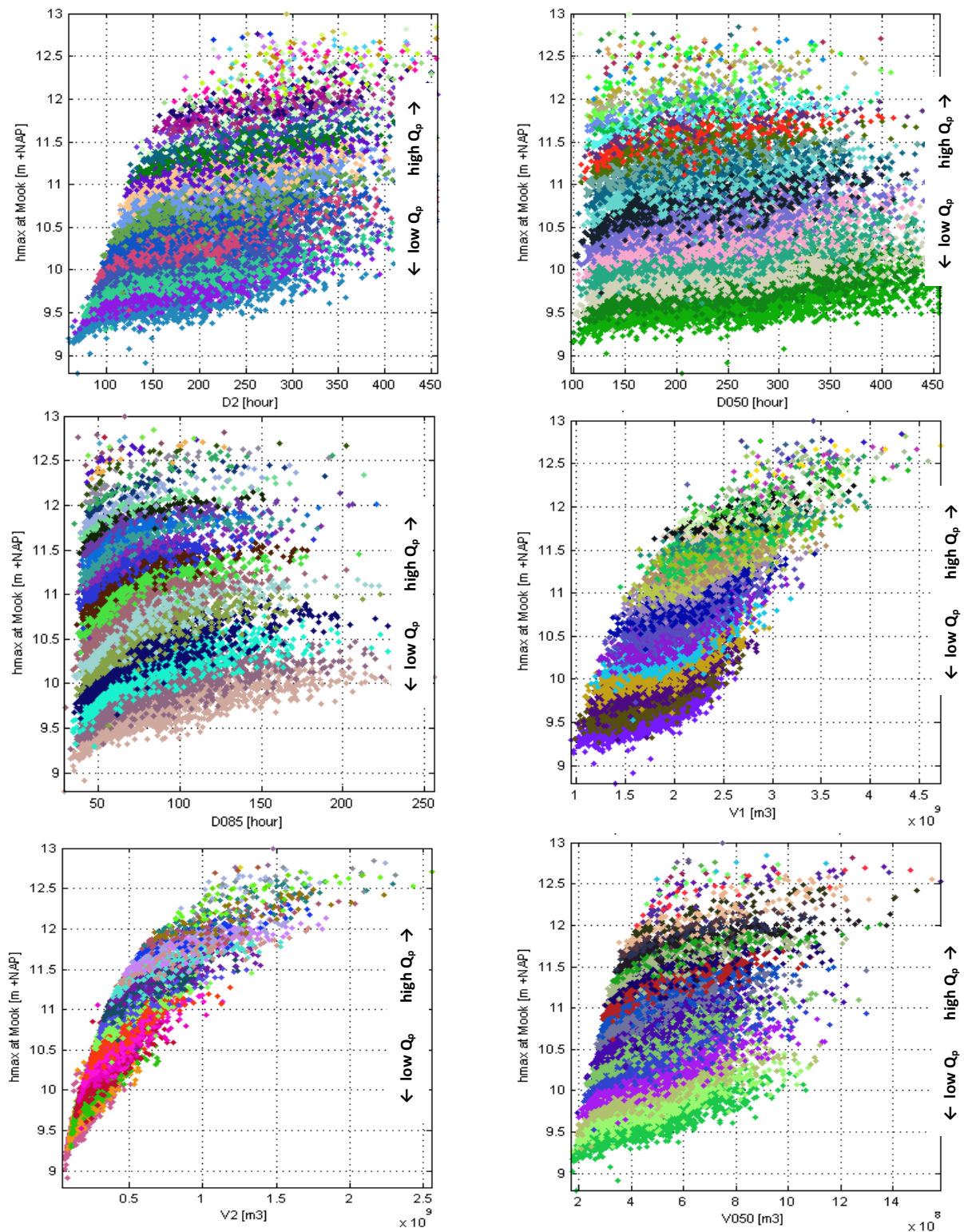


Figure D-1 Conditional scatterplots at Mook, part 1

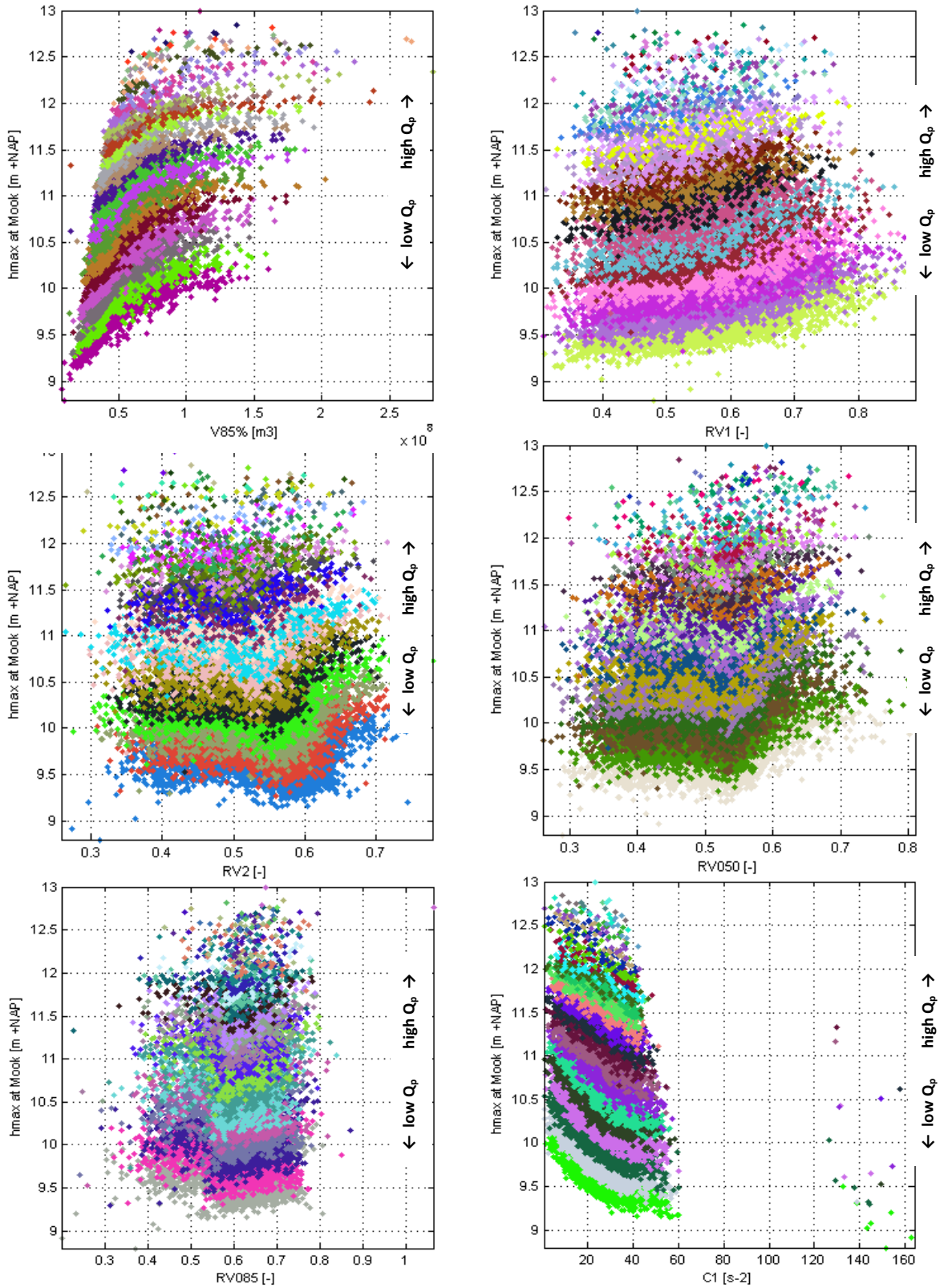


Figure D-2 Conditional scatterplots at Mook, part 2

## Conditional plots of $C_2$ at all locations

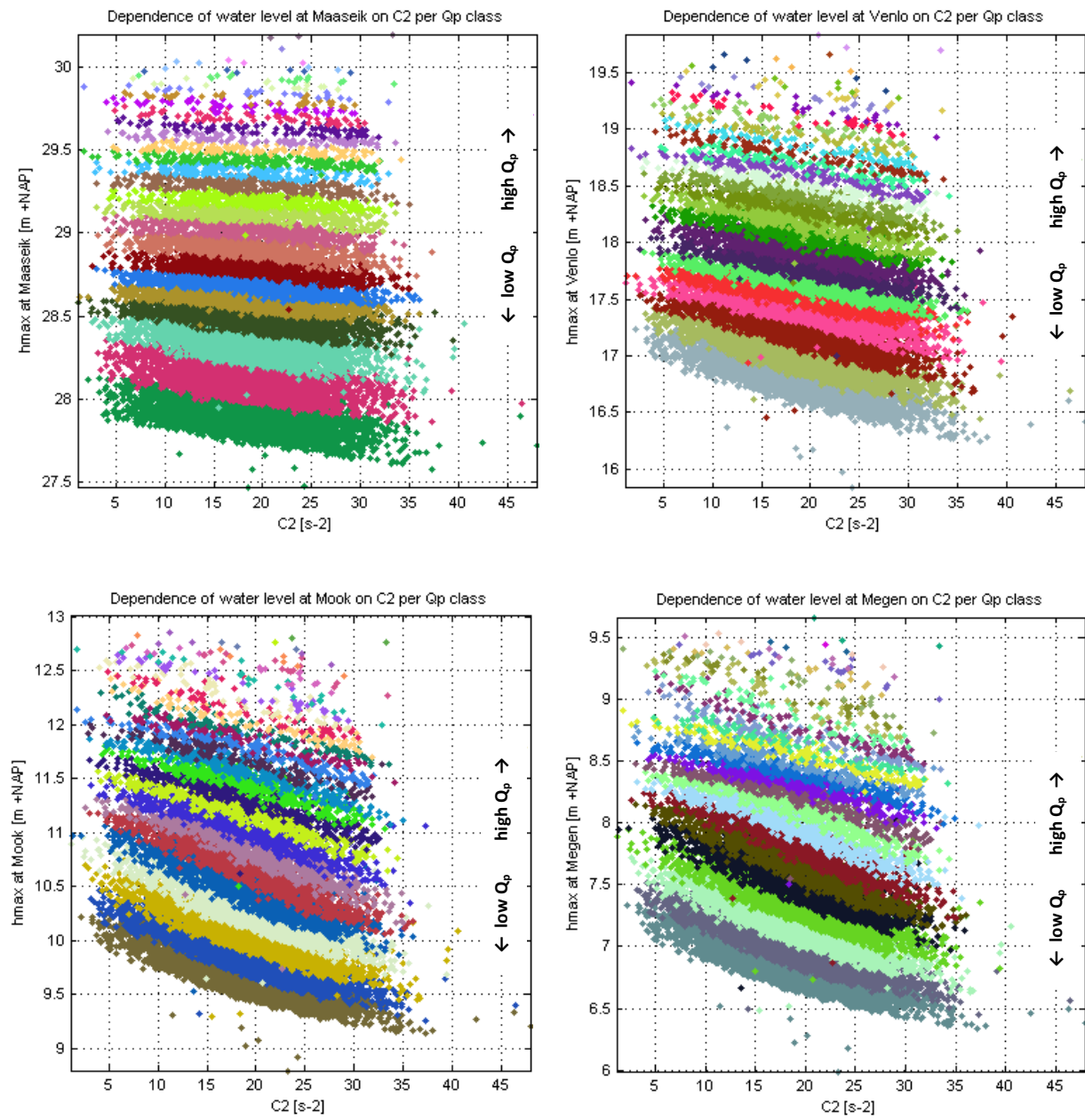


Figure D-3 Conditional scatterplots of  $C_2$

## Probability distributions

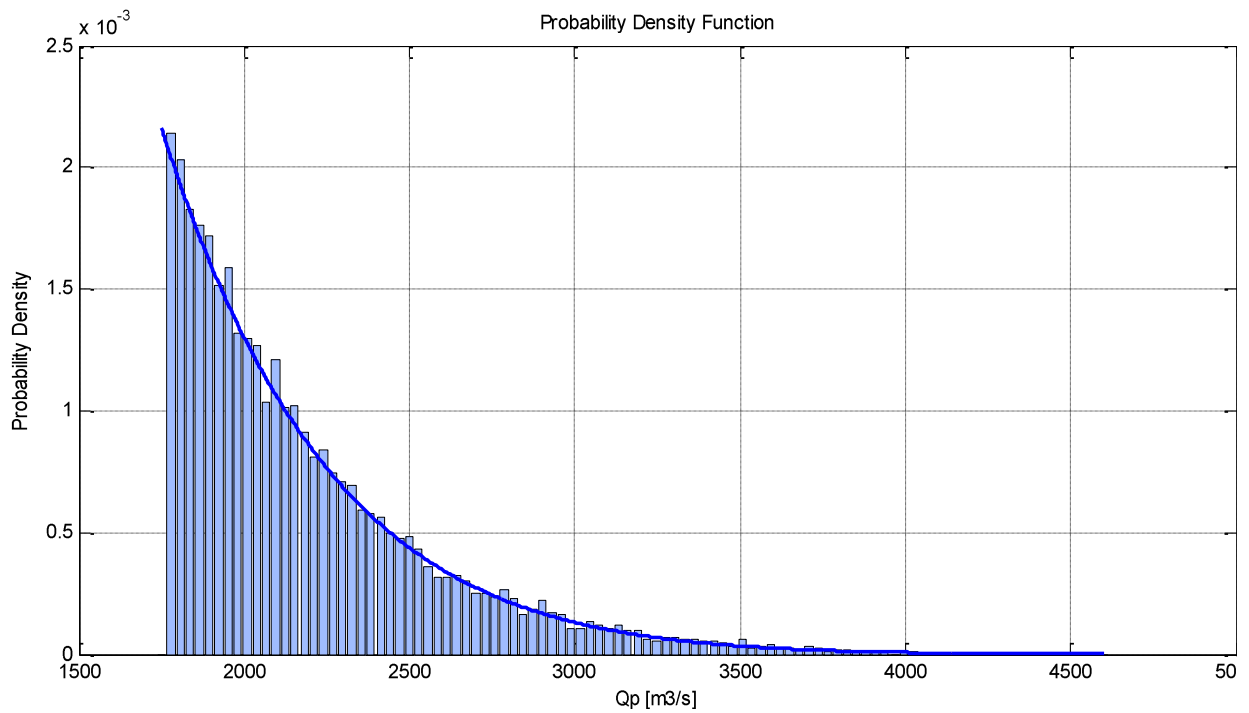


Figure D-4  $Q_p$  distribution: Generalized Pareto,  $k = -0.0806$ ,  $\sigma = 462.98$ ,  $\theta = 1750$ ,  $NLogL = 1.2161e+05$

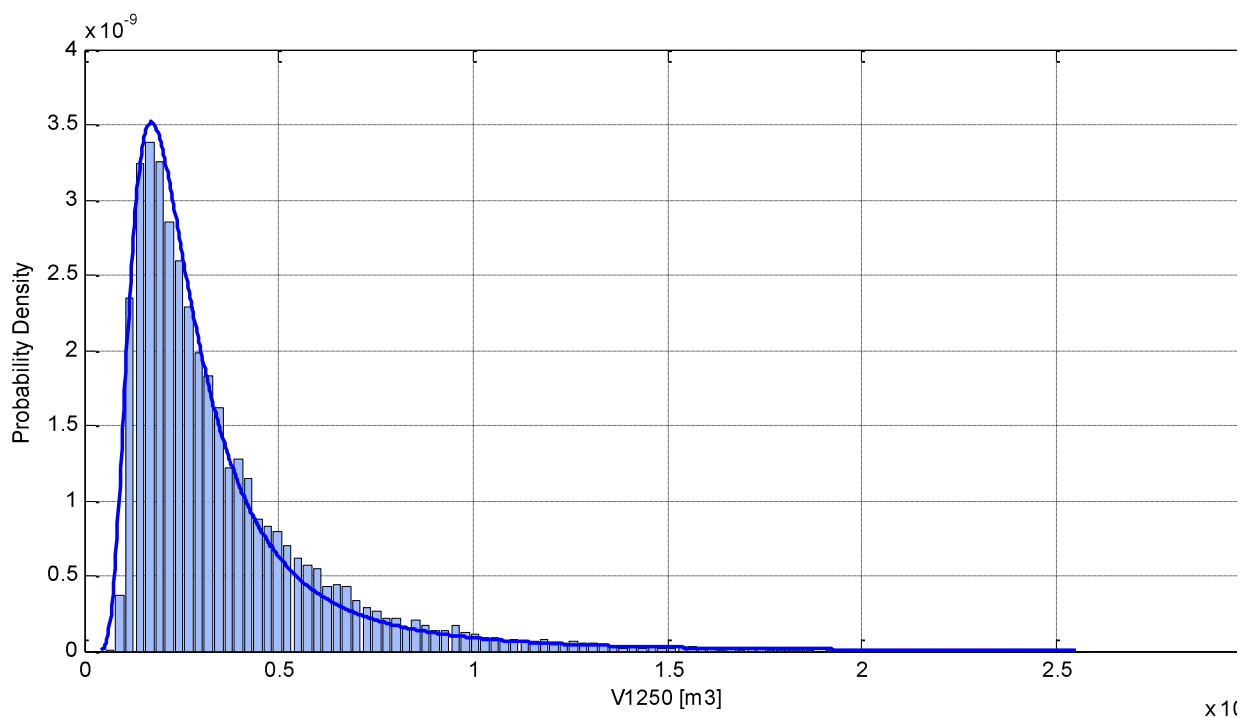
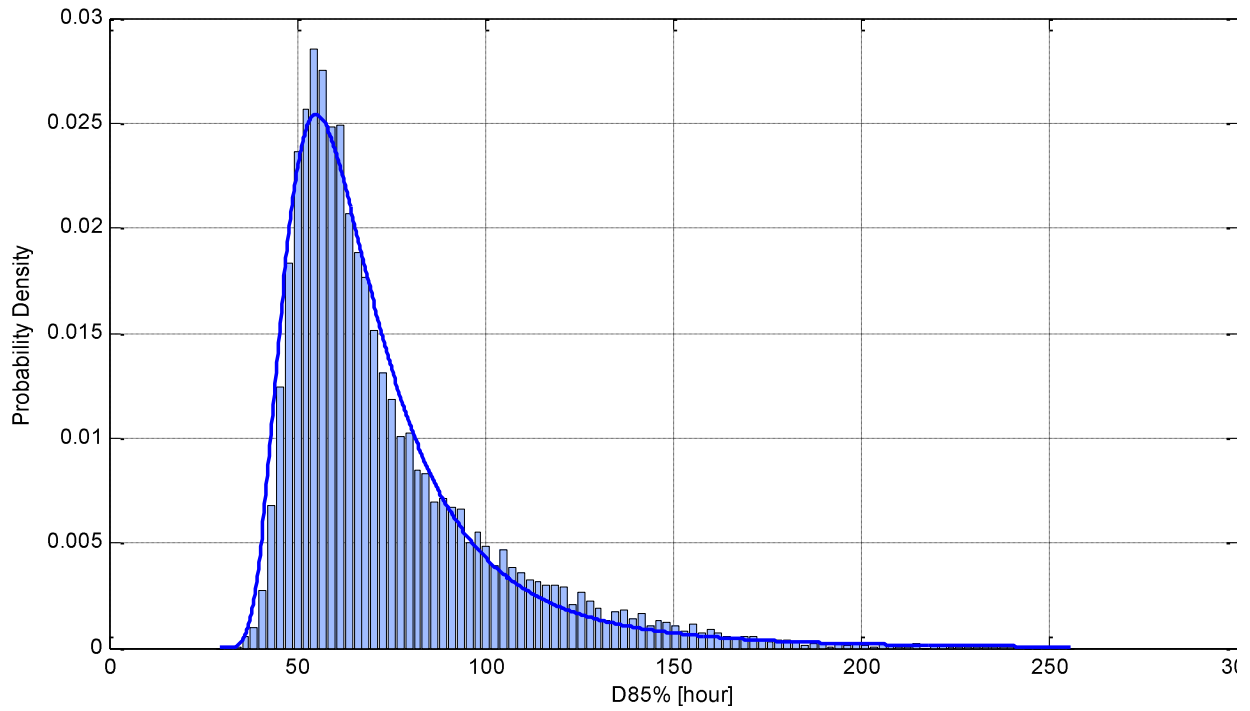
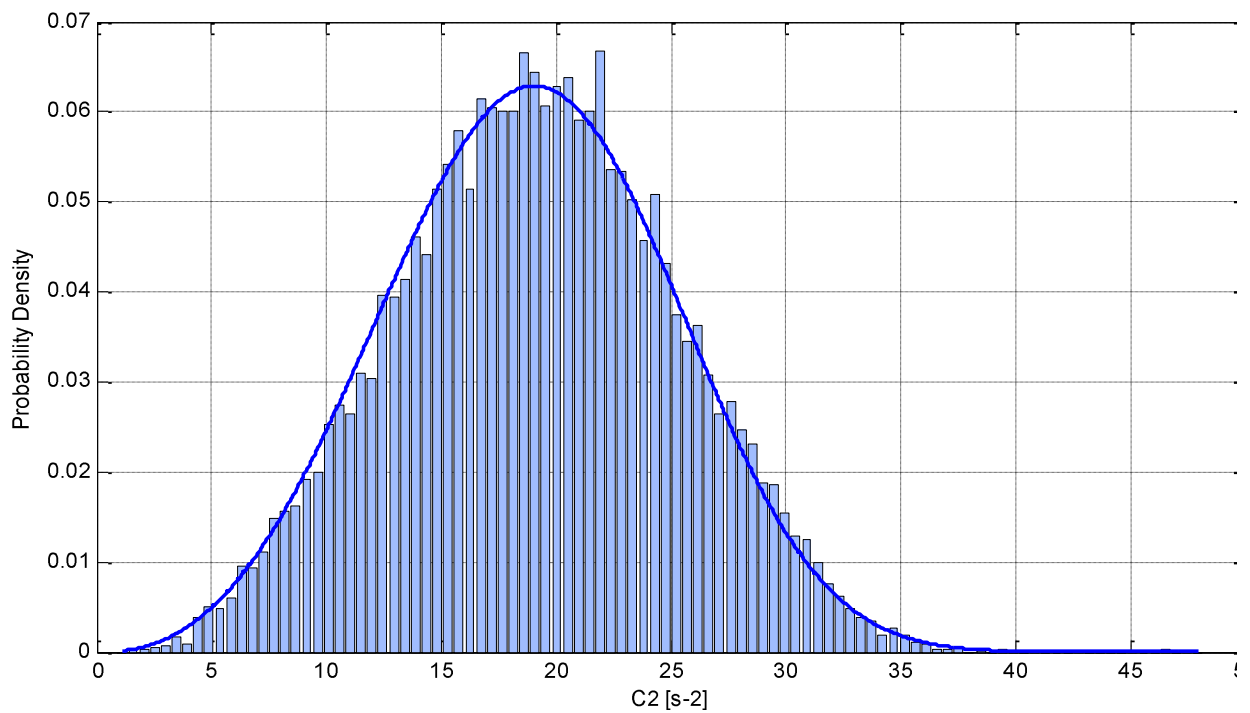


Figure D-5  $V_{1250}$  distribution: GEV,  $k = 0.440$ ,  $\sigma = 1.1589e+08$ ,  $\mu = 2.1720e+08$ ,  $NLogL = 3.5142e+05$



**Figure D-6  $D_{85\%}$  distribution: GEV,  $k = 0.295$ ,  $\sigma = 15.1$ ,  $\mu = 58.8$ ,  $N\text{LogL} = 7.687e+04$**



**Figure D-7  $C_2$  distribution: Weibull,  $a = 21.1$ ,  $b = 3.43$ ,  $N\text{LogL} = 5.55e+04$**

### Scatterplots of shape variables

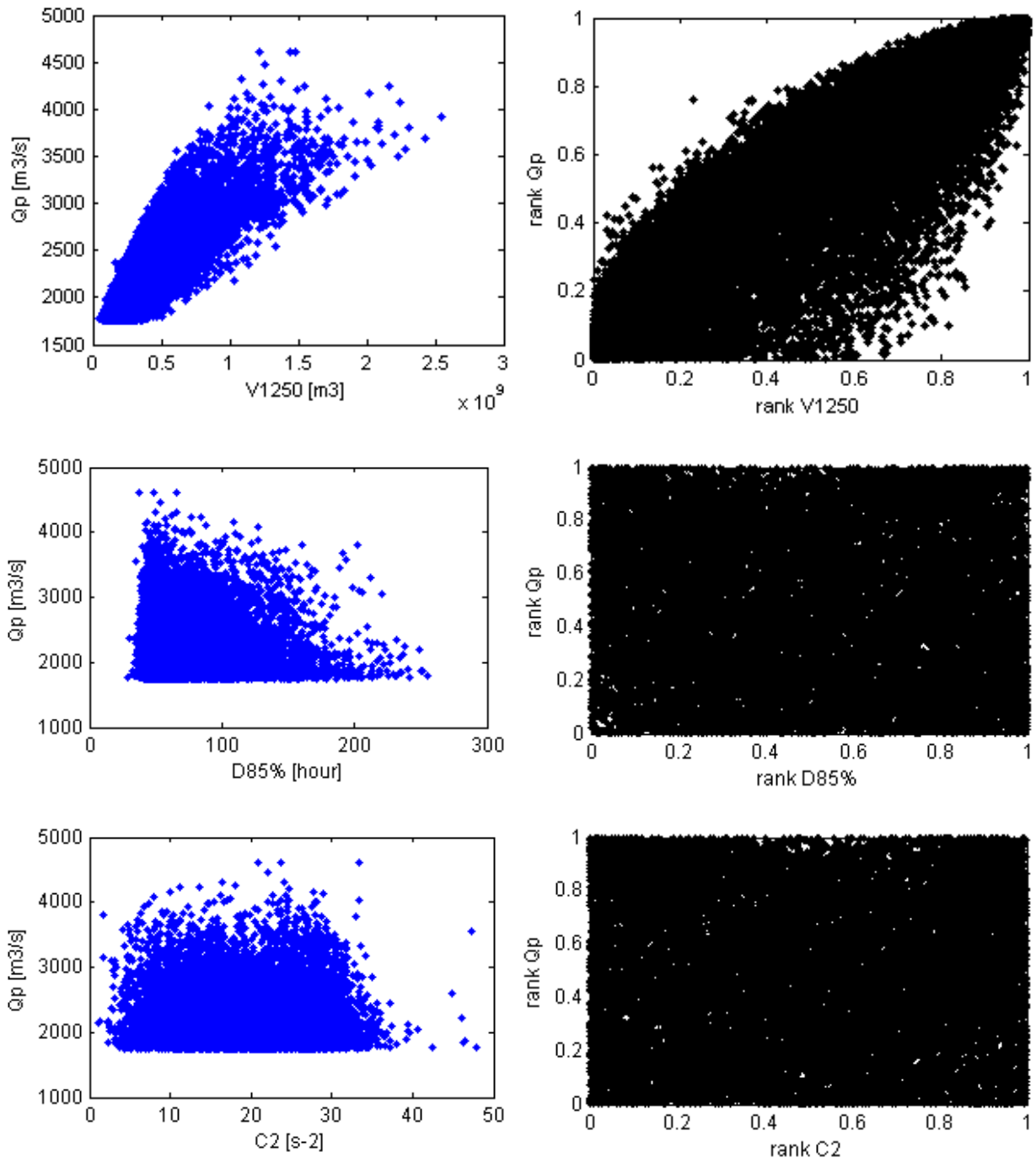


**Figure D-8 scatterplot (left) and rank scatterplot (right)**

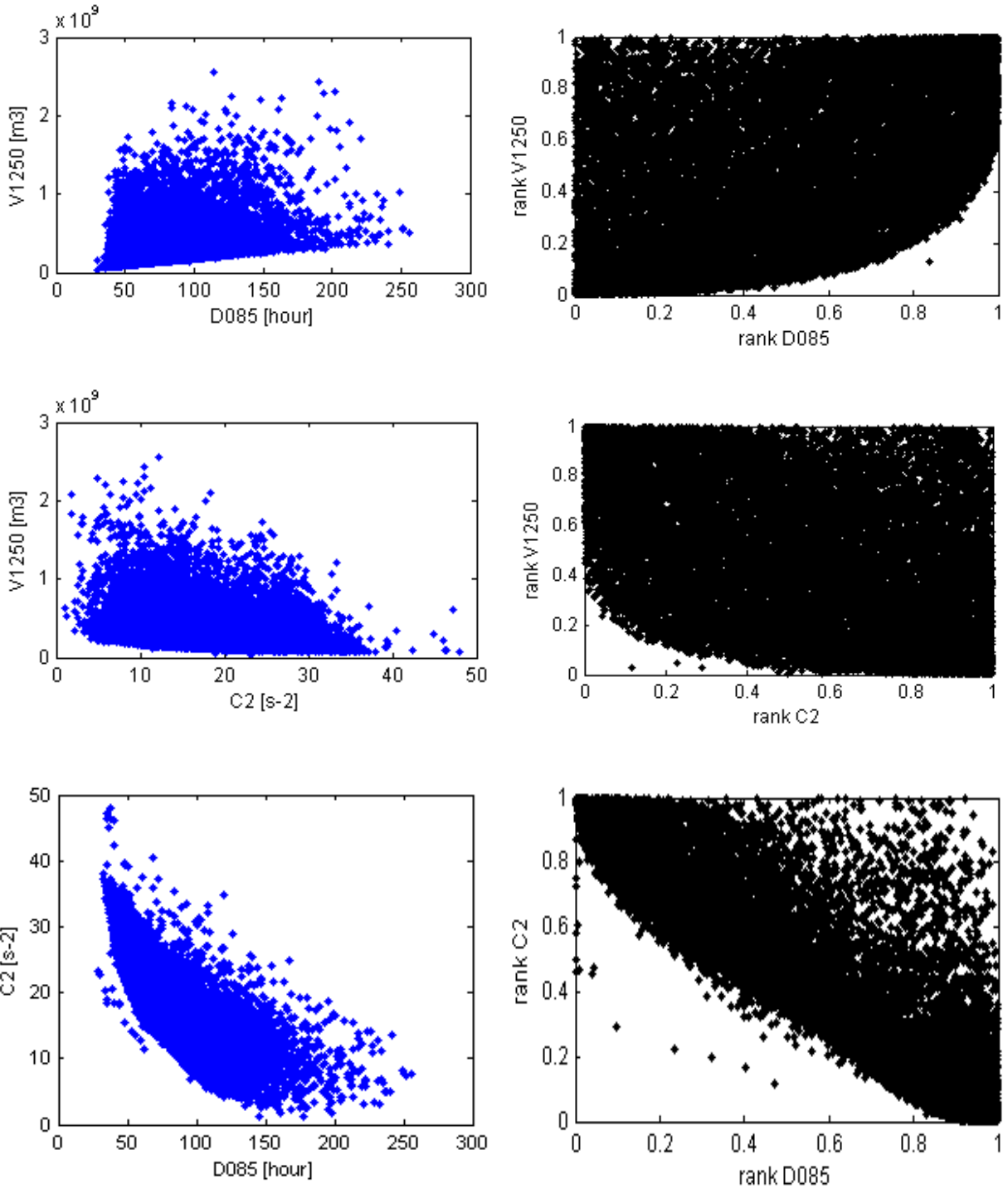


**Figure D-9 scatterplot (left) and rank scatterplot (right)**



**Appendix E. Results of complete simulations in SOBEK**

### Histogram and return period line of local water levels

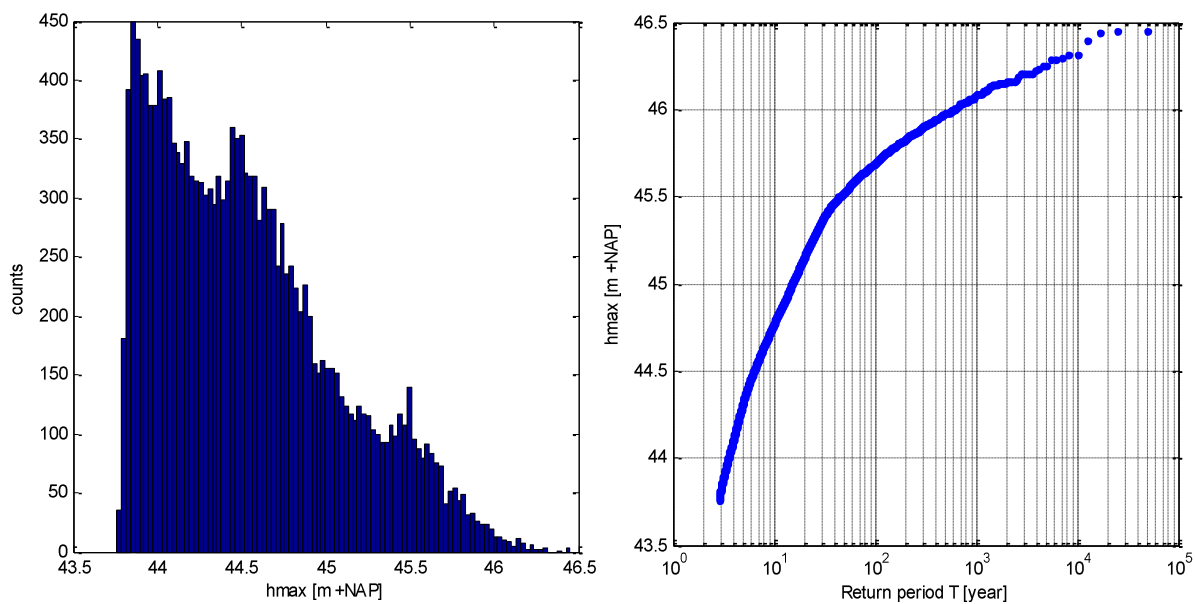


Figure E-1 Water levels at location Borgharen

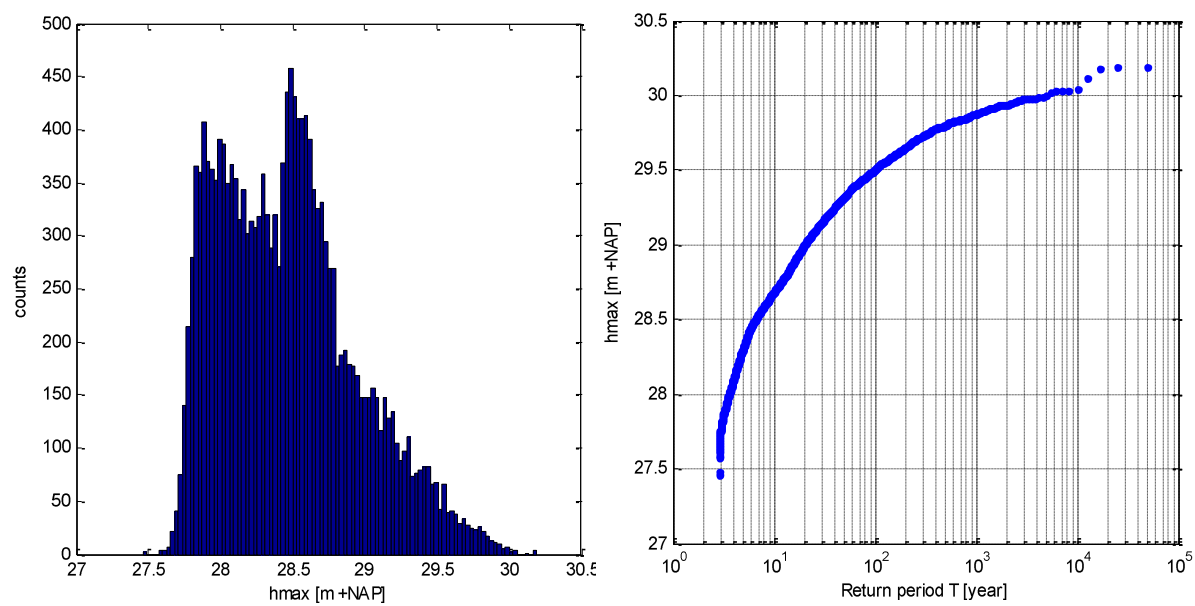
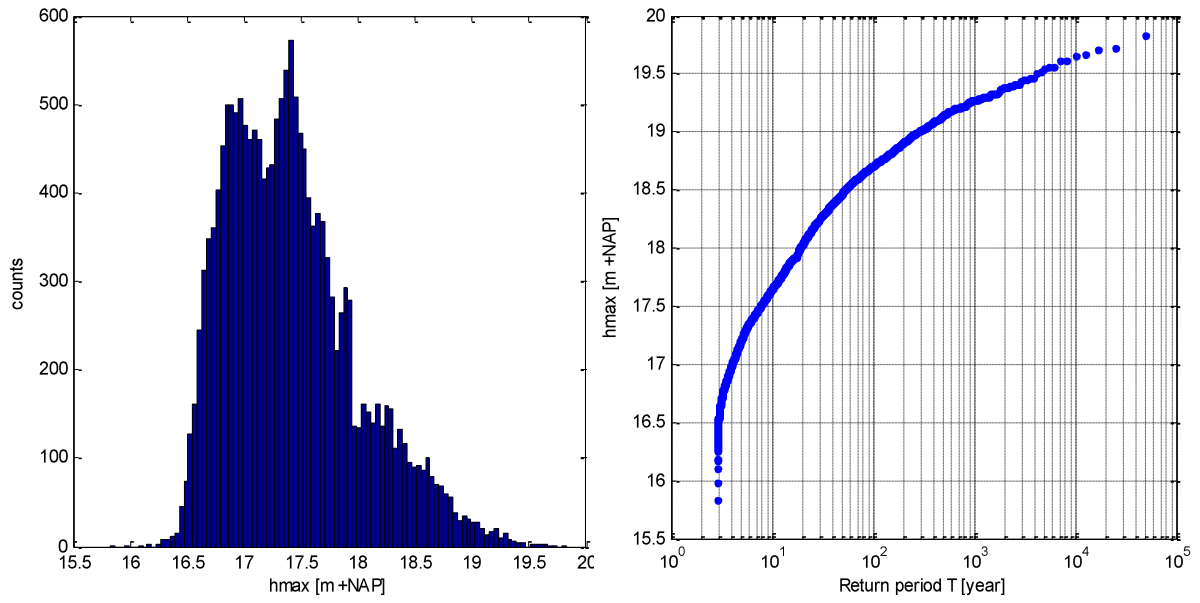
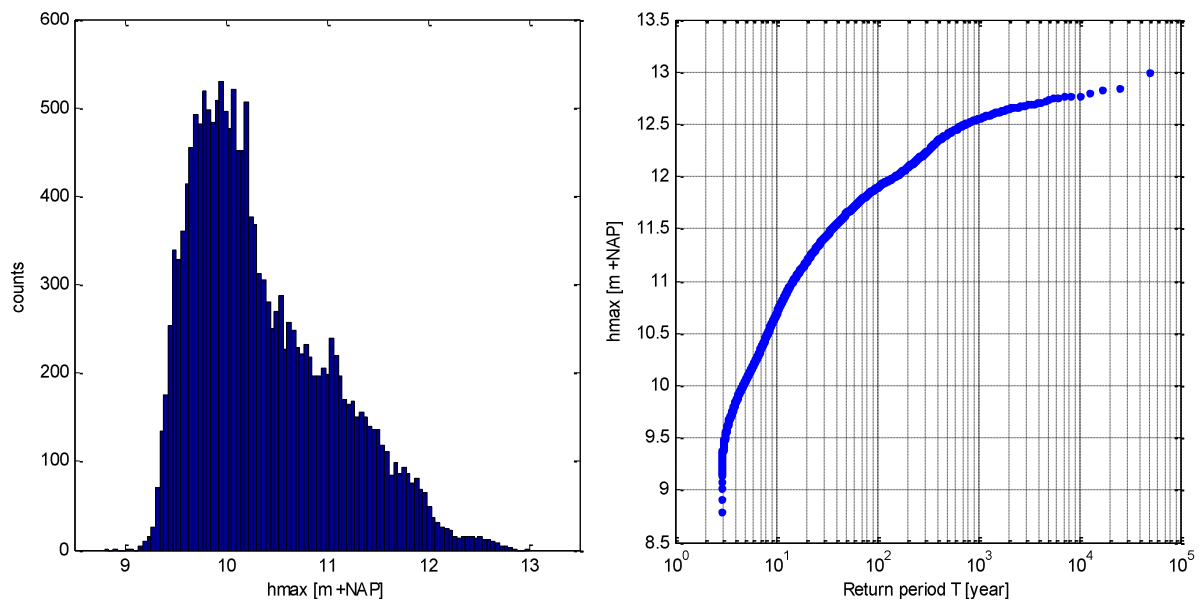


Figure E-2 Water levels at location Maaseik



**Figure E-3 Water levels at location Venlo**



**Figure E-4 Water levels at location Mook**

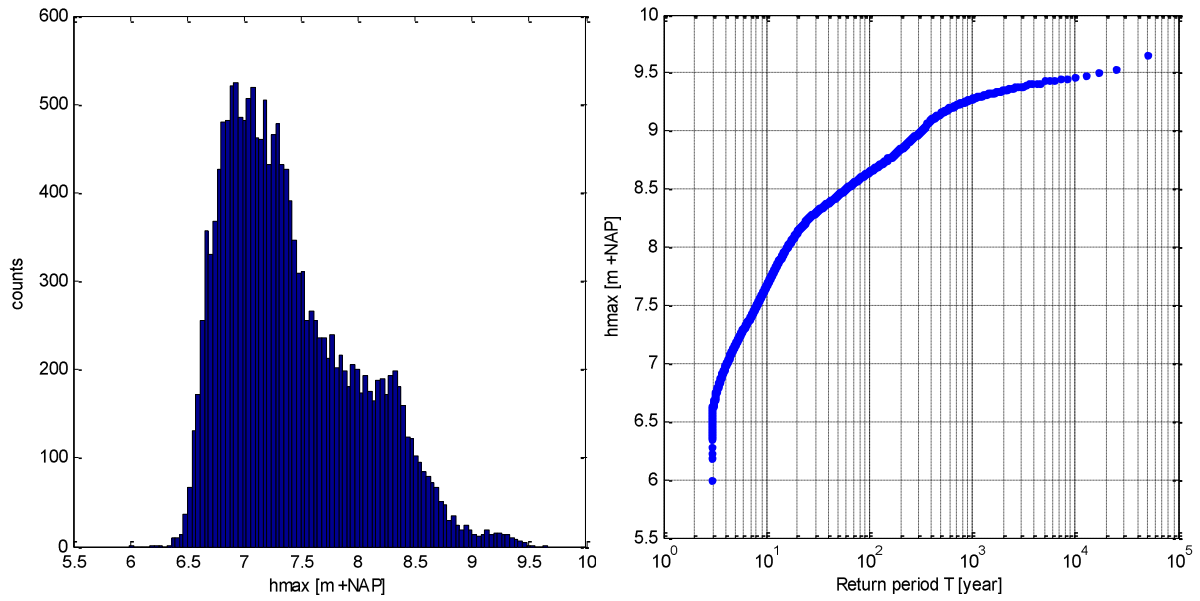


Figure E-5 Water levels at location Megen

### Sensitivity of frequency curve for the number of simulations

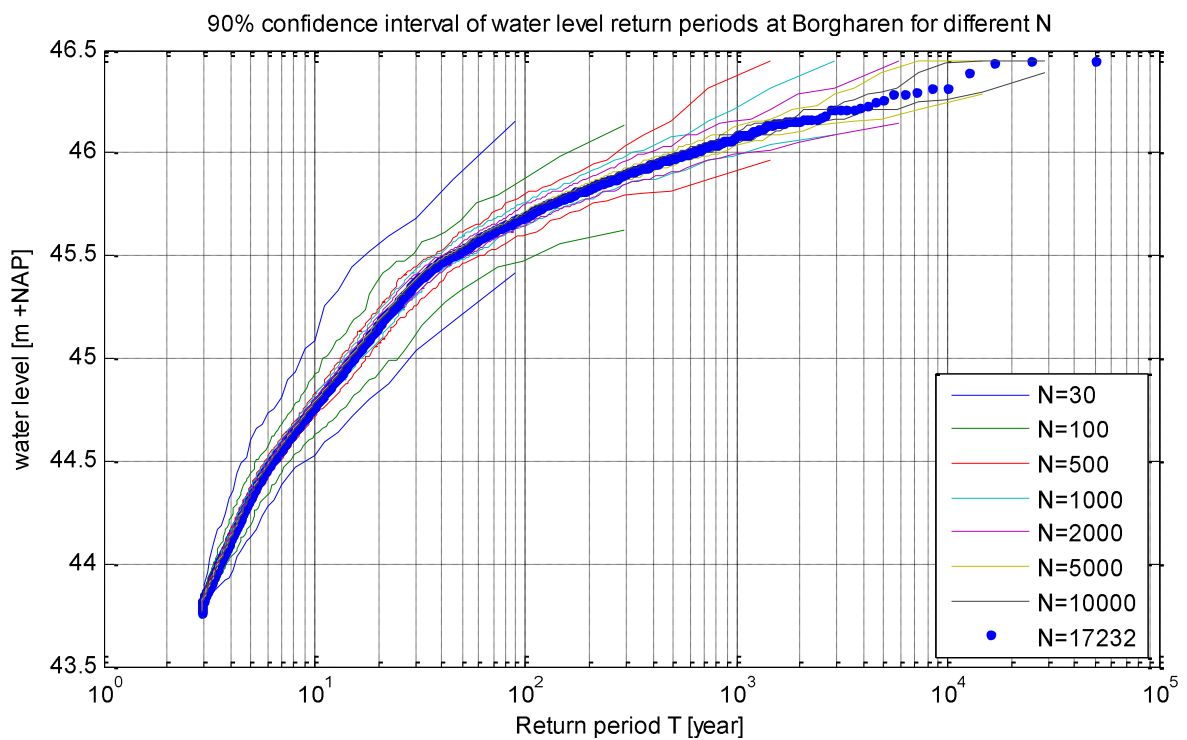


Figure E-6 90% confidence interval at Borgharen

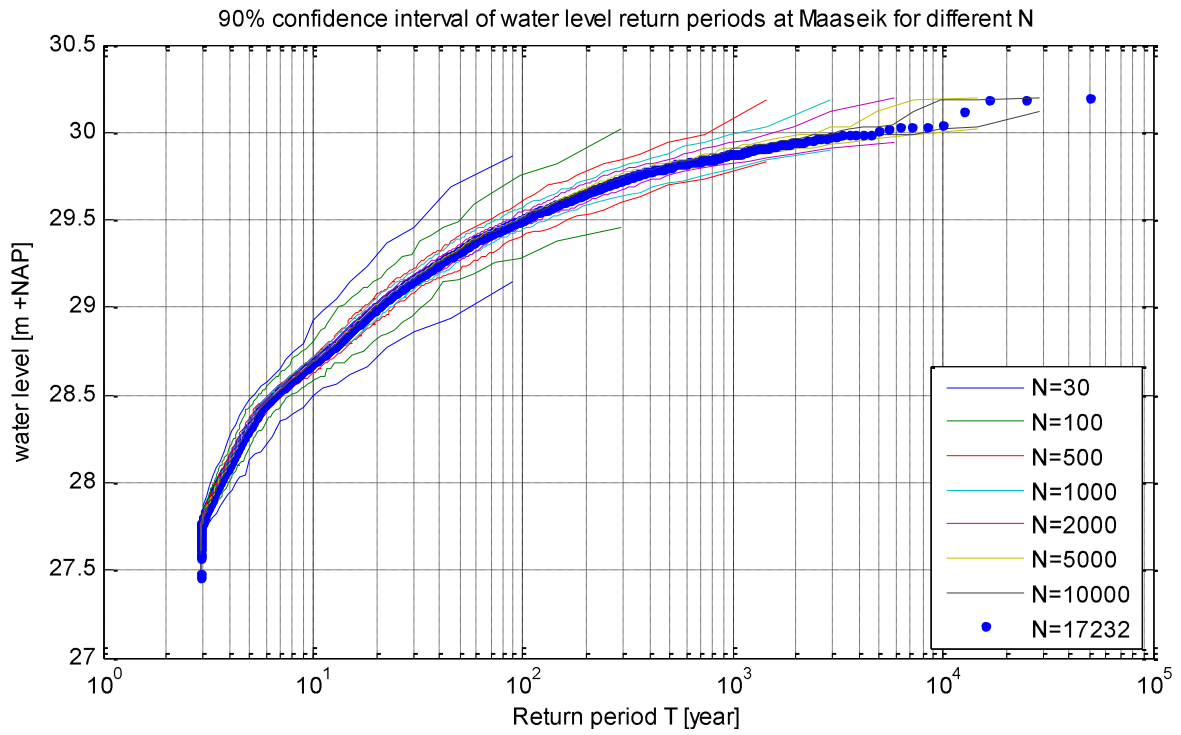


Figure E-7 90% confidence interval at Maaseik

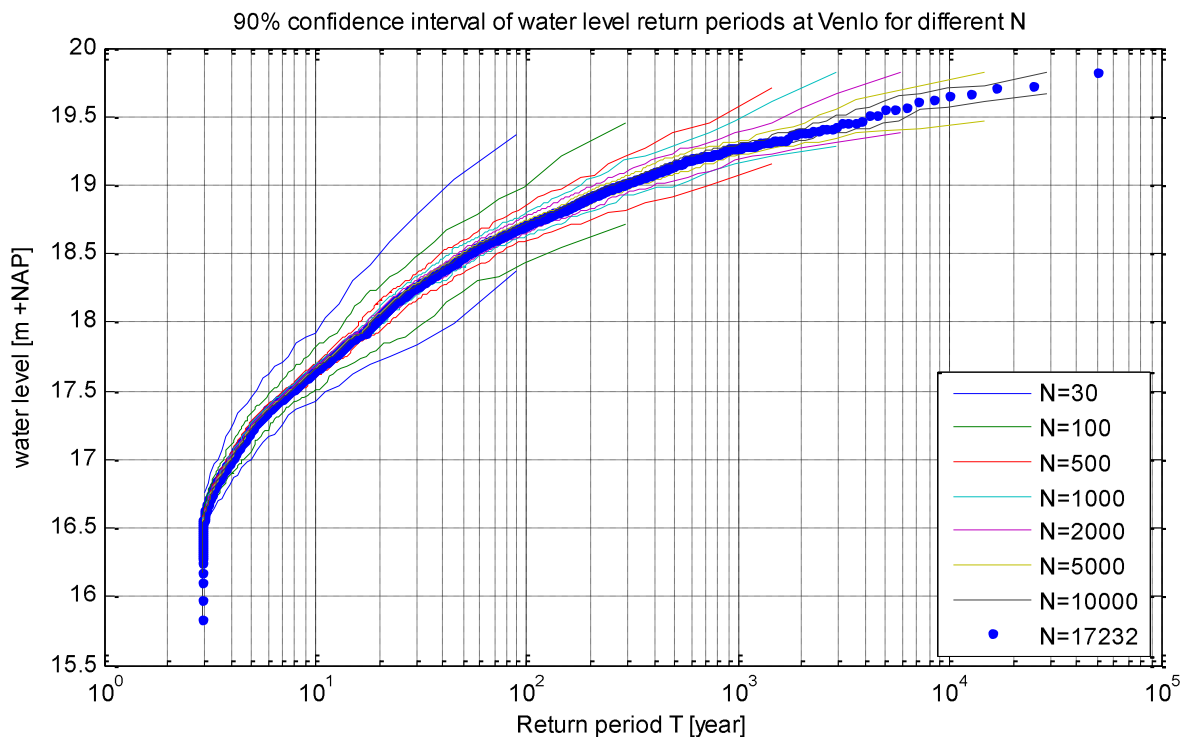


Figure E-8 90% confidence interval at Venlo

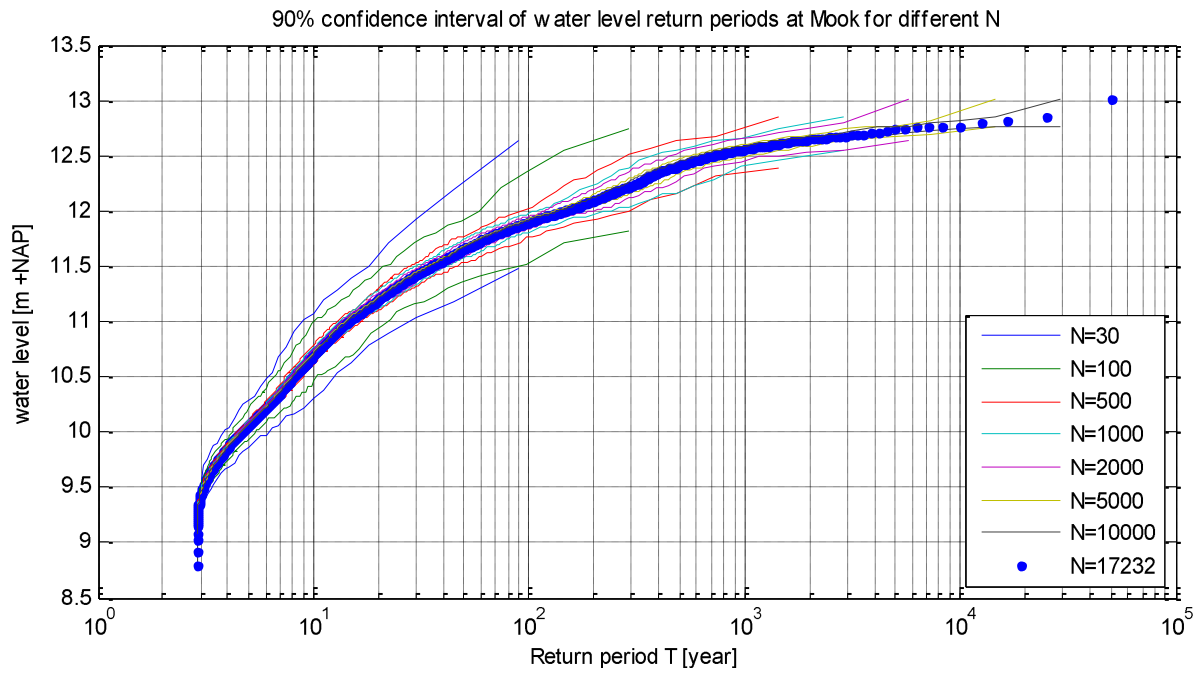


Figure E-9 90% confidence interval at Mook

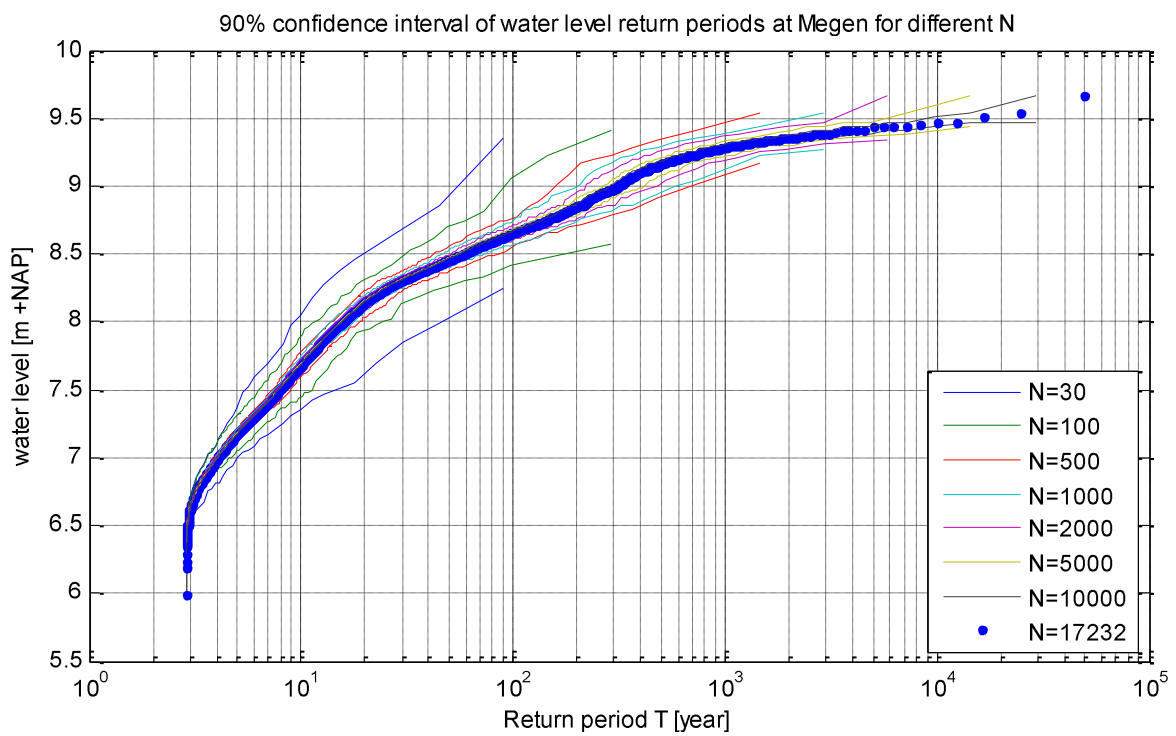


Figure E-10 90% confidence interval at Megen

## **Appendix F. Results of design hydrograph methods**

## Standard hydrographs GRADE vs. Measured dataset

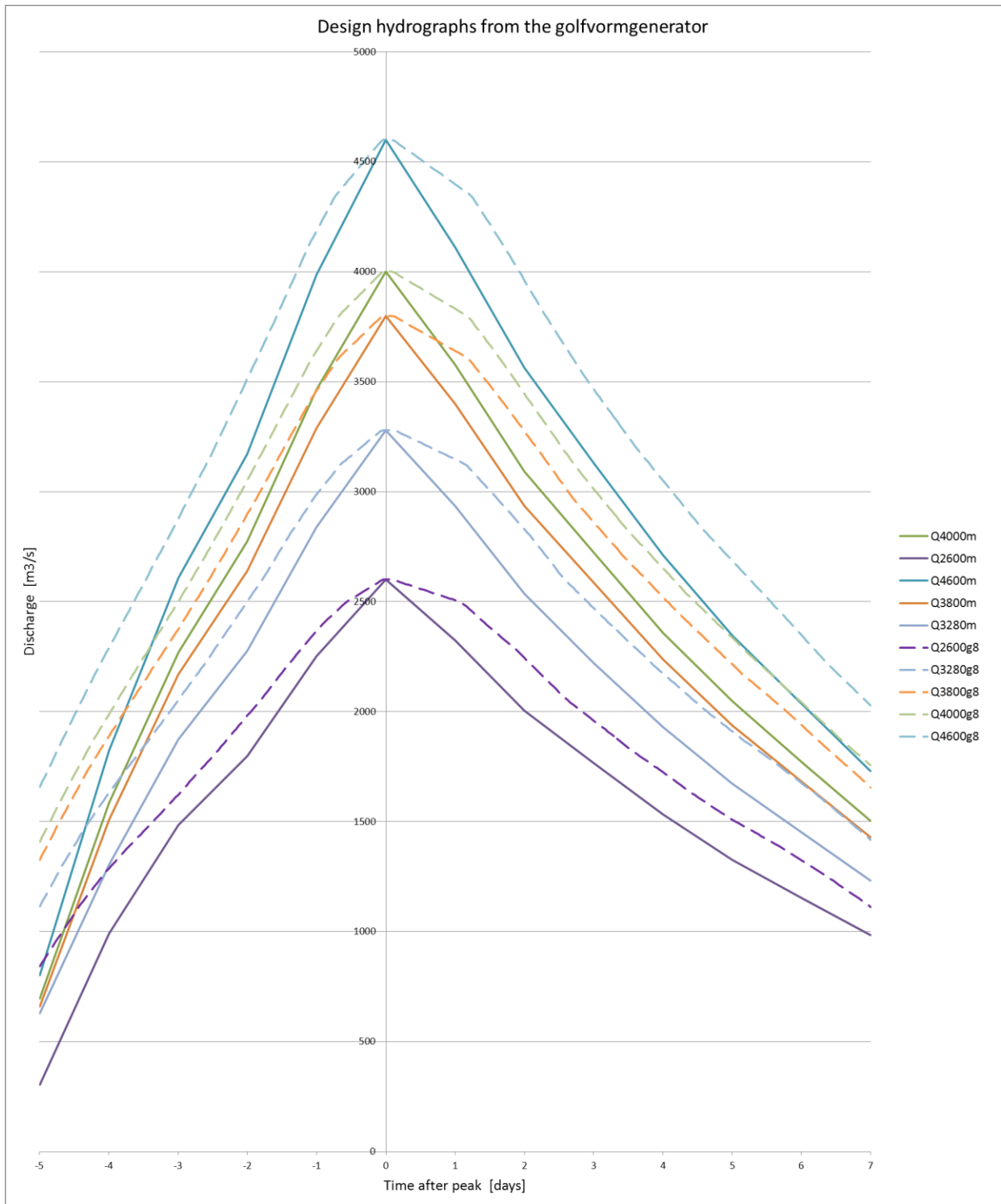


Figure F-1 Standard hydrographs based on GRADE (- -) and based on measurements (-)

## Frequency curves GRADE vs. Measured

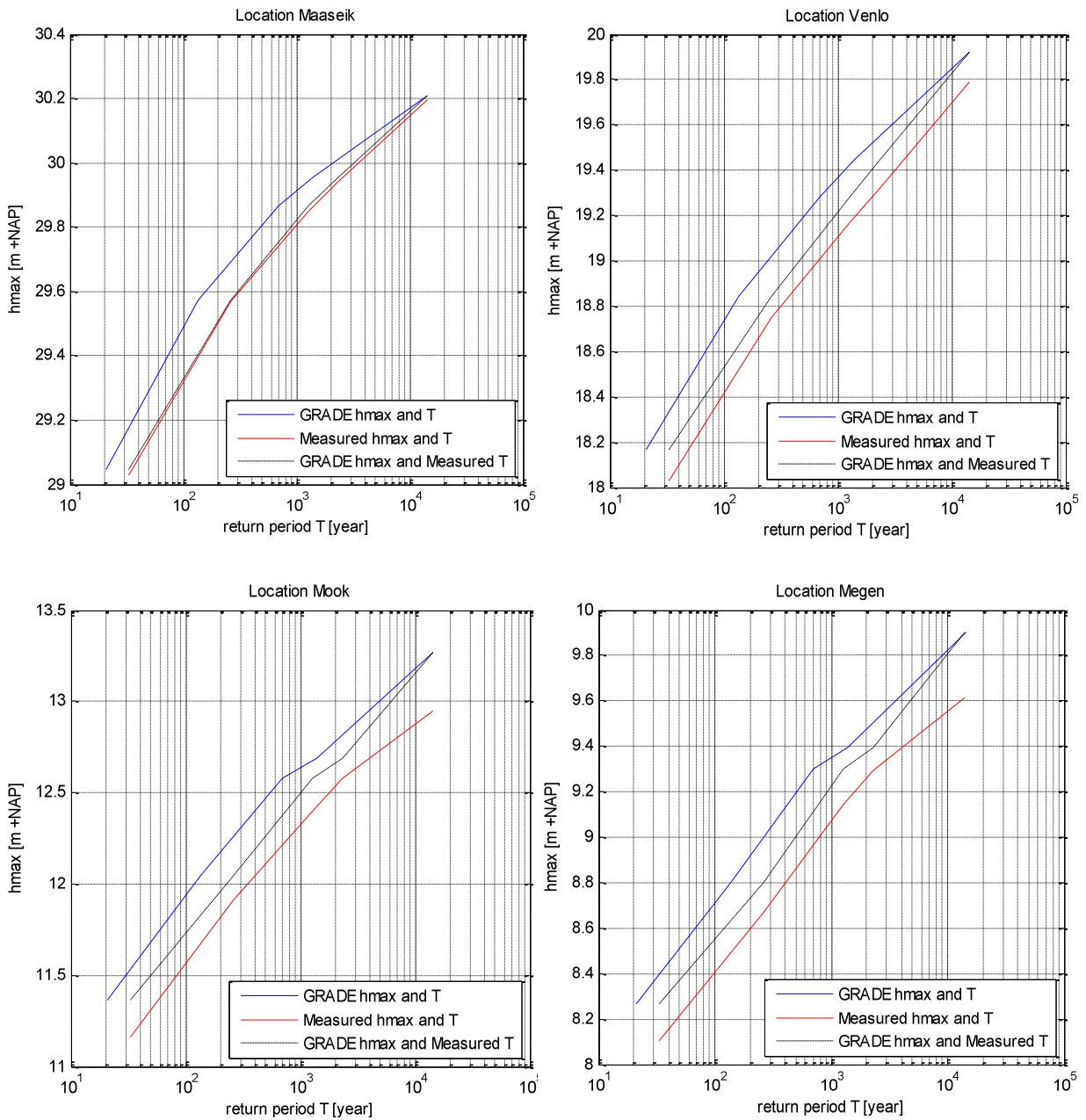


Figure F-3 Water level return periods, GRADE vs Measured ( $T_{GRADE}$  according to GPD)

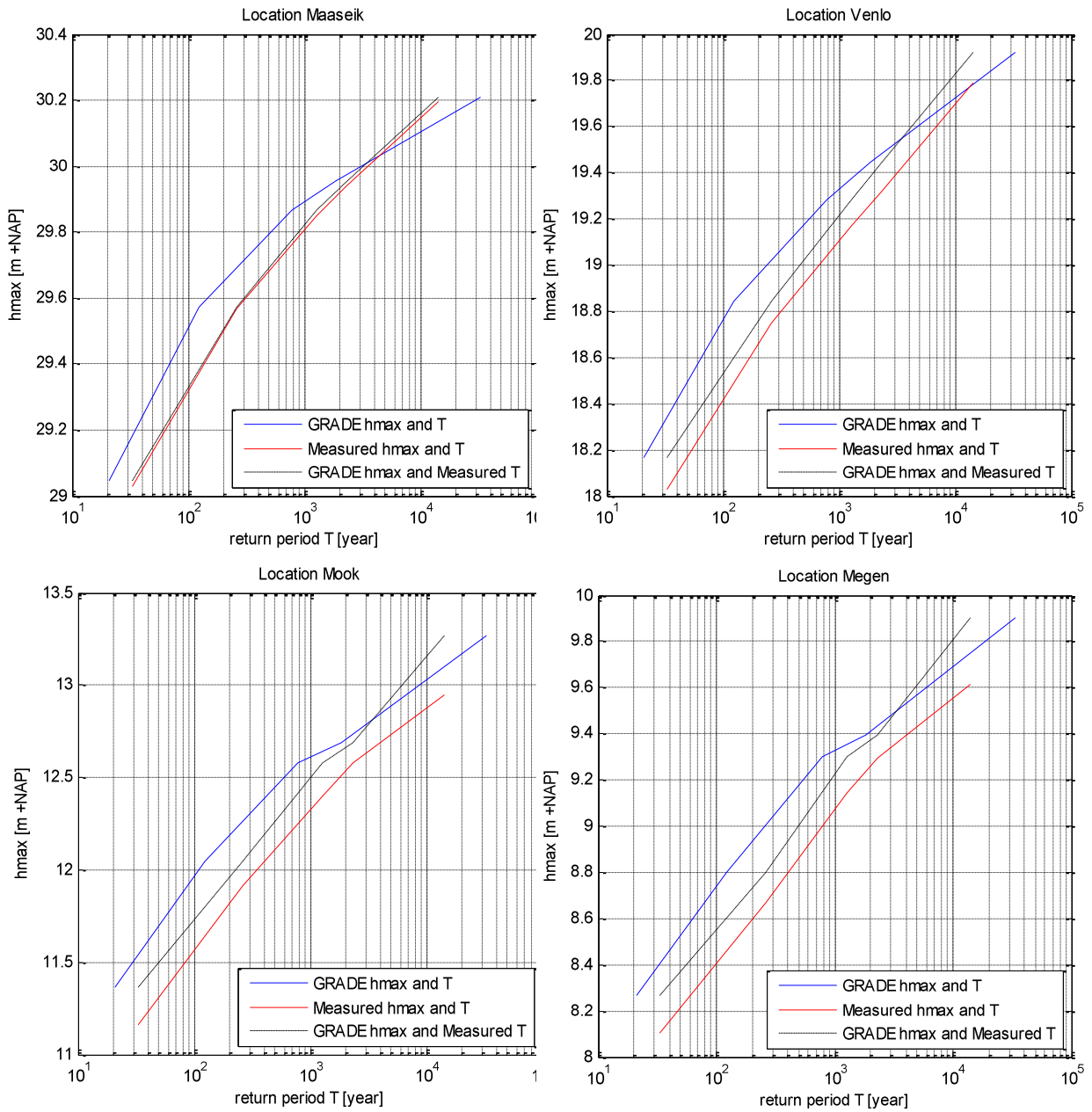


Figure F-4 Water level return periods, GRADE vs Measured ( $T_{GRADE}$  according to Kernel)

### Design hydrographs with modified selection interval

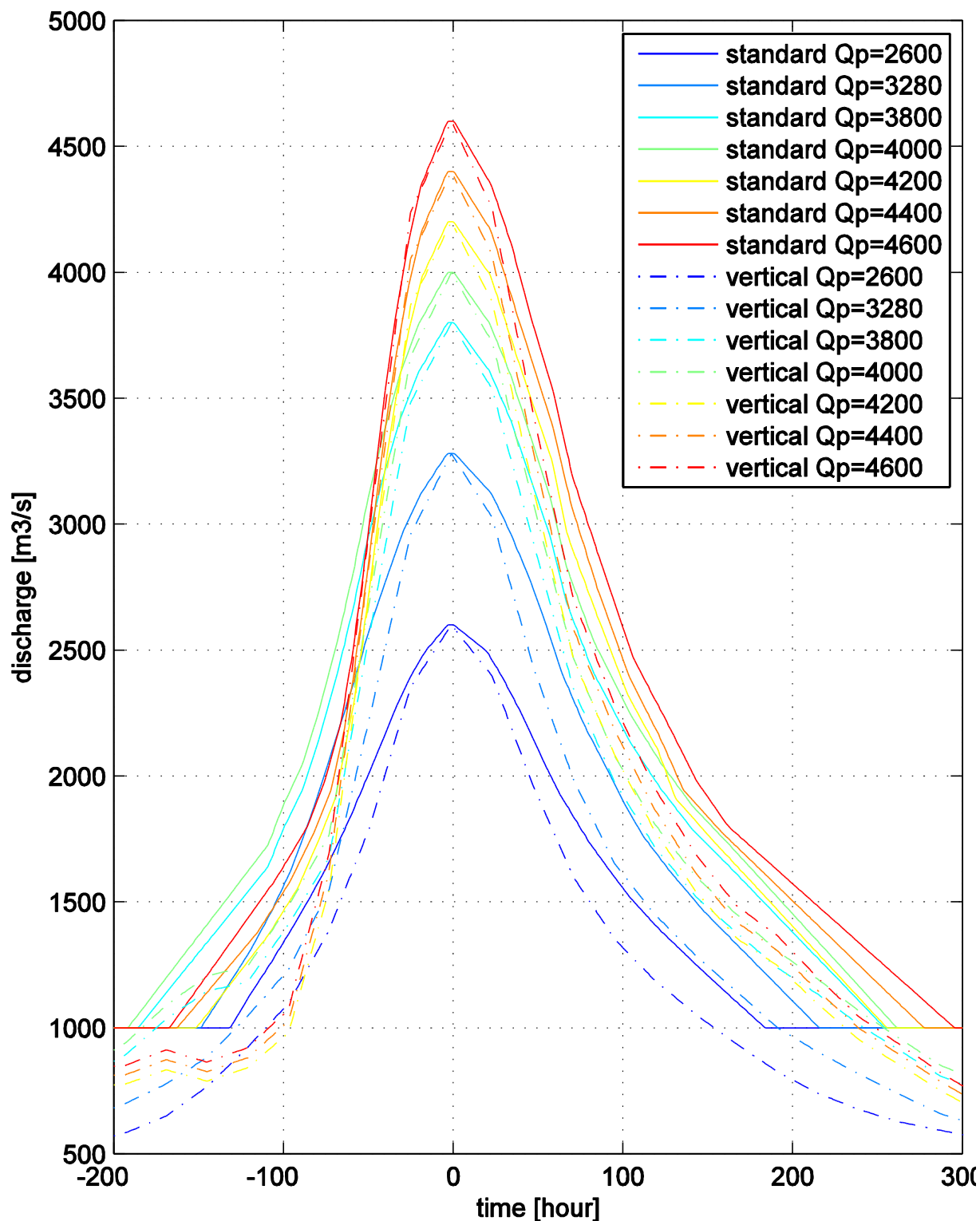


Figure F-5 Hydrographs with modified selection interval that depends on the design peak discharge

## Design water levels based on the design hydrograph methods

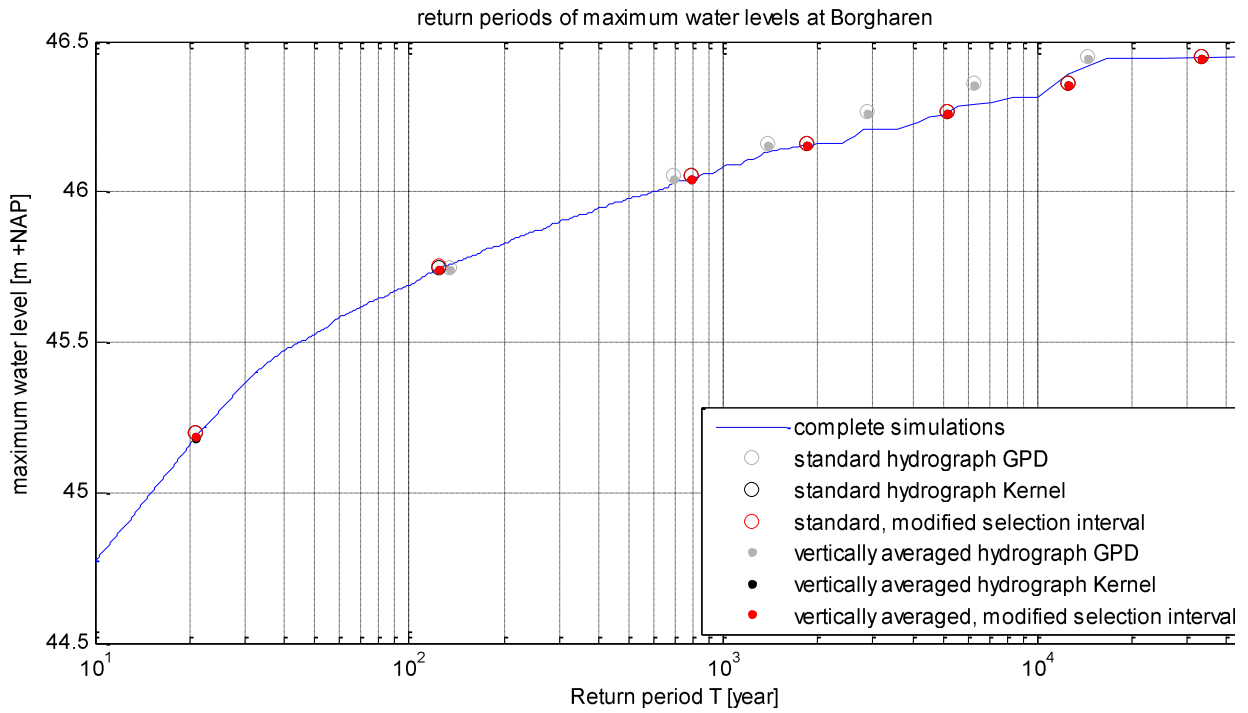


Figure F-6 Design water levels at Borgharen with modified selection interval

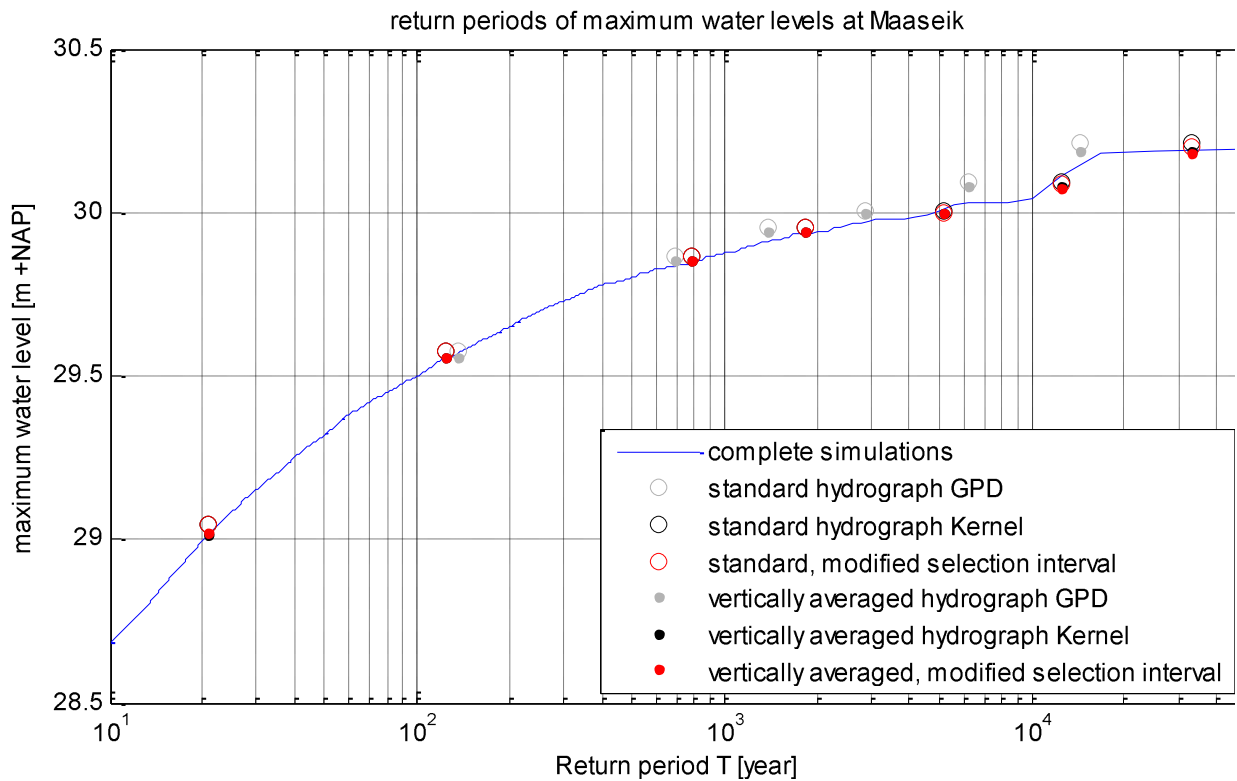
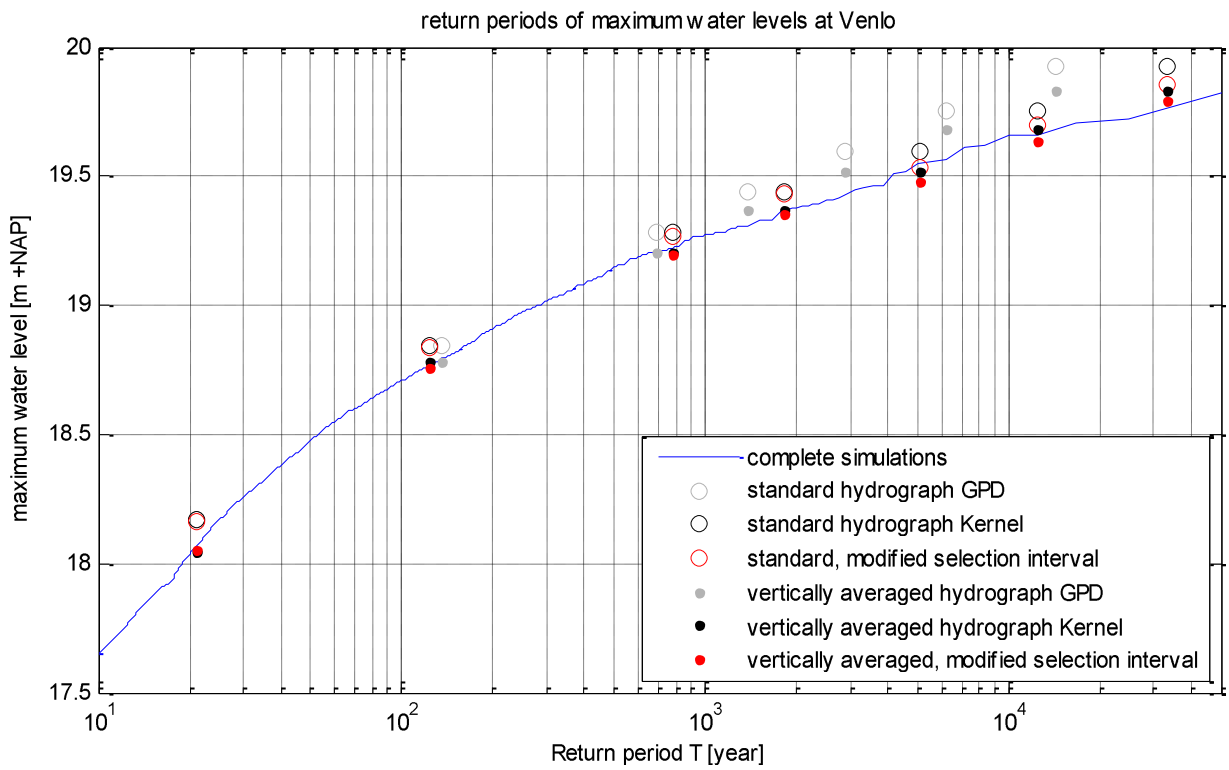
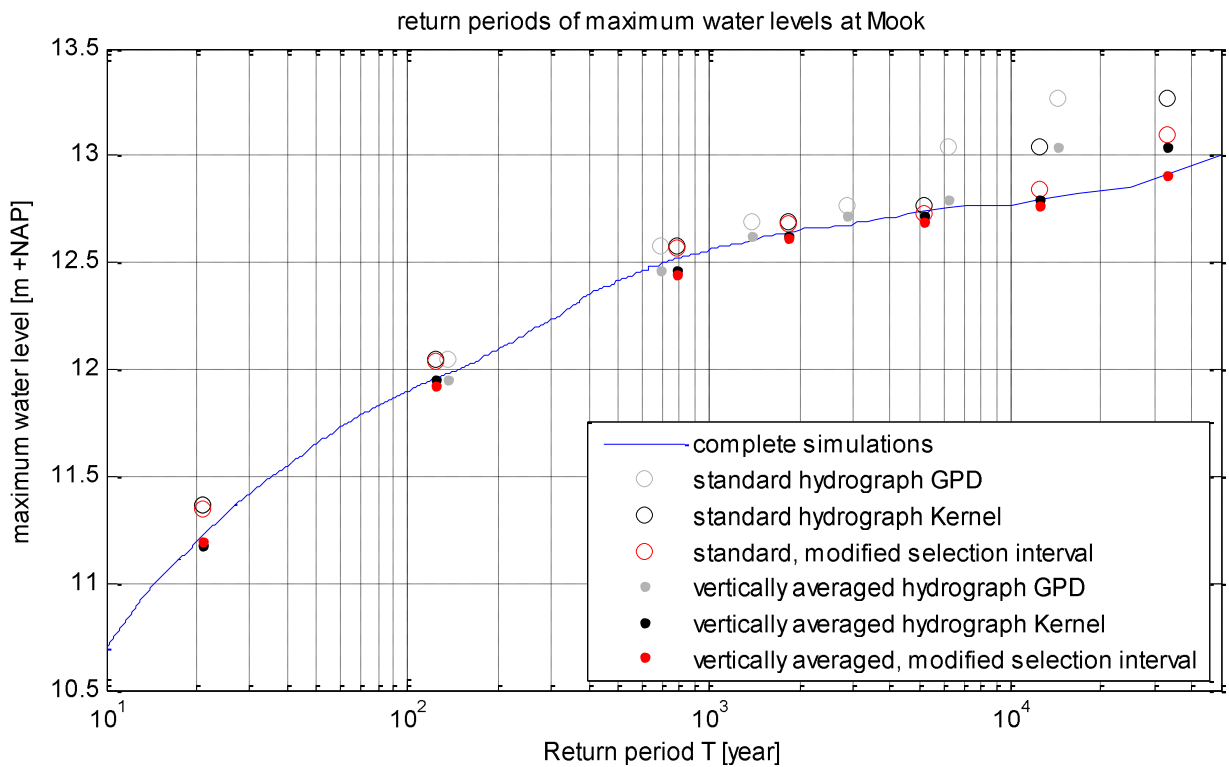


Figure F-7 Design water levels at Maaseik with modified selection interval



**Figure F-8 Design water levels at Venlo with modified selection interval**



**Figure F-9 Design water levels at Mook with modified selection interval**

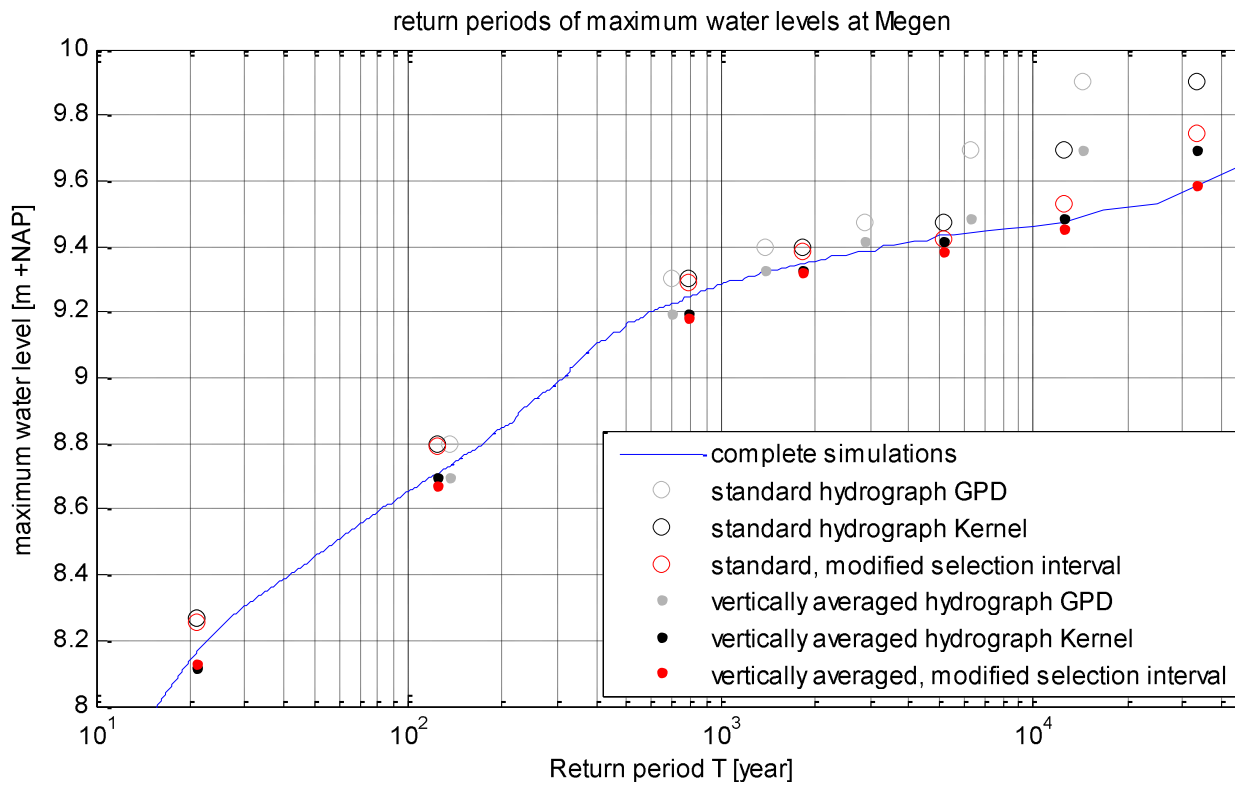


**Figure F-10 Design water levels at Megen with modified selection interval**

## **Appendix G. Results of probabilistic methods**

## Transformation functions

		25x SOBEK	25x WAQUA	17232x SOBEK
Peak discharge	Shape variable	R <sup>2</sup> , RMSE	R <sup>2</sup> , RMSE	R <sup>2</sup> , RMSE
1 <sup>st</sup> order in Q <sub>p</sub>	1 <sup>st</sup> order in C <sub>2</sub>	0.9832, 0.0925	0.9919, 0.0620	0.9575, 0.1436
1 <sup>st</sup> order in ln(Q <sub>p</sub> )	1 <sup>st</sup> order in C <sub>2</sub>	0.9920, 0.0640	0.9890, 0.0725	0.9811, 0.0957
2 <sup>nd</sup> order in Q <sub>p</sub>	1 <sup>st</sup> order in C <sub>2</sub>	0.9953, 0.0515	0.9924, 0.0629	0.9844, 0.0870 <sup>(1)</sup>
2 <sup>nd</sup> order in ln(Q <sub>p</sub> )	1 <sup>st</sup> order in C <sub>2</sub>	0.9953, 0.0515	0.9924, 0.0630	0.9844, 0.0870 <sup>(2)</sup>
1 <sup>st</sup> order in ln(Q <sub>p</sub> )	1 <sup>st</sup> order in ln(D <sub>85%</sub> )	0.9820, 0.0959	0.9844, 0.0860	0.9770, 0.1055
2 <sup>nd</sup> order in ln(Q <sub>p</sub> )	1 <sup>st</sup> order in ln(D <sub>85%</sub> )	0.9873, 0.0843	0.9880, 0.0792	0.9811, 0.0957 <sup>(2)</sup>
1 <sup>st</sup> order in ln(Q <sub>p</sub> )	2 <sup>nd</sup> order in D <sub>85%</sub>	0.9887, 0.0796	0.9882, 0.0785	0.9782, 0.1027
2 <sup>nd</sup> order in ln(Q <sub>p</sub> )	2 <sup>nd</sup> order in D <sub>85%</sub>	0.9891, 0.0802	0.9914, 0.0687	0.9820, 0.0933 <sup>(2)</sup>
1 <sup>st</sup> order in ln(Q <sub>p</sub> )	2 <sup>nd</sup> order in ln(D <sub>85%</sub> )	0.9938, 0.0589	0.9898, 0.0730	0.9817, 0.0941
2 <sup>nd</sup> order in ln(Q <sub>p</sub> )	2 <sup>nd</sup> order in ln(D <sub>85%</sub> )	0.9941, 0.0591	0.9936, 0.0595	0.9855, 0.0839 <sup>(3)</sup>
1 <sup>st</sup> order in ln(Q <sub>p</sub> )	1 <sup>st</sup> order in ln(V <sub>85%</sub> )	0.9818, 0.0962	0.9863, 0.0808	0.9761, 0.1077
2 <sup>nd</sup> order in ln(Q <sub>p</sub> )	1 <sup>st</sup> order in ln(V <sub>85%</sub> )	0.9873, 0.0845	0.9871, 0.0820	0.9807, 0.0968
1 <sup>st</sup> order in ln(Q <sub>p</sub> )	2 <sup>nd</sup> order in ln(V <sub>85%</sub> )	0.9904, 0.0732	0.9913, 0.0675	0.9802, 0.0981
2 <sup>nd</sup> order in ln(Q <sub>p</sub> )	2 <sup>nd</sup> order in ln(V <sub>85%</sub> )	0.9917, 0.0701	0.9913, 0.0690	0.9826, 0.0920
2 <sup>nd</sup> order in ln(Q <sub>p</sub> )	2 <sup>nd</sup> order in V <sub>85%</sub>	0.9865, 0.0892	0.9890, 0.0777	0.9795, 0.0997 <sup>(4)</sup>
1 <sup>st</sup> order in ln(Q <sub>p</sub> )	2 <sup>nd</sup> order in V <sub>85%</sub>	0.9855, 0.0900	0.9890, 0.0757	0.9768, 0.1061 <sup>(4)</sup>

**Table G-1 Fits of water level at Mook to shape variables**

		25x SOBEK	25x WAQUA	17232x SOBEK
Peak discharge	Shape variable	R <sup>2</sup> , RMSE	R <sup>2</sup> , RMSE	R <sup>2</sup> , RMSE
1 <sup>st</sup> order in ln(Q <sub>p</sub> )	1 <sup>st</sup> order in C <sub>2</sub>	0.9939, 0.0518	0.9905, 0.0640	0.9860, 0.0678
2 <sup>nd</sup> order in ln(Q <sub>p</sub> )	1 <sup>st</sup> order in C <sub>2</sub>	0.9953, 0.0473	0.9924, 0.0600	0.9901, 0.0571

**Table G-2 Fits of water level at Venlo to shape variables**

		25x SOBEK	25x WAQUA	17232x SOBEK
Peak discharge	Shape variable	R <sup>2</sup> , RMSE	R <sup>2</sup> , RMSE	R <sup>2</sup> , RMSE
1 <sup>st</sup> order in ln(Q <sub>p</sub> )	1 <sup>st</sup> order in C <sub>2</sub>	0.9904, 0.0604	0.9900, 0.0646	0.9776, 0.0874 <sup>(1)</sup>
2 <sup>nd</sup> order in ln(Q <sub>p</sub> )	1 <sup>st</sup> order in C <sub>2</sub>	0.9935, 0.0522	0.9929, 0.0570	0.9816, 0.0792

**Table G-3 Fits of water level at Megen to shape variables**

<sup>1</sup> Less accurate fit for high Q

<sup>2</sup> Good fit for high Q

<sup>3</sup> Good fit for high Q and high D085

<sup>4</sup> Bad fit for high V85%

### Fitted polynomial surfaces for transformation functions

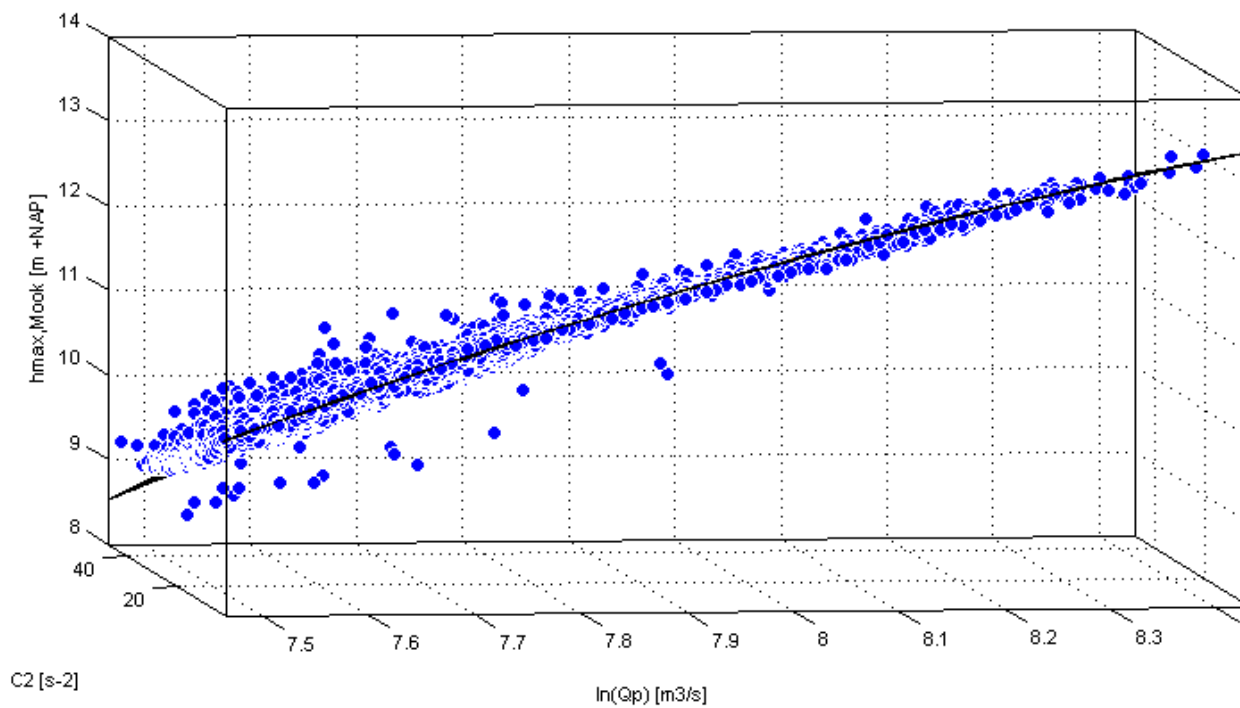


Figure G-1 Polynomial(2,1) fit of  $h_{max,Mook}$  to  $\ln(Q)$  and  $C_2$

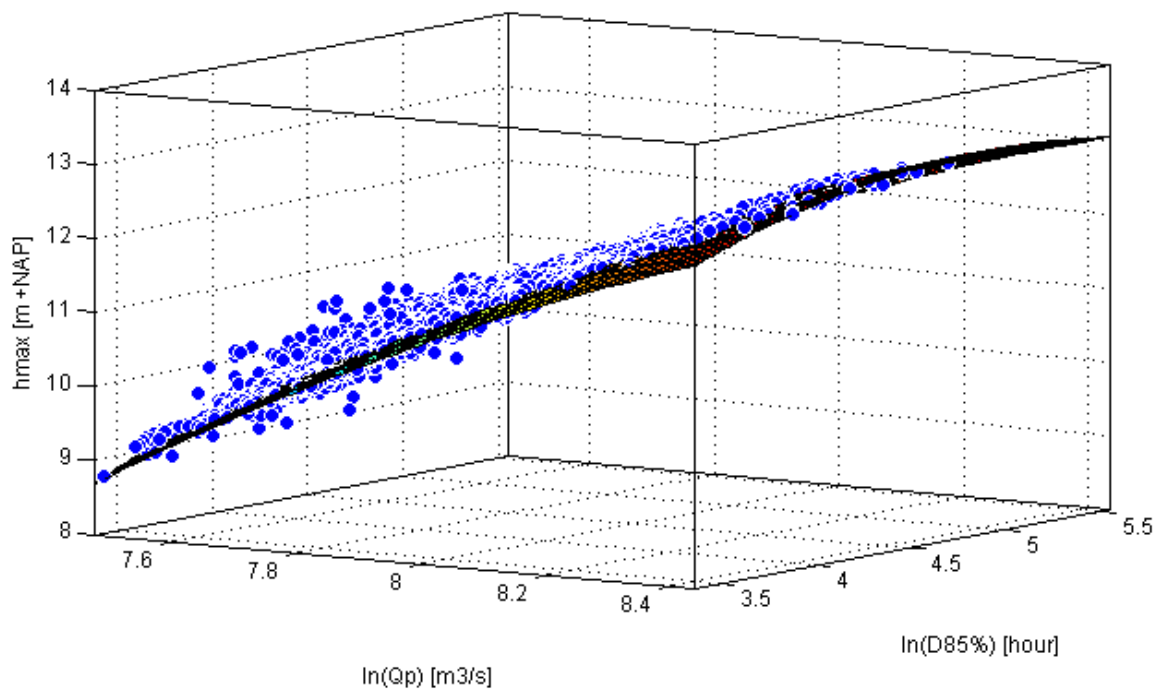


Figure G-2 Polynomial(2,2) fit of  $h_{max,Mook}$  to  $\ln(Q)$  and  $\ln(D_{85\%})$

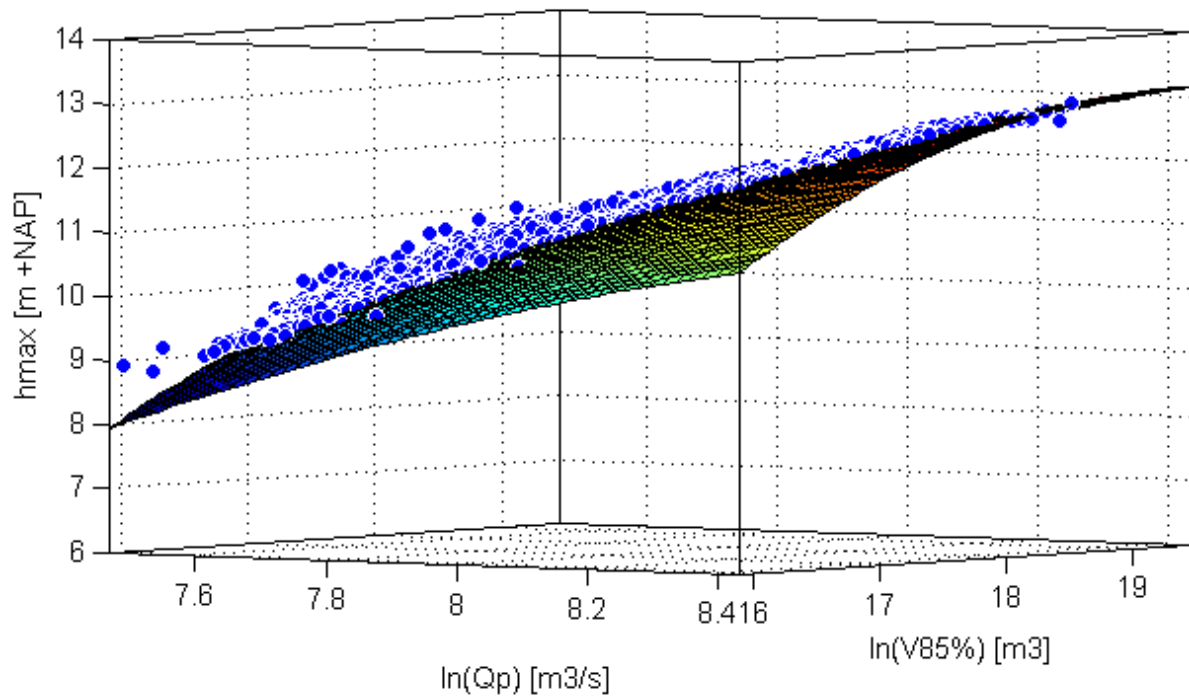


Figure G-3 Polynomial(2,2) fit of  $h_{max,Mook}$  to  $\ln(Q)$  and  $\ln(V_{85\%})$

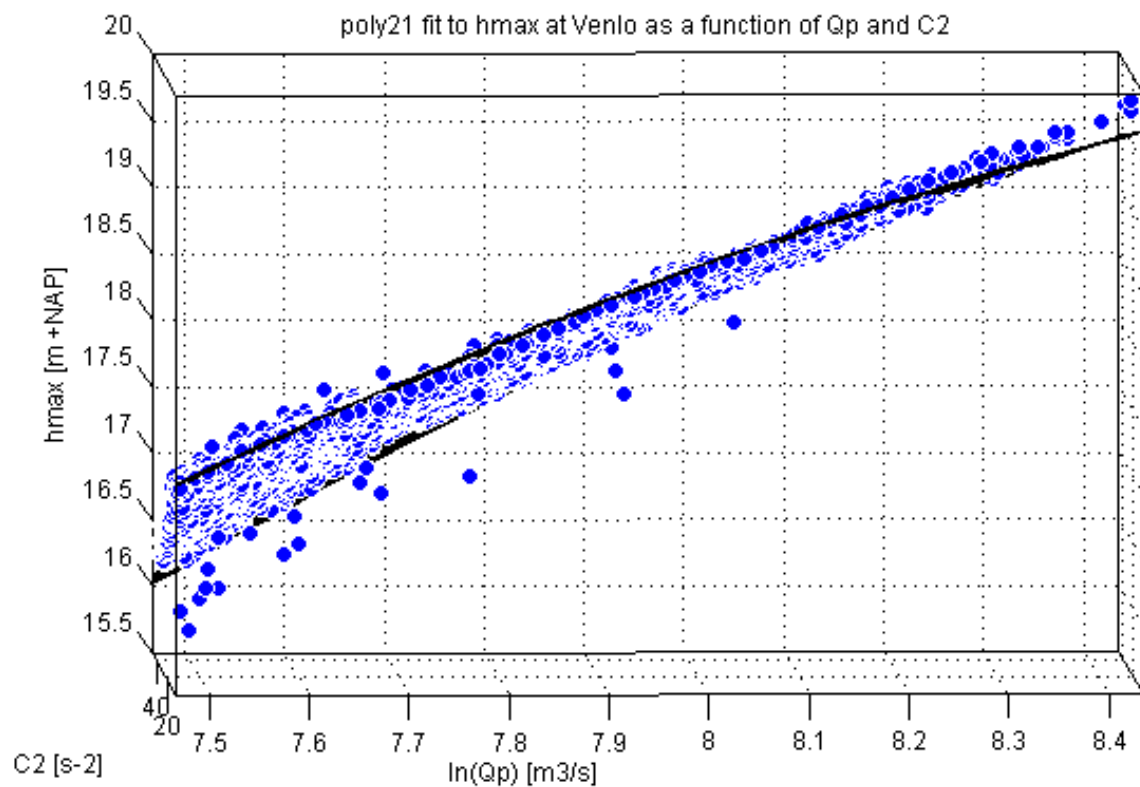


Figure G-4 Polynomial(2,1) fit of  $h_{max,Venlo}$  to  $\ln(Q)$  and  $C_2$

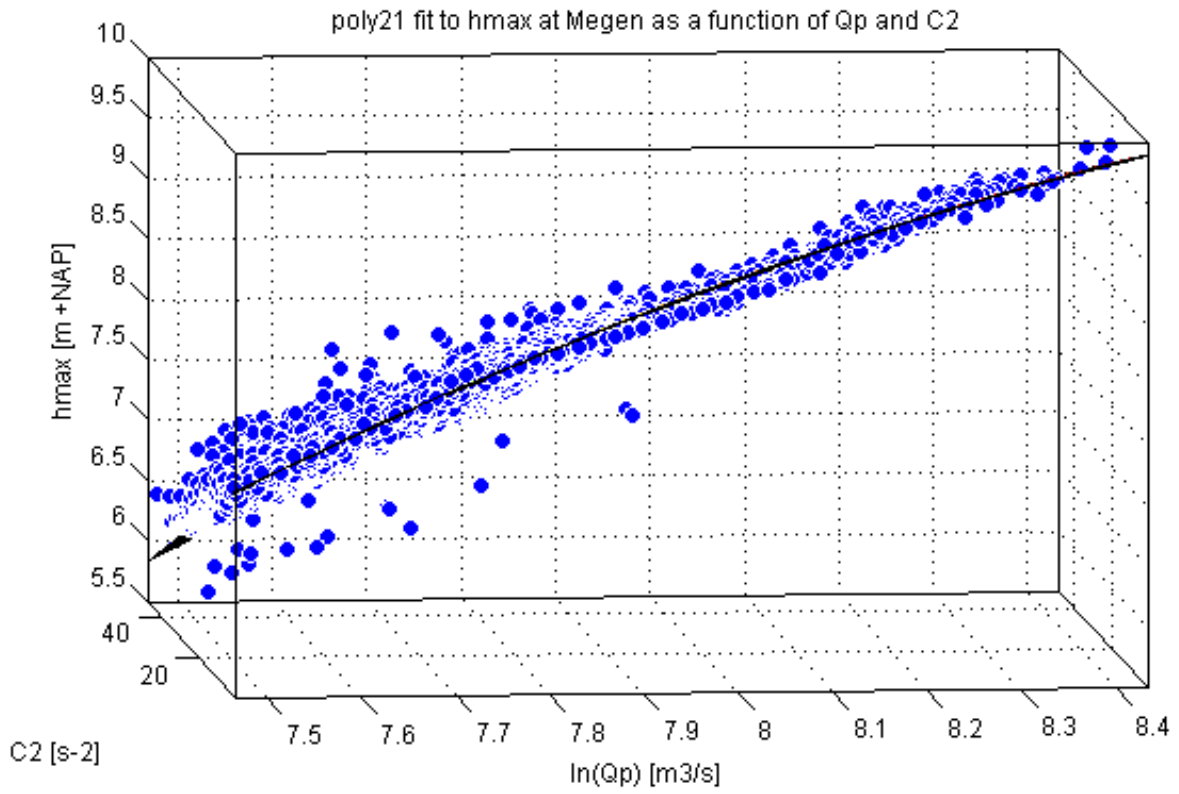


Figure G-5 Polynomial(2,1) fit of hmax,Megen to ln(Q) and C2

## Frequency curve from explicit probabilistic method

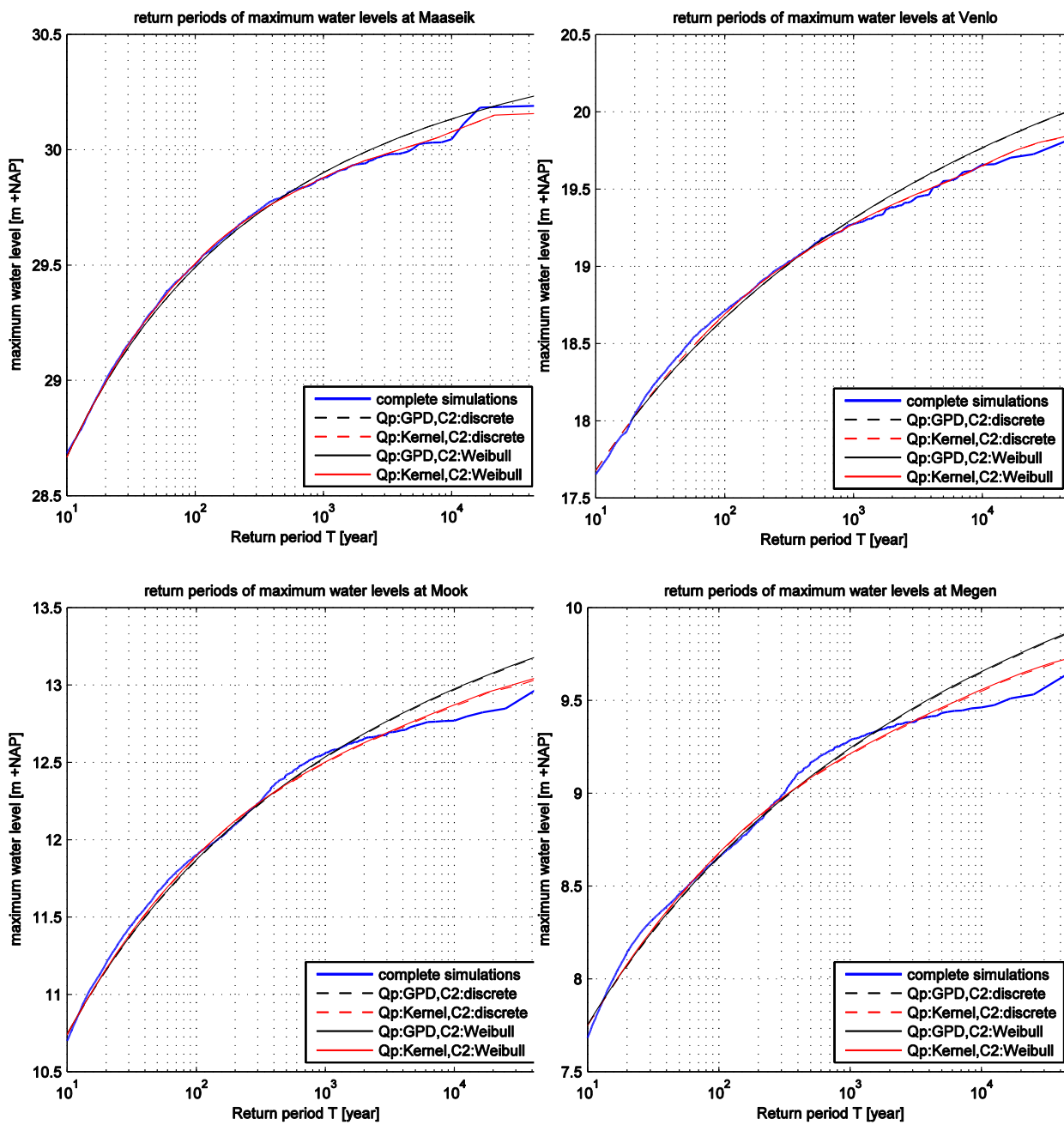


Figure G-6 Frequency curves from explicit probabilistic method

## Goodness of estimate in implicit method

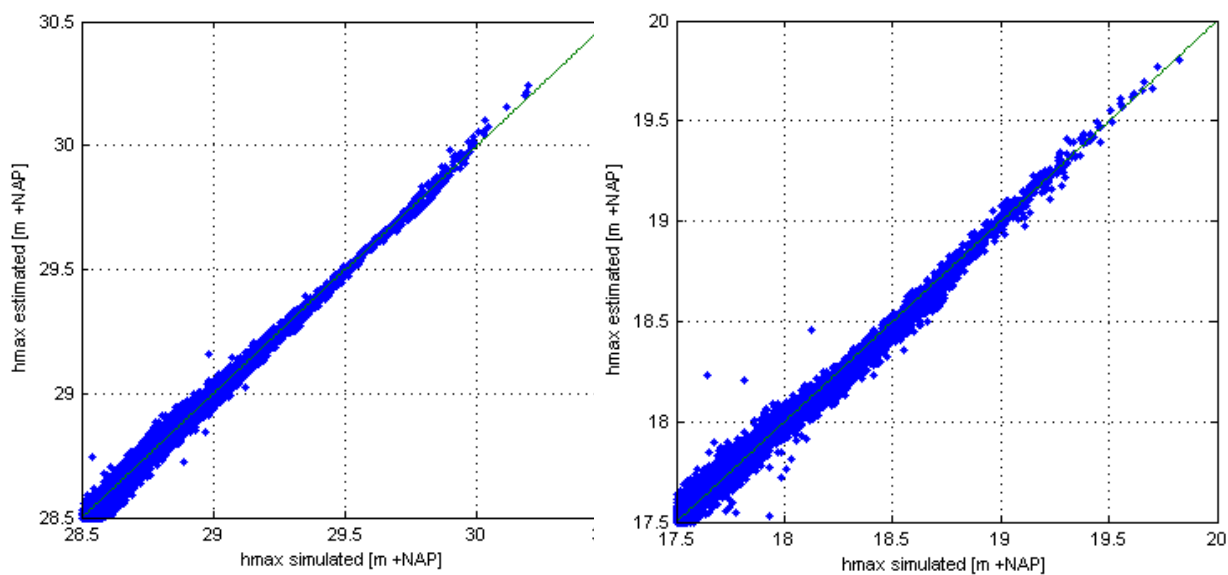


Figure G-7 Goodness of hmax fit at Maaseik (left) and Venlo (right)

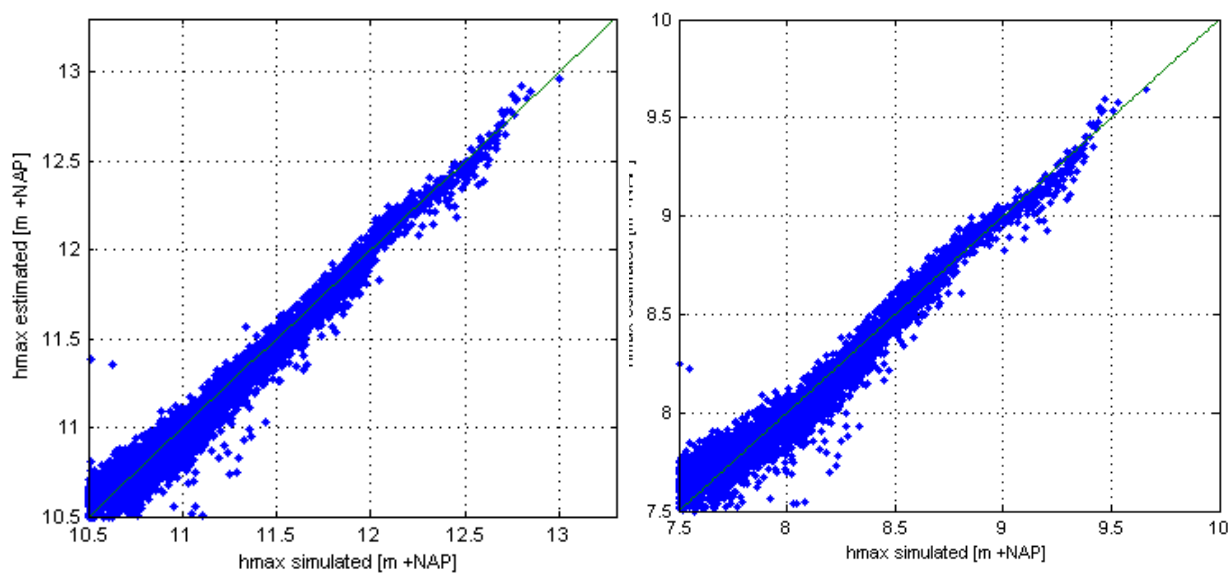


Figure G-8 Goodness of hmax fit at Mook (left) and Megen (right)

### Frequency curve from implicit probabilistic method, compared to other methods

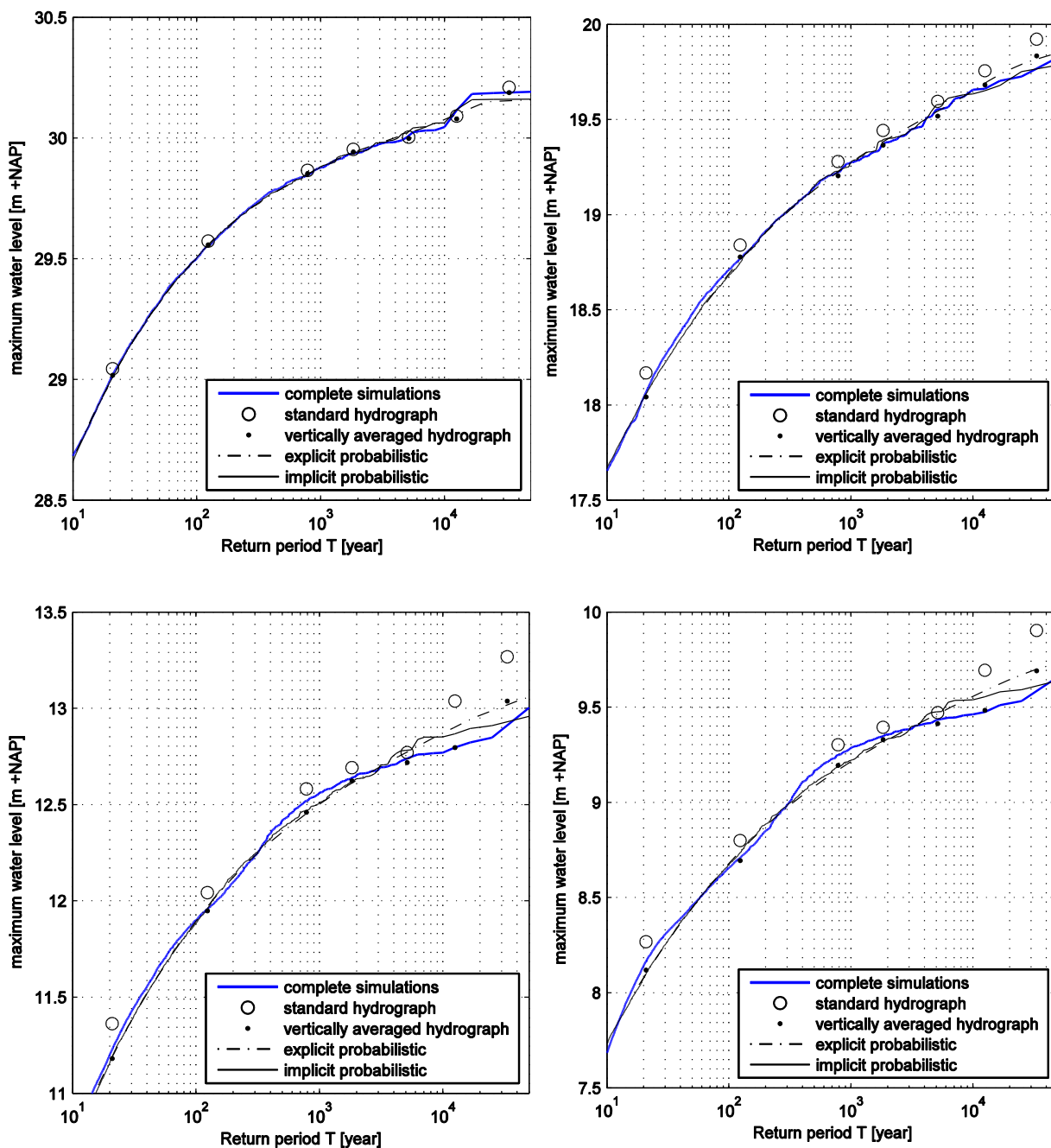
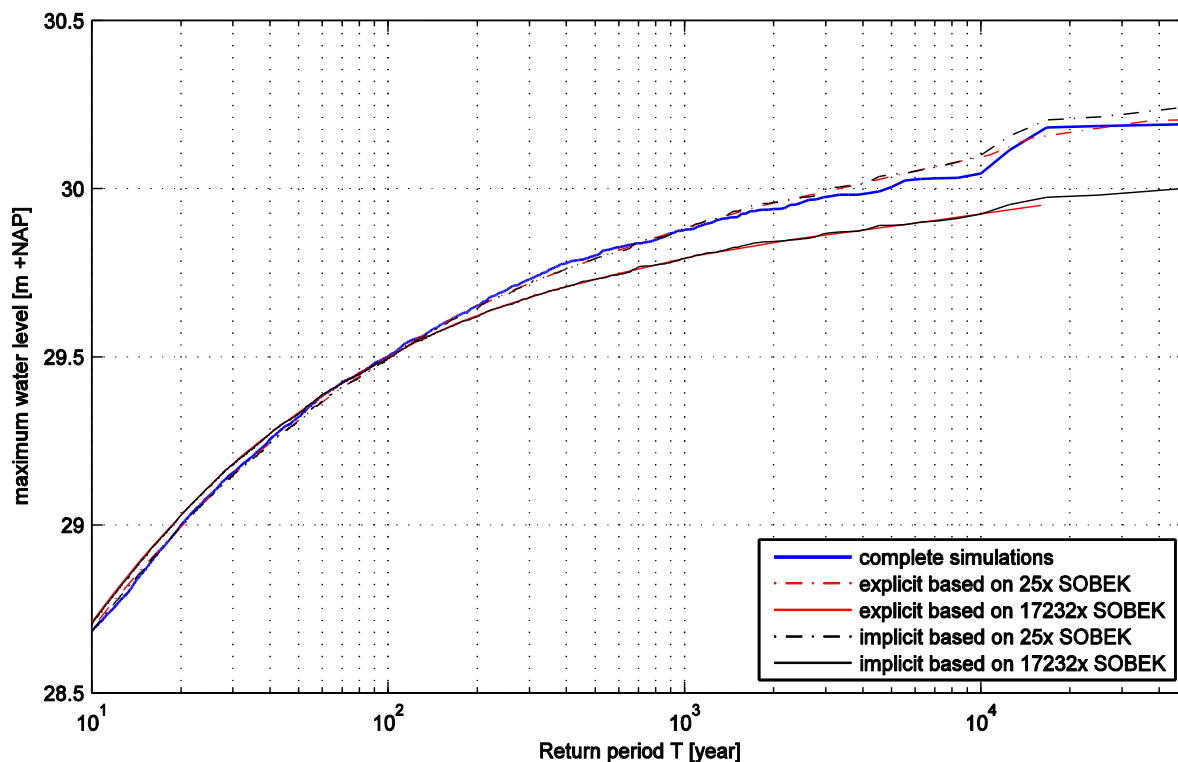
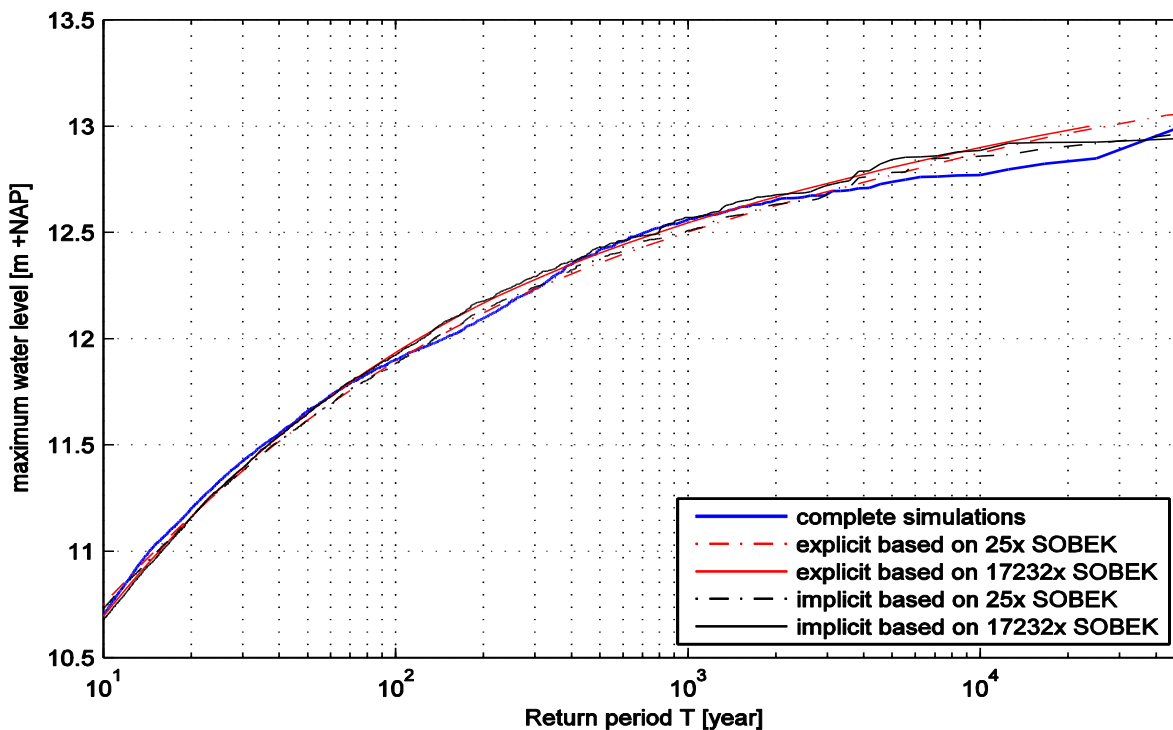


Figure G-9 Frequency curves including implicit probabilistic method (solid black line)

**Frequency curves of probabilistic methods; 2 datasets to fit transformation function**



**Figure G-10 Water level return periods at Maaseik for different SOBEK simulation sets**



**Figure G-11 Water level return periods at Mook for different SOBEK simulation sets**



## **Appendix H. Results of effect of retention basins**

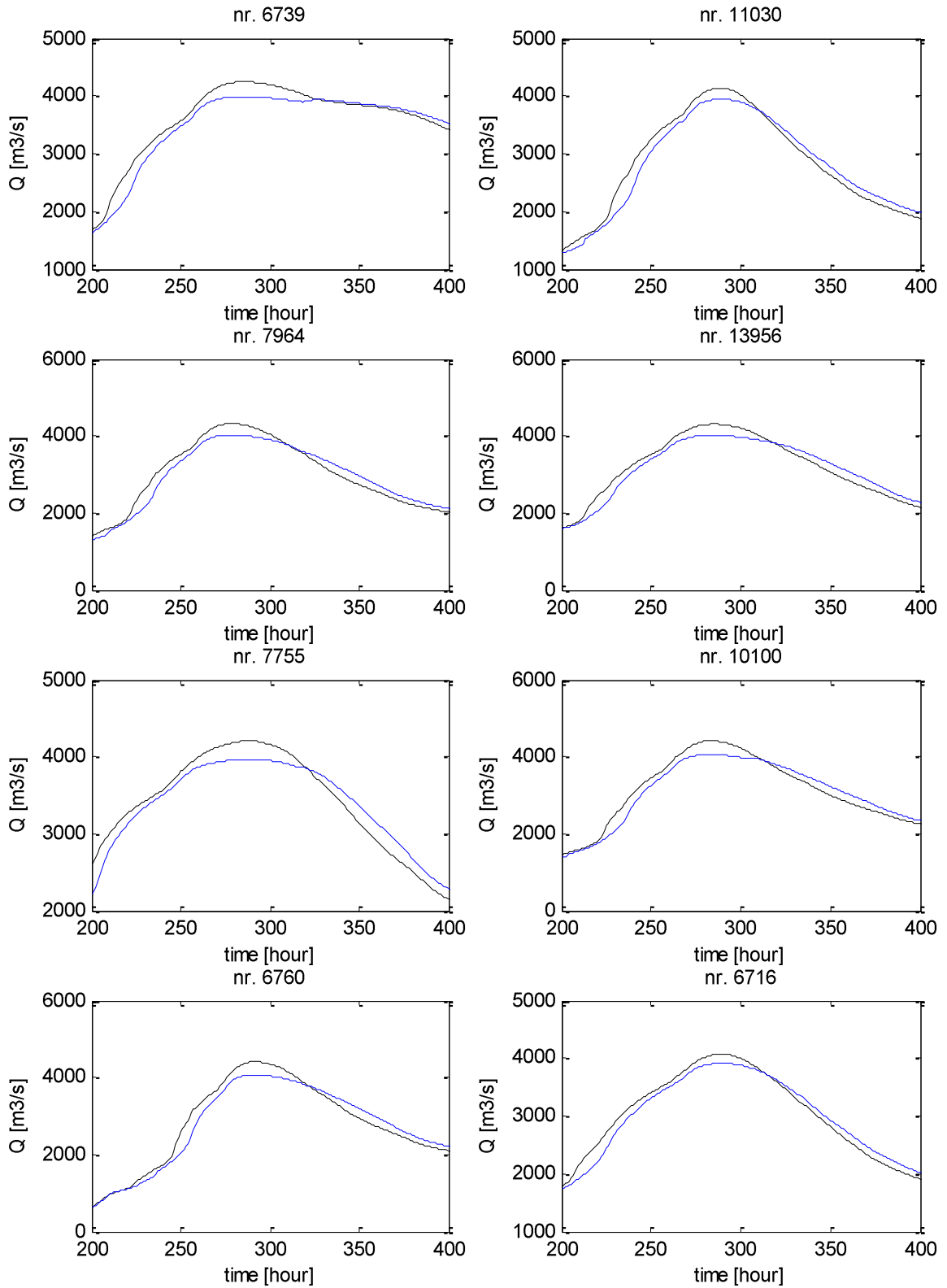


**Figure H-1 Influence of Lob van Gennep on extreme hydrographs (part 1)**

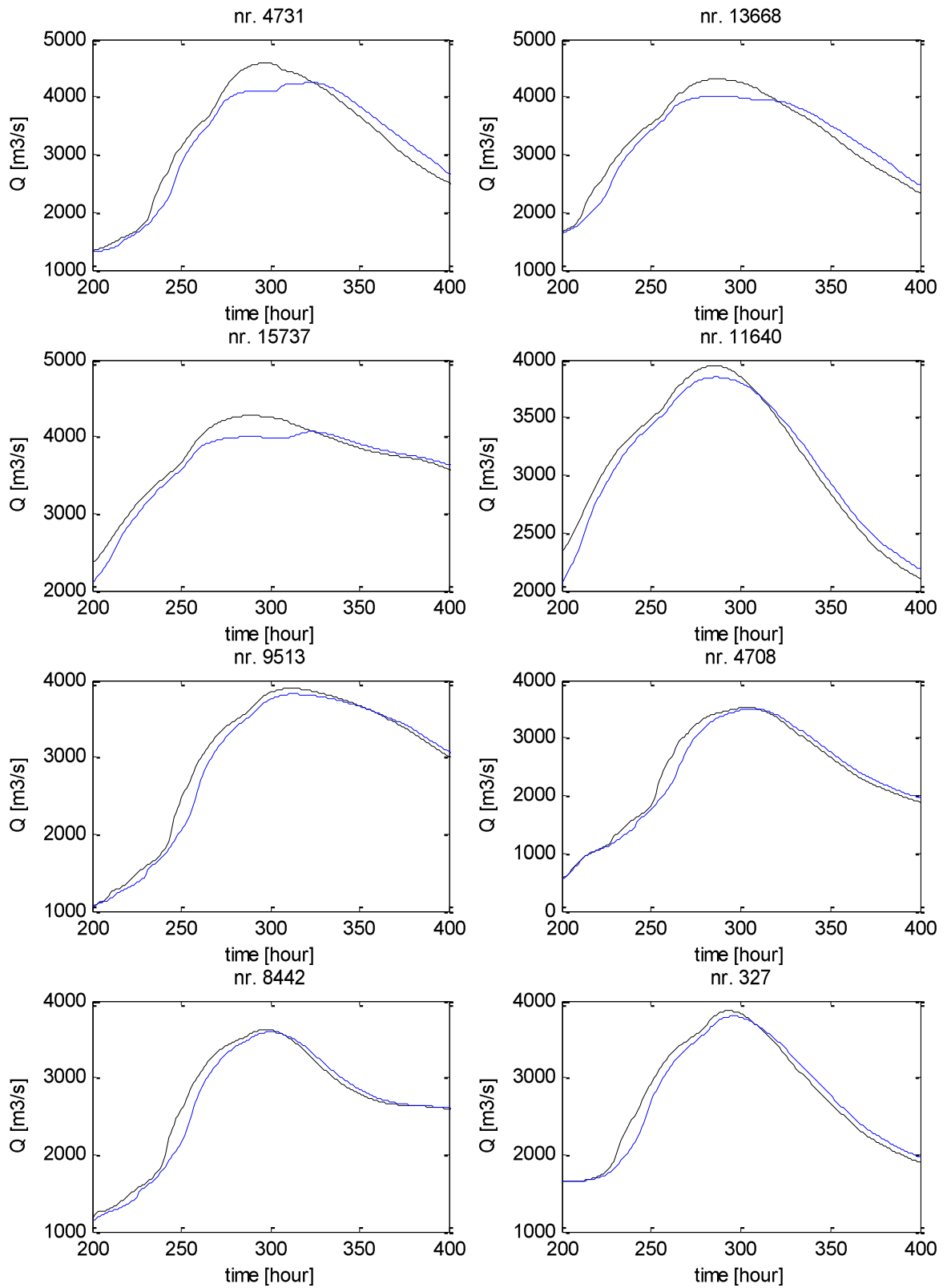


**Figure H-2 Influence of Lob van Gennep on extreme hydrographs (part 2)**

### Frequency curves Meuse system incl. Lob, excl. Lob and without retention

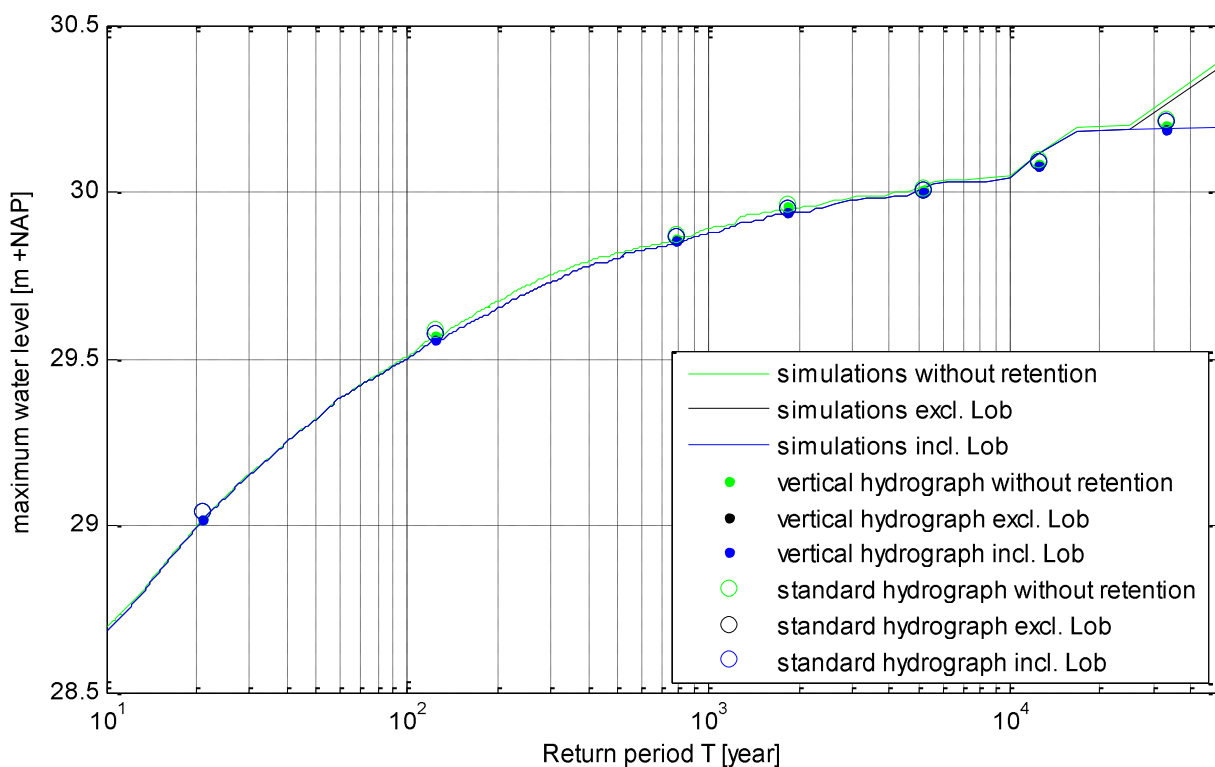


Figure H-3 Design water levels at Maaseik in system without retention (Kernel)

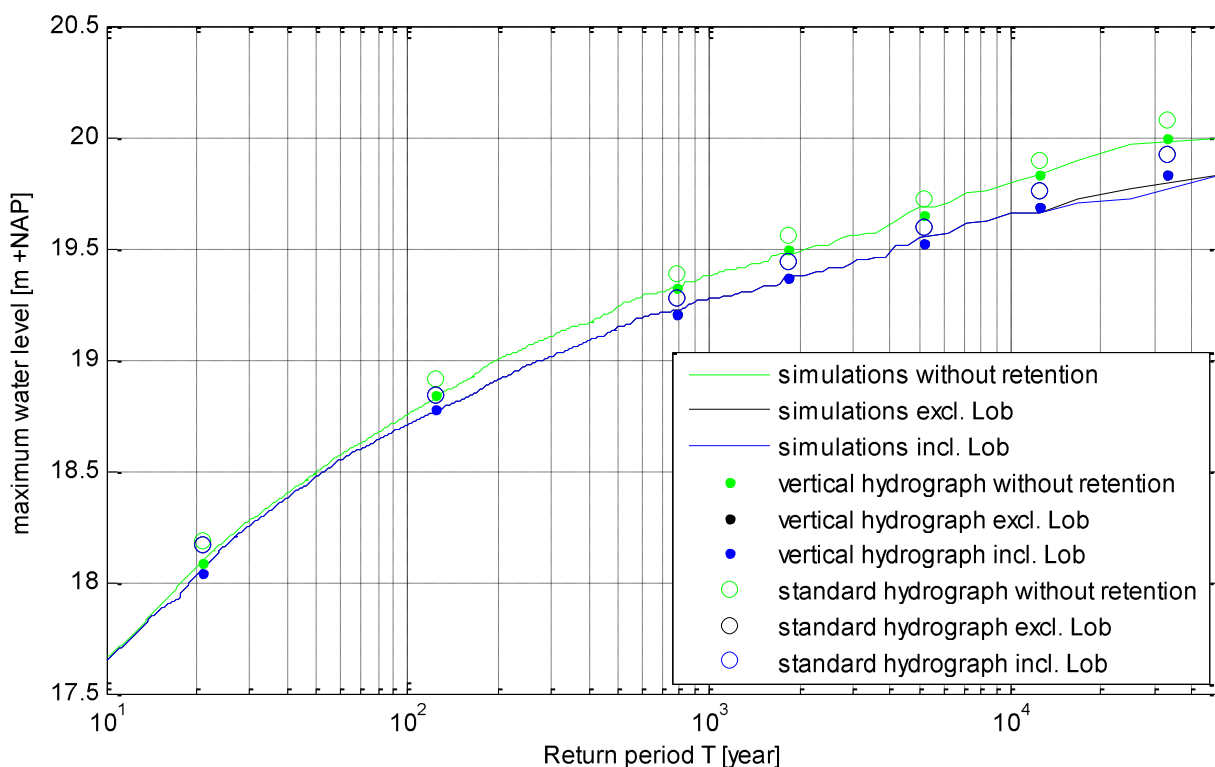


Figure H-4 Design water levels at Venlo in system without retention (Kernel)

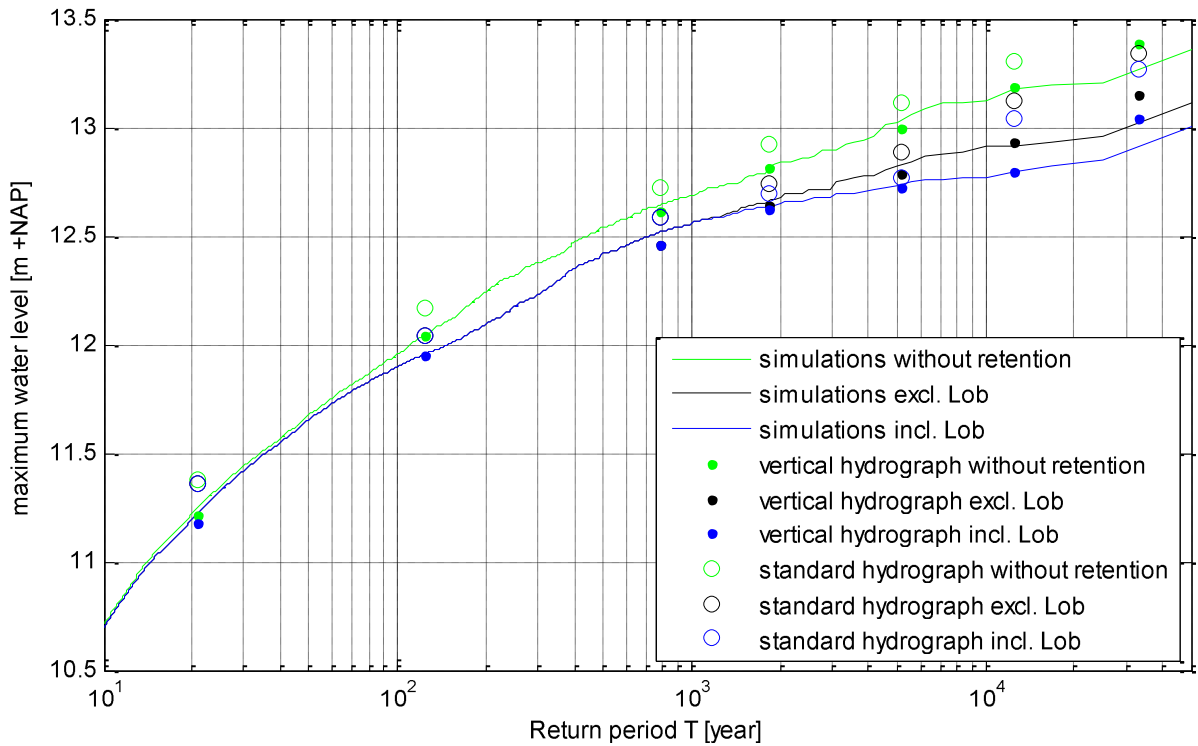


Figure H-5 Design water levels at Mook in system without retention (Kernel)

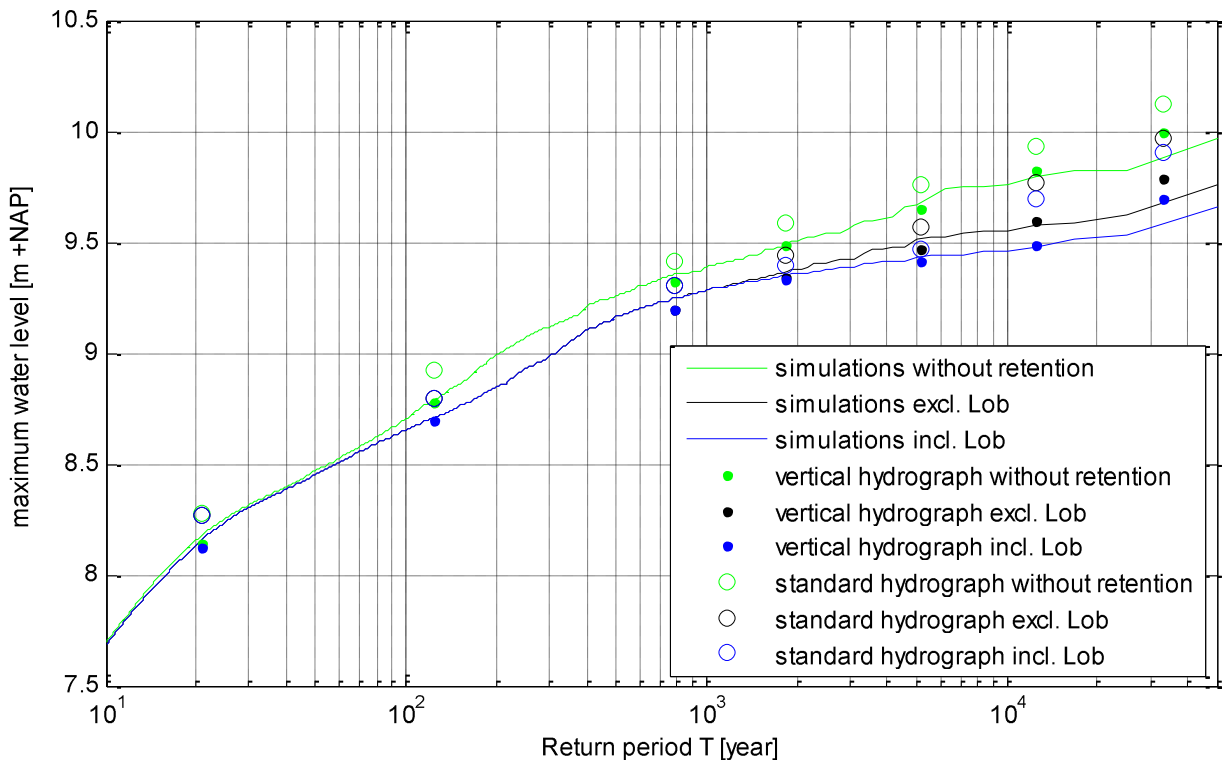


Figure H-6 Design water levels at Megen in system without retention (Kernel)

### Influence of shape variables on retention effect

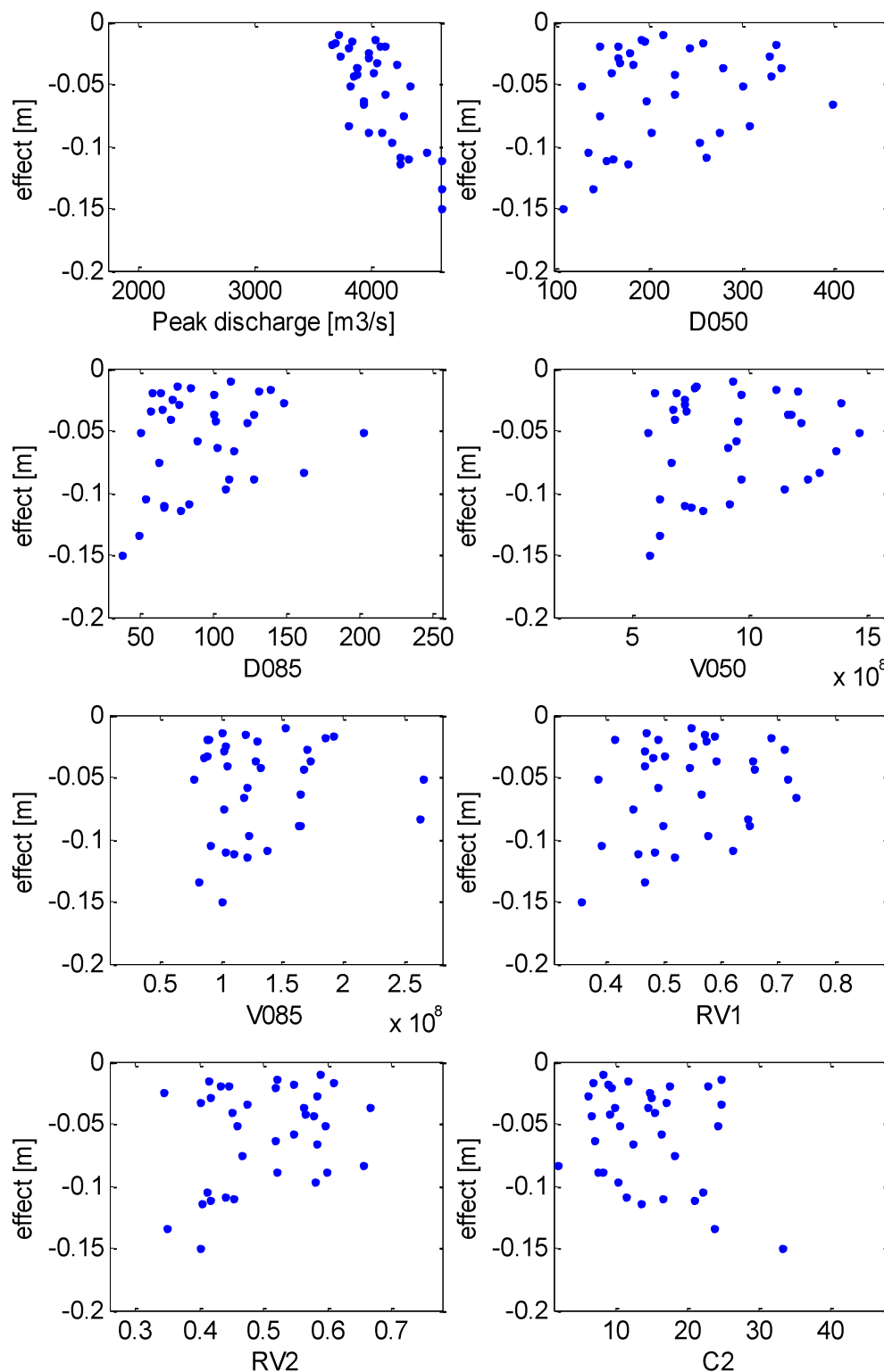


Figure H-7 Relation between retention effect at Mook and shape variables

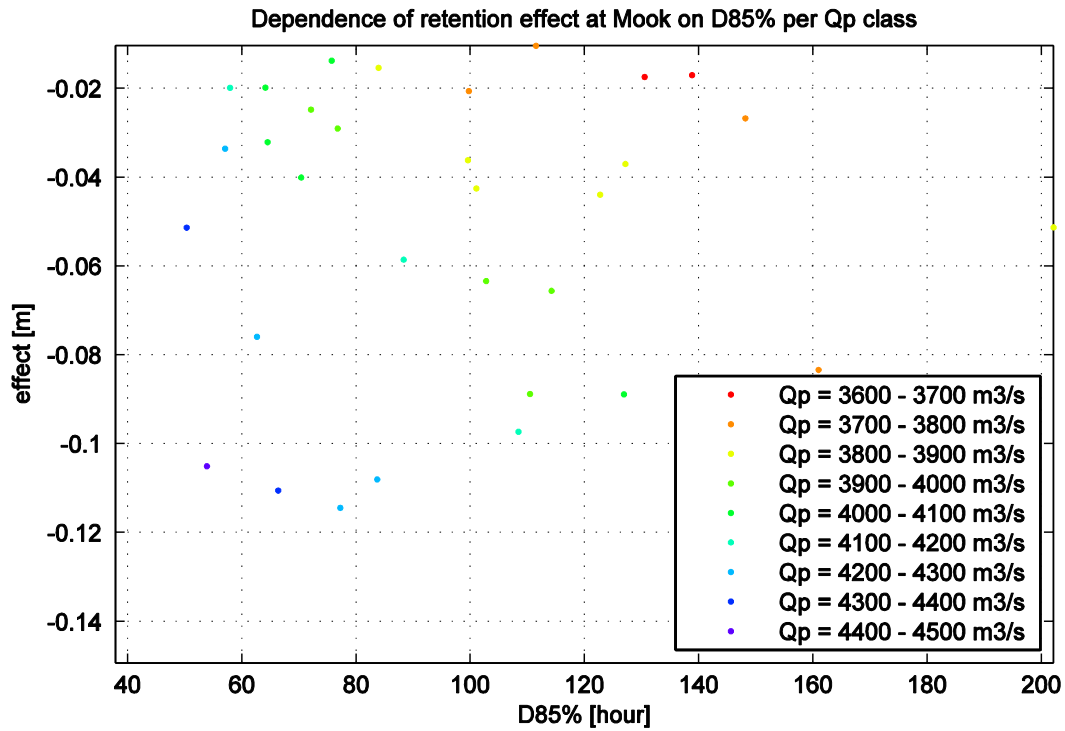


Figure H-8 Dependence of retention effect at Mook on D85%

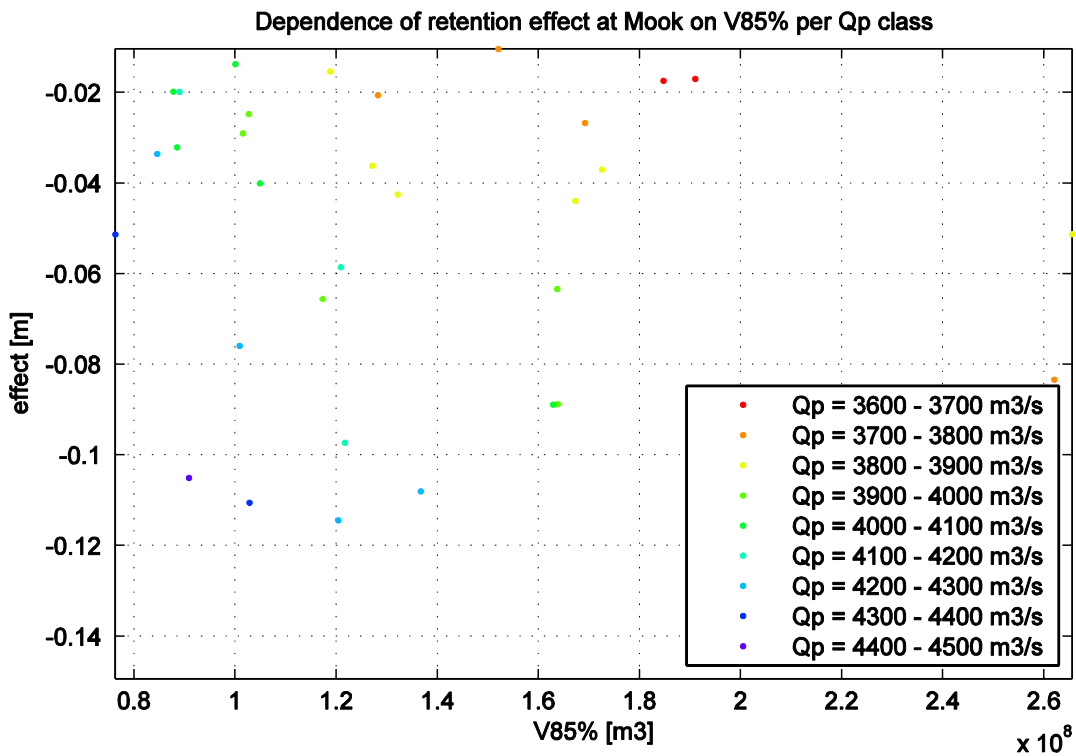


Figure H-9 Dependence of retention effect at Mook on V85%

